A LAGRANGIAN TRAJECTORY AND ISOTOPIC FRACTIONATION (FLEXPART-MCIM) APPROACH TO MODELLING THE ISOTOPIC COMPOSITION OF RAINFALL OVER THE BRITISH ISLES.

A thesis

submitted to the School of Environmental Sciences

of the University of East Anglia

in partial fulfilment of the requirements

for the degree of

Doctor of Philosophy

By

Katherine Ann Teresa Eames

June 2008

Abstract

A novel approach to modelling the oxygen and hydrogen isotope ratios of rainfall over the British Isles is presented. The model process involves two stages. First, a Lagrangian particle dispersion model (FLEXPART) that uses European Centre for Medium Range Weather Forecasting Reanalysis (ECMWF ERA-40) fields to produce ensembles of back trajectories of the three–dimensional path of air parcels prior to rainfall events. Second, physical atmospheric parameters along these trajectories are then input in to a Mixed Cloud Isotope Model (MCIM) to predict the isotopic ratio of rainfall. Models of the movement of oxygen and hydrogen isotopes through the hydrological system are vital to gain understanding of the isotopic systems so as to improve the use of isotopes as palaeoclimate proxies to uncover information about the past.

A case study comparing daily observed isotopic values with modelled values for the same day is presented for Norwich for raindays in November and December 2005. The results of this comparison are very promising for the simulation of δ^{18}O, δD and deuterium excess for events where more than 3 mm but less than 15 mm of rain fell. A positive relationship is seen between the modelled and observed values, i.e. higher modelled values correspond to higher observed values. The regression equation of this relationship for δ^{18}O is y = 0.35x -4.18, which can be compared with the ideal case of modelled = observed (y = x), with an r^2 value of 0.84, significant at the 95% confidence level. The gradient of this relationship and the similar ones seen for δD and deuterium excess reflect the fact that the model sensitivity is too low; the full range of observed values is not captured, though the pattern of variability is reproduced by the model.

Natural variability in the observed data was seen when δ^{18}O values from precipitation

collected at 5 sites around Norwich during November 2005 were compared. However, insufficient observations (only 8 days in one city) were made to allow a general sampling error to be estimated. For the days where multiple samples were collected and analysed, the standard deviation of observed δ^{18}O values varied between 0.11 and 0.92 $^{\circ}/_{\circ\circ}$. This factor should be considered in other studies where modelled values from a grid box are compared with point observations. Similarly, variability was seen across the modelled ensemble of values. For the model runs for Norwich on the 7th November 2005 at 1200 a range of δ^{18}O values of 6.65 $^{\circ}/_{\circ\circ}$ was seen, emphasising the importance of an ensemble of runs being conducted rather than a single trajectory. Comprehensive sensitivity tests of the model were conducted.

Case studies for other U.K. locations in Dublin and Birmingham during November 2005; and for sites at Driby, Lincolnshire and Stock Hill, Somerset during 1977 to 1982 are also presented. Positive correlations were seen between modelled and observed oxygen and hydrogen isotopic ratios and deuterium excess in all cases except for Dublin where there was an insufficient observed sample size. However, as for Norwich, the model sensitivity was too low (the maximum modelled range across all sites was 3.9 times less than that of the observed values for δ^{18}O and 3.5 times too small for δD) .

This approach shows promise for modelling the isotopic composition of rainfall for mid–latitude maritime climatic regions as a complimentary method to the technique of explicitly modelling the isotopic composition of precipitation in General Circulation Models (GCMs). The very nature of GCMs means that it is difficult to identify which processes involved have the largest impact on an individual atmospheric component. The simpler format of model used in this study more easily allows processes to be added or removed in order to investigate the relative importance of each one. Also, smaller scale features are accounted for using the Lagrangian approach used in this study, whereas the resolution of Eulerian GCMs is still limited by the computational times involved. However, more investigation is required into the problems seen in this study in producing a large enough modelled range before this study's approach could be widely used.

Acknowledgements

First and foremost I would like to thank my supervisors at UEA, Dr Adrian Matthews and Dr Peter Rowe, for their unstinting encouragement and support, as well as many interesting discussions throughout the last three and a half years.

In addition thanks to Dr Michiel Helsen (Institute of Marine and Atmospheric Research, Utrecht) and Dr Andreas Stohl (Norwegian Institute for Air Research) for access to and set up help with the MCIM and FLEXPART respectively, and to Paul Dando at ECMWF and Julie Harold and Matthew Livermore at UEA for High Performance computer support.

I would also like to thank Dr Lisa Baldini (University College Dublin) and Professor Andy Baker (University of Birmingham) for collecting precipitation samples at their respective institutions in November 2005; Dr Alina Marca-Bell at UEA for her help and patience in analysing the Norwich November 2005 precipitation samples with a willing but inexperienced lab assistant; Professors Ian Fairchild and Andy Baker for coordinating the analysis of the Dublin and Birmingham precipitation samples at the University of Birmingham; Professors Ian Fairchild and Tim Atkinson for their help in obtaining permission to use the daily observed data sets from Driby and Stock Hill respectively; and Dr Martin Werner for providing the the ECHAM4 climatological fields.

Finally I'd very much like to thank my family and friends, (especially Mum, Dad and Neil) for everything they have done for me over the years.

Contents

Abstract **iii**

Acknowledgements **vii**

1 Introduction **1**

1.1 Preliminary Concepts 1

1.1.1 Isotopes 1

1.1.2 Fractionation 2

1.1.3 Oxygen Isotopes 3

1.1.4 Mass Spectrometry 5

1.1.5 The Hydrological Cycle 6

1.1.6 Air Parcels and Trajectories 8

1.1.7 Eulerian and Lagrangian perspectives 8

1.2 δ^{18}O and its Transport through the Hydrological Cycle 9

1.2.1 Global Network of Isotopes in Precipitation 9

1.2.2 Seasonal Variations 15

1.2.3 Meteoric Water Line 16

1.2.4 Deuterium Excess 17

1.2.5 δ^{18}O as a Climate Proxy 18

1.3 Approaches to Modelling Isotopes in Precipitation 20

1.3.1 Rayleigh–Type Distillation Models 21

1.3.2 Global Climate Models (GCMs) 22

1.3.3 Lagrangian Trajectory Models 24

2 FLEXPART: Model and Methodology **27**

2.1 History of Back Trajectory Models 27

2.2 Evolution of FLEXPART and FLEXTRA 29

2.3 FLEXPART 30

2.3.1 FLEXPART Model Evaluation 32

2.3.2 Turbulence in FLEXPART 36

2.3.3 Mesoscale Velocity Fluctuations 37

2.3.4 Convection and Vertical Motions in FLEXPART 38

2.4 FLEXPART Output 40

2.4.1 Tracer Concentrations 40

2.4.2 Clusters and Cluster Analysis 41

2.5 Model Setup 43

3 Isotope Fractionation Theory and the Mixed Cloud Isotope Model **45**

3.1 Isotope Nomenclature 45

3.2 Rayleigh Distillation Theory 46

3.2.1 Equilibrium Fractionation 47

3.3 Extensions to Rayleigh Distillation Theory 55

3.3.1 Kinetic Fractionation 55

3.3.2 Mixed Clouds Containing Liquid and Solid Condensate 58

3.3.3 Initial Isotopic Composition of Atmospheric Water Vapour 60

3.3.4 Evaporation and Exchange During Precipitation 61

3.3.5 Fractionation in the Middle Atmosphere 62

3.4 Mixed Cloud Isotope Model 63

3.4.1 MCIM Algorithm 63

4 November 2005 Case Study **81**

4.1 Precipitation Collection 81

4.1.1 Collection Sites 81

4.1.2 Precipitation Collection Method 82

4.2 Significance of Correlations 84
4.3 Observed Amount of Precipitation 85
4.4 Observed δ^{18}O 86
4.5 Observed Deuterium Excess 88
4.6 Modelling the Observed Isotopic Composition 90
4.6.1 Norwich 94
4.6.2 Dublin 101
4.6.3 Birmingham 104
4.6.4 Inter–site Comparison 107
4.6.5 Observed and Modelled Monthly Averages 112
4.7 Trajectory Analysis 113
4.8 Modelling the Observed Amount of Rainfall 118
4.9 Norwich Time of Precipitation Data 119
4.10 Intra–site Variability in Norwich 120
4.11 Comparison of Norwich Results and GCM Output 123
4.12 Conclusions 125

5 Sensitivity Studies **129**

5.1 FLEXPART 130
5.1.1 Sampling Error 130
5.1.2 Timestep of FLEXPART Output 132
5.1.3 Duration of Back Trajectories 136
5.1.4 Horizontal Size of Initial Release Grid Box 139
5.1.5 Release Height in the Atmosphere 139
5.1.6 Effect of Convection 141
5.1.7 Within Day Sampling 141
5.2 MCIM 145
5.2.1 Isotopic Composition of Ambient Air 145
5.2.2 Threshold Relative Humidity at Which Precipitation Occurs . . . 146
5.2.3 Relative Proportions of Ambient and Internal Air Mixing 148

5.2.4 Temporal Resolution of Ambient Isotopic Composition Fields . . 149
5.3 Post–production Processing 150
5.3.1 Sampling of Raining Parcels Only 151
5.4 The Model Set–up 152
5.4.1 FLEXPART Parameters 152
5.4.2 MCIM Parameters 155
5.4.3 Data Processing 155

6 Driby, Lincolnshire and Stock Hill, Somerset Case Studies 157
6.1 Observed Precipitation Amount at Driby and Stock Hill 159
6.2 Observed Isotopic Ratio of Precipitation 161
6.2.1 The Seasonal Cycle of δ^{18}O 164
6.2.2 Extreme Observed δ^{18}O 168
6.3 Modelling the Observed Isotopic Composition 172
6.3.1 Modelling the Daily Values 172
6.3.2 Stock Hill Sensitivity Tests 179
6.3.3 Modelling Monthly Averages 182
6.3.4 Observed and Modelled Averages 185
6.3.5 Modelling the Seasonal Cycle 185
6.3.6 Lamb Classifications 186
6.4 Conclusions 189

7 Conclusions 193
7.1 Further Work 199

References 203

Appendix 215

A Photographs of Norwich Precipitation Collection Sites 219

B Observed and Modelled δ^{18}O and δD values, and amount of precipitation for Norwich, Dublin and Birmingham **225**

C Observed δ^{18}O and δD values, and amount of precipitation for all 5 Norwich precipitation collection sites **229**

D Observed and Modelled δ^{18}O and δD values, and amount of precipitation for Stock Hill **233**

E Observed and Modelled δ^{18}O and δD values, and amount of precipitation for Driby **237**

F Observed versus modelled δ^{18}O for all raindays with over 3 mm of rain at Stock Hill split by month **243**

G Observed versus modelled δ^{18}O for all raindays with over 3 mm of rain at Driby split by month **247**

List of Tables

1.1 *Percentage global abundance of each oxygen and hydrogen isotope* 4

3.1 *Example of calculated isotopic composition initial conditions of an air parcel* 68

3.2 *Example of calculated isotopic composition of the initial air parcel before and after mixing in of external air* 72

3.3 *Glossary of terms: Part I* 78

3.4 *Glossary of terms: Part II* 79

4.1 *Mean observed $\delta^{18}O$, δD and d-excess at Norwich, Dublin and Birmingham* 88

4.2 *Observed $\delta^{18}O$ for Dublin, Norwich and Birmingham on days where precipitation was experienced at all three sites* 110

4.3 *Mean observed and modelled $\delta^{18}O$, δD and d-excess at Norwich, Dublin and Birmingham* 113

4.4 *Categories for trajectory analysis with a brief description of each situation* 118

4.5 *Isotopic composition of precipitation collected from 5 sites in Norwich, days with less than a 1 ‰ difference in $\delta^{18}O$ between sites* 124

4.6 *Isotopic composition of precipitation collected from 5 sites in Norwich, days where the difference in observed $\delta^{18}O$ between sites is greater than 1 ‰* 124

5.1 *Modelled isotopic composition for 10 runs with different initial particle locations, for the release of 100 and 1000 particles* 132

5.2 *Modelled oxygen isotopic composition from FLEXPART trajectories with different release box sizes and observed Norwich $\delta^{18}O$* 140

5.3 *Modelled oxygen isotopic composition from FLEXPART trajectories with convection turned on and turned off and observed $\delta^{18}O$ at Norwich* 143

5.4 *The variation in $\delta^{18}O$ during each FLEXPART sensitivity test* 156

6.1 *Maximum and minimum observed $\delta^{18}O$ and δD at Stock Hill and Driby* . 164

6.2 *Mean observed $\delta^{18}O$ and δD at Norwich, Dublin, Birmingham, Stock Hill and Driby* 164

6.3 *Summary of the monthly split of modelled vs observed $\delta^{18}O$ at Stock Hill* . 180

6.4 *Summary of the monthly split of modelled vs observed $\delta^{18}O$ at Driby* . . . 181

6.5 *Mean observed and modelled $\delta^{18}O$, δD and d-excess at Norwich, Dublin, Birmingham, Stock Hill and Driby* 185

7.1 *Locations of daily data sites and the dates $\delta^{18}O$ data is available for each* 194

7.2 *Regression equations and r^2 values for observed versus modelled $\delta^{18}O$ and d-excess for all days where more than 3 mm of rainfall occurred at all sites* 199

B.1 *Observed and modelled $\delta^{18}O$ and δD values, and amount of precipitation for all Norwich raindays collected at the roof site at 87 Bury Street* 226

B.2 *Observed and modelled $\delta^{18}O$ and δD values, and amount of precipitation for all Dublin raindays* 226

B.3 *Observed and modelled $\delta^{18}O$ and δD values, and amount of precipitation for all Birmingham raindays* 227

C.1 *Observed $\delta^{18}O$ and δD values, and amount of precipitation for all Norwich raindays collected at both 87 Bury Street precipitation collection sites* 230

C.2 *Observed $\delta^{18}O$ and δD values, and amount of precipitation for all Norwich raindays collected at all University of East Anglia precipitation collection sites* 231

D.1 *Observed and modelled $\delta^{18}O$ and δD values, and amount of precipitation for all Stock Hill raindays* 234

D.1 *continued* 235

D.1 *continued* 236

E.1 *Observed and modelled $\delta^{18}O$ and δD values, and amount of precipitation for all Driby raindays* 238

E.1 *continued* 239

E.1 *continued* 240

E.1 *continued* 241

E.1 *continued* 242

List of Figures

1.1 *Schematic of the structure of the 3 naturally occurring isotopes of hydrogen* 3

1.2 *Simple schematic of a mass spectrometer* 7

1.3 *The hydrological cycle* 9

1.4 *Schematic showing typical $\delta^{18}O$ values for each stage of the hydrological cycle* 11

1.5 *Map of amount–weighted annual $\delta^{18}O$ of precipitation* 12

1.6 *The Global Meteoric Water Line* 17

2.1 *Comparison of total column carbon monoxide tracer in $mg\ m^{-2}$ from FLEXPART simulations using ECMWF data and GFS NCEP data* 34

2.2 *An example of a divergent particle situation from FLEXPART* 42

3.1 *Saturation vapour pressures calculated using the Claussius–Clapeyron equation* 49

3.2 *Plot of all experimentally obtained oxygen fractionation factors from 0.75 to 350°C, obtained by Horita and Wesolowski (1994), and reported in other literature* 53

3.3 *Values of 10^3 ln α for the fractionation of ^{18}O obtained using the empirical equations of Majoube (1971b) and Horita and Wesolowski (1994)* . . 54

3.4 *Modelled $\delta^{18}O$ and d-excess as a function of condensation temperature as predicted by three different isotope distillation models* 59

3.5 *Flowchart of the MCIM algorithm* 64

3.6 *Saturation vapour pressures calculated using the Claussius–Clapeyron and Goff–Gratch equations* 67

4.1 *Map of the British Isles showing the location of Birmingham, Dublin and Norwich.* 83
4.2 *Critical r^2 values for sample sizes between 3 and 28* 86
4.3 *Scatter plot of observed $\delta^{18}O$ against the daily precipitation total amount during November 2005 for the sites at (i) Norwich, (ii) Dublin and (iii) Birmingham* 87
4.4 *Time series of observed $\delta^{18}O$ and precipitation amount at (i) Norwich, (ii) Dublin and (iii) Birmingham* 89
4.5 *Observed $\delta^{18}O$ versus δD for Dublin, Birmingham and Norwich* 91
4.6 *FLEXPART trajectories for days when d-excess values below the Global Meteoric Water Line were observed* 92
4.7 *FLEXPART trajectories for Dublin 0600 on the 1st December 2005, when the most negative $\delta^{18}O$ value was observed* 95
4.8 *FLEXPART trajectories for the sample day when the least negative $\delta^{18}O$ value was observed* 96
4.9 *Mean sea–level pressure and fronts charts for 10th and 11th November 2005 at 1200 UTC* 97
4.10 *Observed versus modelled for all Norwich raindays for (i) $\delta^{18}O$, (ii) δD, and (iii) deuterium excess* 99
4.11 *Observed versus modelled for Norwich raindays where no snow occurred (i) $\delta^{18}O$, (ii) δD, and (iii) deuterium excess* 100
4.12 *Observed versus modelled for Norwich raindays where the amount of rain was greater than 3 mm (i) $\delta^{18}O$, (ii) deuterium excess* 102
4.13 *Observed versus modelled for all Dublin raindays for (i) $\delta^{18}O$, (ii) δD, and (iii) deuterium excess* 103
4.14 *Observed versus modelled for Dublin raindays where the amount of rain was greater than 3 mm (i) $\delta^{18}O$, (ii) deuterium excess* 105
4.15 *Observed versus modelled for all Birmingham raindays for (i) $\delta^{18}O$, (ii) δD, and (iii) deuterium excess* 106

4.16 *Observed versus modelled for Birmingham raindays where the amount of rain was greater than 3 mm (i) $\delta^{18}O$, (ii) deuterium excess* 108

4.17 *FLEXPART trajectories at 0000 on the 2nd November 2005 for (i) Norwich and (ii) Dublin* 109

4.18 *Modelled versus observed $\delta^{18}O$ for (i) all raindays and (ii) raindays with over 3 mm at Norwich, Dublin and Birmingham* 111

4.19 *Comparison of modelled $\delta^{18}O$ at the start and end of each individual trajectory at Norwich, Dublin and Birmingham* 113

4.20 *Observed versus modelled $\delta^{18}O$ for Norwich and Birmingham split into "Main source" categories* 115

4.21 *Examples of "Main direction" FLEXPART trajectory categories* 116

4.22 *Examples of "Main source" FLEXPART trajectory categories* 117

4.23 *Timing and amount of rainfall falling in Norwich from 24th November 2005 to 8th December 2005* 121

4.24 *Modelled versus observed $\delta^{18}O$ for 8 Norwich raindays where time of precipitation data was also collected* 122

4.25 *Comparison of modelled and observed $\delta^{18}O$ with climatological values from the ECHAM4 GCM for all Norwich raindays* 126

5.1 *FLEXPART particle trajectories for Norwich on the 15th November 2005 using (i) a 3 hour timestep (ii) a 1 hour timestep* 133

5.2 *Modelled isotopic composition from FLEXPART trajectories with different timesteps* 135

5.3 *Modelled isotopic composition from FLEXPART trajectories using the Lagrangian timestep method* 135

5.4 *Modelled versus observed isotopic composition for all Norwich raindays from FLEXPART trajectories using a 1 hour and 3 hour non-Lagrangian timestep and a 1 hour Lagrangian timestep method* 137

5.5 *Modelled isotopic composition with trajectories of varying length* 138

5.6 *Modelled isotopic composition of trajectories initiated at different release heights* 142
5.7 *Modelled isotopic composition of trajectories initiated at 8 times throughout the sample day* 144
5.8 *Modelled versus observed $\delta^{18}O$ for all Norwich raindays. Modelled values are from 4 run averages and 8 run averages* 146
5.9 *Modelled $\delta^{18}O$ values of precipitation produced using a single initial and ambient global atmospheric $\delta^{18}O$* 147
5.10 *Modelled isotopic composition from MCIM runs for Norwich raindays with varying rainout relative humidity thresholds* 148
5.11 *Effect of varying the proportions of internal and external air mixed into the parcel* 150
5.12 *Modelled isotopic composition of all particles and only raining particles* . 153
6.1 *Map of the British Isles showing the location of Birmingham, Dublin and Norwich, as well as Driby and Stock Hill* 158
6.2 *Scatter plot of observed $\delta^{18}O$ against the daily precipitation total amount during the sampling periods at (i) Stock Hill, and (ii) Driby* 160
6.3 *The amount of precipitation observed at Stock Hill throughout the sampling period.* 162
6.4 *The amount of precipitation observed at Driby throughout the sampling period.* 163
6.5 *Observed $\delta^{18}O$ versus δD for Stock Hill* 165
6.6 *Observed $\delta^{18}O$ versus δD for Driby* 165
6.7 *The observed $\delta^{18}O$ of precipitation for Stock Hill* 166
6.8 *The observed $\delta^{18}O$ of precipitation for Driby* 167
6.9 *FLEXPART trajectories for Stock Hill on the 16th February 1978* 170
6.10 *FLEXPART trajectories for Stock Hill on the 25th March 1978* 171
6.11 *Surface pressure chart for 0000 on the 25th March 1978* 172
6.12 *FLEXPART trajectories for Driby on the 8th February 1981* 173

6.13 *Surface pressure chart for 0000 on the 25th March 1978* 174
6.14 *Observed versus modelled $\delta^{18}O$, δD and d-excess for all raindays with over 3 mm of rain at Stock Hill* 176
6.15 *Observed versus modelled $\delta^{18}O$, δD and d-excess for all raindays with over 3 mm of rain at Driby* 177
6.16 *Observed versus modelled $\delta^{18}O$ for all raindays with between 3 and 15 mm of rain (i) Stock Hill, (ii) Driby* 178
6.17 *Observed versus modelled for all Stock Hill raindays with over 3 mm of rain with varied humidity and supersaturation* 183
6.18 *Monthly averages of observed versus monthly averages of modelled $\delta^{18}O$ values (i) Stock Hill, (ii) Driby* 184
6.19 *The modelled $\delta^{18}O$ of rainfall for Stock Hill* 187
6.20 *The modelled $\delta^{18}O$ of rainfall for Driby* 188
6.21 *Modelled versus observed $\delta^{18}O$ for all Stock Hill raindays, split by Lamb categories* 190
6.22 *Modelled versus observed $\delta^{18}O$ for all Driby raindays, split by Lamb categories* 191
6.23 *Modelled versus observed $\delta^{18}O$ for all Stock Hill raindays, split into 3 groups of Lamb categories* 192
6.24 *Modelled versus observed $\delta^{18}O$ for all Driby raindays, split into 3 groups of Lamb categories* 192
A.1 *The roof precipitation collection site at 87 Bury Street, Norwich* 220
A.2 *The garden precipitation collection site at 87 Bury Street, Norwich* 221
A.3 *The Sainsbury Centre precipitation collection site at the University of East Anglia, Norwich* 222
A.4 *The Zicer precipitation collection site at the University of East Anglia, Norwich* 223

Chapter 1

Introduction

This study aims to investigate a system for modelling the oxygen and hydrogen isotopes (see section 1.1.1) of precipitation. As different processes control the isotopic cycle in different areas of the world (section 1.2), this study will concentrate on precipitation over the British Isles. With a better understanding of this isotopic system and much more data it is possible that the use of heavy to light oxygen isotope ratios as a climate proxy could be improved, therefore potentially improving the datasets used to verify and develop climate models. This chapter will introduce the theory behind this study and the details of the modelling approach used, which involves combining a Lagrangian trajectory model (to trace the path taken by precipitating air) and a second model that deals with the changes in isotopes along that path (section 1.3.3). This is the first study using this approach to model isotopes in precipitation over the British Isles.

1.1 Preliminary Concepts

1.1.1 Isotopes

Atoms of elements have a fixed number of protons and electrons, but may have differing numbers of neutrons. Therefore atoms of elements may possess different atomic masses (e.g. ^{12}C and ^{14}C). Each different mass is referred to as a different isotope of the element. Figure 1.1 shows the three naturally occurring isotopes of hydrogen. Deuterium, (^{2}H

or D), contains 1 neutron, tritium (^{3}H), has two, and protium (the most common and often referred to purely as hydrogen, (^{1}H)) has none. The extra neutrons are indicated in notation when their presence is relevant by stating the atomic mass after the element name e.g. carbon-12 or carbon-14, or before the symbol of the element as shown above. As neutrons have no charge they do not affect the way in which isotopes chemically react, but they do affect the strength of covalent bonds formed with atoms of other elements and also the strength of hydrogen bonds, i.e. intermolecular bonds or bonds between molecules. For some isotopes the extra mass makes the atom unstable (radioactive) and it breaks down by emitting energy or small particles. Tritium is one such unstable isotope.

1.1.2 Fractionation

Fractionation is an important consequence of isotopes having differing masses. Chapter 3 contains more detailed theory on this process. Isotopic fractionation of water molecules occurs during evaporation and condensation. Molecules containing heavier isotopes form stronger and therefore more stable bonds with other molecules in their environment than their lighter counterparts. Therefore more thermal energy is required to break these intermolecular bonds, to cause the atoms to evaporate and then to keep them in vapour form.

In a gaseous state the differences in isotopic mass affects the molecular velocities. Kinetic energy (KE) is equal to

$$KE = \frac{1}{2}mv^2 \tag{1.1}$$

where m is the mass of a molecule and v is its' velocity. All molecules of an ideal gas have the same kinetic energy at a specified temperature. Therefore to keep the kinetic energy equal, lighter molecules must have a higher velocity than heavy molecules (Faure and Mensing, 2005). These differences in relative velocities cause fractionation during condensation as the heavier molecules with lower velocity and therefore lower vapour pressure preferentially form water droplets. The ratios of heavy to light isotopes at different points in the hydrological cycle can provide information as to the conditions that the vapour has experienced, and therefore, in some cases, where the vapour has come from.

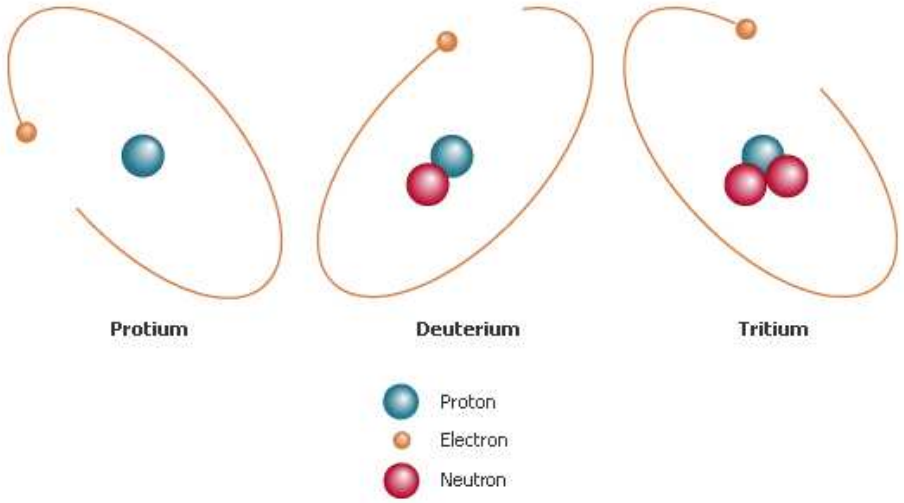

Figure 1.1: *Schematic of the structure of the 3 naturally occurring isotopes of hydrogen (Picture obtained from Encarta MSN).*

1.1.3 Oxygen Isotopes

There are 3 naturally occurring, stable isotopes of oxygen; oxygen-16 (^{16}O), oxygen-17 (^{17}O) and oxygen-18 (^{18}O). Any one of these oxygen isotopes can combine with any two hydrogen isotopes (H or D) to make a water molecule (H_2O). This allows for 9 different isotopic possibilities for a water molecule:

$H_2{}^{16}O$, $H_2{}^{17}O$, $H_2{}^{18}O$, $HD^{16}O$, $HD^{17}O$, $HD^{18}O$, $D_2{}^{16}O$, $D_2{}^{17}O$, $D_2{}^{18}O$

However these isotopes are not present in equal quantities on Earth. Table 1.1 shows the percentage abundance of each hydrogen and oxygen stable isotope. As a consequence, each of the nine different water molecule possibilities will also occur with different frequencies. Only three of the nine forms are naturally present in measurable quantities. These three are: $H_2{}^{16}O$, $H_2{}^{18}O$ and $HD^{16}O$ (Araguás-Araguás et al., 2000). The relative ratios of each isotope will vary on smaller spatial scales due to physical parameters such as temperature and humidity. ^{18}O has previously been used along with tritium (^{3}H) and deuterium (^{2}H or D) to study the hydrological cycle. Water molecules containing oxygen-18 ($H_2{}^{18}O$) require more thermal energy to evaporate and remain in vapour form than water molecules containing the lighter isotope, oxygen-16, ($H_2{}^{16}O$). This means that water vapour will be depleted in heavy isotopes relative to ocean water. A second frac-

Isotope	Abundance, % by number
	Hydrogen
^{1}H	99.985
^{2}H	0.015
	Oxygen
^{16}O	99.762
^{17}O	0.038
^{18}O	0.200

Table 1.1: *Percentage global abundance of each oxygen and hydrogen isotope, from Faure and Mensing (2005).*

tionation occurs during condensation preceding precipitation from a cloud: $H_2{}^{18}O$ preferentially condenses. Therefore cloud droplets and precipitation are enriched in heavy isotopes relative to the water vapour in the cloud, and the cloud moisture becomes progressively more depleted in heavy isotopes as rainout occurs. When the ratios between these heavier and less abundant isotopes and their more common versions are measured (in precipitation, surface waters or groundwaters) this information can provide clues as to where the water has come from, (i.e. tracing groundwaters even after limited mixing, and for precipitation, information as to the conditions the air parcel has experienced since the water vapour source region). This tracing process is also aided by the fact that once water has infiltrated to a certain depth its isotopic composition remains almost constant during subsurface movement and storage (Sonntag et al., 1983). Subsequently, the hydrological cycle can be reconstructed and understood in more detail. In natural waters the heavy stable isotopes of deuterium, D, and ^{18}O, are present almost exclusively in the molecular forms of water, HDO and $H_2{}^{18}O$ (Sonntag et al., 1983). Fractionation of HDO can be up to 8 to 10 times greater than for $H_2{}^{18}O$ making joint analyses of both hydrogen and oxygen isotopes important (Jouzel et al., 1996).

The ratio of ^{18}O to ^{16}O isotopes is conventionally expressed as permil ($^{\circ}/_{\circ\circ}$) relative to Vienna Standard Mean Ocean Water (VSMOW) and termed $\delta^{18}O$ where,

$$\delta^{18}O = \left[\frac{(^{18}O/^{16}O)_{sample}}{(^{18}O/^{16}O)_{VSMOW}} - 1 \right] \times 1000 \tag{1.2}$$

where ^{18}O is the concentration of oxygen-18 and ^{16}O is the concentration of oxygen-16. A similar expression describes δD, the ratio of deuterium to hydrogen. VSMOW is an international reference standard against which the isotopic compositions of samples are compared. The isotopic content of VSMOW is (Clark and Fritz, 1997),

$$\left(\frac{^{18}O}{^{16}O} \right)_{VSMOW} = (2005.2 \pm 0.45) .10^{-6} \tag{1.3}$$

$$\left(\frac{^{2}H}{^{1}H} \right)_{VSMOW} = (155.76 \pm 0.05) .10^{-6} \tag{1.4}$$

Values of δ^{18}O can be positive, negative or zero. A positive value indicates that the sample has a higher $^{18}\mathrm{O}/^{16}\mathrm{O}$ ratio than the standard, which is expressed by saying that the sample is enriched in ^{18}O relative to the standard seawater. A negative value means the sample is depleted in ^{18}O relative to seawater (Faure and Mensing, 2005). By convention when referring to the relative concentrations of oxygen and hydrogen isotopes the state of the heavier isotope concentration is the one described. For example, the statement 'the sample is depleted relative to seawater' would mean the same as 'sample is depleted in ^{18}O relative to seawater'. Whether hydrogen or oxygen is being discussed should be clear from the surrounding text though the two species vary concurrently in most cases.

1.1.4 Mass Spectrometry

Mass spectrometry is an analytical tool that can be used to measure the isotopic content for most elements in the majority of materials. A schematic of an isotope ratio gas source mass spectrometer is shown in figure 1.2. To measure the δ^{18}O values of water samples, the water is equilibrated with CO_2. The CO_2 is then passed through an inlet system and into the mass spectrometer source area where it is ionised. The resultant ions (figure 1.2) are then accelerated and focused according to their mass/charge ratio by a magnetic field (Willard et al., 1988), creating individual ion beams for each mass (i.e. a mass of 44

for $^{12}C^{16}O^{16}O$, and 46 for $^{12}C^{16}O^{18}O$). Each of these beams can then be collected and measured separately by the Faraday collectors and an isotope ratio output is given by the mass spectrometer.

δD values for this study were measured using a continuous flow mass spectrometer. For this method the water sample is injected into the gas stream where it is then reduced to H_2 and CO in a high temperature pyrolysis reaction. These ions are then passed via the mass spectrometer inlet system to the ionising source and the isotopic masses measured as described above for oxygen.

1.1.5 The Hydrological Cycle

The hydrological cycle consists of a series of reservoirs connected by processes such as evaporation, precipitation and runoff. The reservoirs are the oceans, ice sheets, glaciers, terrestrial water, the biosphere and the atmosphere. The oceans, covering 71% of the Earth's surface, hold over 97% of all Earth's water (Barry and Chorley, 1998). Water has very different residence times in each of the reservoirs, ranging from hundreds or thousands of years in the oceans and ice caps, to only 10 days in the atmosphere (Gat, 2000). The global distribution of water is very closely linked to the distribution of energy received from the sun. Energy is required to evaporate water, and cooler global temperatures allow more water to be held in ice. Figure 1.3 is a schematic summary of the main processes involved in cycling water. Evaporation occurs from the oceans around the world, particularly in the tropics where incoming solar radiation is greatest and the trade winds decrease humidity above the water surface thus increasing the rate of evaporation across a steeper humidity gradient. This evaporated water then rises in the atmosphere and circulates until the temperature (energy) of the air falls enough that it can no longer provide sufficient heat to keep the water in vapour form. Precipitation then occurs. Interception occurs when precipitation is prevented from falling immediately on the ground and instead falls on either plants or buildings. Some of this water will evaporate from these surfaces without reaching the ground, causing it to cycle more quickly. Any water that reaches the ground can then either evaporate, infiltrate into the groundwater flow or

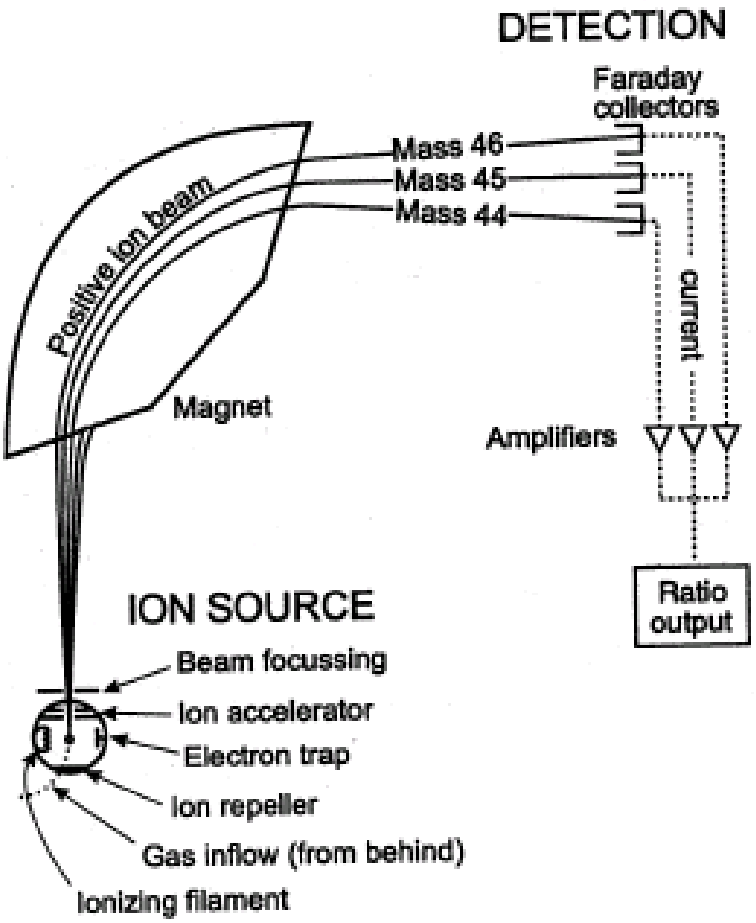

Figure 1.2: *Simple schematic of a mass spectrometer for oxygen isotope measurements showing the ion source and the creation of the ion beams segregated according to mass. The intensity of each beam are measured by the Faraday collectors. The mass ratios are output and compared with internal laboratory standards, which for $\delta^{18}O$ and δD have been calibrated against VSMOW. (Picture obtained from Wikipedia images.)*

move over the surface back to the oceans. Water loss from the soil via intake through the roots then loss from the leaves of plants is termed transpiration (Barry and Chorley, 1998).

1.1.6 Air Parcels and Trajectories

The concept of an air parcel is used in many meteorological explanations and modelling studies. An air parcel is an imaginary body of air that obeys all of the basic dynamic and thermodynamic properties of atmospheric air. A parcel is large enough to contain a large number of molecules, but small enough so that the properties given to it are uniform throughout and so that its movements with respect to the atmosphere do not cause marked compensatory motions within the atmosphere. For visualising purposes, a body of air up to a few metres in diameter is accurate for an air parcel. The path an air parcel takes through the atmosphere is called a trajectory. If an air parcel is tracked backwards through time the path taken is then termed a "back trajectory".

1.1.7 Eulerian and Lagrangian perspectives

There are two ways of viewing the motions of air parcels: Eulerian —- enlisting fixed space coordinates with the observer passively viewing changes within the defined area or volume over a time period; and Lagrangian — where a fixed subject, for example an air parcel, is actively followed by the observer through time and space. The difference between these two methods can be visualised through Eulerian representing an observer on the ground watching the path of a hot air balloon, and Lagrangian being an observer in the basket of the balloon. Lagrangian methods have the advantage that non–linear advection terms are included implicitly, without approximation, following the motion of a fluid across time (Wilson and Sawford, 1996).

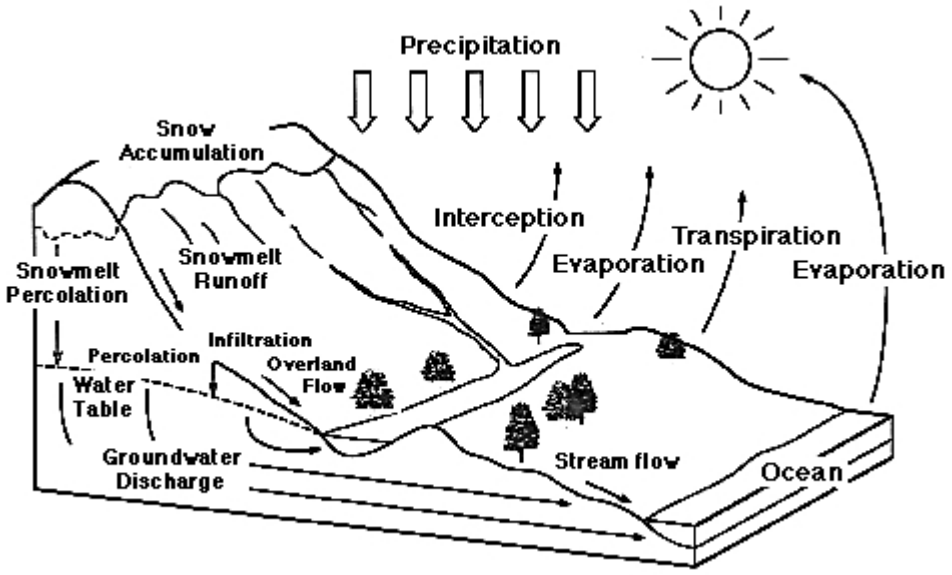

Figure 1.3: *The hydrological cycle (Picture obtained from Wikipedia Images)*

1.2 δ^{18}O and its Transport through the Hydrological Cycle

1.2.1 Global Network of Isotopes in Precipitation

The Global Network of Isotopes in Precipitation (GNIP), was established in 1961 as a response to a recognised need for monitoring and collection of data on isotopes in precipitation. Much of what we know about the global distribution of isotopes has been discerned through analysis of data collected by this project. The database is accessible at http//isohis.iaea.org, and as of the 28th April 2008 contains data collected up to and including 2002. There are some entries dating back to 1953. GNIP was initiated and is maintained by the International Atomic Energy Agency (IAEA) in cooperation with the World Meteorological Organisation (WMO). The IAEA publish guidelines on how samples are to be collected and analysed so as to ensure that the results are comparable. For example, all sites produce statistically averaged values of conditions on the 15th of each month for the preceding month (Schotterer et al., 1996).

The IAEA also conducts quality controls on the incoming data sets such as removing

inconsistent data, obvious outliers, and typing errors (Rozanski et al., 1993). Since the programme started there have been a total of 515 stations operational with an uneven global distribution. The maximum number of stations collecting data at the same time was 220 in 1962-1963 (Schotterer et al., 1996). Information available on the isotopic compositions of precipitation includes the tritium content (^{3}H/^{1}H given in tritium units), and the stable isotope ratios (δD and δ^{18}O). Average physical data such as precipitation type, precipitation amount, surface air temperature and vapour pressure are also given for each month. Dansgaard (1964) conducted the initial analysis of the GNIP data set and the conclusions that he reached, including those concerning Rayleigh fractionation theory, are still used today when studying isotopes in precipitation.

The isotopic ratio of precipitation varies due to many forcing factors, such as temperature and distance from the source region, and many studies have been conducted first to map, and then to understand these variations. The results of these studies are summarised in the remainder of this section. All these factors must be considered as potential influences when attempting to analyse any isotopic data. Figure 1.4 shows typical δ^{18}O values at different stages throughout the hydrological cycle (for example ocean water is shown to have a δ^{18}O of 0 $‰$ and the δ^{18}O of snowfall over ice sheets is given as -45 $‰$. Figure 1.5 shows the global distribution of δ^{18}O in precipitation as observed by the GNIP network. Typical values of δ^{18}O over Britain are shown to be between -10 and -2 $‰$.

The major global source of water vapour is the tropical oceans. Peixoto and Oort (1983) found that approximately 65% of global evaporation over the oceans occurs between 30°S and 30°N (Rozanski et al., 1993). Poleward transfer of this water through atmospheric circulation results in a gradual rainout of vapour containing heavier isotopes due to the distance travelled and lower temperatures experienced, see figure 1.4. Therefore precipitation in polar regions is isotopically lighter than in low–latitudes as can be seen in figure 1.5. Depending on the latitude, either precipitation amount or temperature may dominate the spatial and seasonal distribution of isotopes in local precipitation. In mid– to high–latitudes the isotope ratios tend to correlate positively with temperature variations. This relationship is not seen at low–latitudes due to tropical regions being predom-

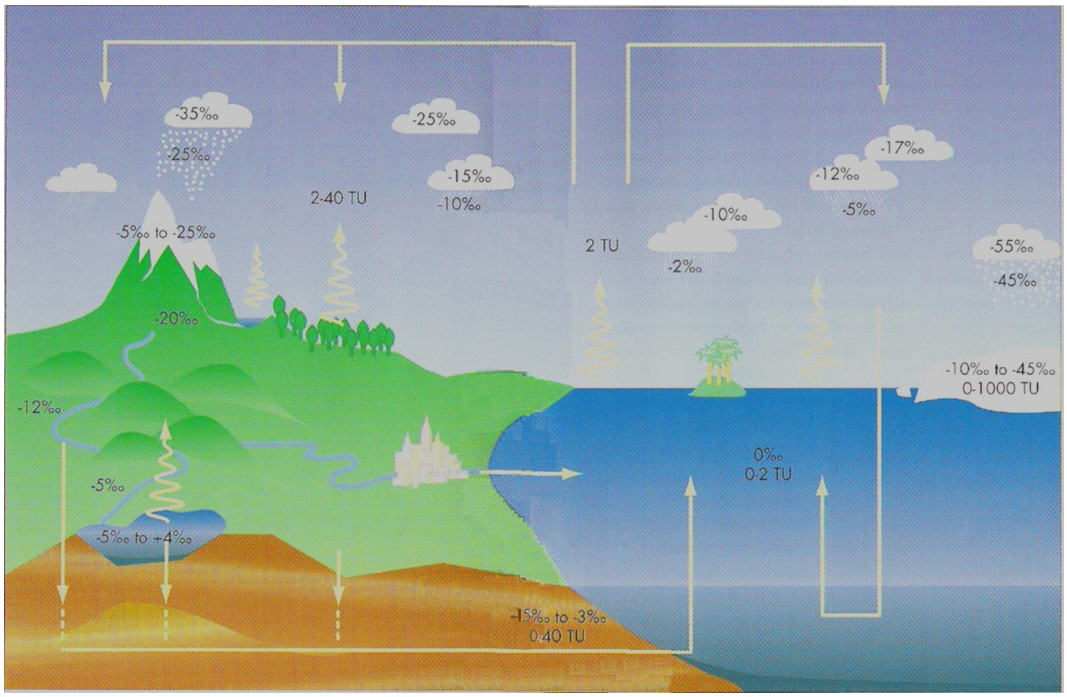

Figure 1.4: *Schematic showing typical $\delta^{18}O$ values in permil (‰) for each stage of the hydrological cycle. (TU = Tritium units). Taken from (Schotterer et al., 1996).*

inantly affected by converging air masses that are forced to move vertically rather than horizontally and experiencing surface temperature gradients that are very small (Fricke and O'Neil, 1999). In tropical areas the isotopic ratio of precipitation has instead been observed to vary inversely with precipitation volume in the so called amount effect (see lower in this section for more details on this effect) (Schotterer et al., 1996).

Analyses of isotope distributions in precipitation over Europe have concluded that variations in isotope ratios have a strong positive correlation with interannual temperature changes making Europe a good region for studying this relationship (Jouzel et al., 1996). Dansgaard (1964) suggested that a one degree temperature change would induce a change in δ^{18}O of 0.69 ‰. In the North Atlantic region these changes are of the same sense due to the positive relationship between temperature and isotopic ratios (i.e. increase in temperature leads to an increase in δ value). Studies conducted since that time have shown that in fact this coefficient varies from place to place. A theoretically derived relationship between δ^{18}O and temperature suggests a slope of between 0.72 and 0.52 ‰ per degree Celsius between 0 and 20 °C, respectively (Rozanski et al., 1992). However even greater

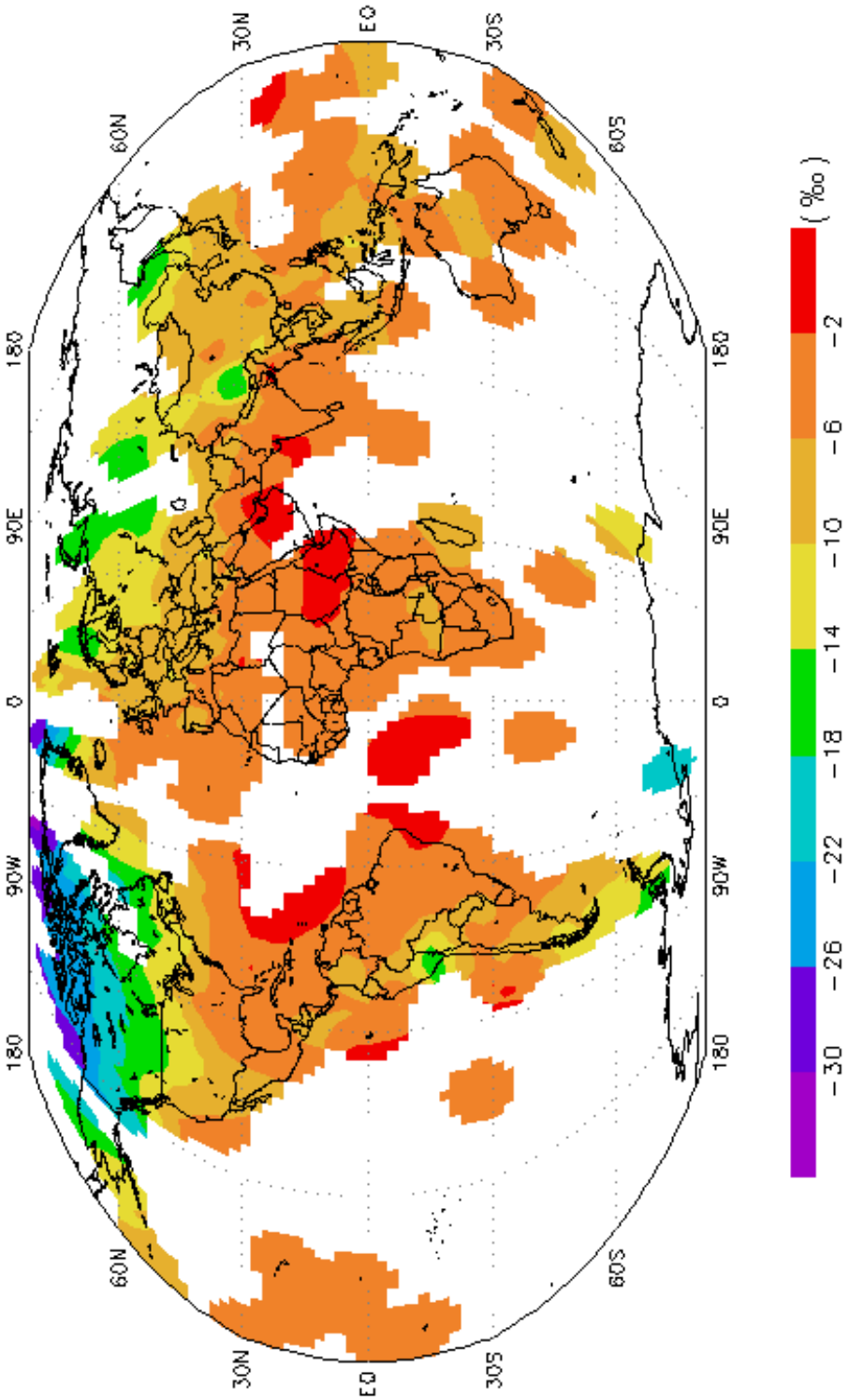

Figure 1.5: *Map of amount–weighted annual $\delta^{18}O$ of precipitation taken from the GNIP database on the IAEA website. Data is a summary spanning the period 1961-1999. Only consecutive 12 month periods were used in calculating the annual means. Oranges and reds indicate less depleted precipitation, blues and purples are regions of more depleted precipitation.*

variation in the slope of the relationship is seen in observations. Darling and Talbot (2003) suggested the "normal" European slope to lie between 0.2 and 0.45 $^{\circ}/_{\circ\circ}$ per degree Celsius and measured a slope of 0.25 $^{\circ}/_{\circ\circ}$ per degree Celsius over the British Isles.

The following observations can be made about the isotopic spatial pattern apparent in the GNIP dataset (figure 1.5) for both δ^{18}O and δD:-

The Continental Effect

As air masses move inland across continents, precipitation becomes more and more depleted in heavy isotopes. Therefore the δ^{18}O value of precipitation becomes more negative. This is known as the continental effect and occurs due to progressive rainout of the heavier isotopes from an air parcel as the air moves away from its source of water vapour (Rozanski et al., 1993). This phenomena is illustrated in the left hand side of figure 1.4 where the initial δ^{18}O of water vapour from the tropical oceans is given as -10 $^{\circ}/_{\circ\circ}$, this decreases through -25 to -35 $^{\circ}/_{\circ\circ}$ as the air parcel moves inland. Figure 1.5 shows real world observations of δ^{18}O in precipitation and the continental effect can be clearly seen to occur south to north across the Northern Hemisphere continental masses.

The Altitude Effect

The isotopic signatures also reflect the topography of the land over which an air parcel has passed. Mountain chains or elevated land cause air masses passing over them to rise and cool, decreasing the amount of water vapour and ^{18}O that can be held. This is termed the altitude effect and is illustrated in the left side of figure 1.4 with the δ^{18}O values decreasing from -10 to -15 and finally to -25 $^{\circ}/_{\circ\circ}$ as the air parcel is lifted as it meets the land. This effect can be seen in the observations in figure 1.5 over the Tibetan plateau as an isolated green circle (green indicating a more negative δ^{18}O value of between -14 and -18 $^{\circ}/_{\circ\circ}$. The effect is also visible over the Andes on the west coast of South America. Consequently individual air parcels that have passed over areas of higher altitude have more negative δ^{18}O values of precipitation (Rozanski et al., 1993).

The Amount Effect

As with the majority of these effects, the amount effect was first proposed by Dansgaard (1964). He observed a negative correlation between δ values of precipitation and the amount of monthly precipitation all year in tropical locations and in the summer in mid–latitudes. Isotopic studies of individual storm events have shown that δ^{18}O varies throughout a prolonged period of precipitation in one area as a frontal system passes. The most intense rainfall is often more depleted in heavy isotopes due to the reduced time available for equilibration with surface air temperature and increased quantity of droplets to be equilibrated. The range of δ^{18}O in one storm event has been measured to be as large as 12 $^{\circ}/_{\circ\circ}$ (Rozanski et al., 1993).

Dansgaard (1964) linked the amount effect to the fact that as raindrops fall they can evaporate and exchange water vapour with the surrounding atmosphere below the cloud. At the start of a shower the air below the clouds will have a lower humidity encouraging more evaporation. Isotopic values of initial precipitation from a system will therefore tend to be enriched in heavier isotopes as the lighter isotopes preferentially evaporate. As the shower continues, the air beneath the cloud will become more humid due to the evaporation occurring into it. This will reduce evaporation but exchange will mean that the rainfall will have a more negative isotopic ratio closer to that of the incloud conditions (Gat, 1980).

Dansgaard (1964) also linked the amount effect to the altitude effect in the way that heavier precipitation events, especially in the tropics, are usually produced by deep convective systems. Air parcels that have been convected through the system will have experienced very cold temperatures at high altitudes that would tend to lead to more negative precipitation being produced by the deeper convective systems which also produce the most intense precipitation. This precipitation will still be affected by equilibration with water vapour in the lower levels of the cloud formations and evaporation at all stages of falling making these the main impacts.

The Source Effect and Re–evaporation

The type of water vapour source for a precipitation site can have an effect on the isotopic composition of the precipitation received. Areas that lie close to oceanic sources will receive water vapour and therefore precipitation with an isotopic composition close to VSMOW. Re–evaporated water is the term given to all water vapour that is sourced from land areas. When precipitation occurs over land masses it does not all immediately infiltrate into the ground and some of the remaining surface water will evaporate. As a water source this surface water will be isotopically lighter than ocean water. As a consequence, vapour from this alternative water source will be lighter than water vapour evaporated directly from the oceans even before any rainout has occurred. Evapotranspiration produces water vapour with the same isotopic composition as the groundwater of the area in which the plants are growing as all water taken up by the roots must be lost from the leaves with no phase change and therefore no fractionation occurring in between (Cole et al., 1999; Sonntag et al., 1983). This effect is not illustrated clearly in figure 1.5 due to this figure showing annual averages and not all precipitation at coastal regions throughout the year being deposited from air parcels that have come in directly over the oceans. Figure 1.4 suggests a δ^{18}O of precipitation from water vapour directly over the source region of $-2\ ‰$.

All of the above "effects" were suggested as explanations for the distribution of isotopes in the early analysis of the GNIP dataset (Dansgaard, 1964). The effects are all linked through the basic physical processes of temperature dependent fractionation (section 1.1.2) and rainout.

1.2.2 Seasonal Variations

The continental and altitude effects are only pronounced when the ocean is the dominant moisture source and re–evaporated water is not a significant component of cloud water content. Re–evaporation is more likely to occur in the summer months due to increased temperatures, as well as extra plant cover, which adds water vapour to the atmosphere through evapotranspiration. Isotope gradients are therefore stronger in winter. Summer

precipitation is less depleted than winter precipitation due to generally higher temperatures and higher humidities over the water vapour source regions. Fractionation is less pronounced when humidity is high leading to initially less depleted water vapour at the source that then continues through the water cycle (Darling and Talbot, 2003).

Another seasonal variation is in the amount of precipitation falling. This can have a great impact on δ^{18}O–temperature correlations over longer time periods. If the majority of a region's precipitation falls in the summer months then annual δ^{18}O values will be biased towards the higher summer temperatures. It can therefore be important to consider the relationship between average δ^{18}O and precipitation–weighted temperature rather than mean annual temperature for a region. The precipitation–weighted temperature is a yearly average temperature calculated to give more importance to temperatures at times of the year when greater amounts of precipitation occurred. However, caution is required when using the relationship to infer palaeotemperatures, as the relationship will change if precipitation seasonality has altered (Jouzel et al., 1996).

1.2.3 Meteoric Water Line

Due to the fact that hydrogen and oxygen atoms are coupled throughout the water cycle, the isotopes of both elements experience the same evaporation and condensation processes. Subsequently, when the isotopic ratios of samples of each of these elements collected from around the world are plotted against one another they form a linear data array. A regression equation with gradient 8 can be fitted to these observations as shown in figure 1.6 (taken from Faure and Mensing (2005)). This line is called the Global Meteoric Water Line, and its' equation is,

$$\delta\mathrm{D} = 8 \times \delta^{18}\mathrm{O} + 10 \tag{1.5}$$

Other meteoric water lines exist for individual regions. All observations collected by the IAEA have been used to create δD - δ^{18}O relations for Europe in winter (Rozanski et al., 1982)

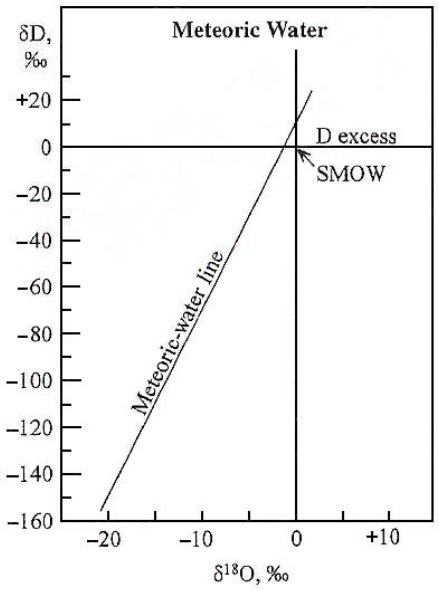

Figure 1.6: *The Global Meteoric Water Line. A best fit line for the isotopic compositions of all global precipitation when $\delta^{18}O$ is plotted against δD with equation $\delta\mathrm{D} = 8\times\delta^{18}\mathrm{O}+10$ (taken from Faure and Mensing (2005) based on data from Rozanski et al. (1993))*

$$\delta\mathrm{D} = (7.6 \pm 0.2)\,\delta^{18}\mathrm{O} + (6.5 \pm 2.1) \tag{1.6}$$

and for Europe in summer

$$\delta\mathrm{D} = (6.0 \pm 0.4)\,\delta^{18}\mathrm{O} - (6.3 \pm 2.8) \tag{1.7}$$

The large difference between the summer and global relationships reflecting the impacts of the seasonal cycle (section 1.2.2).

1.2.4 Deuterium Excess

The deuterium excess, (d-excess as used by Helsen et al. (2006)), is defined as

$$d = \delta\mathrm{D} - 8 \times \delta^{18}\mathrm{O} \tag{1.8}$$

and measures the deviation of a given data value from the Meteoric Water Line (Faure and Mensing, 2005). Values of d-excess vary depending on conditions such as temperature

and relative humidity at the source region of an air mass. d-excess values in vapour above the ocean surface increase when the sea surface temperature increases (+0.35 $^{\circ}/_{\circ\circ}$ per °C) and decrease with increasing relative humidity (-0.43 $^{\circ}/_{\circ\circ}$ per %) (Vimeux et al., 1999). There is evidence from simple models that the initial d-excess of an air parcel is to a certain extent preserved during movement towards polar regions (Vimeux et al., 1999). The imprint of the initial relative humidity on d-excess decreases with distance inland. Due to this decreasing signal of relative humidity and also the fact that model simulations show that relative humidity over ocean regions has varied little over time, the most useful relationship for climate studies is that between deuterium excess and sea surface temperature (Vimeux et al., 2001). The deuterium excess provides a possible way of identifying the source region and mixing of air masses. d-excess will be altered by vapour entering the air mass from re–evaporation over continents so this must also be considered (Araguás-Araguás et al., 2000). Values of d-excess lower than 10 $^{\circ}/_{\circ\circ}$ may indicate the presence of vapour from secondary evaporative processes.

Deuterium excess records can be less noisy than those of individual isotopes, making studying it potentially easier than investigating δ values. This feature of isotopic records is not entirely understood though it is possible that it is seen due to the fact that d-excess varies less between precipitation events (Vimeux et al., 2001).

1.2.5 δ^{18}O as a Climate Proxy

The isotopic ratio of rainwater reaching the ground is positively correlated with surface temperatures due to isotopic exchange of the raindrops with surrounding moisture as they fall. (It should be noted that snow and hail reflect cloud conditions, as sufficient isotope equilibration cannot occur during their descent (Rozanski et al., 1993).) This makes δ^{18}O a potentially useful quantitative climate proxy as the ratios can be preserved in ice layers (Barlow et al., 1993) as well as other palaeo–archives. For example the ratios can be preserved in layered rock formations such as stalagmites and stalactites through rainwater infiltrating into the ground above caves and undergoing fractionation with calcite that dissolves in the liquid. This calcite solution then enters the cave system, and the calcite,

now containing the atmospheric δ^{18}O signal due to the fractionation process, forms the next layer of deposit on the cave formations (Lauritzen and Lundberg, 1999). Hoffmann et al. (2000) showed that water isotopes are accurate proxies for temperature variations in high–latitudes. However, many other factors may also cause water isotope ratios to vary. These include: the condensation temperature; changing conditions in the source region; microphysical processes in clouds during snow formation; changes in magnitude of the ratio between advective and diffusive transport; changes in the strength of the inversion layer; and seasonality of precipitation (Helsen et al., 2006).

δ^{18}O of past precipitations may be preserved in ice sheets, groundwaters and fluid inclusions in speleothems, the latter being derived from cave dripwaters (Dennis et al., 2001). A value can also be obtained via transfer functions from skeletal remains of animals, lake sediments, and soil minerals that formed in equilibrium with surface or groundwaters (Fricke and O'Neil, 1999). Many often used climate proxies, such as ice sheets and oceanic sediments, do not have a large continental coverage. The relationship between δ^{18}O and temperature recorded in layered rock formations has the potential to reduce this spatial bias in climate reconstructions.

Like many other physical properties of the atmosphere, the isotopic composition of water vapour, and subsequently of precipitation, exhibits variability on different time scales. Studies into the long–term (decadal timescale) relationship between mean surface temperature fields and δ^{18}O in precipitation show that the positive correlation essentially vanishes when average annual temperatures at the site of precipitation rise above approximately 15°C (Jouzel et al., 1997). Rozanski et al. (1992) found that over the period 1960 to 1990, in mid– and high–latitude regions, isotopic composition in precipitation varied with surface air temperature with an average δ^{18}O–temperature coefficient of 0.6 $^{\circ}/_{\circ\circ}$ $^{\circ}$C^{-1}. This study also concluded that isotopic composition of precipitation over areas of high–altitude were more sensitive to long term temperature variations than those at low–altitudes (Rozanski et al., 1992).

One important question still to be answered is whether or not a relationship determined between δ^{18}O and temperature for the present will be valid when extended back

in time (Fricke and O'Neil, 1999; Hendricks et al., 2000). Jouzel (1999) suggested that the δ^{18}O–temperature relationship is only valid so long as factors such as the evaporative source of water vapour and the seasonality of precipitation remain constant. Jouzel et al. (2003) concluded that using the present day spatial relationship between isotopes and temperature in Greenland across time creates underestimates of climatic temperature changes of up to a factor of 2. Jouzel et al. (2003) also concluded that using the present day spatial relationship across time works better for some Antarctic sites. However, to use δ^{18}O records as a palaeothermometer to provide an estimate of past temperatures in current studies, it must be assumed that the present–day spatial isotope–temperature relationship has not altered over time. Evaporative origin of moist air masses passing a region may change due to large scale atmospheric circulation variations, as could the seasonality of precipitation. Variations of either would seriously affect the accuracy of the palaeothermometer. This problem can be reduced by calibrating the palaeothermometer with instrumental data and comparing results with independent, co–located palaeotemperature estimates such as exist for the Last Glacial Maximum in ice sheets (Jouzel et al., 1996).

Previous studies have shown that combinations of data sets from different proxy sources through multivariate regression yields better results than using a single proxy source (Schmutz et al., 2000). Schmutz et al. (2000) combined NAO index reconstructions created using the following proxies: tree ring data from Northern Fennoscandia and the Eastern United States; ice accumulation rates in Greenland; and tree ring data from Morocco and Finland with ice core data. The combined index was compared with an index series created using early instrumental and documental data and the study concluded that the skill of the combined index was comparable with or higher than the individual indices.

1.3 Approaches to Modelling Isotopes in Precipitation

Concentrations of HDO and $H_2{}^{18}O$ in precipitation vary both spatially and temporally due to isotopic fractionation whenever a phase change of water occurs, see section 1.1.3.

Many different types of models have been developed to understand the water isotope cycle. A selection of these models will be discussed in this section.

1.3.1 Rayleigh–Type Distillation Models

Rayleigh–type distillation models are the simplest models used to investigate the hydrological isotopic system. These models include the main physical controls on δD and δ^{18}O in global precipitation as defined by Dansgaard (1964) (section 1.2), but are simple enough for large scale atmospheric and efficient first–order sensitivity studies (Jouzel et al., 2000).

Initially simple multibox Rayleigh models of the mean west–east horizontal transport of atmospheric water vapour across Europe were used to investigate deuterium variations in the hydrological cycle over Europe (Rozanski et al., 1982). Only zonal transport was modelled because of information on atmospheric circulation that shows that meridional transport is nearly absent in winter and negligible in summer over the European continent. These simulated values were then compared with observations. In most cases fairly close agreement between predicted and actual values was achieved. The continental and seasonal effects were particularly well reproduced by Rozanski et al. (1982). This study also concluded that the isotopic composition of local precipitation is related to the whole travel history of precipitating air masses not just the simple relationship with local air temperature as initially suggested by Dansgaard (1964). They suggested that the remaining water vapour fraction, F, was the most important factor in describing the past history of an air parcel. The local surface temperature (through the saturation vapour pressure) together with the source region surface temperature, have an overall control on F.

Covey and Haagenson (1984) used a more advanced Rayleigh model that predicted the isotopic composition of snow when given the composition of source water and the trajectory of the air mass from water vapour source to sink (Covey and Haagenson, 1984). They stated that the ideal way of comparing the model results with observations of the isotopic composition of present–day precipitation would be through using three–dimensional back trajectories of the air parcel. They were thwarted in this by a lack of resolution of the back

trajectories and a lack of isotope data at a sufficient resolution to allow comparisons with single meteorological events. Results of their model depend strongly on:

- The degree to which non–equilibrium processes act during evaporation.
- The height to which saturated air is raised after its formation.
- The temperature at which precipitation is formed.

Simple Rayleigh–type models do not cope well with isotopes in convective systems where droplet size becomes important. Some idealised extensions of Rayleigh theory have been used to study individual convective clouds, though they are limited to being useful only for such applications (Gedzelman and Arnold, 1994).

However, Rayleigh theory models do *"reproduce the basic behaviour of δD and $\delta^{18}O$ in precipitation, at least in mid– and high–latitudes"* (Jouzel et al., 1997). The theoretical basis of Rayleigh theory is described in detail in Chapter 3.

1.3.2 Global Climate Models (GCMs)

GCMs have been used together with Rayleigh models in recent isotope studies. A GCM can be used to "tag" water evaporating from a well–defined region, and follow this parcel in a Eulerian coordinate system until it precipitates. This process provides information on the relative contributions of evaporative regions to precipitation in a certain location. GCMs allow more complex atmospheric processes to be considered when studying the movement of isotopes than can be taken into account when using a Rayleigh model though this can sometimes make interpretation of results more difficult. They are, however, particularly useful in verifying the assumption that the spatial isotope–temperature relationship is valid over time by modelling the seasonality and main atmospheric circulations in the past (Jouzel et al., 1996), and in providing initial isotopic ratio values for source regions for other isotope studies (Jouzel and Koster, 1996).

The global–scale modelling of deuterium and ^{18}O distribution has been carried out using GCMs of the atmosphere with the major patterns generally being well reproduced

(Rozanski et al., 1993). Joussaume et al. (1984) was the first study to use a GCM (the AGCM of the Laboratoire de Météorologie Dynamique) to model stable water isotopes. The observed global climate for January was well reproduced by the model. Jouzel et al. (1987) extended this approach into the NASA GISS (Goddard Institute for Space Studies) GCM and performed sensitivity studies on this model (Jouzel et al., 1991). Further studies extending the GISS GCM ModelE version isotope parameterisations into the stratosphere were conducted by Schmidt et al. (2005) and Schmidt et al. (2006). Water isotopes have also been included in the ECHAM GCM, with the latest version being documented by Hoffmann et al. (1998). Each of these models reproduce the main latitudinal and continental observed pattern of isotopic values but with some local discrepancies, and some magnitudinal inconsistencies. Generally there is an overestimation of δ values at the poles and a slight underestimation in the mid– and high–latitudes (Jouzel et al., 1997, 2000). More recently water isotopes have been added to the GENESIS GCM (Mathieu et al., 2002) with good results on large scales though still with some regional problems, the Melbourne University AGCM (Noone and Simmonds, 2002) that performs well when compared to GNIP monthly data, and to the National Center for Atmospheric Research Community Atmospheric Model version 2 (NCAR CAM2) (Lee et al., 2007).

Cole et al. (1999) modelled the relationship between interannual variability in climate and δ^{18}O of precipitation. They used the NASA–GISS model 2 which follows water isotopic and geographic source tracers throughout the model's water cycle and calculates fractionation through all phase transitions, except evaporation from land. No fractionation is assumed during evaporation from land surfaces and ocean isotopic composition is fixed. When forced by 12 years of sea surface temperature data, changes in precipitation amount and the relative contributions of local water vapour sources were identified as being the most important factors in determining isotopic composition changes (Cole et al., 1999). The authors observed that changes in vapour source regions over geologic timescales can create fluctuations as large as $\pm$ 10-15% in the total precipitation and therefore also alter the isotopic composition seen in nearly all grid cells (8° by 10° resolution).

Although GCMs take account of all aspects of the water cycle, results from GCMs in

climate mode cannot be compared to specific precipitation events. Due to the complexity of GCMs it is also difficult to isolate specific processes and their individual effect on isotopic ratios. The resolution of GCMs is still a limiting factor especially in describing crucial processes like cloud formation, and precipitation in polar regions. Besides which the coarse resolution of GCMs makes direct comparison with observations of a single precipitation event difficult, (though Hoffmann et al. (1998) and Noone and Simmonds (2002) performed such comparisons), which hampers full model validation (Helsen et al., 2006). Smaller scale models are therefore relied upon to provide knowledge about these specific processes and to model specific events.

Sturm et al. (2005) presented results of a regional circulation model (RCM) called REMO 5.0, forced with ECMWF and ECHAM boundary conditions. The model resolution used was a 0.5° grid. Model results were compared with yearly, monthly and event averages of observations. Major spatial patterns were again well produced, as was the seasonal cycle. The event based comparison was less conclusive.

1.3.3 Lagrangian Trajectory Models

More recently, back trajectory models have been combined with Rayleigh isotope type models to allow more detailed investigations of the individual forcing factors of variations in δ^{18}O and δD in precipitation. Studies to date using this approach have been limited to Greenland and Antarctica but have given positive indications as to the validity of the approach. Helsen et al. (2004) used 6 five–day back trajectories and the Mixed Cloud Isotope Model (MCIM) of Ciais and Jouzel (1994) to model an observed snowfall event that occurred in January 2002 at Dronning Maud Land, Antarctica. The trajectory model used was the Royal Netherlands Meteorological Institute trajectory model (TRAJKS) which does not take account of convective processes. The initial model results gave isotopic values that were too high. The initial isotopic composition of the parcel was then varied iteratively to reproduce the observed value and give an estimated source region for the water vapour beyond the 5–day trajectories. This study was developed further by Helsen et al. (2006) when the observed isotopic record from snow accumulated between

1998 and 2001 was modelled. In this second study instead of using the observed isotopic value to work backwards to the initial isotopic composition, the δ values at the start of each five–day back trajectory were taken from a 20–year run of the ECHAM4 GCM. Mixing in of water vapour from the surrounding atmosphere along the trajectories was also permitted. A threshold for fractionation to occur was included as a relative humidity value of 80%. This limited fractionation to occur only when a phase change was seen. Again convection was not included in the trajectory model and a single start time for the back trajectories was chosen for each event. There were difficulties in matching layers of snow with specific snowfall events. When this matching was possible (using a sonic height ranger to measure depths of snow deposited from each event) good correlations between modelled and observed values were seen. The approach is also capable of reproducing most of the observed spatial gradients of δ values and qualitatively describing the seasonal cycle (Helsen et al., 2007). Sodemann (2006) used a Lagrangian trajectory model and the MCIM to model seasonal δ values of precipitation over Greenland. In this case the isotopes were mainly used to test the validity of the trajectory model though modelled values tended to not be depleted enough when compared to observations. Sodemann (2006) hypothesised that this was due to insufficient tuning to Greenland conditions and initialising the isotopic composition with surface level δ values that would be less depleted than at the height of the actual trajectory starting position.

The Lagrangian trajectory approach, where trajectories are based on reanalysis fields, is utilised by this study. This is the first study to apply this method to the isotopic composition of mid–latitude precipitation. The back trajectory model used in this study is described in Chapter 2 and is called FLEXPART. Chapter 3 summarises isotope theory, in particular the theory utilised by the Mixed Cloud Isotope Model (MCIM) used in this work. A case study comparing model results to observed values from Norwich, Dublin and Birmingham is then presented in Chapter 4. Sensitivity testing of the model is presented in Chapter 5. Chapter 6 contains the results of a longer case study based in Lincolnshire and Somerset. Finally Chapter 7 summarises the conclusions of this study.

Chapter 2

FLEXPART: Model and Methodology

2.1 History of Back Trajectory Models

Trajectory models have been used to study atmospheric dynamics for several decades. As early as 1940, Petterssen introduced a graphical technique to construct isobaric trajectories manually from weather charts using the assumption that at any given time the wind vector at a point is tangential to the trajectory. Subsequent points in time and space could therefore be linked together to create a trajectory (Petterssen, 1956).

With the advent of computer modelling more complex methods of calculating trajectories have been developed and the reliability of results improved. Danielsen (1961) developed a method of constructing trajectories using not only wind fields but also semiconservative atmospheric properties such as potential temperature. This method was known as a dynamic technique. Versions where only wind vectors are used are termed kinematic. Dynamic techniques were used extensively, as they allowed the use of long intervals between wind fields. Accurate wind fields with high space and time resolution are now available so kinematic trajectories have become the more reliable. However, errors of 20% of the distance travelled are typical for single trajectories computed using analysed wind fields.

There are many different types of kinematic trajectories:-

- Isobaric trajectories follow pressure surfaces. The height in pressure coordinates of

the required pressure level must be determined at each timestep and then the wind at that height and time is used to advect the trajectory (Stohl, 1999).

- Isentropic trajectories follow lines of constant potential temperature.
- Iso–eta trajectories move along model surfaces that follow the terrain.
- Iso–sigma trajectories follow the model surfaces in sigma coordinates.
- Mixing layer trajectories are two dimensional trajectories that are advected by the horizontal wind averaged across a specified mixing layer height.
- Three–dimensional trajectories use all 3 wind components to trace the path through time.

Stohl and Seibert (1998) used the conservative properties, in the absence of diabatic processes, of potential vorticity, specific humidity and potential temperature to investigate the relative accuracies of isentropic, isobaric, iso–eta and three–dimensional trajectories. They concluded that three–dimensional trajectories are the most accurate, followed by kinematic isentropic trajectories, both in the troposphere and stratosphere. Isobaric and iso–eta trajectories came third, and finally dynamic isentropic trajectories, which tended to perform unrealistic ageostrophic oscillations after 24 to 48 hours (i.e. they began to rotate at increasing and soon implausible speeds). Stohl et al. (1995) conducted a similar study using conservative tracers and found that temporal interpolation is a significant error source for trajectory calculations. However, for travel times greater than 24 hours, three–dimensional trajectories calculated with 24 hourly wind fields were found to be more accurate than isentropic, isobaric and iso–eta trajectories with 3 hourly input. Three dimensional trajectories should therefore be used even if available windfield resolution for this trajectory type is poorer. Other sources of errors for trajectory modelling are truncation errors, interpolation errors, inaccurate knowledge of the starting position and inaccuracies in the input wind fields (Stohl and Seibert, 1998).

Another method for following transport in the planetary boundary layer (PBL) is that of vertically integrated transport vectors (VITV) which describe the mass mean transport

across the PBL. Haagenson et al. (1987, 1990) used tracer–derived trajectories to evaluate the relative accuracy of each trajectory type and found that VITV trajectories performed better than three–dimensional trajectories. However, this method does require an accurate estimate of boundary layer height, which is not always readily available. Stohl and Wotawa (1995) developed an iterative scheme to calculate this value along a preliminary trajectory as an input for an improved–guess final trajectory that improved the method greatly. VITV calculations still only produce a single trajectory.

The latest method to be used to calculate air parcel movements is that of Lagrangian Particle Dispersion Models (LPDM). Single trajectories are unable to accurately portray air parcel movements especially once turbulent mixing occurs. LPDMs improve on single trajectories by following the Lagrangian transport and diffusion of many so–called particles (tens or hundreds of thousands) through the atmosphere. The particles do not represent individual molecules but rather infinitesimally small air parcels (section 1.1.6). LPDMs can therefore represent transport in the PBL more realistically than traditional trajectory models, especially when turbulence is important (Stohl, 1998). LPDMs are also used to describe the dispersion of passive tracers in the turbulent PBL (Stohl and Thompson, 1999).

2.2 Evolution of FLEXPART and FLEXTRA

The LPDM used to provide information on the past movements of air particles in this study has evolved through contributions by many authors. It has been adjusted when problems were discovered or when newer process descriptions were included. The initial model was intended for use in the simulation of long–range air pollutant transfer from point, line, area or volume sources and was called FLEXTRA.

FLEXTRA is a kinematic trajectory model and is still used in studies today when single trajectories are required. FLEXTRA uses bicubic horizontal, quadratic vertical, and linear time interpolation to determine the three wind components at a trajectory position and employs the numerical method of Petterssen (1940) for the trajectory calculations (Forster et al., 2001). FLEXTRA is capable of producing three–dimensional trajecto-

ries, iso–eta trajectories (by setting the vertical wind to zero), mixing layer trajectories, isobaric trajectories, and isentropic trajectories. FLEXTRA also has the feature of calculating potential vorticity along the trajectory path, which can then be used as a measure of accuracy for upper level trajectories. FLEXTRA can also calculate an ensemble of trajectories by slightly varying the start location for each member of the ensemble. The deviation of the ensemble members from one another is then another method by which accuracy can be determined.

FLEXPART was developed using aspects of the trajectory model FLEXTRA such as input data handling when the use of LPDMs began and takes into account turbulent dispersion which FLEXTRA is not able to. Version 1 was developed during FLEXPART's primary author's (Andreas Stohl) military service, version 2 saw the addition of code to describe the deposition of pollutants. By version 3 performance optimizations were required and a density correction using Langevin equations was added. Version 4 included other updates, the most important being the inclusion of a convection scheme and cluster analysis (see sections 2.3.4 and 2.4.2 respectively). The backward calculation capabilities were improved, as were the input and output management routines in version 5. The current version 6.2 has a domain–filling option, the ability to output nests, and improvements to the convection system (Stohl et al., 2005a). The domain–filling option allows particles to be initiated on a larger scale to allow the study of atmospheric motions such as stratospheric ozone intrusions.

2.3 FLEXPART

The FLEXPART model is an open source LPDM the most recent version of which is described by Stohl et al. (2005a). Only functions specific to this study are described within this chapter. The FLEXPART code and user guide are freely available on the web through Stohl's website at "http://zardoz.nilu.no/∼andreas/flextra+flexpart.html". The model can release thousands of particles at many different heights, plot a trajectory for each through time using atmospheric wind fields created by numerical predication centres combined with subgrid–scale parameterisations, and then output either all trajectories, a cluster

analysis or a source/receptor probability footprint map for air parcels released from a specified location. Currently there are versions of FLEXPART that can be driven with meteorological analysis data from the following sources:-

- European Centre for Medium–range Weather Forecasting (ECMWF) 15 year re-analysis data (ERA-15) for the years 1979-1993 (Gibson et al., 1999)

- ECMWF 40 year reanalysis data (ERA-40) over the time period 1958-2001. These are available on a 1° x 1° latitude–longitude resolution with 60 hybrid model levels in the vertical (with approximately 14 levels below 1500 m and 23 below 5000 m (Stohl and James, 2004). Analysis fields are available every six hours (0000, 0600, 1200 and 1800 UTC) and are supplemented by forecast fields (0300, 0900, 1500, 2100 UTC) where UTC stands for Coordinated Universal Time.

- the Aviation (AVN) model of the National Center of Environmental Prediction (NCEP). Available on 26 vertical levels from 1000 hPa and 10 hPa.

- the Global Forecasting System (GFS) of NCEP. These are now available at a 0.5° x 0.5° latitude–longitude resolution with 26 pressure levels between 1000 hPa and 10 hPa in the vertical. Analysis fields are available every six hours (0000, 0600, 1200 and 1800 UTC) with forecast fields (0300, 0900, 1500, 2100 UTC).

The ECMWF data was available at higher resolutions than the other analysis data until 2003 when the GFS analysis model was improved. This thesis will use the ECMWF ERA-40 analysis data as most previous studies that have used FLEXPART, including many validation tests, have used this input data. The other advantage of using ECMWF input data is that some of the capabilities of the later versions of FLEXPART are not transferred as quickly e.g. the convection scheme added to the 2001 version of FLEXPART was not a part of the AVN version as late as 2004 (Forster et al., 2004).

FLEXPART was designed to be run both forwards and backwards through time in order to predict the dispersion of pollutant from a known source or to trace a measured pollutant back to a probable source. It therefore has many inbuilt features such as wet

and dry deposition simulation, and radioactive decay of certain tracer species, that will not be used in this study. The flexibility of the model has enabled it to be used as a tool to investigate many aspects of the atmosphere. For example, Cooper et al. (2005) traced the path of mid–latitude stratospheric ozone into the lower troposphere and marine boundary layer, and Stohl (2006) used FLEXPART to investigate sources of pollution measured in the Arctic. FLEXPART can also be used in forward mode with ECMWF forecasts to predict the movement of air parcels into the future. This forecasting capability has been used to plan the flight paths of scientific aeroplane mounted chemical sampling expeditions with favourable results (Stohl et al., 2003, 2004a; Lawrence et al., 2003; Forster et al., 2004). FLEXPART has also been used in longer term analyses to calculate average transports over extended time periods, (e.g. 15 years of Asian carbon monoxide transport (Forster et al., 2004) and 5.5 years continuous simulation to find the transport routes and sources of Arctic pollution (Stohl, 2006)). In the Stohl (2006) study, FLEXPART used a polar stereographic projection to maintain accuracy around the North Pole that has since been added to the generally available code. The flexibility of FLEXPART is part of what makes it such a useful model.

Perhaps most importantly for this thesis, FLEXPART has previously been used to model the transport of water vapour through the atmosphere. Stohl and James (2004) used FLEXPART to connect regions of net evaporation with regions of net precipitation by trajectories, which could then be used to examine the relationship between the two regions. Berto et al. (2004) used FLEXTRA to identify water sources of precipitation events over the Trentino region of Italy.

2.3.1 FLEXPART Model Evaluation

No matter how varied its potential uses, no model would be useful if it could not be proved to produce reliable results. FLEXTRA has been validated with constant level balloon flight data (Stohl and Koffi, 1998), manned gas balloon flight observations (Baumann and Stohl, 1997) and meteorological tracers as in section 2.1 (Stohl and Seibert, 1998). Stohl et al. (2001) conducted an intercomparison between FLEXTRA and two other tra-

jectory models (LAGRANTO and TRAJKS) concluding that the the output from all three models was very similar if the same linear spatial interpolation scheme was used. The FLEXPART model has been, and continues to be, investigated thoroughly through comparisons of modelled tracer dispersions with measured observations following controlled releases of a tracer (Stohl et al., 1998). FLEXPART was also tested during intercontinental air pollution transport studies, over northern Canada and the Atlantic (Spichtinger et al., 2001; Forster et al., 2001), from North America to the Azores (Stohl and Trickl, 1999) and central Europe (Trickl et al., 2003), from the North Atlantic to the west coast of Ireland (Stohl et al., 2002), and while traversing the Indian Ocean on the way to Australia (Wenig et al., 2003). The modelled results on most occasions for each of these case studies closely matched the observed data.

Stohl and James (2004) validated their FLEXPART results of the movements of water vapour through the atmosphere by comparisons with a traditional Eulerian method (assuming that globally, evaporation equals precipitation), ECMWF forecasts and precipitation fields from the Global Precipitation Climatology Project (GPCP). For an extreme precipitation event case study moisture fluxes from FLEXPART agreed well with results from the Eulerian method, and both closely matched the forecasted and observed fields (Stohl and James, 2004).

An especially useful validation was conducted by Damoah et al. (2004). Boreal forest fires in southeast Russia created smoke plumes that after 17 days extended across most of the Northern Hemisphere and were visible in satellite images and lidar measurements from eastern Asia, North America and Europe. As well as comparing FLEXPART output with the observations, this study also compared FLEXPART runs using ECMWF ERA-40 and the GFS NCEP reanalysis data as shown in Figure 2.1. Differences were seen between the simulations using the different input data sets in small scale features, though some of the fine–scale structure was reproduced well. However, both simulations agreed well with each other and with observations on larger scales. The study was inconclusive as to which data set, if either, gave the better results. More observational data would be required to test this further.

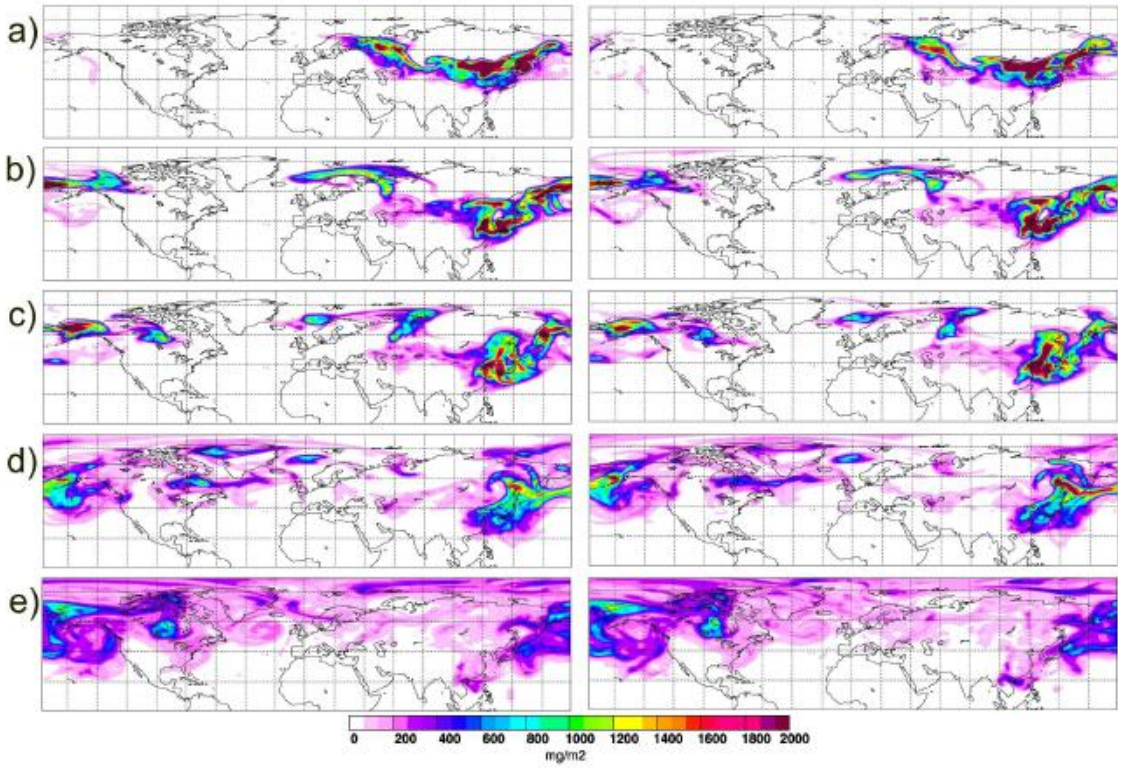

Figure 2.1: *Comparison of total column carbon monoxide tracer in* $mg\ m^{-2}$ *from FLEXPART simulations using ECMWF data (left column) and GFS NCEP data (right column) on (a) 18 May 2003 at 00 UTC, (b) 21 May at 00 UTC, (c) 22 May at 06 UTC, (d) 26 May at 06 UTC, and (e) 31 May at 06 UTC (taken from Damoah et al. (2004)*

Another useful validation was conducted by Meloen et al. (2003) and Cristofanelli et al. (2003). These studies compared how nine different models and methods reproduced a stratosphere–troposphere exchange event that occurred from 26th May 00 UTC until the 7th June 00 UTC 1996. The observational data consisted of measurements of surface ozone, beryllium-7, and beryllium-10 concentrations and meteorological parameters collected at four European high mountain stations, as well as atmospheric profiles from ozone soundings and high–resolution lidar. FLEXPART was compared with three trajectory models (LAGRANTO, TRAJKS and FLEXTRA), a Lagrangian chemistry transport model (STOCHEM), a Eulerian transport model (TM3), two GCMs (ECHAM4 and MA-ECHAM4) and a trajectory method. All models and methods were forced with ECMWF input data and were initialised as similarly as possible. The conclusions of the studies were that all the models produced the same temporal evolution and geographical pattern of the event, which matched the general behaviour of the observed data. Variations in the modelled event occurred more in the amplitude of the features shown. Similar stratospheric intrusion observation data from 20-21 June 2001 was compared with FLEXPART output by Zanis et al. (2003). This second study also observed that FLEXPART produced similar fields to those observed. Therefore, as this study uses FLEXPART purely in a spatial context, it can be used with some confidence.

In forecasting mode, FLEXPART's predictions have been compared with infrared satellite observations and insitu measurements after the fact (Forster et al., 2004), and with the output of other forecasting models (Lawrence et al., 2003). All such comparisons have shown that FLEXPART does reproduce most of the features and those missed could be as much due to inaccuracies in the ECMWF forecast fields as in the FLEXPART code used.

Calculating an ensemble of trajectories by varying the start position slightly and accounting for random interpolation is suggested as a way of assessing trajectory uncertainties. If all trajectories produced follow a similar path then the trajectory error is assumed to be small. If large deviations occur, such as those due to complex meteorological conditions, then uncertainties are larger (Baumann and Stohl, 1997). FLEXPART 6.2

automatically varies both horizontal and vertical positions within the initial release grid box dimensions specified to create these ensemble trajectories. However, even with this measure of uncertainty the interpolation schemes and spatial resolution of the wind fields can introduce errors into each individual trajectory in the order of 1000 km after 5 days backward calculation (Stohl et al., 1995). This can be further increased due to convective systems and the parcel losing its identity if it comes into contact with the Earth's surface. These errors are difficult to quantify, so care must be taken when using the trajectories. However if sufficient trajectories are used together in analyses, the errors can be greatly reduced (Stohl et al., 2002). Clustering trajectories further reduces the positional errors (section 2.4.2). Unfortunately clustering removes the continuity of trajectories so cannot be used in this study.

2.3.2 Turbulence in FLEXPART

FLEXPART stochastically parameterises three–dimensional turbulence in the PBL and free troposphere, which are not resolved by the input meteorological data fields, by solving Langevin equations assuming a Markov process (or stochastic differential equations) for the three wind components with an added density correction term (Stohl and Thompson, 1999). The density correction term takes into account the fact that in deep PBLs the density at the top of the layer may be more then 20% less than at the surface. Neglecting this can lead to errors in predicted concentrations on the order of 10% (Stohl and Thompson, 1999). In the PBL, the magnitude and the Lagrangian decorrelation times of the turbulent wind components are obtained using a parameterisation by Hanna (1982) and assuming that turbulence is always Gaussian in this region. Boundary layer heights are found using a combined Richardson number and lifting parcel technique developed by Vogelezang and Holtslag (1996). Above the PBL, the turbulent components are set to small values dependent on the wind shear. The main assumption made by this part of the model is that if particles are well mixed in the flow then they should remain so (Stohl and Thompson, 1999). If a particle reaches the top of the PBL or the surface then it is reflected back into the boundary layer and the sign of its turbulent velocity is reversed.

If a particle reaches the top level of the model it is set back to a position just below the highest level for the next timestep. Finally if there is a lateral domain set on the model and a particle reaches this point then the computation of that trajectory is stopped (Stohl et al., 2005b).

It should be considered that the turbulence parameterisations are only as good as the wind fields from which they are calculated. Stohl et al. (2004b) demonstrated that analysis wind fields can introduce artificial mixing into calculations. This problem occurs as subsequent timesteps are dynamically inconsistent with each other due to a lack of dynamical constraints between them. This is caused during the nudging of forecasts towards observations to create the analyses. Forecast–only fields performed better at conserving meteorological tracers (i.e. potential vorticity) along trajectories than analysed fields. However, the authors did not conclude that analysis fields should no longer be used, on the contrary, they still argued that analysis fields are the best option at this time as forecast fields lose accuracy with time into the future. They instead cautioned that users of analysis fields should be aware of this impact when forming conclusions.

It has been noted that this parameterisation of turbulence does not truly reflect what is occurring in the atmosphere. In the model, free tropospheric turbulence is simulated continuously whereas in the real atmosphere there are extended periods with no turbulence punctuated by short bursts of strong turbulence. There have been investigations into adding a clear air turbulence (CAT) scheme to FLEXPART, such as those used by air–traffic safety, which would theoretically improve the handling of turbulence. However, these investigations have yet to yield a scheme that functions satisfactorily with currently available meteorological data. Validation of any scheme would also be difficult due to a lack of observational data (Trickl et al., 2003).

2.3.3 Mesoscale Velocity Fluctuations

Gupta et al. (1997) drew attention to a spectral gap between parameterised turbulence in trajectory models and the turbulent processes accounted for in the meteorological input data fields. ECMWF grid boxes at a 1° x 1° resolution are on a scale of about 120 km.

Turbulence is usually parameterised to scale with boundary layer height, at approximately 1 km. This gap in the scales accounted for can cause the particle movement rate to be underestimated. To deal with this, FLEXPART solves another Langevin equation using mesoscale wind fields obtained by assuming that the variation of winds on the ECMWF grid scale must be of a similar magnitude to the variation within a grid box. Mesoscale velocity fluctuations are not so important in the PBL as they constitute a much smaller process than both mixing caused by vertical shear of the horizontal fields and vertical turbulent motions. However, mesoscale turbulence is important for long–range transport in the free troposphere and must therefore be included (Stohl et al., 2005b).

2.3.4 Convection and Vertical Motions in FLEXPART

Convection in trajectory models has been problematic to deal with. The meteorological input data already contains the effects of large–scale convection but it does not resolve subgrid–scale convection such as individual deep convective cells i.e. thunderstorms (Beirle et al., 2006).

In 2002 the convection scheme presented by Emanuel (1991) and developed in a joint paper by Emanuel and Živković-Rothman (1999) was included in FLEXPART version 4.0 to account for subgrid–scale convection (Seibert et al., 2002; Seibert and Frank, 2004). This scheme greatly improved the ability of FLEXPART to take account of convection, and especially moist convection, at every time when a subsequent ECMWF windfield is input, (i.e. every 3 or 6 hours). However, it also increased computation time especially as particle numbers were increased. Therefore in FLEXPART version 6.0 the convection scheme was again rewritten. The underlying scheme is still that of Emanuel and Živković-Rothman (1999) based on the buoyancy sorting principle of Raymond and Blyth (1986), but the redistribution of particles is now totally stochastic (Stohl et al., 2004a). This change has decreased processing time, so allows the convection scheme to be called at each stage of FLEXPART's calculations and therefore increases its accuracy. The time points are usually every 15 or 30 minutes, interpolated across the 3 or 6 hour ECMWF reanalysis data. The scheme relies on the grid–scale temperature and humidity fields from

the ECMWF reanalysis data.

Convection in a grid cell is triggered whenever the virtual temperature of a parcel is greater than the temperature of the level above the parcel's lifting condensation level by more than 0.9 K (the lifting condensation level is the level in the atmosphere at which condensation would occur within an air parcel if it were lifted to that height adiabatically, i.e. without heat input or output from the parcel). The scheme then accounts for upward and downward saturated mass fluxes within the clouds and unsaturated precipitating downward movement outside of the clouds using entrainment and detrainment motions. A vertical displacement matrix is then produced which contains the mass fractions that are displaced through convective motion. Each mass fraction M $A^{i,j}$ displaced from level i to level j is calculated using

$$MA^{i,j} = \frac{M^i \left(|\sigma^{i,j+1} - \sigma^{i,j}| + |\sigma^{i,j} - \sigma^{i,j-1}|\right)}{(1 - \sigma^{i,j}) \sum_{j=LCL}^{LNB} \left[|\sigma^{i,j+1} - \sigma^{i,j}| + |\sigma^{i,j} - \sigma^{i,j-1}|\right]} \tag{2.1}$$

where M^i is the mass fraction displaced from the surface to level i. LCL is the lifting condensation level and LNB is the level of neutral bouyancy of a surface air parcel. $\sigma^{i,j}$ varies between [0,1] and is the mixing fraction between two layers i and j. $\sigma^{i,j}$ is determined by

$$\sigma^{i,j} = \frac{\theta^j - \theta^{i,j}_{lp}}{\theta^{i,j}_{l} - \theta^{i,j}_{lp}} \tag{2.2}$$

where θ^j is the environmental potential temperature, $\theta^{i,j}_l$ is the liquid potential temperature of air displaced adiabatically from i to j, and $\theta^{i,j}_{lp}$ is the liquid potential temperature of air displaced adiabatically first to i and then to j (Stohl et al., 2005a).

The particles in a grid column are then redistributed according to this probability matrix among the input model level layers. Note that when backward modelling is occurring the transposed matrix has to be used (Seibert et al., 2002). Whether a specific particle is moved or not is decided by calling a random number between 0 and 1. This number also determines where in its new layer a particle will be placed. Finally, mass conservation is used to calculate the compensating subsidence required in the atmosphere that is then converted to a vertical velocity that is allowed to act upon all the particles in the grid box even those that were not affected by convective drafts (Stohl et al., 2005a,b).

Due to the stochastic nature of the parameterisation, and the general unpredictability of small–scale convective systems, it is unlikely that convection is always modelled to occur in exactly the right place and time (Trickl et al., 2003). However, the positive validations of FLEXPART through comparisons with observed data suggest that the parameterisations perform more than adequately. The convection scheme can easily be switched on or off as individual studies require. James et al. (2003) showed that turning the scheme off has very little impact in the extratropics but it has a significant influence on transport in the tropics.

2.4 FLEXPART Output

2.4.1 Tracer Concentrations

FLEXPART was designed to help investigate the movement of pollution through the atmosphere. It can follow chemicals and non–reactive tracers from known sources to potential areas of deposition or it can be used to locate potential source regions for known pollution events. Part of the advantage of FLEXPART over traditional trajectory models (though not used in this study) is its ability to produce maps of potential source or sink areas rather than a single point value. One of the ways in which FLEXPART achieves this is through tracer concentration output. Particles are initiated in FLEXPART with a certain mass. Each trajectory therefore has a certain mass at each location and time. FLEXPART determines the tracer concentration in each grid cell of the three–dimensional output grid by summing up the mass fractions of all the particles located in the cell and dividing this value by the cell volume. This process is made more efficient through the use of a uniform kernel method where the mass of a particle is divided between the nearest grid cells that fall within a grid box resolution from the central location of the particle as described by Stohl et al. (1998), who found that it performed similarly on average to other methods of calculating tracer concentrations. To avoid artificial smoothing of the results, the kernel method is not used until 3 hours after the particles are released (Forster et al., 2004).

2.4.2 Clusters and Cluster Analysis

FLEXPART also has the ability to condense the trajectory output using cluster analysis. This facet of the model was introduced to encourage the use of the more accurate LPDMs rather than models that produce single trajectories that remain popular due to the simplicity of the output (Stohl et al., 2002). FLEXPART can now use the iterative approach described below at every output time to cluster the positions of all the particles belonging to each release point. Each timestep is clustered independently with no direct link to the trajectory as a whole, so unfortunately no cluster trajectories can be drawn. The clustered output is similar to traditional trajectories with added uncertainty bounds and inclusion of turbulence and convection. First the central position of all particles, then the latitude and longitude of the centre of each cluster is given, as well as the fraction of the total particles that is included in the cluster, and the root mean square distance of cluster member particles from the central location (Stohl et al., 2005b).

Cluster analysis is a multivariate statistical technique. In FLEXPART it is used to split the particles released into groups or clusters with similar trajectories. It then outputs the mean path of each cluster. This is especially useful in atmospheric studies where strongly divergent air patterns could cause the mean of all particle movement to lie in a completely different direction to the paths actually taken by the air parcels, (see figure 2.2). It should also be noted that a real air parcel of finite size could potentially be torn apart by strongly divergent air movements (Stohl, 1998).

Cluster analysis can be conducted in many varying ways but the method FLEXPART uses follows the steps outlined below:-

- At each timestep a user specified number of random seed locations are created which are representative of the spread of the particles.
- Each of the real particles is then assigned to the seed location position to which it is closest creating clusters of particles around each seed.
- The mean position of the particles in each cluster is then calculated and this value becomes the seed location of the cluster.

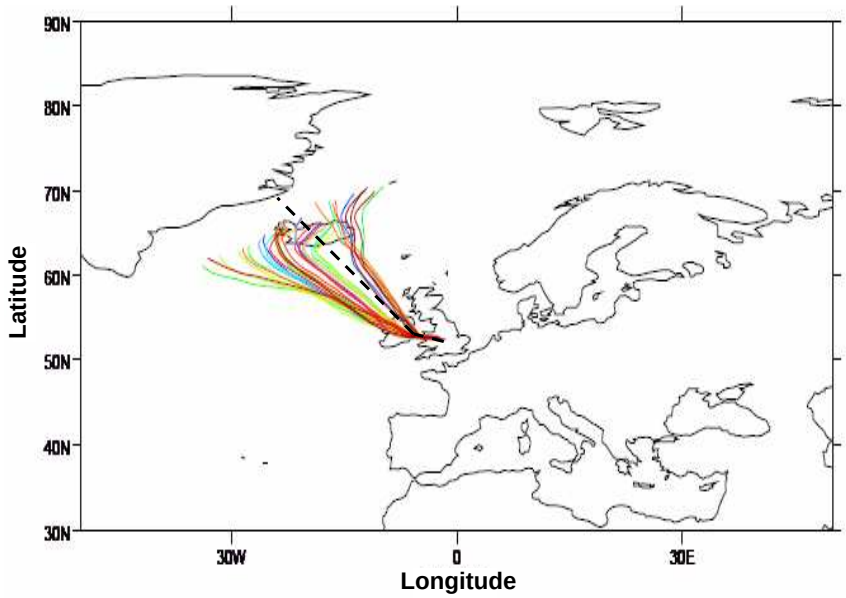

Figure 2.2: *An example of a divergent particle situation from FLEXPART in which a possible mean of the trajectories (black dashed line) does not follow any of the potential particle trajectories (coloured lines).*

- Due to the calculation of a new mean some particles may now be in the wrong cluster, i.e. their location is closer to another clusters' mean. Each particle is therefore checked to ensure it is in the correct cluster and then mean locations for each cluster are recalculated.

- FLEXPART then loops through this calculation and reassignment part of the analysis until the total Root Mean Square distance of all the particles from their respective cluster average position decreases only slightly between two loops. These cluster positions at successive timesteps then comprise the cluster trajectories output by the model.

As the trajectories and therefore clusters have been constructed using wind fields, each one can be clearly associated with a synoptic pattern, or evolution of a synoptic pattern over the period investigated (Dorling et al., 1992).

2.5 Model Setup

This chapter has introduced the main features of FLEXPART and back trajectory models in general. This study uses FLEXPART to trace particles back in time from a known rainday in order to gain temperature, pressure and humidity data about the path taken by each particle. As mentioned previously (section 2.3), the input to FLEXPART used in this study is ECMWF ERA-40 reanalysis fields at 0000, 0600, 1200 and 1800 hours UTC. Specifically temperature, pressure, humidity and all three wind components are required. Due to the Lagrangian nature of FLEXPART it does not run on any grid, instead a continuous positional output is possible though this is dependent on interpolation between the 1° x 1° horizontal resolution of the ECMWF data.

For this study neither the cluster output nor the footprint output options are useful as later stages of modelling require continuous trajectories that these methods do not provide. Instead, at every output step throughout the model run the particle positions are output and then trajectories for each particle can be reconstructed from this position data.

A parameterisation to take account of subgrid scale terrain effects is also used. The tracer used for this study is purely an air tracer. Smaller scale processes within the tracked air parcels that are related directly to water will be modelled later by the Mixed Cloud Isotope Model (MCIM) described in Chapter 3. FLEXPART is purely used to gain multiple trajectories with temperature and specific humidity data at each timestep along each trajectory. The release of the tracer occurs over the first 3 hours of the simulation. This staggered release means that the first time that all particles can be looked at together is 3 hours previous to the initialisation time. Subsequently at the first output time point some particles will already have travelled away from the release site potentially introducing an error into the results. This error is, however, likely to be minimal when compared to errors caused by interpolating between the ECMWF ERA-40 wind fields and uncertainties within the trajectories themselves.

Other internal settings of the model were investigated for sensitivity for this studies' use of FLEXPART. Details of these tests and the final parameters chosen are discussed in Chapter 5. The next chapter introduces the theory behind isotope modelling and in

particular the theory used in the second model utilised for this study, the MCIM.

Chapter 3

Isotope Fractionation Theory and the Mixed Cloud Isotope Model

The Mixed Cloud Isotope Model (MCIM) is the second model used in this investigation. It uses the locational data and atmospheric parameters provided by FLEXPART to calculate an isotopic ratio for precipitation falling from the tracked parcels. Since the isotopic composition of precipitation was first modelled, many different methods have been used. This chapter gives a summary of leading isotope theory and then introduces the specific theory used in the MCIM. Tables 3.3 and 3.4 at the end of this chapter are a summary of the terms described.

3.1 Isotope Nomenclature

Throughout this chapter δ^{18}O will be used to express the ratio of oxygen-18 (^{18}O) to oxygen-16 (^{16}O) isotopes relative to Vienna Standard Mean Ocean Water (VSMOW) as explained in section 1.1.3, where,

$$\delta^{18}O = \left[\frac{(^{18}O/^{16}O)_{sample} - (^{18}O/^{16}O)_{VSMOW}}{(^{18}O/^{16}O)_{VSMOW}} \right] \times 1000 \tag{3.1}$$

which can be simplified to,

$$\delta^{18}O = \left[\frac{(^{18}O/^{16}O)_{sample}}{(^{18}O/^{16}O)_{VSMOW}} - 1 \right] \times 1000 \tag{3.2}$$

where ^{18}O is the concentration of oxygen-18 and ^{16}O is the concentration of oxygen-16 in either the sample being measured or the standard VSMOW. A similar expression can be used to describe δD, the ratio of deuterium to hydrogen. These δ values are always expressed in permil ($^{\circ}/_{\circ\circ}$) or parts per thousand.

3.2 Rayleigh Distillation Theory

As mentioned in section 1.2.1, the Global Network of Isotopes in Precipitation (GNIP) project was set up in 1961. The initial purpose of the central database of isotopes in precipitation was to track excess tritium released from the testing of nuclear weapons, which began in 1952 and peaked in 1963. It soon became apparent that this database would also be extremely useful in hydrological, oceanographical, meteorological and climatological studies (Schotterer et al., 1996). Dansgaard (1964) conducted the first analysis of this global dataset after sufficient data had been collected. His conclusions still form the basis of stable isotope fractionation theory today, even though at the time he did not put forward a complete physical explanation of the processes.

Observations of the isotopic composition of sea water, (δ_w), water vapour, (δ_v), and precipitation, (δ_p), showed that precipitation was usually more depleted in heavy isotopes than seawater but less depleted than atmospheric water vapour,

$$\delta_w > \delta_v < \delta_p \tag{3.3}$$

This pattern can be explained by isotopic fractionation, which was briefly introduced in section 1.1.2. The specific nature of fractionation for water molecules is explored next.

3.2.1 Equilibrium Fractionation

One–phase Rayleigh Model

If a phase change occurs slowly enough, then the vapour phase will be saturated with respect to the liquid phase (100% relative humidity) and an equilibrium is obtained. The factor by which the isotopic composition of one phase is different from that of another phase is determined by the ratio of the saturation vapour pressure (e_s) of the lighter isotope ($e_{s\ light}$), to that of the heavier isotope ($e_{s\ heavy}$) (Dansgaard, 1964). This factor is termed the equilibrium fractionation factor, α_{eq},

$$\alpha_{eq} = \frac{e_{s\ light}}{e_{s\ heavy}} \tag{3.4}$$

These saturation vapour pressures are theoretical values with $e_{s\ light}$ being the saturation vapour pressure of a pure sample of the light isotope e.g. all oxygen present in both liquid and vapour is ^{16}O. Similarly $e_{s\ heavy}$ is the saturation vapour pressure of a pure sample of the heavier isotope e.g. all oxygen present in both liquid and vapour is ^{18}O. The saturation vapour pressures are dependent on temperature as described by the Claussius–Clapeyron equation,

$$\frac{de_s}{dT} = \frac{Le_s}{R_w T^2} \tag{3.5}$$

in differential form. Equation 3.5 can be solved to become,

$$e_s = e_{s_0} \exp\left[\frac{L}{R_w}\left(\frac{1}{T_0} - \frac{1}{T}\right)\right] \tag{3.6}$$

where e_s is the saturation vapour pressure and e_{s_0} is the saturation vapour pressure at some reference temperature T_0. L is the latent heat of evaporation and is equal to 2.50 x 10^6 J kg^{-1} for normal water that contains a mix of the different isotopes. Values of e_s calculated using the Claussius–Clapeyron equation can be seen in figure 3.1. The value of L will change for water containing 100% of one isotope. R_w is the specific gas constant for water vapour and also varies depending on which isotope is being considered due to,

$$R_w = \frac{R^*}{M_w} \tag{3.7}$$

where R^* is the Universal gas constant equal to 8.314 J mol^{-1} K^{-1}. M_w is the molecular mass of the water molecules being considered, so for $H_2^{16}O$, M_w = 0.018, and for $H_2^{18}O$, M_w = 0.020. The mass dependent variables in equation 3.6 (i.e. L, R_w, and e_{s_0}) ensure that the saturation vapour pressure of the heavy isotope is always less than that of the lighter isotope ($e_{s\ heavy} < e_{s\ light}$) making the fractionation factor (α_{eq}) greater than 1.

As the fractionation factor, α_{eq} is a measure of the difference in isotopic composition between the two phases, it can also be expressed as,

$$\alpha_{eq} = \frac{r_A}{r_B} \tag{3.8}$$

where r_A and r_B are the ratio of the heavy to light isotope, e.g. $^{18}O/^{16}O$, in the two phases A and B (Faure, 1977).

The magnitude of the isotopic difference, and so the fractionation factor, between each phase, depends on the temperature and rate at which the phase change occurs (Dansgaard, 1964). This can also be seen from the Claussius–Clapeyron equation (equation 3.6) as all factors other than temperature are mass dependent and therefore constant when considering an isotope pair at a time. It should be noted that as fractionation is dependent on mass, fractionation affects HDO 8-10 times more than $H_2^{18}O$ (Jouzel et al., 1997). This is because a deuterium (D) atom has twice the mass of a hydrogen (H) atom, but an ^{18}O atom has only 18/16 the mass of an ^{16}O atom.

Fractionation factors, α, are dimensionless values and for water molecules they are very close to 1. They are therefore sometimes expressed as ε, an enrichment factor, in $^{\circ}/_{\circ\circ}$.

$$\varepsilon\,(^{\circ}/_{\circ\circ}) = [\alpha - 1] \times 1000 \tag{3.9}$$

This allows the change in δ value induced by the fractionation factor, α, to be seen more clearly. So, for example, a value of α = 1.009 would be equivalent to ε = 9 $^{\circ}/_{\circ\circ}$. Therefore ε also shows the effect of the fractionation factor in $^{\circ}/_{\circ\circ}$ on the δ value after a phase change.

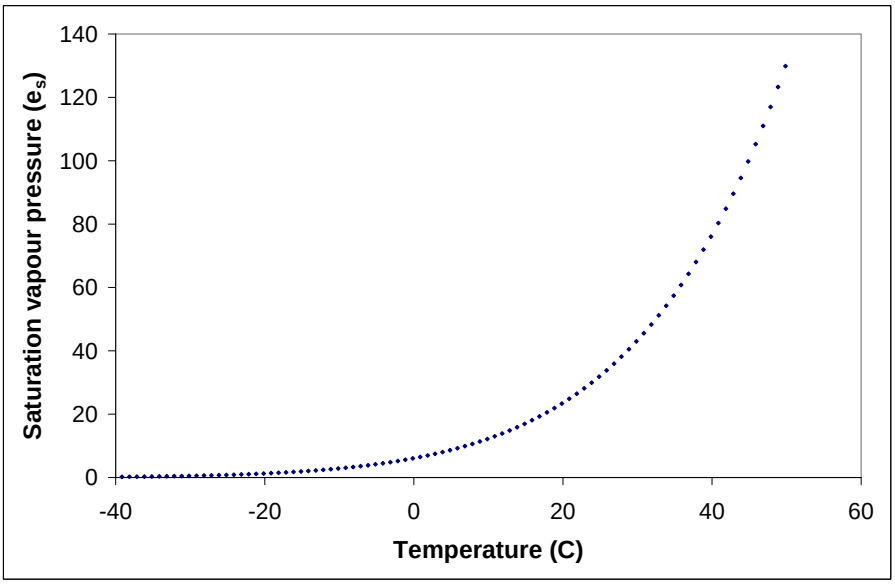

Figure 3.1: *Saturation vapour pressures (e_s) calculated using the Claussius–Clapeyron equation. Note that though the temperature in the graph is given in °C, the equation requires the temperature in Kelvin.*

As the fractionation factor is a measure of the isotopic difference between two phases, if the isotopic composition of one phase is known then the isotopic composition of the other can be found using,

$$a_v = \frac{e_{s\ heavy}}{e_{s\ light}} a_w = \frac{a_w}{\alpha_{eq}} \tag{3.10}$$

where a denotes the absolute isotope content of the heavy isotope and the subscripts v and w are vapour and water phases respectively (Dansgaard, 1964). The absolute isotopic content is a mass mixing ratio in kg kg^{-1} equal to,

$$a_v = \frac{^{18}O_v}{^{16}O_v + {}^{18}O_v} \approx \frac{^{18}O_v}{^{16}O_v} \tag{3.11}$$

where $^{18}O_v$ is the concentration of oxygen-18 and $^{16}O_v$ is the concentration of oxygen-16, in the vapour. As $^{18}O_v$ is very much less than $^{16}O_v$ it can be neglected in the denominator of equation 3.11 to simplify the expression as shown. a can therefore be taken as the ratio of heavy to light isotopic components within a single phase.

Equation 3.10 can then be converted into the more useful δ notation, assuming that the water is VSMOW, by using equation 3.1,

$$\delta_v\,(^\circ\!/_{\circ\circ}) = \frac{a_v - a_w}{a_w} = \frac{\frac{a_w}{\alpha_{eq}} - a_w}{a_w} = \left[\frac{1}{\alpha_{eq}} - 1\right] \times 1000 \tag{3.12}$$

This equation can then be used to calculate the isotopic composition of vapour evaporating from sea water with an isotopic composition equal to the VSMOW standard, δ = 0 (see section 1.1.3), as long as the temperature and so the fractionation factor is known. For example, at a temperature of 20°C, the equilibrium fractionation factors for deuterium and ^{18}O are 1.08 and 1.009 respectively. This means that under equilibrium conditions, vapour that has evaporated from sea water will have δD = -80 $^\circ\!/_{\circ\circ}$ and δ^{18}O = -9 $^\circ\!/_{\circ\circ}$ (Dansgaard, 1964). For ice and water Craig and Gordon (1965) suggested that the δ^{18}O of ice would be 2 $^\circ\!/_{\circ\circ}$ heavier than liquid water if they were in equilibrium with each other, this different phase change requiring a different fractionation factor due to the new saturation vapour pressures involved.

Equation 3.10 can also be rearranged in order to calculate the absolute isotopic composition of liquid precipitation when it condenses from vapour,

$$a_p = \frac{e_{s\ light}}{e_{s\ heavy}} a_v = \alpha_{eq}\, a_v \tag{3.13}$$

which can again be converted to the more useful δ notation by using equation 3.1 and becoming,

$$\delta_p\,(^\circ\!/_{\circ\circ}) = [\alpha_{eq} - 1] \times 1000 \tag{3.14}$$

in δ notation (Dansgaard, 1964). Unfortunately this expression is only valid for the first condensation event from an air parcel whose water vapour has evaporated in equilibrium from water with an isotopic composition equal to VSMOW. This limits its application to real world situations. Dansgaard (1964) therefore further developed these expressions into Rayleigh distillation/fractionation theory. *"A Rayleigh distillation model computes the isotopic content of an idealised, isolated air parcel travelling from an oceanic source towards a region where condensation and finally precipitation takes place."* (Dansgaard,

1964). Condensate forms when the air is saturated (in equilibrium with the surrounding vapour), at the temperature of the cloud base, and is removed immediately from the parcel. This means that the water vapour in the air parcel will alter its isotopic composition every time condensation occurs, becoming more and more depleted in heavy isotopes. Condensation and precipitation from the parcel will also become progressively more depleted, though enriched compared to the vapour, as Rayleigh theory does not allow for any evaporation into the air parcel after the initial evaporation. Therefore the isotopic content of precipitation at any point is a function of the initial δD and δ^{18}O values, determined by the assumed temperature–dependent fractionation factors, and the fraction of the initial water vapour remaining in the parcel, (f = amount of water vapour at current time ÷ initial amount of water vapour),

$$\delta_p\ (^{\circ}/_{\circ\circ}) = \left[\frac{\alpha_{eq}}{\alpha_0} f^{(\alpha_m - 1)} - 1\right] \times 1000 \tag{3.15}$$

and for the water vapour left behind,

$$\delta_v\ (^{\circ}/_{\circ\circ}) = \left[\frac{1}{\alpha_0} f^{(\alpha_m - 1)} - 1\right] \times 1000 \tag{3.16}$$

where α_{eq}, α_0 and α_m are the fractionation factors at the current, initial and mean temperatures respectively (Dansgaard, 1964).

Two–phase Rayleigh Model

The two–phase or closed model was discussed by Craig and Gordon (1965) and again by Gat (1996). Merlivat and Jouzel (1979) used this model to study the relationship between deuterium and ^{18}O in precipitation. The model involves a modification of the original Rayleigh theory to take into account the fact that not all liquid condensation is immediately lost from an air parcel. Instead some liquid is retained in the parcel, adding a second phase to the atmospheric component of the model. Precipitation leaving the parcel (δ_p) has the same isotopic ratio as the condensed liquid in the parcel at that time δ_c). Therefore $\delta_c = \delta_p$, and,

$$\delta_c = \frac{\delta_{v\,0} - \varepsilon_{eq}\,(1-f)}{\alpha_{eq} - f\,(\varepsilon_{eq}/10^3)} \tag{3.17}$$

where $\delta_{v\,0}$ is the isotopic composition of the initial water vapour, f is the fraction of the initial water vapour that remains, and ε_{eq} is the equilibrium enrichment factor.

Equilibrium Fractionation factors

All of the above equations require a value for the fractionation factor at the relevant temperature. Many studies have attempted to measure fractionation factors experimentally and then fit an empirical equation to the results obtained to calculate other values not explicitly investigated experimentally. Majoube (1971b) used the results of their own experiments to create the relationship,

$$ln\;\alpha_{eq} = \frac{1137}{T^2} - \frac{0.4156}{T} - 0.0020667 \tag{3.18}$$

whereas Horita and Wesolowski (1994) collected experimental data of their own and collated data created by many other authors including Majoube (1971b) data to conclude that,

$$ln\;\alpha_{eq} = \left[0.35041 \times \frac{10^6}{T^3}\right] - \left[1.6664 \times \frac{10^3}{T^2}\right] + \left[6.7123 \times \frac{1}{T}\right] - \left[7.685 \times 10^{-3}\right] \tag{3.19}$$

In both equations T is the air temperature in Kelvin. Figure 3.2 shows the empirical data collected and collated by Horita and Wesolowski (1994) and the best fit line described by equation 3.19.

These empirical equations can be used to obtain α_{eq} values for oxygen isotope fractionation, without the need to know an array of vapour pressures.

The α_{eq} values obtained through using equations 3.18 and 3.19 are very similar as can be seen in figure 3.3. It should be noted that the temperatures shown in figure 3.3 are in °C whereas the equations require the temperature to be in Kelvin.

For deuterium, expressions for α_{eq} are calculated using,

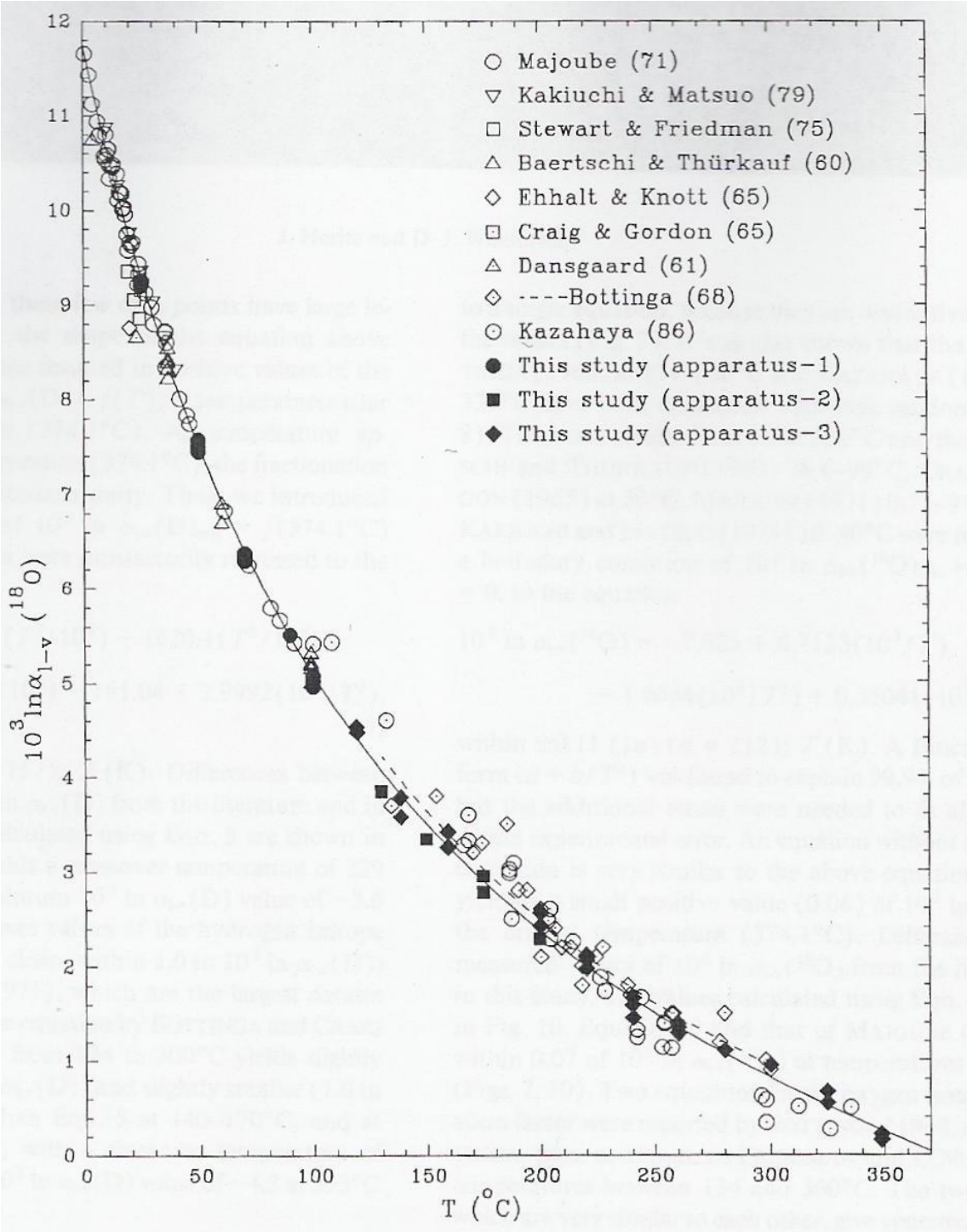

Figure 3.2: *Plot of all experimentally obtained oxygen fractionation factors from 0.75 to 350°C, obtained by Horita and Wesolowski (1994) (marked this study), and reported in other literature. Solid line is calculated using equation 3.19 in the text. (Figure taken from Horita and Wesolowski (1994))*

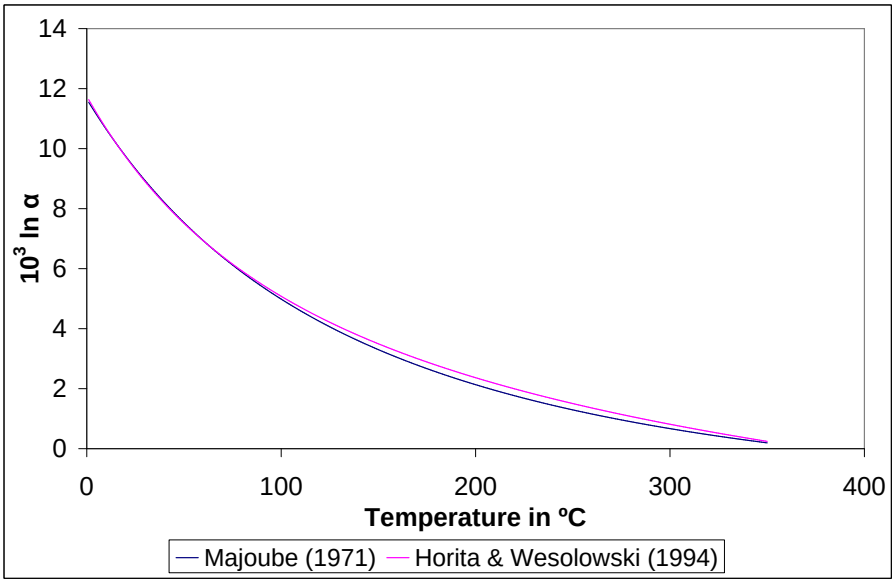

Figure 3.3: *Values of 10^3 ln α for the fractionation of ^{18}O obtained using the empirical equations of Majoube (1971b) (blue line) and Horita and Wesolowski (1994) (purple line).*

$$ln\ \alpha_{eq} = \frac{24844}{T^2} - \frac{76.248}{T} + 0.052612 \tag{3.20}$$

$$ln\ \alpha_{eq} = \left[1.1588 \times \frac{T^3}{10^9}\right] - \left[1.6201 \times \frac{T^2}{10^6}\right] + \left[0.79484 \times \frac{T}{10^3}\right] - 0.16104 + \left[2.9992 \times \frac{10^6}{T^3}\right] \tag{3.21}$$

from Majoube (1971b) and Horita and Wesolowski (1994) respectively. These equations were also empirically obtained. The Horita and Wesolowski (1994) equations were developed from data collected in the temperature range from 25 °C up to the critical temperature of water (374.1 °C). The experimental temperature range of Majoube (1971b) was 0 to 100 °C. Investigation by Horita & Wesolowski showed that results of their equations were *"in excellent agreement"* with those of Majoube between 25 and 100 °C (Horita and Wesolowski, 1994). At temperatures lower than 25 °C there is still good agreement, especially with the oxygen fractionation factors. The hydrogen fractionation factors calculated differ by a greater amount but the fractionation factors themselves are larger.

However, supercooled drops and droplets are present in clouds at temperatures down

to -15 °C that were not investigated by Majoube (1971b) or Horita and Wesolowski (1994). It is therefore worth noting that these equations may not be as accurate for liquid to vapour processes occurring outside the investigated experimental range.

A different set of equations is required to calculate the fractionation factors for the solid to vapour transition under equilibrium conditions. Majoube (1971a) looked at oxygen isotope fractionation between water vapour and ice in the temperature range 0 to -34 °C,

$$ln\ \alpha_{eq} = \frac{11.839}{T} - \left[28.224 \times 10^{-3}\right] \tag{3.22}$$

Merlivat and Nief (1967) investigated hydrogen isotope fractionation between 0 and -40°C, finding,

$$ln\ \alpha_{eq} = \frac{16288}{T^2} - \left[9.34 \times 10^{-2}\right] \tag{3.23}$$

3.3 Extensions to Rayleigh Distillation Theory

3.3.1 Kinetic Fractionation

In addition to the fractionation processes occurring when a liquid and vapour are in equilibrium, (see section 3.2.1), further non–equilibrium or kinetic processes can be important. Dansgaard (1964) suggested that kinetic fractionation is due to differences in the molecular diffusivities of the molecules in air and liquid. Quantitative values of the kinetic effect on fractionation could not be given conclusively by Dansgaard (1964) as there were insufficient observations of these processes available at that time. Since then it has been suggested that through conservation of kinetic energy, E,

$$E = \frac{1}{2}mv^2 \tag{3.24}$$

where m is mass and v is velocity of a molecule, molecules containing lighter isotopes must have higher velocities than the heavier molecules to conserve kinetic energy (section 1.1.2). This translates to a faster rate of diffusion of lighter molecules than heavy

molecules in response to a concentration gradient at a constant temperature (Faure and Mensing, 2005). There is a concentration gradient between the few millimetres thick laminar marine boundary layer, which is in equilibrium with the ocean, and the free atmosphere. Lighter molecules diffuse between the boundary layer and the free atmosphere faster leading to kinetic fractionation. An unusual observation made by Craig (1961) and Dansgaard (1964) is that kinetic effects are important during evaporative processes but do not seem to occur during condensation. This is most likely due to the fact that condensation occurs at relative humidities of approximately 100%, at which point equilibrium conditions are maintained (Gat, 1996).

Notably, it was Dansgaard (1964) who first introduced the concept of deuterium excess (d-excess). His use for it was not purely to see how far it deviated from the Meteoric Water Line, see section 1.2.3, but to use this information as an indication of the extent of non–equilibrium fractionation that occurred during evaporation at the source region. The extent of non–equilibrium fractionation occurring is a function of temperature and humidity. This phenomenon has been used to locate source regions of precipitation before modelling was an option, and even since models have been available (Petit et al., 1991). For example precipitation sourced in the Eastern Mediterranean generally has higher d-excess value of around 37 $^{\circ}/_{\circ\circ}$ (Gat, 1980). A d-excess value of lower than 10 $^{\circ}/_{\circ\circ}$ suggests that a second evaporation stage has been involved, e.g. evaporation of raindrops below a cloud (Araguás-Araguás et al., 2000). Merlivat and Jouzel (1979) concluded that d-excess depends on the relative humidity at the oceanic origin of the air parcel.

Kinetic fractionation is extremely hard to measure but seems to enrich samples in heavier isotopes relative to the value expected with purely equilibrium fractionation. The equations most often used are derived from wind tunnel experiments conducted by Vogt (1976),

$$\varepsilon_k = 12.4(1 - h_{0.1})\,(^{\circ}/_{\circ\circ}) \quad \text{for } (^2H) \tag{3.25}$$

$$\varepsilon_k = 14.3(1 - h_{0.1})\,(^{\circ}/_{\circ\circ}) \quad \text{for } (^{18}O) \tag{3.26}$$

where $h_{0.1}$ is relative humidity measured about 10 cm above the evaporating surface, expressed as a fraction of unity (Araguás-Araguás et al., 2000). Remembering that $\varepsilon = (\alpha - 1) \times 1000$. Similar expressions were found by Gonfiantini (1986). Using a typical value of $h_{0.1}$ = 0.8 gives a ε_k value for oxygen fractionation of 2.86 $^{\circ}/_{\circ\circ}$, which is much smaller than the 10 $^{\circ}/_{\circ\circ}$ of ε_{eq}.

Modelling Kinetic Fractionation

Merlivat and Jouzel (1979) redesigned the equations for initial evaporation from sea water by including a kinetic fractionation factor, thus improving the modelled *d*-excess values. Jouzel and Merlivat (1984) further improved modelled *d*-excess values, particularly at temperatures lower than -20°C by introducing a kinetic fractionation effect (α_k) to simulate differences in diffusivity of heavy and light water molecules (The Rayleigh Model with Kinetic fractionation or RMK). This kinetic effect occurs especially during snow formation as a result of vapour deposition onto ice crystals in an environment that is supersaturated with respect to ice. Their model did not take into account freezing of water drops and droplets as that process occurs without any fractionation occurring. They surmised that through adding the kinetic effect, the effective fractionation coefficient (α) becomes,

$$\alpha = \alpha_{eq}\alpha_k = \frac{\alpha_{eq} S_i}{\alpha_{eq}\left(D/D'\right)\left(S_i - 1\right) + 1} \tag{3.27}$$

where D' and D are diffusion coefficients for heavy and light molecules, respectively, and S_i is the supersaturation of vapour with respect to ice. The modelled *d*-excess values are highly sensitive to S_i so Jouzel and Merlivat (1984) proposed several parameterisations of S_i based on condensation temperature, T_c, in degrees Celsius, (e.g. equation 3.28). However they did acknowledge the need for more data sets to be investigated with this model to refine the formulation of S_i as a function of temperature. For the observed data tested by Petit et al. (1991) a simple linear function,

$$S_i = a + [b \times T_c] \tag{3.28}$$

where $a = 1.02$ and $b = -0.0038$ was found to reproduce the observed d-excess values plotted against measured δD. To vary the supersaturation value, coefficients a and b must be varied (Petit et al., 1991). However, Fisher (1991) concluded that S_i most likely varies from one precipitation event to the next, or even possibly within the same cloud. Jouzel et al. (1991) investigated values of S_i using the NASA GISS GCM and concluded that changing the values within the ranges they looked at did not greatly alter the δ^{18}O values output.

Modelled δ and d-excess values had been seen to deviate from observations when calculated using Rayleigh theory with only equilibrium processes at temperatures below -20°C. Figure 3.4 shows an example of Rayleigh modelled values (solid black line) compared to observations (grey dots). The extended Rayleigh expression containing a kinetic component produces modelled δ values that are much closer to observations of snow formation at low temperatures in polar regions, (dashed lines in figure 3.4) (Jouzel and Merlivat, 1984).

However Jouzel and Merlivat (1984) pointed out that because their Rayleigh model assumes constant saturation, isotopic exchange will continuously occur between the vapour and the liquid remaining in the cloud. Therefore the use of this Rayleigh theory must be restricted to clouds with low water contents.

3.3.2 Mixed Clouds Containing Liquid and Solid Condensate

In cold regions both liquid droplets and ice crystals can exist in clouds at the same time between -15 and -40°C, thus "mixed clouds" are present (Ciais and Jouzel, 1994). This coexistence causes liquid droplets to evaporate and water vapour to condense directly onto ice crystals due to the differing saturation conditions over water and ice. This is the Bergeron–Findesein process and it means that neither droplets nor crystals will be in isotopic equilibrium with the vapour (Ciais and Jouzel, 1994). Bergeron in 1935 described the process saying that in mixed clouds *"The vapour tension will adjust itself to a value in between the saturation values over ice and water. The effect of this must then be that condensation will take place continually until the liquid phase is entirely consumed."*

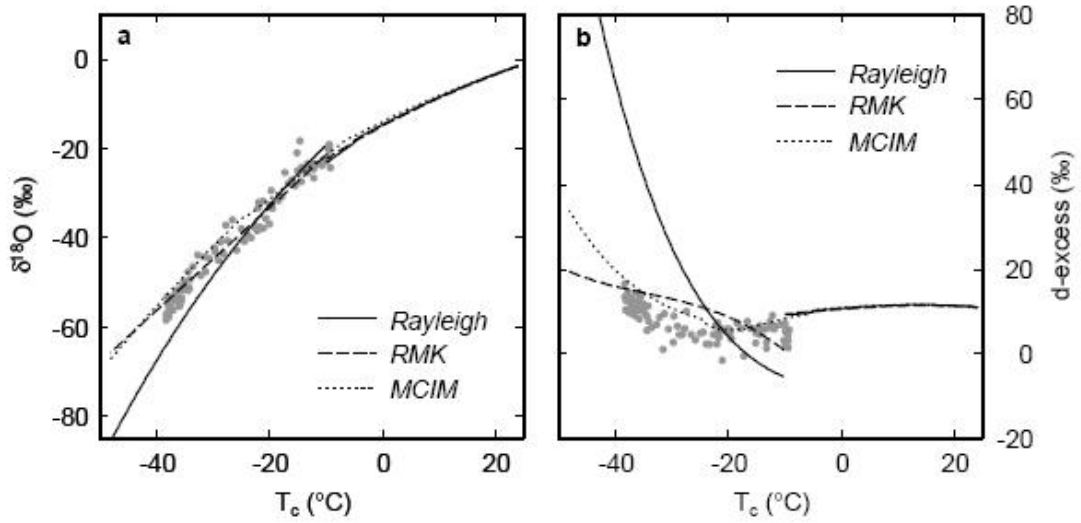

Figure 3.4: *Modelled (a) $\delta^{18}O$ and (b) d-excess as a function of condensation temperature (T_c) as predicted by three different isotope distillation models: the Rayleigh model from Dansgaard (1964) (solid line); the Rayleigh model including the kinetic isotopic effect (dashed line, RMK: Jouzel and Merlivat (1984)) and the Mixed Cloud Isotope Model (dotted line, MCIM: Ciais and Jouzel (1994)). Antarctic observations (gray dots) are from Dahe et al. [1994], for which values of T_c are calculated from surface temperatures (T_s) using T_c = 0.67T_s - 1.2 (Jouzel and Merlivat, 1984). Figure taken from Helsen (2006)*

Therefore the differing saturation vapour pressures cause the liquid droplets to evaporate. Direct deposition of vapour onto existing ice crystals by inverse sublimation will then take place and kinetic fractionation will occur during this process. Little or no fractionation occurs when supercooled droplets freeze (Ciais and Jouzel, 1994).

In this original MCIM, "*moist air is lifted up till its dew point is reached, then starts the condensation process; a certain amount of liquid is kept in the cloud and the vapour is saturated with the liquid (the liquid is in isotopic equilibrium)*" (Ciais and Jouzel, 1994). Over the interval -15 to -40°C both liquid and ice are present in the cloud. Below -40°C only ice and vapour remain. The phase change from liquid–vapour requires a different fractionation factor to that of solid–vapour, section 3.2.1. Changing the fractionation factors when a certain temperature is reached causes a discontinuity in the model, (solid line in figure 3.4). By allowing ice and liquid to coexist, as in the MCIM, this discontinuity is removed and a much improved set of modelled values is produced (dotted line in figure 3.4). This model method was shown to be able to reproduce the main

characteristics of mid– and high–latitude stable isotope variability (Jouzel et al., 1997).

Ciais and Jouzel concluded that accounting for these processes is not absolutely necessary so it does not invalidate previous studies of isotope ratios (Ciais and Jouzel, 1994). However, these mixed cloud processes do occur, especially within stratiform clouds, and should be included if time and computational power permits to increase the accuracy of the results.

3.3.3 Initial Isotopic Composition of Atmospheric Water Vapour

As discussed before, Dansgaard (1964) used equation 3.14 to describe the isotopic composition of the initial evaporation from sea water with the composition of VSMOW. However, this expression is only of use if equilibrium conditions are maintained, the sea water is of the same composition as VSMOW, and there is no water vapour already in the atmosphere. These conditions are very unlikely to be met.

Therefore Craig and Gordon (1965) suggested 2 other methods of calculating the isotopic composition of water vapour evaporating from the sea surface:-

1. By considering all exchange processes at the water surface, and knowing the δ values of the background atmospheric vapour before evaporation occurs.

2. By assuming that mean annual evaporation must equal mean annual precipitation and mean continental run–off on a global scale.

Craig and Gordon (1965) concluded that the first method would ideally be used, especially for smaller scale studies, and summarised the process with,

$$\delta_{v\,o} = \frac{\left(\frac{\delta_w}{\alpha_{eq}}\right) - \delta_a h_A - \varepsilon_{eq} - \varepsilon_k}{(1 - h_A) + \frac{\varepsilon_k}{10^{-3}}} \tag{3.29}$$

where δ_w and δ_a are the isotopic composition of sea water and background atmospheric vapour respectively. h_A is the relative humidity of the atmosphere expressed as a fraction of unity (e.g. 0.8 for 80%). α and ε are fractionation and enrichment factors, either equilibrium (eq) or kinetic (k). Unfortunately, the detail of knowledge required to properly use this first method is rarely available.

The second method can be used much more widely. Craig and Gordon (1965) looked at global precipitation samples and concluded that mean global precipitation would have an δ^{18}O equal to $-4‰$ and a δD equal to -22 ‰. These values were then equated with those of mean global evaporation. The isotopic composition of the net evaporation flux can then be taken as equal to that of the water vapour over the ocean assuming that the hydrological cycle is in isotopic steady state on a global scale, therefore $\delta_E = \delta_{v\,o}$ (Merlivat and Jouzel, 1979).

However, the assumption that $\delta_E = \delta_{v\,0}$ has been questioned for models where a regional value for $\delta_{v\,0}$ is being sought (Jouzel et al., 1996). This is due to the fact that measurements have shown that the vapour and ocean surface waters are not in isotopic equilibrium. Using this assumption can actually introduce a bias into the model of between 2 and 6 ‰ for δ^{18}O. The bias becomes especially important when considering deuterium excess. Jouzel and Koster (1996) suggested that a more accurate initial condition for isotope models could be obtained from GCMs and have made data sets available for both present day and Last Glacial Maximum (LGM) conditions created using the Godard Institute for Space Studies (GISS) isotope GCM.

3.3.4 Evaporation and Exchange During Precipitation

Dansgaard (1964) concluded that as water droplets fall from the atmosphere they experience isotopic exchange with surrounding background atmospheric water vapour and also some may re–evaporate into the higher atmosphere, though as with kinetic fractionation he was unable to quantify these processes. Observations of the δ values of atmospheric water vapour and precipitation presented by Jacob and Sonntag (1991) supported this theory in most situations. It should be remembered that if vapour and water are in equilibrium after exchange, the vapour will still be more depleted in heavy isotopes than the water, to the order of 80 ‰ for deuterium and 9 ‰ for oxygen. Miyake et al. (1968) found that mixing by exchange between falling raindrops and the surrounding vapour was important. Exchange occurs at different rates depending on both the size of the falling droplets and the number of droplets present. Heavy rain (large drops with a high terminal velocity)

may not exchange to equilibrium whereas light rain (small drops with a low terminal velocity) will under most circumstances. Exchange for solid precipitation i.e. snow or hail can only affect the outer layers so is considered negligible (Dansgaard, 1964). Equilibration of raindrops will mean that raindrops will equilibrate with water vapour in the lowest part of the atmosphere.

Evaporation of cloud droplets beneath the cloud base preferentially removes lighter isotopes from precipitation (Cole et al., 1999). This process may be significant in arid and semi–arid regions (Araguás-Araguás et al., 2000) as well as in warm, more moist conditions (Rozanski et al., 1982) and can be calculated dependent on the relative humidity (Stewart, 1975). More evaporation beneath the cloud base occurs when the air below the cloud is not saturated with vapour, a condition characteristic of less intense precipitation events (Cole et al., 1999).

3.3.5 Fractionation in the Middle Atmosphere

Observations of water vapour in the stratosphere and mesosphere have been made in the last few decades to allow a better understanding of the water cycle. These observations have revealed a trend of increasing water vapour content in the middle atmosphere over the observation period e.g (Oltmans and Hofmann, 1995). Isotope modelling of this atmospheric region, which had been previously conducted by Kaye (1990), then became a valuable tool in the analysis of these changes. Fractionation in these regions is no longer primarily linked to changes of state. Instead "chemical" fractionation mechanisms dominate (Zahn et al., 2006). Chemical fractionation is caused by the nature of molecular bonds. It requires less energy to break bonds involving lighter isotopes. Fractionation mainly occurs during the production of H_2O due to the oxidation of methane. However recycling of H_2O via the HO_x family and general isotope exchange reactions all cause fractionation. Another difference between these processes and those that occur from physical fractionation, is that all of the chemical reactions enrich the water vapour in heavier isotopes. Enrichments of 250 $^{\circ}/_{\circ\circ}$ over the atmosphere between the tropopause, at around 11 km, and 40 km have been observed (Zahn et al., 2006). This modelling approach is

still in it's infancy with large uncertainties in some of the reaction rates and also in the fractionation factors. However, results are promising.

These "chemical" fractionation factors should ideally be considered as soon as an air parcel travels above 11 km from the surface though very few models as yet include these processes.

3.4 Mixed Cloud Isotope Model

The MCIM used in this study accounts for mixed cloud processes i.e. it allows liquid droplets and ice crystals to coexist in clouds when the temperature of the air parcel is between -5.16 and -25°C. This temperature range is set due to previous model testing against observations (Ciais and Jouzel, 1994; Hendricks et al., 2000). It is based on the MCIM created by Ciais and Jouzel (1994), see section 3.3.2, but has been modified by Michiel Helsen (Helsen et al., 2006).

The main alteration made by Helsen et al. (2006) was to move away from the theoretical temperature and pressure variations framework that had been used previously to investigate processes under ideal conditions. Instead actual temperature and pressure variations occurring along a trajectory modelled from reanalysis fields were used (Helsen et al., 2006). These "observed" trajectories could then be used to model δ values of observed precipitation events.

However, the modified MCIM does not take into account either evaporation or exchange as rain falls, or any chemical fractionation in the middle atmosphere. Details of the model algorithm are given below and illustrated in figure 3.5.

3.4.1 MCIM Algorithm

Calculating the initial humidity mixing ratio

One of the functions of the MCIM is to output the amount and isotopic composition of water in each phase at each point along the path of the air parcel. The humidity mixing ratio, r, is a measure of the amount of water vapour in the air parcel and is equivalent to

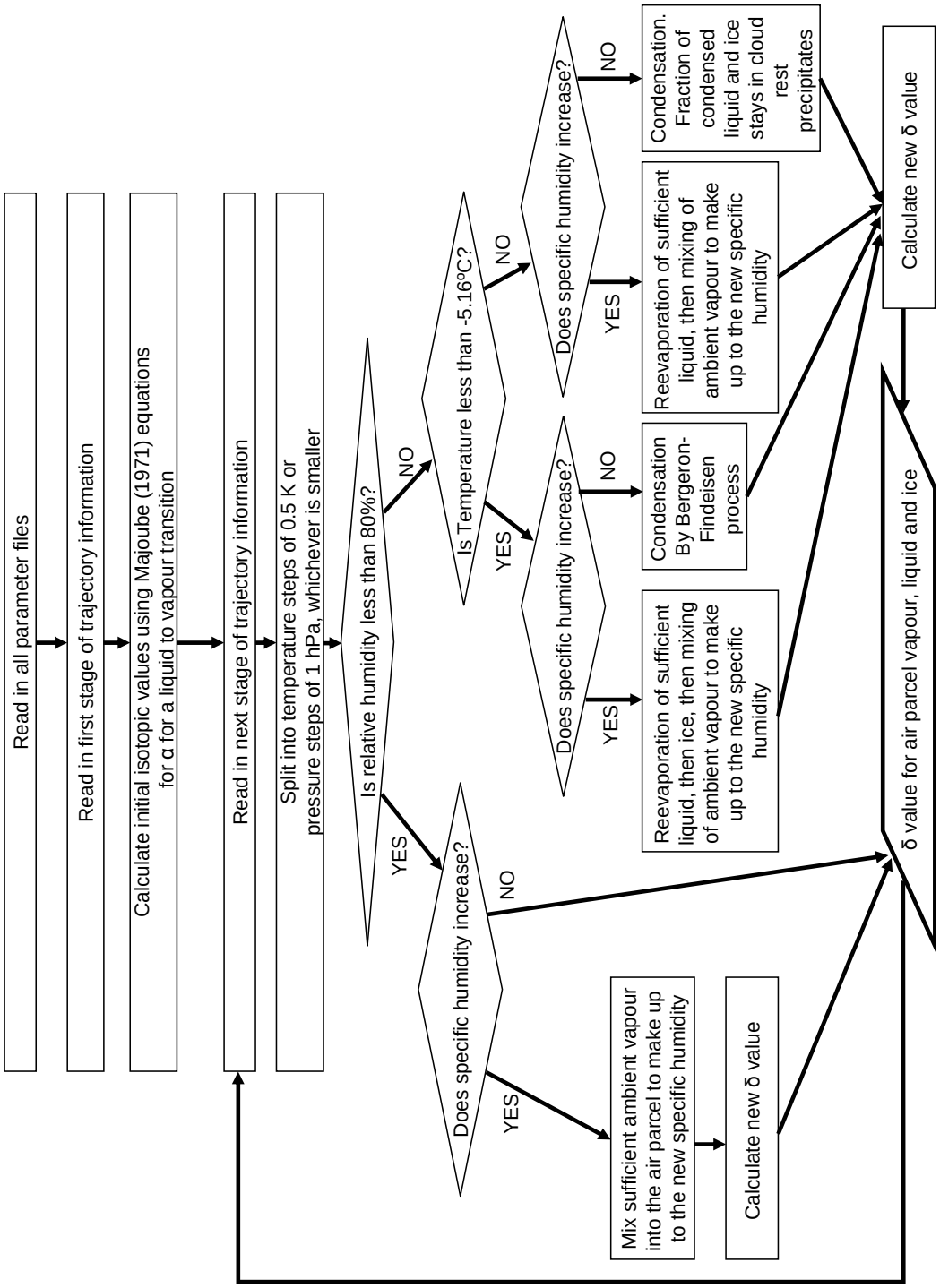

Figure 3.5: *Flow chart illustrating the basic steps and decisions taken by the MCIM algorithm.*

$$r = \left[\frac{\rho_v}{\rho_d}\right] \times 1000 = \left(g\, kg^{-1}\right) \tag{3.30}$$

where ρ_v is the density of water vapour in the air parcel and ρ_d is the density of dry air in the parcel.

To calculate this from the temperature and pressure data available from FLEXPART a saturation vapour pressure, e_s, must be found. The saturation vapour pressure over water (e_s) is the vapour pressure when water vapour and liquid water are in thermodynamic equilibrium, i.e. the rate of evaporation is equal to the rate of condensation. Similarly, the saturation vapour pressure over ice (e_{s_i}) is the vapour pressure when water vapour and ice are in thermodynamic equilibrium, i.e. the rate of sublimation of ice is equal to the rate of deposition.

The MCIM assumes that the initial air parcel is saturated with water vapour, but contains no liquid or ice to simplify the first stage. The MCIM does not use the Clausius–Clapeyron equation given in section 3.2.1, (equation 3.6). Instead it uses another empirically derived equation recommended by the World Meteorological Organisation in 1988. This second equation is known as the Goff–Gratch equation for liquid, where the saturation vapour pressure, e_s, is entirely dependent on the temperature, T, in Kelvin, by

$$\begin{aligned} log\, e_s \;=\; & \left[-7.90298\left(\frac{373.16}{T}-1\right)\right] + \left[5.02808\, log_{10}\left(\frac{373.16}{T}\right)\right] \\ & - \left[\left(1.3816\times10^{-7}\right)\left(10^{11.344\left(1-\frac{T}{373.16}\right)}-1\right)\right] \\ & + \left[\left(8.1328\times10^{-3}\right)\left(10^{-3.49149\left(\frac{373.16}{T}-1\right)}-1\right)\right] + log_{10}\,1013.25 \end{aligned} \tag{3.31}$$

For example, if the initial temperature of an air parcel is 259.30 K then the saturation vapour pressure, e_s, would be 2.04 hPa. This can then be converted to a humidity mixing ratio using the pressure, p, and the saturation vapour pressure, e_s,

$$r = \frac{\epsilon \times e_s}{p - e_s} \times 1000 \tag{3.32}$$

where ϵ is the ratio of the molecular weights of water vapour to dry air (M_w/M_d) equal to 0.622. Using this expression gives a saturation humidity mixing ratio of 1.74 g kg^{-1} for

this example.

Values of saturation vapour pressures calculated using both the Claussius–Clapeyron equation and the Goff–Gratch equation are shown in figure 3.6. It should be noted that although the temperature in figure 3.6 is given in °C, both equations require the temperature in Kelvin. The values match well in the temperature range for which the Claussius–Clapeyron equation is valid (-20 to 35°C) but then start to deviate from each other. The Goff–Gratch equation also is simpler to use as e_s is only a function of temperature. The Claussius–Clapeyron equation requires added information about the latent heat of evaporation (L) at the relevant temperature, as well as data on the mix of isotopes present as variations. Changes in the isotope ratio will change the specific gas constant, (R_w), altering the Claussius–Clapeyron equation.

Calculating initial isotopic composition

As covered previously, there are many methods by which an initial value for the isotopic composition of a modelled air parcel may be calculated. Most of these methods are either extremely complex or inaccurate on the small scale that this model uses, see section 3.3.3. The modified MCIM therefore uses GCM output to initialise the air parcel isotopic composition as suggested by Jouzel and Koster (1996). The GCM output used is a climatology of data from the ECHAM4 model, which produces an isotopic value for each 1.1° x 1.1° grid cell on 19 atmospheric layers. The closest ECHAM4 model location to the starting location of the parcel is used as the initial composition of the water vapour in the parcel. The MCIM then uses this value to find the theoretical isotopic composition of any liquid water held in the parcel as these values are required for subsequent calculations. For liquid water this is achieved using the previously explained equations of Majoube (1971b) (section 3.2.1) to find the required fractionation factors, α_{eq}. For oxygen,

$$ln\ \alpha_{eq} = \frac{1137}{T^2} - \frac{0.4156}{T} - 0.0020667 \tag{3.33}$$

and for deuterium,

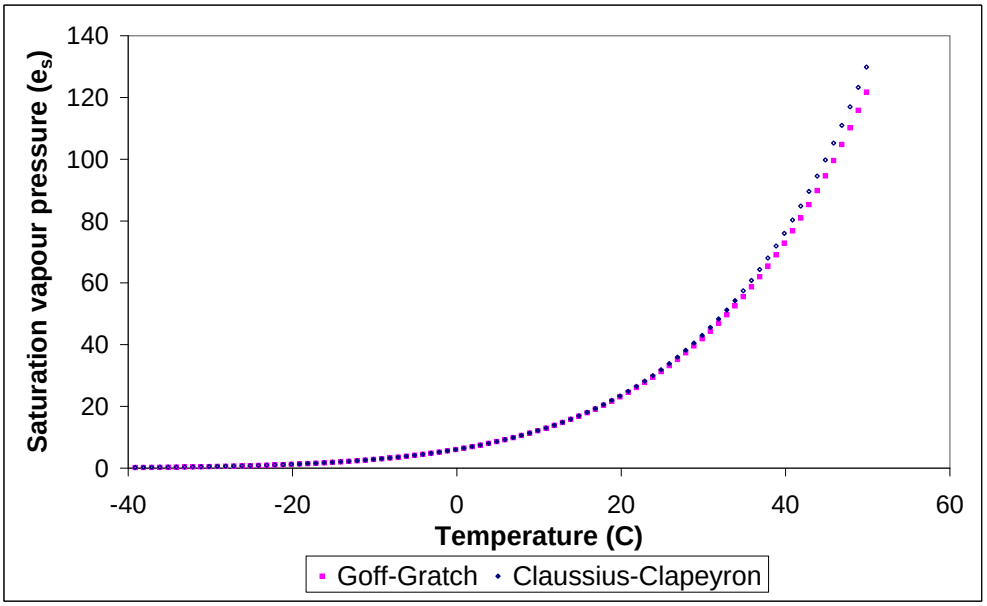

Figure 3.6: *Saturation vapour pressures (e_s) calculated using the Claussius–Clapeyron (blue) and the Goff–Gratch (pink) equations. The Claussius–Clapeyron equation is not valid beyond the range -20 to $35°C$, so e_s values calculated for temperatures outside this range are shown as blue diamonds with a white centre. Note that though the temperature in the graph is given in $°C$, both equations require the temperature in Kelvin.*

$$ln\ \alpha_{eq} = \frac{24844}{T^2} - \frac{76.248}{T} + 0.052612 \tag{3.34}$$

where T is temperature in degrees Kelvin. The theoretical isotopic composition of any liquid present, δ_l, can then be found using a derivation of equation 3.13,

$$\delta_l = [\alpha_{eq} \times (\delta_v + 1)] - 1 \tag{3.35}$$

where the δ values are expressed as raw values rather than $^{\circ}/_{\circ\circ}$. For example, consider an air parcel at temperature 259.30 K at a location where the ECHAM4 output gives a raw δ^{18}O value of -0.0254 (equal to $-25.4\ ^{\circ}/_{\circ\circ}$) and a raw δD value of -0.1938 (equal to $-193.8\ ^{\circ}/_{\circ\circ}$). These values are assigned to the air parcel water vapour and then the isotopic composition of liquid condensed from this vapour can be found, (for summary see table 3.1).

Though it is assumed that there is no liquid or ice in the air parcel for this initial step, for subsequent steps an ice isotopic composition is required. Therefore it is assumed that the ice has an identical isotopic composition to the liquid as it would do if liquid froze so $\delta_l = \delta_i$.

Vapour to Ice fractionation

Though the initial air parcel does not experience fractionation of isotopes due to deposition of water vapour onto ice crystals, this process does occur during the lifetime of the air parcel. Different fractionation factors are required for the vapour to ice transition than for vapour to liquid. Also, the vapour to ice fractionation process is slightly more complicated than that for the vapour to liquid transition. Initially the oxygen fractionation factor

Water Phase	Oxygen α_{eq}	δ^{18}O ($^{\circ}/_{\circ\circ}$)	Deuterium α_{eq}	δD ($^{\circ}/_{\circ\circ}$)
Ambient vapour from GCM	N/A	-25.4	N/A	-193.8
Parcel vapour	N/A	-25.4	N/A	-193.8
Parcel liquid	1.013	-12.4	1.137	-83.7

Table 3.1: *Example of calculated isotopic composition initial conditions of an air parcel.*

is calculated similarly to that for liquid though this time using the equation of Majoube (1971a),

$$ln\ \alpha_{eq} = \frac{11.839}{T} - \left[28.224 \times 10^{-3}\right] \tag{3.36}$$

and for deuterium, the equation of Merlivat and Nief (1967),

$$ln\ \alpha_{eq} = \frac{16288}{T^2} - \left[9.34 \times 10^{-2}\right] \tag{3.37}$$

where again T is temperature in degrees Kelvin. However, an extra kinetic factor must then be considered (Jouzel and Merlivat, 1984). This kinetic effect is dependent on the supersaturation ratio with respect to ice, S_i. Any ice formed but not lost from the parcel will maintain its isotopic composition, and not equilibrate with liquid or vapour until it melts again. At the point of melting it introduces an "isotopic memory" from the point in time at which the water froze. This remembered isotopic composition is then remixed through the vapour and liquid (Ciais and Jouzel, 1994).

In the MCIM the supersaturation ratio at temperatures greater than 268 K is found using

$$S_i = \frac{e}{e_{s_i}} \tag{3.38}$$

where e is the vapour pressure of the water vapour and e_{s_i} is the saturation vapour pressure over ice. e_{s_i} is calculated using the Goff–Gratch equation for ice,

$$\begin{aligned} log\, e_{s_i} &= \left(-9.09718 \times \left(\frac{273.16}{T} - 1\right)\right) - \left(3.56654 \times log\left(\frac{273.16}{T}\right)\right) \\ &\quad + \left(0.876793\left(1 - \frac{T}{273.16}\right)\right) + log\, 6.1071 \end{aligned} \tag{3.39}$$

where T is the air temperature in Kelvin.

At temperatures lower than 248 K the supersaturation over ice is taken to be a linear function of temperature with $S_i = 1.02 - 0.0038T$ (section 3.3.1). Between temperatures 248 and 268 K a linking function is used to smooth the transition across the mixed cloud temperature interval.

The calculated supersaturation value over ice, S_i, is then used to adjust the fractionation factors to include the kinetic component,

$$\alpha = \alpha_{eq}\alpha_k \quad \text{where} \quad \alpha_k = \frac{S_i}{\frac{S_i - 1}{m} + \frac{1}{\alpha_{eq}}} \tag{3.40}$$

where m is the coefficient of diffusion of the molecules in air, equal to 0.9723 for δ^{18}O, and 0.9755 for δD (Merlivat, 1978).

Clear Sky Conditions

Once the initial saturated air parcel has been created, it moves through the atmosphere experiencing different temperature, pressure and relative humidity conditions. In the real atmosphere cloud will not be formed unless the local (cloud scale) relative humidity reaches at least 100%. To simulate this in models, cloud forms only after a relative humidity threshold is exceeded. Helsen et al. (2006) added a similar scheme to the MCIM with a large (model) scale humidity threshold set to 80%. This takes into account errors in input data and model processes, as well as cloud size versus model resolution incompatibility, section 5.2.2. Previous Rayleigh studies, including the original MCIM (Ciais and Jouzel, 1994), assumed constant saturation from the source regions to the precipitation site in question and calculated fractionation continuously along a trajectory, purely as a function of temperature and pressure. Using a threshold such as a relative humidity of 80%, limits the calculation of fractionation to conditions where condensation is likely to be occurring according to relative humidity information provided by the trajectory. This allows a more realistic approximation of atmospheric conditions and isotopic concentrations (Helsen et al., 2006).

During clear sky (no cloud) conditions, i.e. when the relative humidity is less than the 80% threshold value, there can still be variations in the relative and specific humidities, especially as re–analysis observations of these parameters are being used. On occasion an increase in specific humidity and therefore in the water mass contained within the parcel will be seen to occur when comparing the new specific humidity with the one from the previous timestep. This change is due to the mixing of external water vapour into the air

parcel in the real atmosphere. The modified MCIM must account for this, and does so by mixing in water vapour from the surrounding atmosphere. The isotopic composition of this "external" water vapour is obtained from the ECHAM4 climatological fields at the location of the air parcel.

This mixing is accomplished by calculating the amount of δ^{18}O, q_{18anc}, in the air parcel before mixing occurs,

$$q_{18anc} = q \times (\delta_v + 1) \times \left({}^{18}O/{}^{16}O\right)_{VSMOW} \tag{3.41}$$

where q is the specific humidity of the air parcel before the change occurred. δ_v is again a raw isotopic value, in this case that of the water vapour before mixing. $({}^{18}O/{}^{16}O)_{VSMOW}$ is the absolute isotopic content for the VSMOW standard equal to 2.0052×10^{-3}. A similar equation can be used for the deuterium content using $(D/H)_{VSMOW} = 1.5575 \times 10^{-4}$ (Clark and Fritz, 1997). Multiplying by the VSMOW value reduces the δ value to the absolute isotopic content of the sample as explained by equation 3.2.

Equation 3.41 can then be used again to find the absolute content of heavy isotope in the external water vapour to be mixed in, q_{18gcm}. This time however, q is the change in specific humidity and δ_v is the raw isotopic value given by the ECHAM4 output. The absolute values of the internal and external water vapours are then known and due to their being multiplied by the specific humidities, they are scaled as to the amount from each source.

These two absolute values can then be combined into the new (raw) δ composition of the water vapour in the air parcel after mixing,

$$\delta_v = \frac{\frac{q_{18anc}+q_{18gcm}}{q}}{({}^{18}O/{}^{16}O)_{VSMOW}} - 1 \tag{3.42}$$

where q is the specific humidity of the parcel after mixing. Table 3.2 gives examples of the numbers generated continuing from the initial parcel previously calculated. The table shows that in this case, the change in specific humidity and the variation between external and internal was sufficient to decrease the δD value of the parcel by 0.2 $^{\circ}/_{\circ\circ}$. The change in δ^{18}O values was minimal though cumulative changes seen across timesteps are larger.

Stage of Mixing	Internal δD (‰)	Specific Humidity g kg^{-1}	External δD (‰)	Amount of ^{18}O
Internal before mixing	-193.8	1.12	-193.8	1.41 x 10^{-4}
External added	N/A	0.05	-190.1	6.31 x 10^{-6}
Internal after mixing	-193.6	1.17	-190.1	N/A

Table 3.2: *Example of calculated isotopic composition of the initial air parcel before and after mixing in of external air.*

As for the initial isotopic composition, a theoretical value for liquid condensed from this vapour can be obtained. However as the relative humidity threshold has not been exceeded there is still no liquid or ice present. The theoretical ice isotopic composition is therefore still equal to that of the theoretical liquid.

Liquid Only Clouds

If the relative humidity of the air parcel exceeds the 80% threshold described previously then clouds start to form. The type of cloud formed depends on the temperature of the air parcel. Another internal threshold of the model is that if the temperature is greater than a model obtained threshold temperature of -5.16°C then any condensation will be to liquid water droplets, i.e. any clouds will be entirely formed of liquid drops with no ice present. Where clouds are formed there is also the possibility of precipitation falling from that cloud.

Whether or not precipitation will occur from the parcel at any given point is dependent on the amount of cloud liquid droplets present at two consecutive time points and is determined through mass conservation by comparing the two consecutive humidity mixing ratios obtained from the ECMWF humidity fields. If the humidity mixing ratio of the air parcel increases, i.e. the amount of water vapour in the parcel has increased, then water vapour must have been added to the parcel not lost as precipitation. This extra water vapour is obtained either by re–evaporation of cloud liquid water if sufficient is present, or it must be mixed in from the surrounding atmosphere external to the air parcel. This increase in internal water vapour can take the following forms:-

1. **Re–evaporation of all liquid and external mixing**

   If insufficient liquid is present in the air parcel to evaporate and provide the extra water vapour required then more water vapour must be obtained from outside the air parcel, i.e. if the change in internal water vapour amount between two timesteps is larger than the amount of cloud liquid water present inside the parcel at the earlier of the two timesteps then more water must be obtained from outside the parcel to make up the shortfall. This is achieved in much the same way as was described in section 3.4.1 for mixing in of external air. The main variation in methods is the presence of the liquid phase. Equation 3.42 must therefore include the liquid phase so cannot use specific humidity as a measure of the amount of water present. Instead a humidity mixing ratio, r, can be used to scale the proportions of each phase involved. Equation 3.42 becomes,

$$\delta_v = \frac{\frac{r_{18anc_v} + r_{18anc_l} + r_{18gcm}}{r}}{({}^{18}O/{}^{16}O)_{VSMOW}} - 1 \tag{3.43}$$

   with a similar equation for deuterium, where r_{18anc_v} and r_{18anc_l} are the δ value of the air parcel vapour and liquid phases respectively, scaled by the humidity mixing ratio, r. r_{18gcm} is the scaled δ value of the external water vapour to be mixed in, and $({}^{18}O/{}^{16}O)_{VSMOW}$ is the absolute isotopic content for the VSMOW standard equal to 2.0052×10^{-3}.

2. **Re–evaporation of some liquid droplets**

   Another possibility is that all the extra water vapour has come from liquid droplets within the parcel, but not all of the liquid has re–evaporated i.e. the difference in amount of water vapour between two timesteps is smaller than the amount of liquid water in the parcel at the earlier timestep. In this case fractionation due to evaporation must be taken into account. The change in the δ value of the liquid in the cloud due to the re–evaporation is expressed as a raw value by

$$\Delta\delta_l = \frac{\left(\left[(\alpha_{eq} - 1) \times \frac{\Delta r_v}{r_v}\right] + \frac{\Delta\alpha_{eq}}{\alpha_{eq}}\right) \times (1 + \delta_l)}{1 + \left(\alpha_{eq} \times \frac{r_l}{r_v}\right)} \tag{3.44}$$

where Δ values denote the change in the parameter between before and after mixing. α_{eq} is the fractionation factor at the after mixing air parcel temperature. r values are the humidity mixing ratio of liquid and vapour phases, subscripts l and v respectively. The changes in δ^{18}O and δD can then be added to the original δ values of the liquid content of the parcel to give the new δ values after re–evaporation has occurred. The new vapour δ values can then be calculated using a rearranged form of equation 3.35,

$$\delta_v = \left(\frac{1 + \delta_l}{\alpha_{eq}}\right) - 1 \tag{3.45}$$

where again the δ values are raw values.

3. **Condensation occurs**

   There is also the possibility that the water vapour content of the air parcel may have decreased due to condensation. In this case a fraction of the condensed vapour will be retained as liquid within the parcel while the rest is lost as precipitation. The changes in δ values for the liquid and vapour phases are calculated using the same equations as when there is an increase in water vapour, i.e. equations 3.44 and 3.45.

Mixed Clouds

If the relative humidity of the air parcel remains greater than 80% and the temperature drops below -5.16°C then ice crystals start to appear and the clouds become a mixture of liquid droplets and ice crystals. Below -25.16°C clouds are formed entirely of ice crystals. Mass conservation is again used to indicate whether water vapour has been lost or gained by the air parcel, and, in the case of a gain in water vapour, where this vapour has come from.

1. **Re–evaporation of all liquid droplets and all ice crystals, and external mixing**

   The simplest way in which mixed clouds can change along a trajectory is a sufficiently large increase in water vapour to require all liquid droplets and ice crystals within the air parcel to re–evaporate, and external water vapour to be mixed in as well. This situation is described as for re–evaporation of all liquid and external mixing for liquid only clouds but with an extra term for the ice that is now present. Equation 3.43 therefore becomes,

$$\delta_v = \frac{\frac{r_{18anc_v} + r_{18anc_l} + r_{18anc_i} + r_{18gcm}}{r}}{\left({}^{18}O/{}^{16}O\right)_{VSMOW}} - 1 \tag{3.46}$$

   with a similar equation for deuterium, where r_{18anc_i} is the δ value of the air parcel ice phase, scaled by the humidity mixing ratio, r.

2. **Re–evaporation of all liquid droplets and some ice crystals**

   The liquid droplets will evaporate before the ice crystals. Therefore if not all of the condensate contained in the air parcel is required to re–evaporate to conserve water vapour mass then it will be the ice crystals that remain. It is assumed that there is no fractionation involved in the sublimation of ice. Mixing in of external water vapour from the ECHAM4 GCM is not necessary as sufficient water is present in the liquid droplets and ice crystals internal to the air parcel. This process is therefore expressed with a modified version of equation 3.46,

$$\delta_v = \frac{\frac{r_{18anc_v} + r_{18anc_l} + r_{18anc_i}}{r}}{\left({}^{18}O/{}^{16}O\right)_{VSMOW}} - 1 \tag{3.47}$$

   with a similar equation for deuterium, where r_{18anc_i} is calculated by

$$r_{18anc_i} = \Delta r_i \times (\delta_i + 1) \times \left({}^{18}O/{}^{16}O\right)_{VSMOW} \tag{3.48}$$

   where Δr_i is the amount of ice that is required to vapourise. δ_i is the raw isotopic composition of ice crystals.

3. **Re–evaporation of some liquid droplets and no ice crystals**

   It is also possible that the increase in water vapour experienced by the air parcel is so small that only a portion of the liquid droplets present are required to evaporate while the ice crystals remain untouched. In this case the process is the same as that for liquid clouds when only partial re–evaporation occurs. Fractionation must be taken into account with partial liquid evaporation as seen in equations 3.44 and 3.45.

4. **Condensation and Precipitation**

   In mixed clouds condensation and precipitation occur according to the Bergeron–Findeisen process. Due to the saturation vapour pressure over water being greater than the saturation vapour pressure over ice, (section 3.3.2), the liquid droplets evaporate. Direct deposition of vapour onto existing ice crystals by inverse sublimation will then take place and kinetic fractionation will occur during this process. In this case neither the liquid droplets nor the ice crystals are in isotopic equilibrium. Little or no fractionation occurs when supercooled droplets freeze.

   To achieve this, first the amount of liquid in the parcel must be found. Unlike the previous cases, the amount of liquid as a humidity mixing ratio is found to be a fraction (0.04) of the water vapour present as a function of temperature. Temperature is included in this case due to the proportions of liquid to ice in a mixed cloud being dependent on temperature. This total amount of liquid is then split into 3 parts. A fraction of 0.0001 of the liquid freezes to ice with no fractionation. The second split is liquid that evaporates to water vapour. This second fraction is also a 0.0001 fraction, but this is further scaled according to the saturation vapour pressure over the liquid. This second part evaporates but then is deposited to ice immediately, experiencing kinetic fractionation. The remainder of the liquid phase stays as liquid.

   The isotopic composition of the vapour can then be calculated and from these values the δ values of the liquid and ice phases can also be found. A percentage of the ice

present must then be lost as precipitation. This amount is 55% of the ice present unless this is greater than the change in ice content from the last trajectory point. If 55% of the total amount of ice is too much, then 101% of the change in ice is used as the amount of precipitation instead.

After introducing the theory behind both models used in this study over the last two Chapters 2 and 3, the following three chapters detail the results obtained from the model and their relation to observed values from Norwich, Dublin, Birmingham, Lincolnshire and Somerset.

Term	Explanation	Units
a	absolute isotopic content of water a_w, water vapour a_v, liquid precipitation a_p	
$^{\circ}/_{\circ\circ}$	permil or parts per thousand	
VSMOW	Vienna Standard Mean Ocean Water	
δ^{18}O	the standardised ratio of oxygen-18 to oxygen-16	$^{\circ}/_{\circ\circ}$
δD	the standardised ratio of deuterium to hydrogen	$^{\circ}/_{\circ\circ}$
δ_w	the standardised isotopic content of sea water	$^{\circ}/_{\circ\circ}$
δ_v	the standardised isotopic content of water vapour	$^{\circ}/_{\circ\circ}$
$\delta_{v\,0}$	the standardised isotopic content of initial water vapour	$^{\circ}/_{\circ\circ}$
δ_p	the standardised isotopic content of liquid precipitation	$^{\circ}/_{\circ\circ}$
δ_c	the standardised isotopic content of liquid condensation	$^{\circ}/_{\circ\circ}$
δ_E	isotopic composition of the net evaporation flux	$^{\circ}/_{\circ\circ}$
δ_a	isotopic composition of the atmospheric vapour present	$^{\circ}/_{\circ\circ}$
δ_l	isotopic composition liquid precipitation	$^{\circ}/_{\circ\circ}$
δ_i	isotopic composition solid precipitation	$^{\circ}/_{\circ\circ}$
d-excess	deuterium excess	
α	fractionation factor	
ε	enrichment factor	$^{\circ}/_{\circ\circ}$
eq, k	as subscripts for fractionation and enrichment factors denote equilibrium or kinetic processes respectively	
0, m	as subscripts for fractionation factors denote initial or mean fractionation respectively	

Table 3.3: *Glossary of terms: Part I.*

Term	Explanation	Units
R_w	specific gas constant for water vapour	J kg^{-1} K^{-1}
R^*	universal gas constant	J mol^{-1} K^{-1}
M_w	molecular mass of water vapour	kg mol^{-1}
M_d	molecular mass of dry air	kg mol^{-1}
e_s	saturation vapour pressure of heavy $e_{s\ heavy}$,	
	or light $e_{s\ light}$ isotope	hPa
L	latent heat of vapourisation	J kg^{-1}
h	relative humidity (subscripts indicate	% or fraction
	measurement height in metres above surface)	
h_A	relative humidity of the free atmosphere	%
q	specific humidity	g m^{-3}
r	humidity mixing ratio	g kg^{-1}
ρ_v	density of water vapour	kg m^{-3}
ρ_d	density of dry air	kg m^{-3}
ϵ	ratio of the molecular weights of water vapour to dry air	
D' D	diffusion coefficients	
	for heavy and light isotopes respectively	
S_i	supersaturation of vapour with respect to ice	
T	Temperature	degrees
p	Pressure	hPa
f	fraction of the initial water vapour still in an air parcel	

Table 3.4: *Glossary of terms: Part II.*

Chapter 4

November 2005 Case Study

To test the validity of the Lagrangian trajectory model used in this study, observed isotopic composition of precipitation data was required. The GNIP data set has this information but as monthly averages. As the Lagrangian trajectory model is initiated from a single point in time, higher temporal resolution observation data is required for initial testing. Daily data regarding the isotopic composition of precipitation at European sites is rare and fragmented, tending to be collected for a specific study (Darling and Talbot, 2003; Heathcote and Lloyd, 1986). Therefore a collection system was established to obtain daily rainfall samples from 3 sites across the British Isles during November and December 2005. This observed data set is presented here and used as a case study to examine the feasibility of the FLEXPART–MCIM approach to modelling the isotopic composition of rainfall in the British Isles.

4.1 Precipitation Collection

4.1.1 Collection Sites

A collection network was set up to gain an observational daily data set from more than one location across the same time period. The locations of the sites chosen were in Norwich, Birmingham and Dublin, (figure 4.1). These locations were chosen for their similar latitudes and therefore the possibility of observing the movement of synoptic systems across

the British Isles.

In Norwich, five sites were established to see what effect small changes in sampling site have on precipitation amount and isotopic composition. Three of the sites were located around the University of East Anglia (UEA) campus: one on an open field by the Sainsbury's Exhibition Centre, one on an area of grass surrounded by buildings including the Zuckerman Institute of Connective Environmental Research (ZICER), and the last on the roof of the Environmental Sciences School. The other two Norwich sites were situated 1.5 miles away at 87 Bury Street, one on a single storey roof that was sheltered on one side, and the second enclosed at ground level in the garden. Photographs of these sites are shown in Appendix A. Samples collected from the elevated site at Bury Street were analysed for isotopic composition to form the main Norwich observed data set (appendix B.1). This site was chosen to ensure security, which could not be guaranteed at the open access sites at the UEA. Water samples were taken sporadically from the other sites in order to compare the isotopic values experienced across Norwich.

4.1.2 Precipitation Collection Method

The data collected were daily values for the amount of precipitation falling at each of the sites and, where possible, an 8 ml sample of rainwater (corresponding to 0.65 mm of precipitation) to be analysed for isotopes. The collecting equipment consisted of a funnel leading into a closed bottle all contained in a weighted bucket to prevent it from falling over. The samples were collected at 1200 every day for the month of November 2005 at all sites. Measurements at the Norwich sites were continued for the first two weeks of December due to a fault in the tipping bucket raingauge used on the roof site at 87 Bury Street, which was used to gain information about the timing of precipitation. The tipping bucket raingauge used consisted of a funnel that emptied into the "tipping bucket" part of the device. Once one side of the bucket is full with rainwater the weight causes the bucket to tip exposing the second bucket to the water flow from the funnel. Each "tip" of the bucket completes a circuit and the time of the tip can be recorded against the internal clock of the device. The number of tips per minute are counted and as each bucket can

Figure 4.1: *Map of the British Isles showing the location of Birmingham, Dublin and Norwich.*

hold 0.2 mm of rainwater before it tips, the amount and time of precipitation events are recorded.

4.2 Significance of Correlations

Throughout the results chapters of this study, observed δ values will be compared to modelled values to measure the ability of the model to reproduce observed values. This comparison will be conducted through calculating regression equations relating the observed values to the modelled ones. These equations express the correlation between the two values i.e. the statistical probability that the variance in one value is caused by variance in the other. Ideally all modelled ratios would be equal to their respective observed ratio. This is rarely the case in statistical studies so a second coefficient, r^2, is also calculated as a measure of the accuracy of the regression equation in relating the two values. A low r^2 value means that only a low percentage of observed values could be predicted using the modelled value and the regression equation. The r^2 of each regression equation must be compared with a critical r^2 number to see at what significance level the regression equation can be used. To calculate the critical r^2 number:

$$r^2 = (tanh\ z)^2 \tag{4.1}$$

where z equals

$$z = \frac{b}{\sqrt{n-3}} \tag{4.2}$$

where b is a constant equal to 1.645 (for 95% significance) or 1.281 (for 90% significance), and n is the number of data pairs being compared (Wilks, 1995). These r^2 values assume a 1–tailed distribution in the relationship between the two variables being compared. This assumption is valid in this case as a negative relationship between observed and modelled values of the same parameter is not a part of the null hypothesis. The observed and modelled values must be either positively correlated or they have no relation to each other at all. Figure 4.2 shows a suite of critical r^2 numbers for both 90 and 95% significance

level testing. If the r^2 value of a regression equation is larger than the critical r^2 at 95% significance then the probability of the regression relationship occurring by chance is only 5%.

4.3 Observed Amount of Precipitation

The daily amount of precipitation observed at the Norwich sites was measured as a volume of water collected over the 24 hour sampling period. This was converted to an amount of precipitation by,

$$\text{Amount of precipitation (mm)} = \frac{\text{Total volume of water in sampler in mm}^3}{\text{Area of top of sampler funnel in mm}^2} = \frac{V}{\pi r^2} \tag{4.3}$$

The radius of the funnels used was 62.5 mm. The maximum precipitation amount that the 500 ml bottles used could hold was therefore 40.7 mm falling over 24 hours. Similar methods were used at Birmingham and Dublin, but using the respective funnel radius used at each site.

Figure 4.3 shows the amount of precipitation plotted against the measured δ^{18}O observed at Norwich, Dublin and Birmingham. These two parameters are significantly correlated at the 95% level for all sites even though at mid–latitudes there is generally a stronger temperature to δ^{18}O correlation (Schotterer et al., 1996). Temperature information for the sites is not available so no conclusions about the relative strength of the correlations are possible. More than half of the raindays involved less than 3 mm of precipitation (27 out of the 42 samples across the 3 sites), see section 4.6. However the days where more than 3 mm of precipitation fell account for 80% of the total precipitation at Norwich, 76% at Dublin and 89% at Birmingham. The samples collected at Norwich on the 25th and 26th of November 2005 were at least partially composed of snow. All other Norwich samples were entirely composed of rainfall. No information was obtained about rain versus snow content of the Dublin and Birmingham samples.

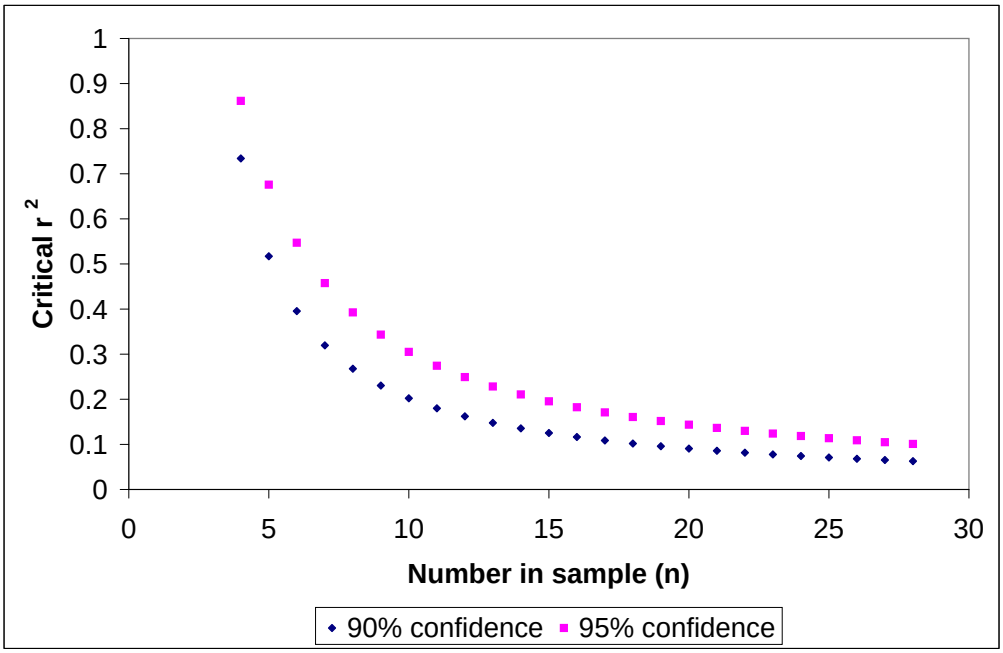

Figure 4.2: *Critical r^2 values for sample sizes between 3 and 28, and significance levels of 90% (navy diamonds) and 95% (purple squares).*

4.4 Observed δ^{18}O

This case study is comprised of a unique dataset of observed measurements of isotopic composition of rainfall from a transect across the British Isles. All samples were collected at the same time each day (1200 hours) and analysed in the same way by mass spectrometry (section 1.1.4). The complete raw data set can be seen in Appendices B and C. Monthly averages of δ^{18}O, δD and d-excess at Norwich, Dublin and Birmingham are shown in table 4.1. Birmingham's averages are the most negative for δ^{18}O and δD at -8.18 and -47.91 $‰$ respectively. However the average d-excess value is largest for Dublin. Figure 4.4 shows a time series across the collection period of δ^{18}O and precipitation amount (mm) for (i) Norwich, (ii) Dublin and (iii) Birmingham. The inverse relationship between δ^{18}O and precipitation amount noted in section 4.3 is visible again in these time series, where peaks in one variable are mirrored by troughs in the other and vice versa. The Norwich time series of δ^{18}O appears to show less negative values throughout the early part of November until the 25th, then more negative δ^{18}O values are seen into early December and to the end of the observation period. This trend is also partly visible

(i)

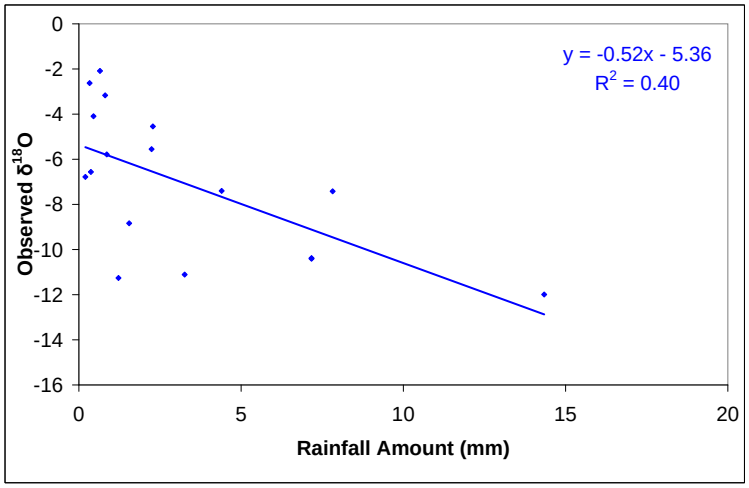

(ii)

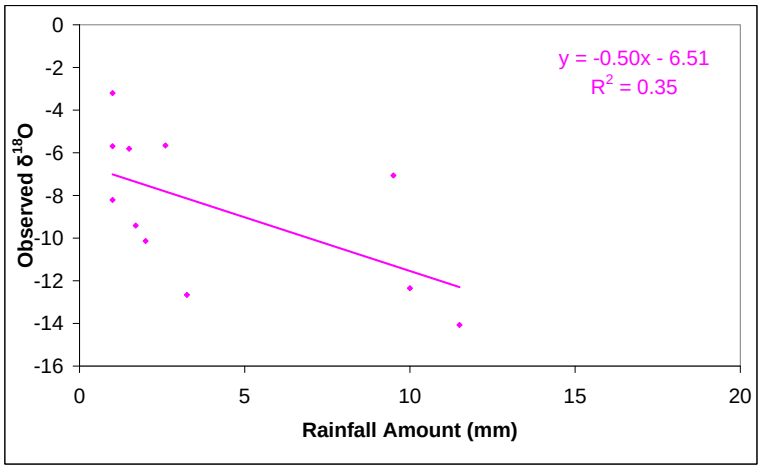

(iii)

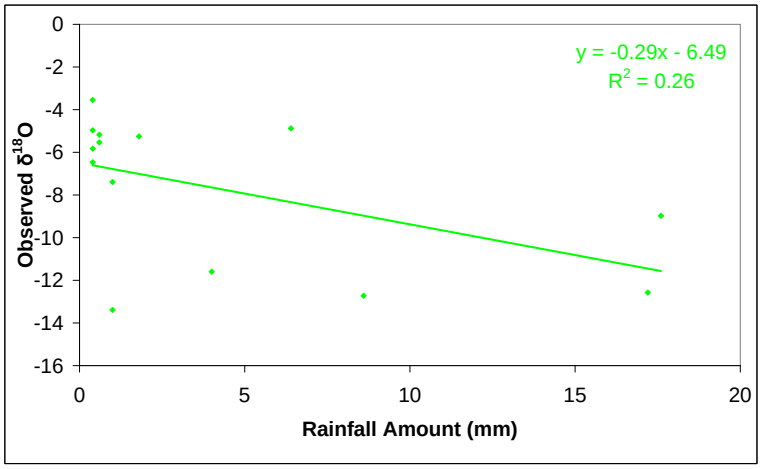

Figure 4.3: *Scatter plot of observed $\delta^{18}O$ against the daily precipitation total amount during November 2005 for the sites at (i) Norwich, (ii) Dublin and (iii) Birmingham. The straight lines are best fits by linear regression; the regression equation and r^2 values of these lines are shown in the upper right of each panel. The error in the observed $\delta^{18}O$ values is 0.02 $^{\circ}/_{\circ\circ}$.*

in the Birmingham and Dublin time series though they do not extend into December so the shift towards more negative values consists of only 2 observations at these locations. This trend can be explained by the fact that the first half of November 2005 was warm whereas the second half was very cold. This change was due to predominantly cyclonic/south–westerly situations until the 12th November 2005 followed by anticyclonic and northerly systems in the second half of the month (Eden, 2006). The warm south–westerlies would bring lots of water vapour straight from an oceanic source in the first half of the month explaining the high amounts of precipitation and the less negative δ values seen at the start of the month. Colder air from the north in the second half of the month would contain less water vapour and fewer heavy isotopes leading to the lower amounts of precipitation and more negative δ values. Exceptions to this trend will be due to smaller scale processes.

4.5 Observed Deuterium Excess

The d-excess parameter can be used to describe the relationship between δD and δ^{18}O such that

$$d = \delta\mathrm{D} - 8 \times \delta^{18}\mathrm{O} \tag{4.4}$$

d-excess values can give an indication of the source region of an air parcel, as described in section 1.2.4. Figure 4.5 shows δD versus δ^{18}O for each of the precipitation samples collected as well as their relation to the Global Meteoric Water Line (GMWL), which is based on global observations. All but four of the samples lie on or above the GMWL as expected in Western European samples collected in the winter (Schotterer et al., 1996). This is further reflected by the Meteoric Water Line calculated from all the observed

Site	δ^{18}O (‰)	δD (‰)	d-excess
Norwich	−7.06	−41.85	14.66
Dublin	−7.34	−41.53	16.00
Birmingham	−8.18	−47.91	15.35

Table 4.1: *Mean observed $\delta^{18}O$, δD and d-excess at Norwich, Dublin and Birmingham.*

(i)

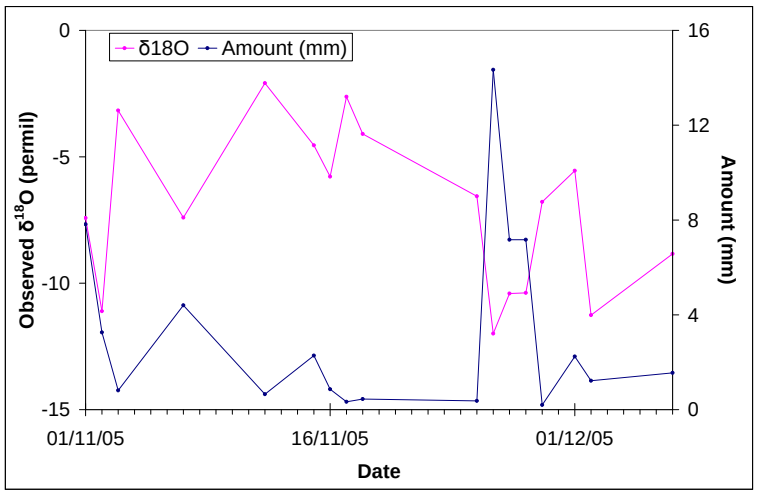

(ii)

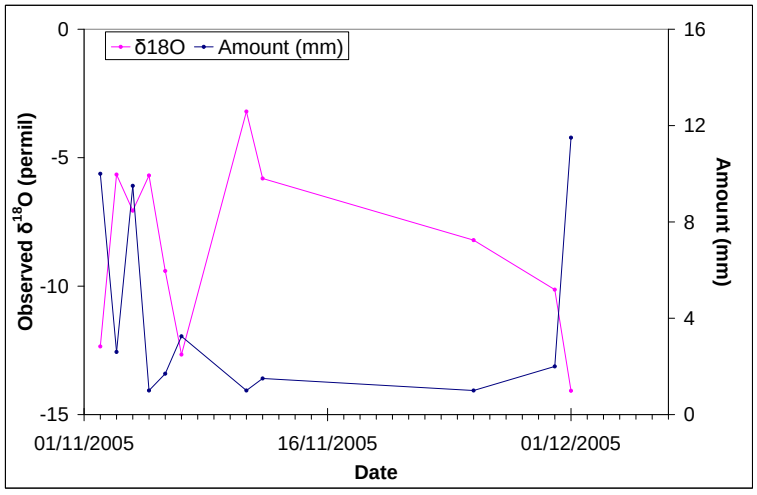

(iii)

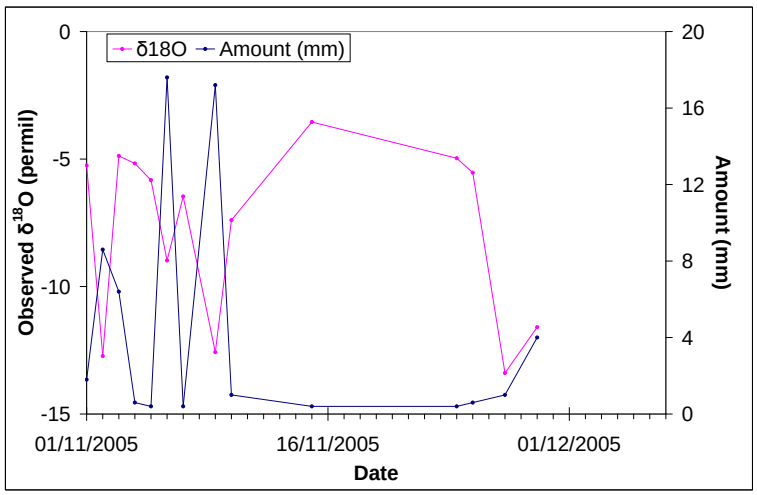

Figure 4.4: *Time series of observed $\delta^{18}O$ and precipitation amount at (i) Norwich, (ii) Dublin and (iii) Birmingham across the collection period.*

data points (y = 7.87x + 14.32) that shows a shift of 4 ‰ towards higher d-excess values. These higher values are caused by lower relative humidity conditions over the water vapour source regions due to the lower temperatures experienced in the winter months. This lower relative humidity causes a greater component of the fractionation process to be made up of kinetic fractionation, which affects oxygen and hydrogen isotopes differently (Rozanski et al., 1993). There are four samples whose d-excess values fall below the GMWL, 3 from Norwich (03/11, 12/11 and 15/11) and 1 from Birmingham (03/11). Example trajectories from these days and locations are shown in figure 4.6. The example time chosen best depicts the conclusion drawn and explained next, though other trajectories for the same days and locations are extremely similar. d-excess values lower than the GMWL theoretically occur due to a portion of the water vapour having been sourced from continental reevaporation (Rozanski et al., 1993). The modelled trajectories for Birmingham (03/11/05) travelled over the Atlantic and then to Birmingham across Devon and Cornwall. For the Norwich low d-excess values: on 3/11/05 some of the modelled trajectories passed over North Spain and part of France before reaching Norwich; the trajectories for 12/11/2005 all arrived at the U.K. in Devon before traversing the country to reach Norwich; and on 15/11/2005 the trajectories arrived from slightly further North but still crossed the British Isles before reaching Norwich. These were by no means the only cases where trajectories passed across the British Isles, but the deuterium excess values suggest that these were the only occasions when a significant amount of water vapour was gained from the British Isles before the precipitation event at the respective sites. It should, however, be noted that though d-excess values may be used as an indication of water vapour source, there are other factors involved that may complicate the situation beyond this simple interpretation.

4.6 Modelling the Observed Isotopic Composition

To obtain a modelled value for the isotopic composition of precipitation on any one day, FLEXPART was run using 100 independent particles each released from a slightly different location in a 0.1° by 0.1° by 100 m box over the respective sampling site. These par-

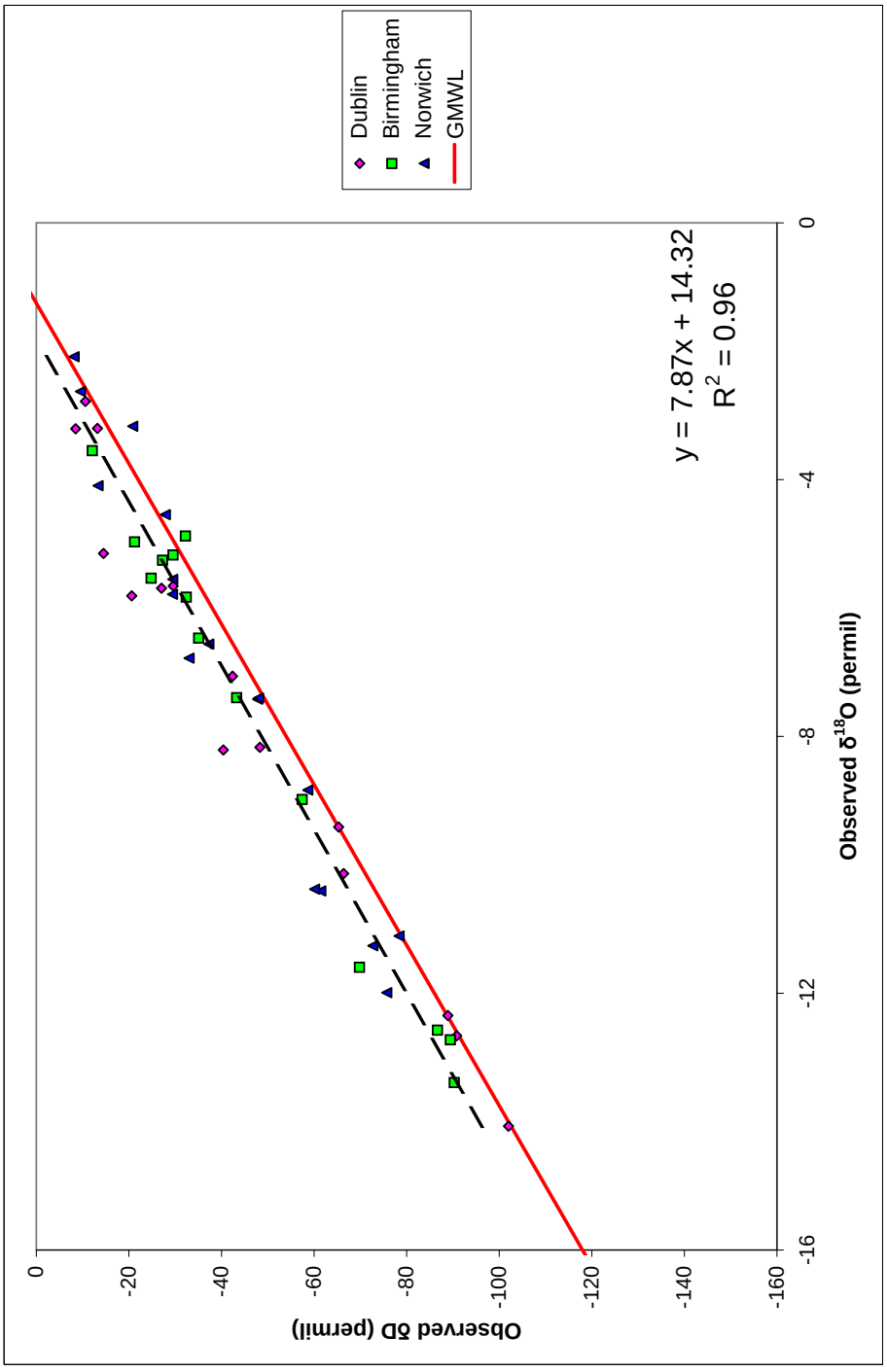

Figure 4.5: *Observed $\delta^{18}O$ versus δD for Dublin (pink), Birmingham (green) and Norwich (blue) raindays in November and December 2005. The Global Meteoric Water Line (red line) is the general ($\delta D = 8*\delta^{18}O + 10$) relationship between the two variables. The black dashed line is the Meteoric Water line for the British Isles for November and December 2005 whose equation is given in the lower right hand corner. The observational errors are 2 $^{\circ}/_{\circ\circ}$ for δD and 0.02 $^{\circ}/_{\circ\circ}$ for $\delta^{18}O$.*

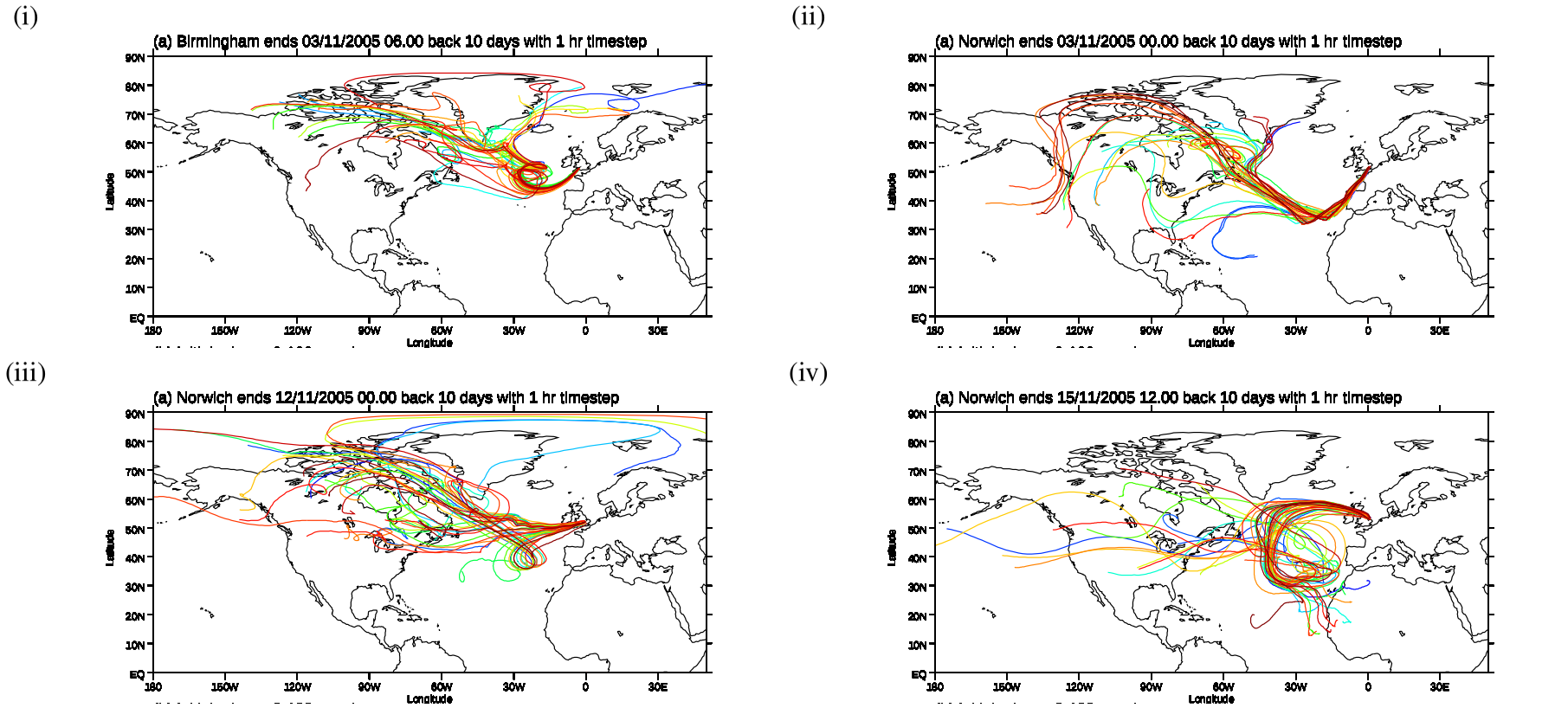

Figure 4.6: *FLEXPART trajectories for (i) Birmingham at 0600 on the 3rd November 2005, (ii) Norwich at 0000 on the 3rd November 2005, (iii) Norwich at 0000 on the 12th November 2005, and (iv) Norwich at 1200 on the 15th November 2005 when d-excess values below the Global Meteoric Water Line were observed due to re–evaporation during final days' travel across the British Isles.*

ticles then traced a trajectory 10 days backwards in time according to ECMWF ERA-40 windfields. Along each of the 100 trajectories information was recorded by FLEXPART about the temperature, pressure and humidity experienced. These atmospheric parameter trajectories provided the input for the MCIM to produce an isotopic value for each of the 100 particles for the initial time point that the particles were released at by FLEXPART. These 100 values are highly variable, for example the δ^{18}O values for the 100 runs for Norwich on the 7th November 2005 at 1200 ranged from a maximum of -5.09 ‰ to a minimum of -11.74 ‰. This variation is caused by the slightly different initial location of each particle, meaning that each particle has a different trajectory experiencing different conditions. The variation also shows the importance of modelling multiple trajectories rather than just a single path as has been used previously. Any small error in the windfields or starting location could have a large impact on the results.

These 100 final isotopic values were then averaged to create a single modelled isotopic value for that date and time. Four model runs were conducted within each 24 hour sampling period at 1800 hours on the day preceding the collection and then 0000, 0600 and 1200 hours on the sampling day. The 4 final results of each of these model runs were then averaged to create a daily modelled value to compare with the daily observed value. Parameters within the model were varied to assess sensitivity. The results of these tests can be seen in Chapter 5.

As Dublin is the most westerly of the 3 sites in this case study it would be expected for it to experience generally less negative isotopic values due to the predominant westerly winds over the U.K. However Dublin actually recorded the most negative δ^{18}O value of -14.07 ‰ on the 1st December 2005, and Norwich, the most easterly site, recorded the least negative δ^{18}O value of -2.08 ‰ on the 12th November 2005. The FLEXPART trajectories produced for these days and locations provided a partial explanation for this. The trajectories ending in Dublin at 0600 on the 1st December 2005 passed over the centre of the Greenland plateau, the only occasion during this case study where the majority of trajectories took this path, (figure 4.7). This would be expected to greatly deplete the air parcels of heavier isotopes due to a combination of rainout across the high altitude areas

and a lack of heavy isotopes present in the ambient atmospheric water vapour mixed into the air parcels. Trajectories arriving at Dublin at 0000 and 1200 hours on the 1st December 2005 also took this path. The situation that caused the least negative δ^{18}O value of -2.08 ‰ to be seen in Norwich is slightly less clear. The trajectories seen for 1800 hours on the 11th November 2005 and 0000, 0600 and 1200 hours on the 12th November 2005 are all different from each other in small scale features (figure 4.8). The only similarities are that they all approach the U.K. from the Atlantic and were sourced over North America. The trajectories for 1800 and 0000 hours did approach the U.K. from the Azores so would be expected to have picked up less depleted water vapour (figure 4.8). However, this path via the Azores was not unusual for November 2005 so it is not conclusive from the trajectory paths as to why this situation should cause the least negative δ^{18}O value seen. Mean sea–level pressure and front charts for the 10th and 11th November 2005 at 1200 (figure 4.9) show a cold front over Norwich at 1200 on the 10th November 2005 and then an intense low pressure system whose cold front is approaching Norwich on the 11th November 2005 at 1200. Gedzelman and Lawrence (1990) observed that the highest δ values of a low pressure synoptic situation occur in the warm sector at the edge of the system which is where Norwich appears to be sited on the 11th November 2005 from figure 4.9 and where most likely it was positioned for the majority of that day. Rain did not fall at either Dublin or Birmingham on this day to allow comparisons across this system but it would appear that the location of the low pressure system with respect to Norwich is what caused the particularly high δ values to be seen.

4.6.1 Norwich

Over the course of the sampling period Norwich experienced 17 raindays when precipitation amount was sufficient to analyse for its isotopic composition. The observed δ values ranged from a maximum of δ^{18}O = -2.09 ‰ and δD = -8.16 ‰ on the 12th November 2005 to a minimum of δ^{18}O = -11.99 ‰ and δD = -75.71 ‰ on the 26th November 2005. Figure 4.10 shows the modelled δ^{18}O, δD and d-excess values for each of the 17 days against the observed δ^{18}O, δD and d-excess values for the same day in

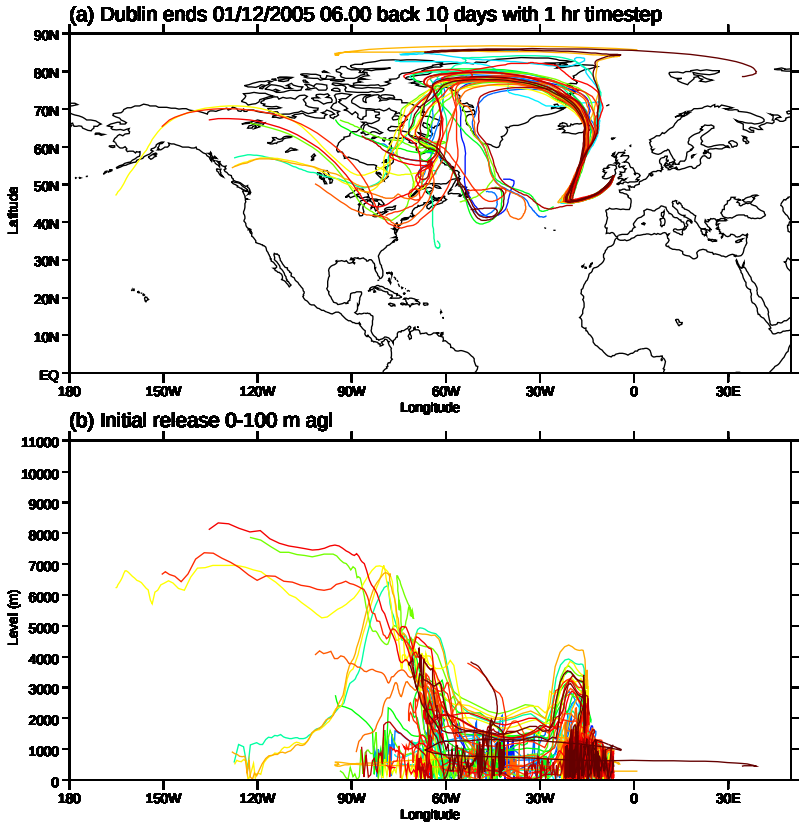

Figure 4.7: *FLEXPART trajectories for Dublin 0600 on the 1st December 2005, when the most negative $\delta^{18}O$ value was observed.*

(i)

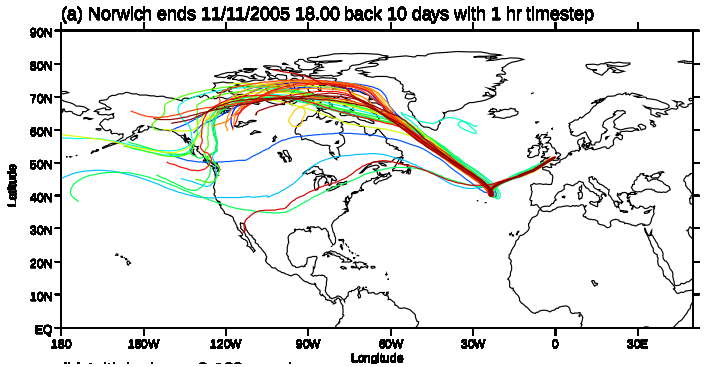

(ii)

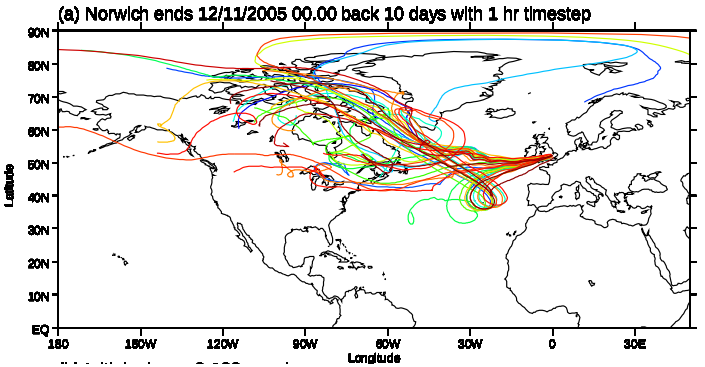

(iii)

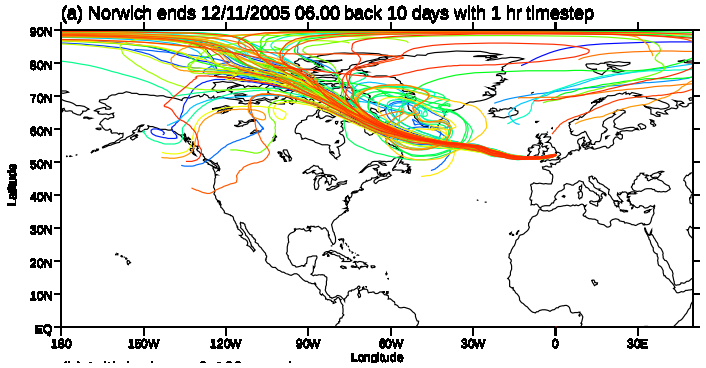

(iv)

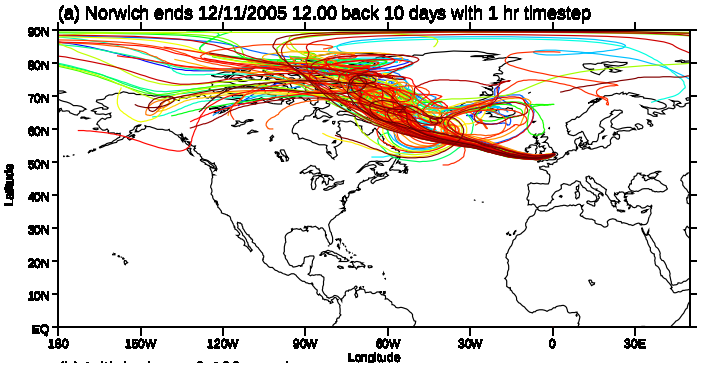

Figure 4.8: *FLEXPART trajectories for Norwich at (i) 1800 on the 11th November 2005, and (ii) 0000 on the 12th November 2005 when the least negative $\delta^{18}O$ value was observed.*

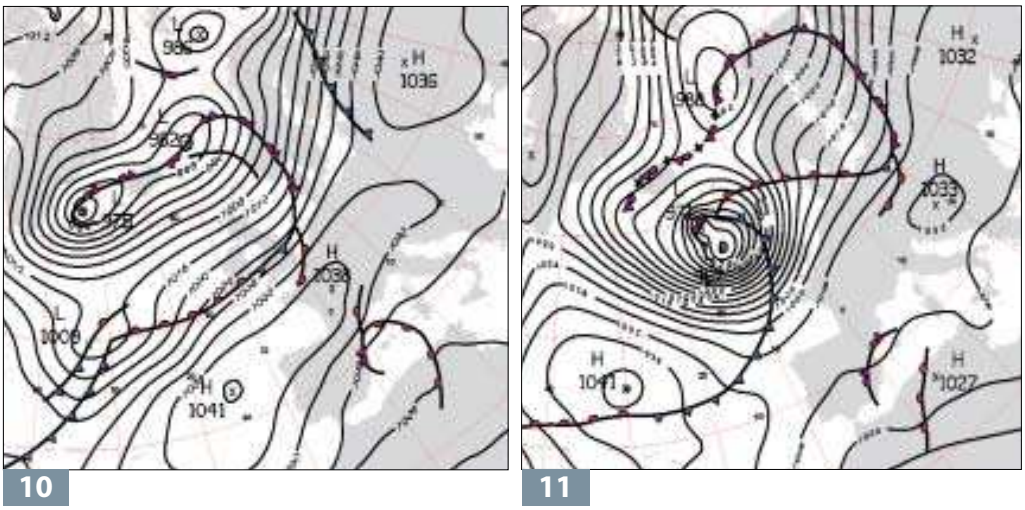

Figure 4.9: *Mean sea–level pressure and fronts charts for 10th and 11th November 2005 at 1200 UTC when the least negative $\delta^{18}O$ value was observed.*

blue. Modelled errors are shown by the vertical black lines above and below each point. These errors are the standard deviation of the 400 modelled δ^{18}O, δD and d-excess values (1 for each particle) for each day, showing the range across the particles as described in section 4.6. Observed errors induced by the mass spectrometry are negligible at 2 $^{\circ}/_{\circ\circ}$ for δD and 0.02 $^{\circ}/_{\circ\circ}$ for δ^{18}O. However, there is an observed error caused by sampling that must be considered. The modelled value is valid for a 0.1° x 0.1° grid box whereas the observed value is a point sample. Where samples were taken and analysed for multiple Norwich sites then the magnitude of this error can be estimated as a standard deviation of these values. Where this information exists it has been shown as black horizontal lines from the data point. The lack of observed errors on the other points does not indicate that there was no error, but only that there is not sufficient data available to allow it to be quantified.

Also on these graphs (figure 4.10) is a red line that shows the ideal observed = modelled (y=x) situation. It can be seen immediately that the data sets do not match the ideal. The regression equations for the best fit lines of these three data sets (δ^{18}O, δD and d-excess) have very low correlation coefficients at 0.17, 0.15 and 0.37 respectively. The values for δ^{18}O and d-excess are, however, just significant at the 95% level when compared to the significance threshold of 0.17. The gradient of distribution is too shallow

at 0.09, 0.09 and 0.13 respectively, and for all δ^{18}O, δD and d-excess there is a large offset from the perfect situation of -6.98 ‰, -44.78 ‰ and 10.47 respectively in the modelled results. Jouzel et al. (1997) also saw an underestimation of δ values in the mid–latitudes. The model sensitivity is very low even when considering the possible modelled error. The modelled values ranged from a maximum of δ^{18}O = -6.43 ‰ on the 7th November 2005 and δD = -39.04 ‰ on the 12th November 2005 to a minimum of δ^{18}O = -8.68 ‰ and δD = -58.59 ‰ on the 7th December 2005. The modelled range of δ^{18}O is therefore 2.25 ‰ compared to an observed range of 9.9 ‰. However, the relationship is of the correct sense, with increasing modelled values corresponding to increasing observed values.

Snowfall was observed during the sampling periods for the 25th and 26th November 2005. Snow does not equilibrate with surrounding atmospheric vapour as it falls so will theoretically not be modelled well by the approach used in this study that models the isotopic composition of the lowest 100 m of the atmosphere and assumes equilibration of any rain falling through this layer (section 3.3.4). The 25th and 26th November were therefore removed from the dataset, and the remaining observed and modelled values were compared again, figure 4.11. Removing these 2 data points made very little difference to the relationships seen between the observed and modelled parameters. The gradients of the regression equations for δ^{18}O and δD decreased from 0.09 to 0.07 and both correlations coefficients decreased by 0.05. For d-excess the gradient of the relationship remained constant and the correlation coefficient actually increased by 0.12 (from 0.37 to 0.48). The improvements caused by removing the samples containing snow are therefore greater than the deteriorations so any samples known to contain snow should be removed from any further datasets.

The relationship between observed and modelled isotopic values improved greatly when the raindays with less than 3 mm of precipitation were removed from the data set, see figure 4.12, (δD is not shown due to its similarity to δ^{18}O). The gradient of the best fit lines for δ^{18}O and d-excess increased from 0.07 and 0.13 to 0.35 and 0.17 respectively, and both relationships are significant at the 95% level. The days where less than 3 mm of

(i)

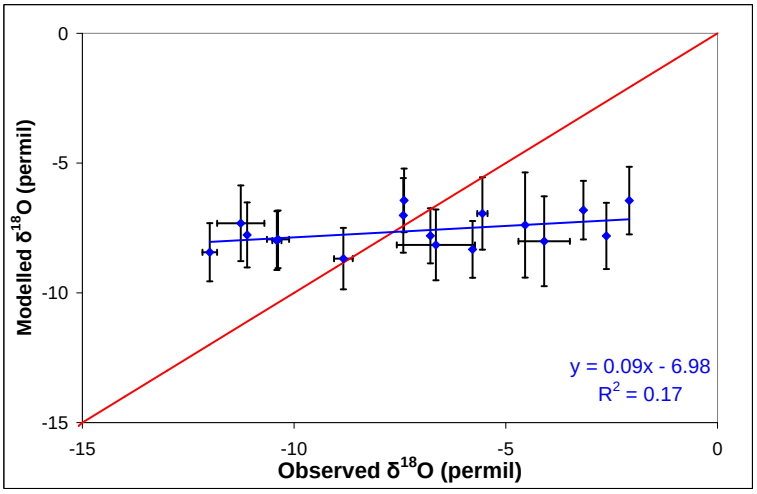

(ii)

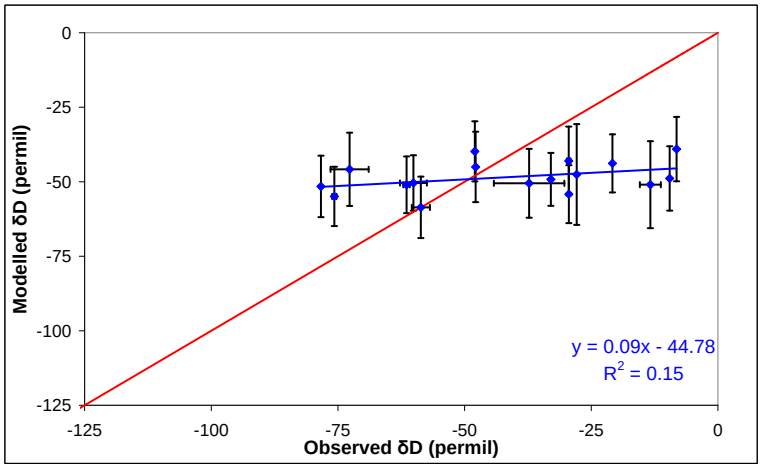

(iii)

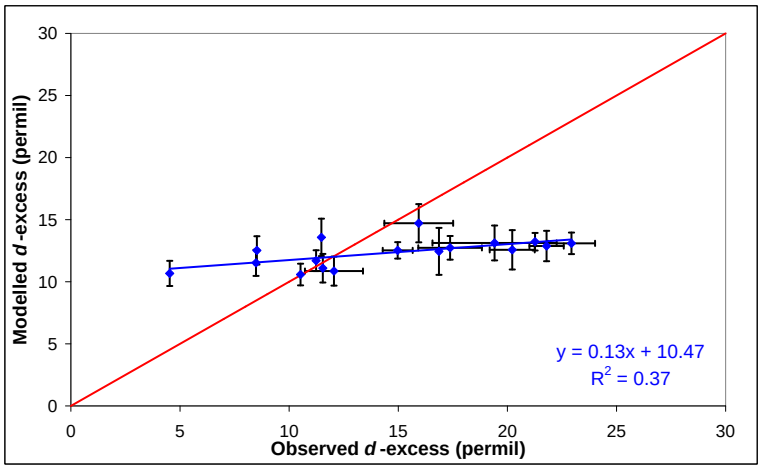

Figure 4.10: *Observed versus modelled for all Norwich raindays for (i) $\delta^{18}O$, (ii) δD, and (iii) deuterium excess, shown in blue, with the regression equation and correlation coefficient shown in the bottom right hand corner. Observed and modelled errors are represented by horizontal and vertical black lines from each data point. The red line in each graph is the optimum 1:1 line.*

(i)

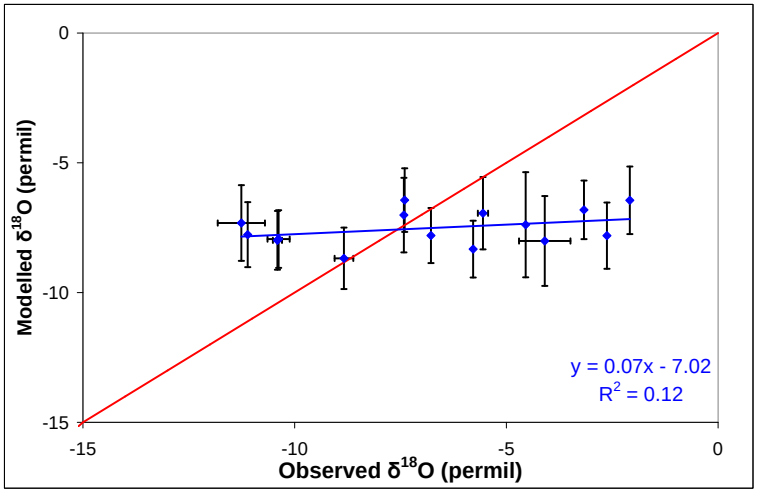

(ii)

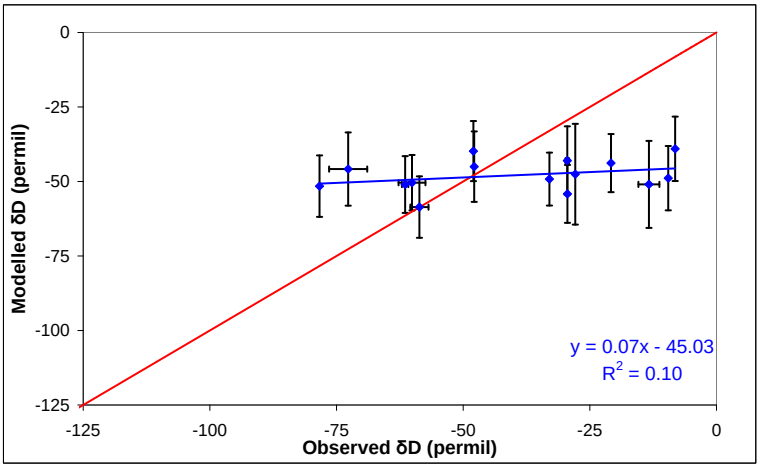

(iii)

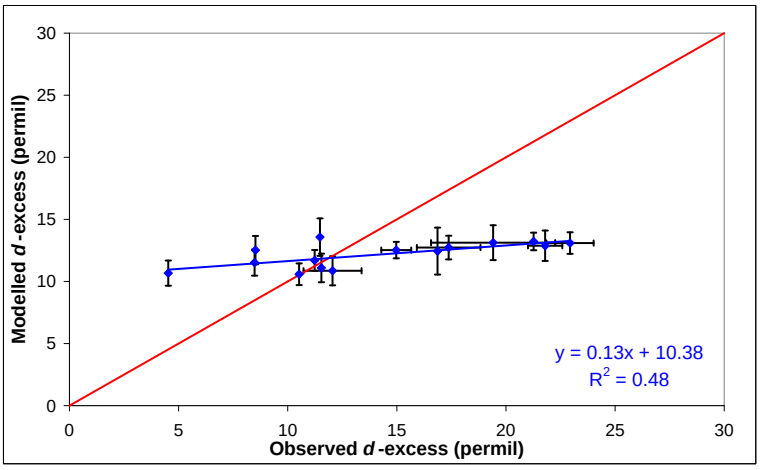

Figure 4.11: *Observed versus modelled for Norwich raindays where no snow occurred (i) $\delta^{18}O$, (ii) δD, and (iii) deuterium excess, shown in blue, with the regression equation and correlation coefficient shown in the bottom right hand corner. Observed and modelled errors are represented by horizontal and vertical black lines from each data point. The red line in each graph is the optimum 1:1 line.*

precipitation occurred were removed because:-

1. There is a greater chance of isotopic exchange with atmospheric vapour occurring when the sample bottles were not full to the top as happened on days where less than 3 mm of rain was recorded.

2. The model resolution is limited by the ECMWF ERA-40 windfields so larger synoptic systems are modelled more accurately than small systems and during the winter months especially it is the larger ones that will produce more precipitation over one location.

3. Slight positional errors of the systems are to be expected, therefore if a site falls at the edge of an actual system and therefore receives only minimal precipitation, it is possible that the modelled system would miss the site entirely.

The application of this model is ultimately intended to be in interpreting annual or decadal averages of δ^{18}O and δD preserved in speleothems or similar archives. The 6 raindays where more than 3 mm of rainfall occurred account for 80% of the total rainfall amount at Norwich. The isotopic signature of these 6 days would therefore dominate any recording of this month's isotopic value.

4.6.2 Dublin

During November 2005, Dublin experienced precipitation on 15 days. The observed isotopic ratios ranged from a maximum of $\delta^{18}\text{O} = -2.78$ ‰ and $\delta\text{D} = -10.60$ ‰ on the 15th November 2005 to a minimum of $\delta^{18}\text{O} = -14.07$ ‰ and $\delta\text{D} = -102.00$ ‰ on the 1st December 2005.

To test the model's ability for Dublin rainfall, all modelled values were initially compared with their relevant observed value. Figure 4.13 shows the results of these comparisons. Each day's values are represented by a blue point, with the modelled error shown by the vertical black lines. No observed error can be calculated for Dublin due to the lack of multiple samples for the same day and different locations. A best fit line was fitted to

(i)

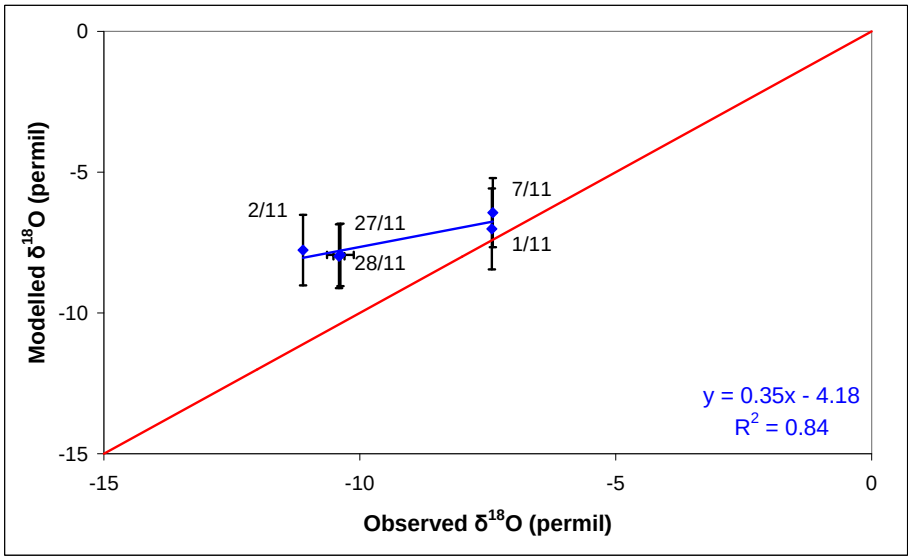

(ii)

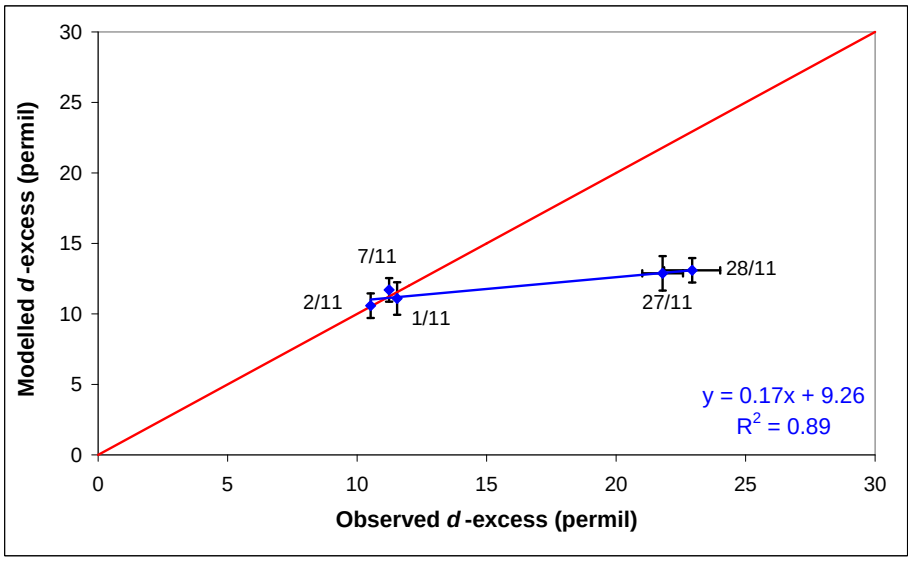

Figure 4.12: *Observed versus modelled for Norwich raindays where the amount of rain was greater than 3 mm (i) $\delta^{18}O$, (ii) deuterium excess, shown in blue, with the regression equation and correlation coefficient shown in the bottom right hand corner. Observed and modelled errors are represented by horizontal and vertical black lines from each data point. The red line in each graph is the optimum 1:1 line.*

(i)

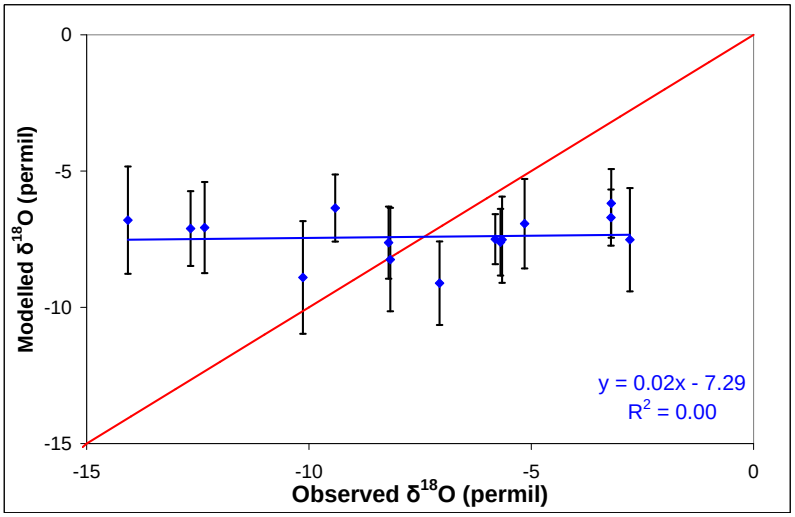

(ii)

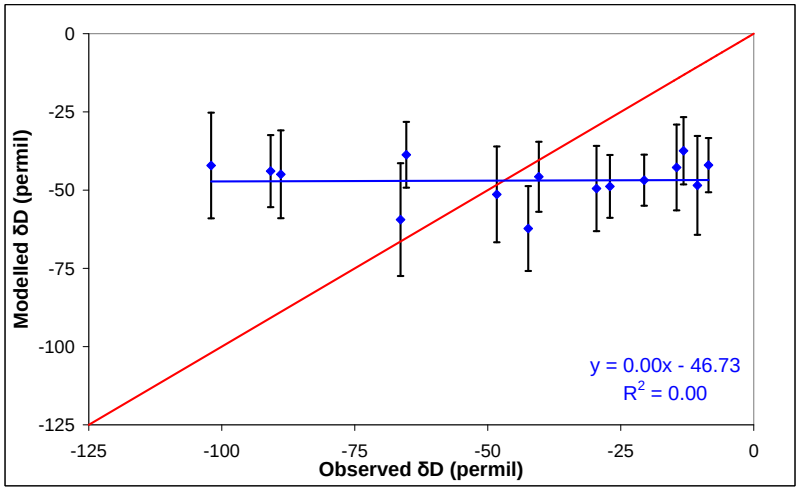

(iii)

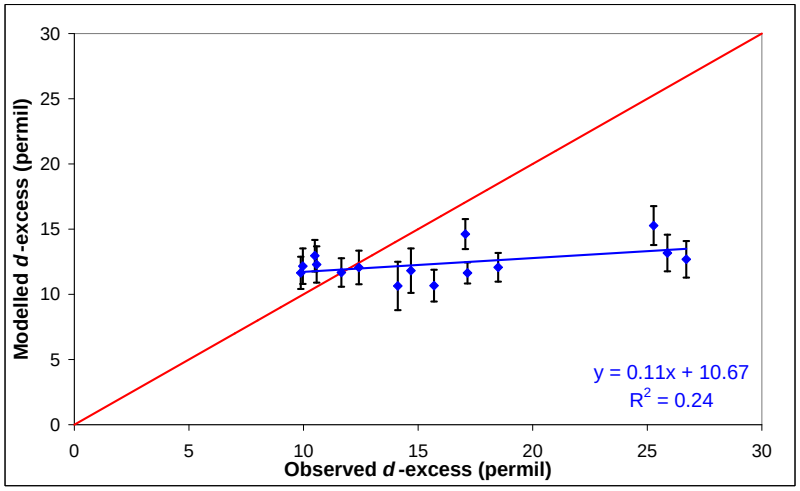

Figure 4.13: *Observed versus modelled for all Dublin raindays for (i) $\delta^{18}O$, (ii) δD, and (iii) deuterium excess, shown in blue, with the regression equation and correlation coefficient shown in the bottom right hand corner. Modelled errors are represented by vertical black lines from each data point. The red line in each graph is the optimum 1:1 line.*

these data points (blue line) and a regression equation given for this line (shown in the bottom right of each graph in figure 4.13). The regression equations were y = 0.02x -7.29 for δ^{18}O, y = 0.00x -46.73 for δD and y = 0.11x + 10.66 for d-excess. Both of these equations illustrate the very small gradients of the best fit lines and the large offset of the modelled values. The d-excess correlation is significant at the 90% level, but this was the only significant relationship. With the Norwich data, introducing a threshold of daily precipitation of 3 mm greatly improved the results. However, this is not the case for the Dublin data. In fact a negative relationship is seen between observed and modelled δ^{18}O for days where more than 3 mm of precipitation fell (figure 4.14). Unfortunately there were only 4 days out of the 15 raindays with greater than 3 mm of rainfall, which is too small a data set from which to draw any robust conclusions.

4.6.3 Birmingham

There were 14 raindays at Birmingham during November 2005. The observed isotopic ratios ranged from a maximum of δ^{18}O = -3.54 ‰ and δD = -12.10 ‰ on the 15th November 2005 to a minimum of δ^{18}O = -13.39 ‰ and δD = -90.3 ‰ on the 27th November 2005.

Modelled and observed isotopic values for all Birmingham raindays were compared. Figure 4.15 shows the modelled values versus the observed values of δ^{18}O, δD and d-excess for all Birmingham raindays as blue points with the best fit line of these points shown in blue. Modelled errors are also shown by vertical black lines. No observed error caused by sampling resolution can be shown due to the lack of measurements at multiple Birmingham sites. The regression equations of the best fit lines are y = 0.06x -6.92 for δ^{18}O, y = 0.06x -44.18 for δD and y = 0.29x +7.74 for d-excess (bottom right of graphs in figure 4.15). Neither the δ^{18}O nor the δD observed to modelled relationship is significant. However, the d-excess regression equation is significant at the 95% level. The δ^{18}O and δD equations, as for the Norwich data, show the small gradient of the relationship and the large offset of the modelled values. The d-excess equation is closer to the ideal of y = x though still has too shallow a gradient.

(i)

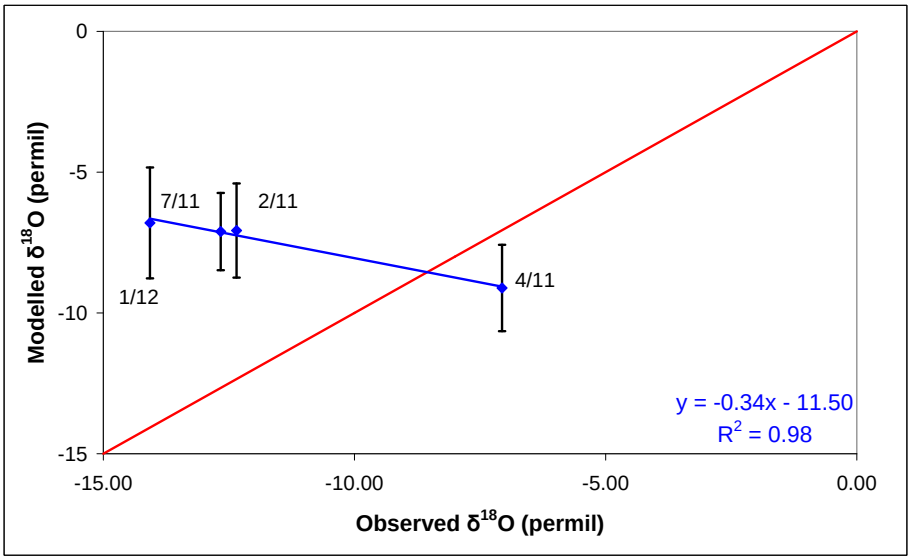

(ii)

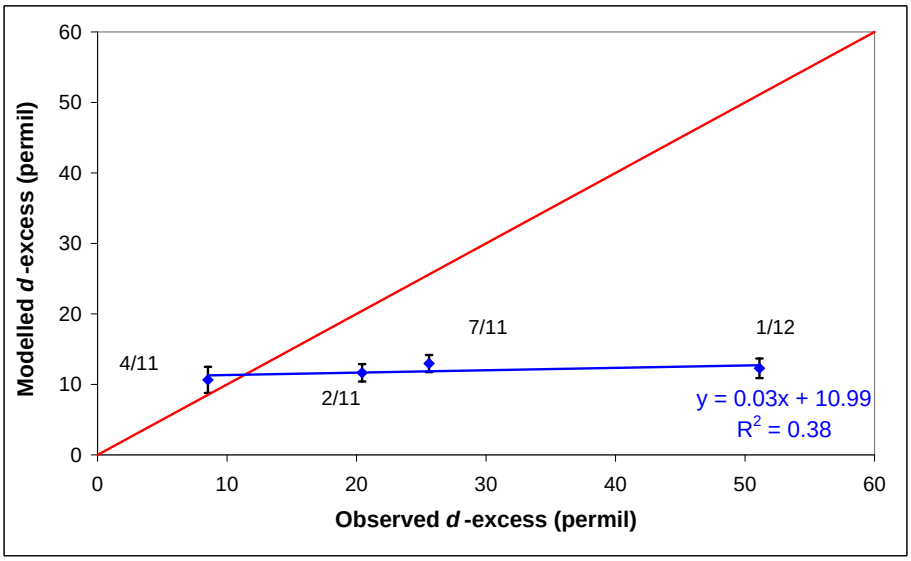

Figure 4.14: *Observed versus modelled for Dublin raindays where the amount of rain was greater than 3 mm (i) $\delta^{18}O$, (ii) deuterium excess, shown in blue, with the regression equation and correlation coefficient shown in the bottom right hand corner. Modelled errors are represented by vertical black lines from each data point. The red line in each graph is the optimum 1:1 line.*

(i)

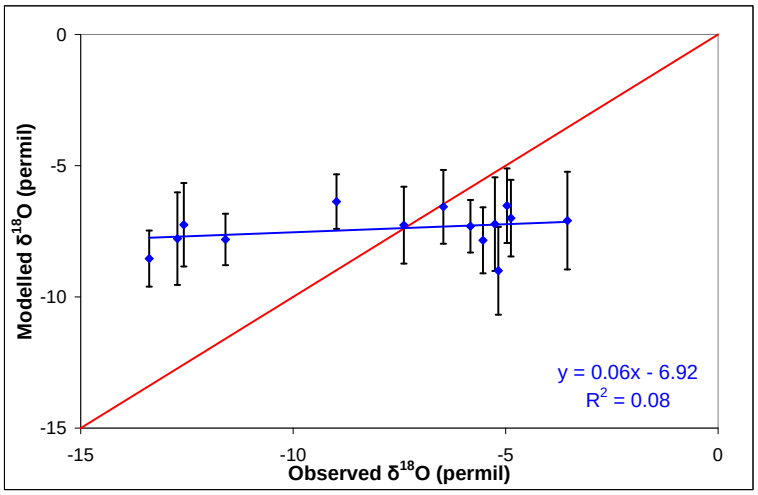

(ii)

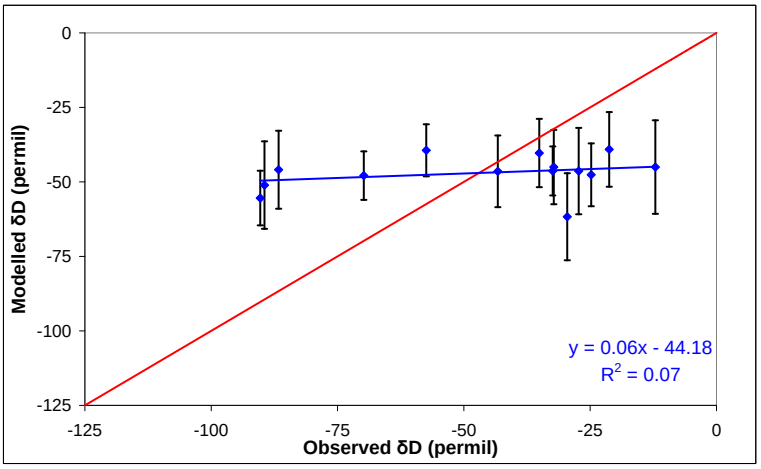

(iii)

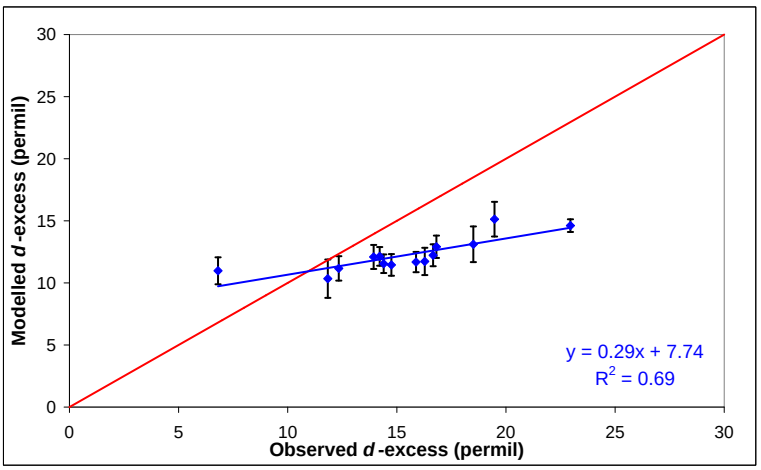

Figure 4.15: *Observed versus modelled for all Birmingham raindays for (i) $\delta^{18}O$, (ii) δD, and (iii) deuterium excess, shown in blue, with the regression equation and correlation coefficient shown in the bottom right hand corner. Modelled errors are represented by vertical black lines from each data point. The red line in each graph is the optimum 1:1 line.*

Figure 4.16 shows the results for δ^{18}O and d-excess when the data is filtered to include only days when more than 3 mm of precipitation occurred. This filtering leaves only 5 of the 14 data points to be compared. The results of this filtered comparison are much improved as was the case for Norwich. Unlike the Dublin data, a positive relationship is seen for all the δ^{18}O, d-excess and deuterium excess values. The deuterium excess modelled to observed relationship is significant at the 95% level even with only 5 data points. The new regression equations are y = 0.10x -6.19 for δ^{18}O and y = 0.24x +8.74 for d-excess, only slightly altered from the initial comparison regression equations.

4.6.4 Inter–site Comparison

Across the sampling period there were 6 days when precipitation occurred at all three sites. The observed δ^{18}O values for all three sites for these 6 days are summarised in table 4.2. On the 2nd November 2005 all three sites recorded δ^{18}O values within 1.5 $^{\circ}/_{\circ\circ}$ of each other. The FLEXPART trajectories within this day were very similar between all sites for all times throughout the day (e.g. trajectory maps for Dublin, Birmingham and Norwich at 1800 on the 2nd November 2005 were all very similar). The more negative δ values experienced on the 2nd November at all sites can be attributed to the majority of trajectories being sourced further to the north and approaching the U.K. from the west. Examples of this trajectory situation from Norwich and Dublin are shown in figure 4.17.

The 7th November 2005 saw Dublin precipitation have a very negative δ^{18}O value of -12.66 $^{\circ}/_{\circ\circ}$ while Birmingham and Norwich δ^{18}O values were -6.47 and -7.40 $^{\circ}/_{\circ\circ}$ respectively, a difference of at least 5 $^{\circ}/_{\circ\circ}$. The FLEXPART trajectories for the 7th November 2005 are similar across the sites and times in their approach to the U.K. across the Atlantic. However, the source regions of the particles vary for the 1800 and 0000 hour trajectories. For Dublin the trajectories at both these times originate mainly over the Davis Strait between Greenland and North Canada. For Norwich the 1800 hour trajectories mainly originate in this region as well whereas the Norwich 0000 and Birmingham 1800 and 0000 hour trajectories originate further south in North America. This variation in source region would explain the most negative values being seen in Dublin where all

(i)

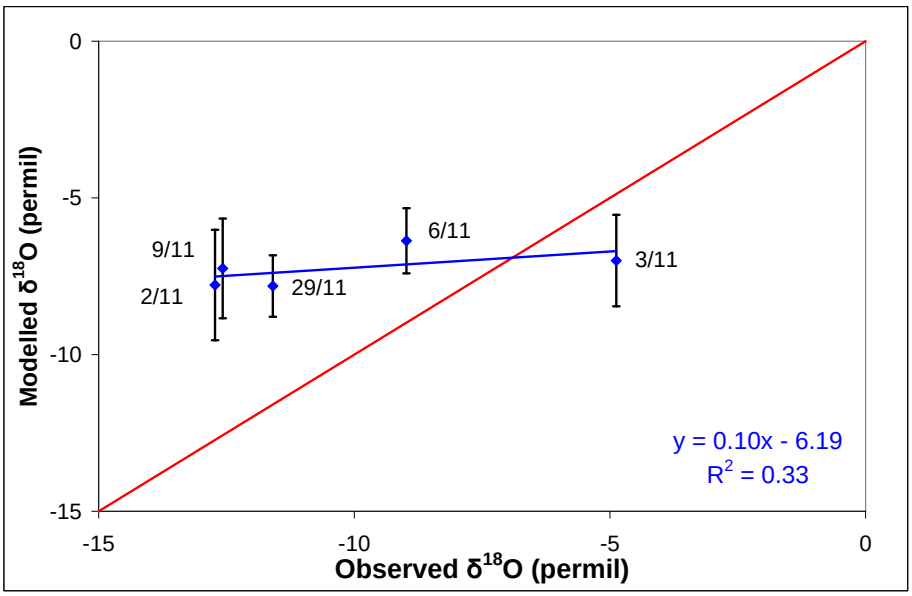

(ii)

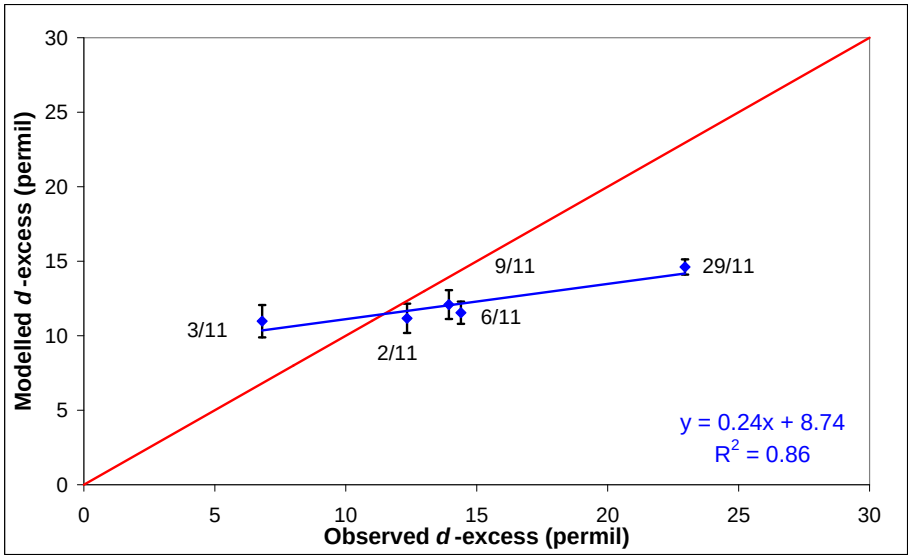

Figure 4.16: *Observed versus modelled for Birmingham raindays where the amount of rain was greater than 3 mm (i) $\delta^{18}O$, (ii) deuterium excess, shown in blue, with the regression equation and correlation coefficient shown in the bottom right hand corner. Modelled errors are represented by vertical black lines from each data point. The red line in each graph is the optimum 1:1 line.*

(i)

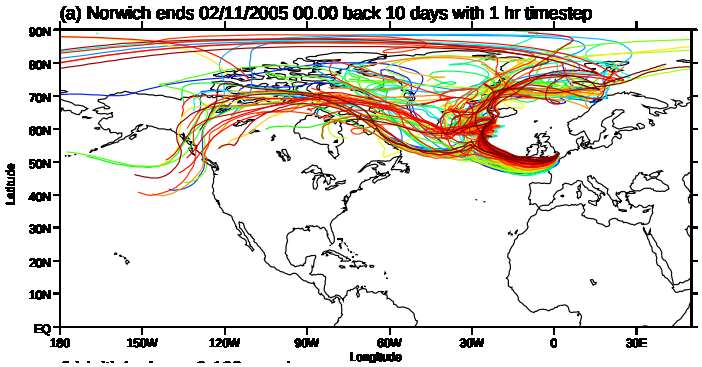

(ii)

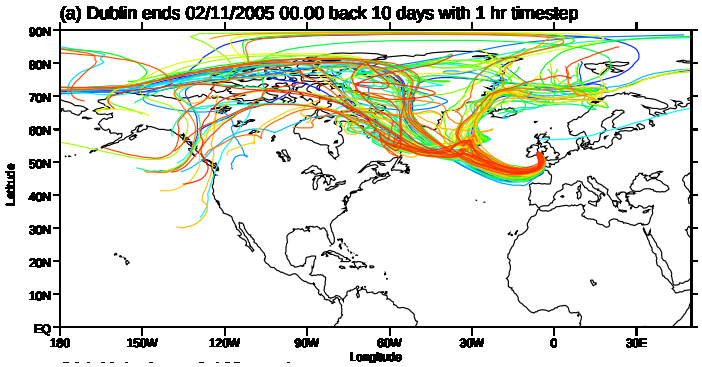

Figure 4.17: *FLEXPART trajectories at 0000 on the 2nd November 2005 for (i) Norwich and (ii) Dublin, when rain occurred at all three British Isles sites.*

trajectories came from the very cold sea near Greenland. The least negative values being seen in Birmingham where the most trajectories start further south. Norwich received a mix of trajectories from both locations and so its isotopic composition fell in between that of the other two sites.

The other days saw ranges of values between these two extremes and were the 3rd, 15th, 25th and 29th November 2005. Other studies (for example Barras and Simmonds (2008); Rindsberger et al. (1990)) were able to look at how isotopic composition varied across low pressure systems (in Tasmania and Israel respectively) by using multiple collection sites. The synoptic situations on the days where precipitation occurred at all three sites for this case study were not resolved sufficiently to allow this sort of analysis to be undertaken. There is no consistent pattern of which of the three sites experienced the most negative value when all three sites received precipitation on the same day but source region appears to influence the δ values.

Comparing all the modelled and observed data for the three locations together shows no coherent relationship between the data, even for those days where more than 3 mm of precipitation fell (figure 4.18). Therefore there are most likely different factors controlling the isotopic signal at each of these three sites and furthermore at any further sites studied with this model. Each site must therefore be investigated separately.

As source region plays an important part in controlling the isotopic ratios, the isotopic ratios at the start and end of the trajectories were compared for Norwich, Dublin and Birmingham (figure 4.19). There was no correlation seen between these two variables at any of the three sites. Mixing in of ambient air along the trajectories must therefore mask the initial atmospheric δ value. This result re–enforces the need to model the entire

Date	Dublin	Birmingham	Norwich
02/11/2005	-12.35	-12.72	-11.11
03/11/2005	-5.66	-4.88	-3.17
07/11/2005	-12.66	-6.47	-7.40
15/11/2005	-2.78	-3.55	-4.55
25/11/2005	-8.21	-5.53	-6.65
29/11/2005	-8.17	-11.59	-6.78

Table 4.2: *Observed $\delta^{18}O$ for Dublin, Norwich and Birmingham on days where precipitation was experienced at all three sites.*

(i)

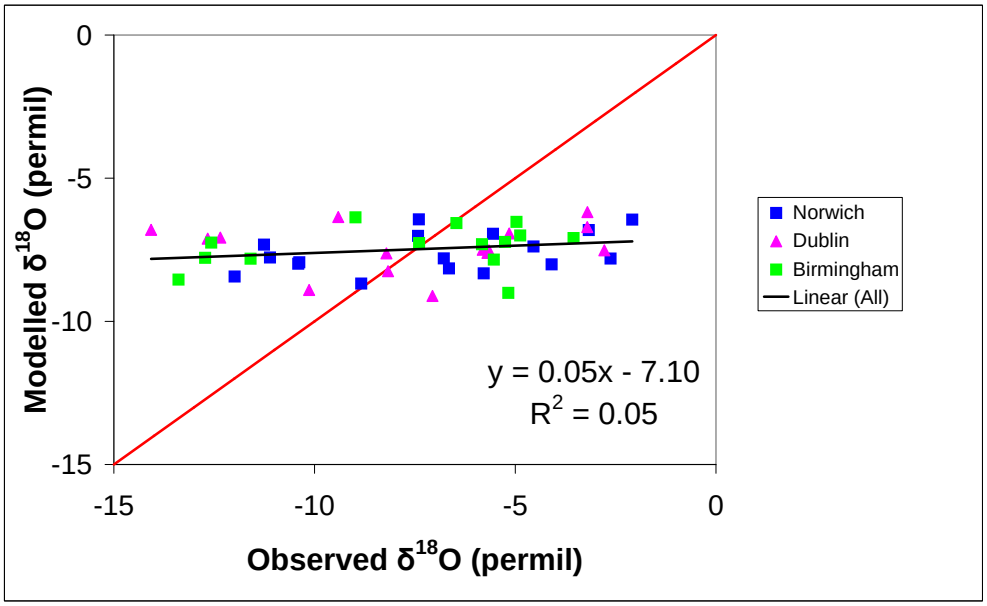

(ii)

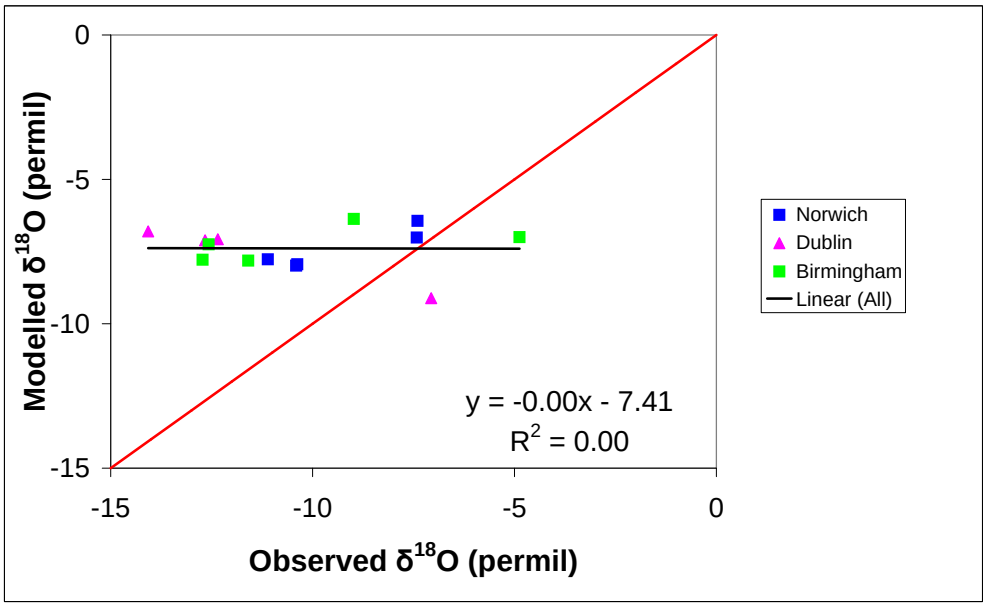

Figure 4.18: *Modelled versus observed $\delta^{18}O$ for (i) all raindays and (ii) raindays with over 3 mm at Norwich (blue), Dublin (pink) and Birmingham (green). The best fit line for all data points is shown in black. The regression equation and correlation coefficient of the best fit line are shown in the bottom right of the graph. The red line is the optimum 1:1 line.*

trajectory and to go far enough back in time so that sufficient mixing in is allowed to occur.

4.6.5 Observed and Modelled Monthly Averages

As the ultimate application of this model would be in interpreting annual or decadal averages of δ^{18}O and δD in palaeoarchives, the observed and modelled averages of all precipitation events were calculated (table 4.3). For all sites the modelled and observed averages for δ^{18}O and δD are very similar. This suggests that even though the model is not producing values of a sufficient range, it is modelling the average conditions well. As an application for this model would be in interpreting seasonal, annual and decadal proxy records this result is very promising.

At all sites the average modelled d-excess is too low when compared with the average observed. This suggests that the kinetic fractionation processes are not being correctly modelled. Cappa et al. (2003) experimentally investigated kinetic effects during evaporation and concluded that the diffusion coefficients used by Merlivat and Jouzel (1979) to calculate the kinetic fractionation in clouds may be incorrect. Merlivat (1978) suggested the use of the diffusion coefficients of 0.9723 for δ^{18}O and 0.9755 for δD which are used in the MCIM (section 3.4.1). Cappa et al. (2003) found these coefficients to be 0.9691 for δ^{18}O and 0.9839 for δD. This is due to surface cooling effects not being accounted for in previous experiments (such as Brutsaert (1975) and Flothmann et al. (1977)). Instead the temperature of the bulk of the liquid was used, which is different from that of the surface layer by around 0.5°C (Schmidt et al., 2005). Schmidt et al. (2005) found that using the Cappa diffusion coefficients raised d-excess values by around 3 $^{\circ}/_{\circ\circ}$ but also reduced the correlation between observed and modelled global fields. The GISS ModelE GCM used by Schmidt et al. (2005) to test this new scheme included evaporation from the sea surface where the impacts of the new scheme are highest. As there is no evaporation from the sea surface in the model used in this study, changes caused by using the Cappa diffusivities would most likely be smaller. However, the Cappa scheme would be likely to raise d-excess values and therefore should be tested. However, adapting and testing the model to

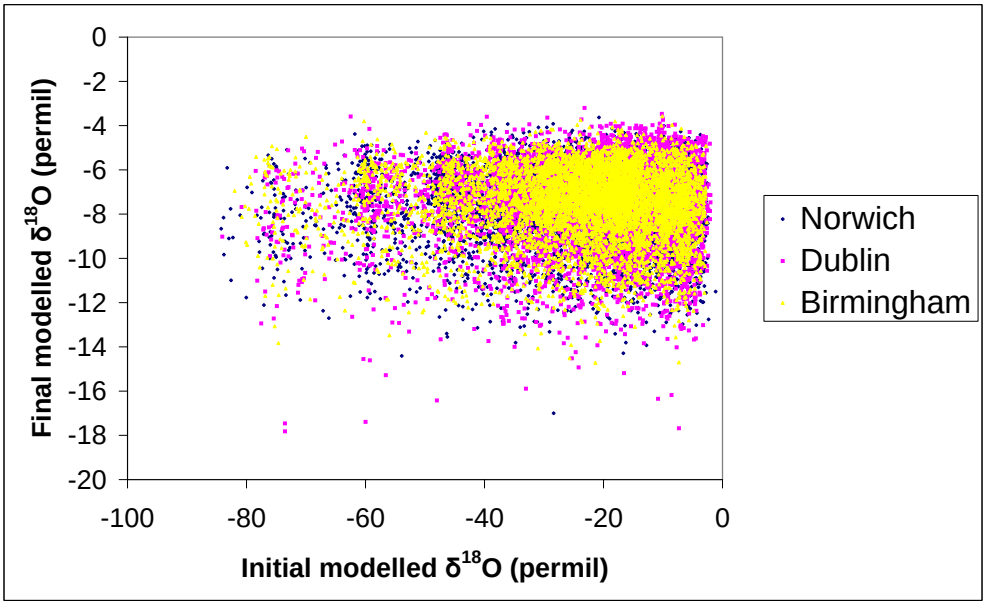

Figure 4.19: *Comparison of modelled $\delta^{18}O$ at the start and end of each individual trajectory at Norwich (navy), Dublin (pink) and Birmingham (yellow).*

include this scheme is outside the scope of the present study.

4.7 Trajectory Analysis

To look in more detail at the trajectory information, all trajectories for Norwich, Dublin and Birmingham were divided into categories according to:

1. Main direction taken by the trajectories in the days preceding the precipitation event.

2. Spread of the 100 trajectories.

3. Main source region.

Site	**Observed**			**Modelled**		
	δ^{18}O (‰)	δD (‰)	d-excess	δ^{18}O (‰)	δD (‰)	d-excess
Norwich	−7.06	−41.85	14.66	−7.60	−48.49	12.34
Dublin	−7.34	−41.53	16.00	−7.41	−46.95	12.36
Birmingham	−8.18	−47.91	15.35	−7.40	−46.97	12.22

Table 4.3: *Mean observed and modelled $\delta^{18}O$, δD and d-excess at Norwich, Dublin and Birmingham.*

The categories for each feature are listed in table 4.4 and examples of main direction and main source region types are shown in figures 4.21 and 4.22 respectively. Although these categories are subjective, it was hypothesised that splitting the trajectories into separate categories and then splitting the modelled versus observed data into these same categories might show a specific process that was less well modelled. This investigation could potentially reveal the location in the model of any errors in how processes are described. Therefore each of the trajectories from each of the 4 times (1800, 0000, 0600 and 1200) were categorised and then each of the 4 was compared with the single observed value from that day. A daily category was not assigned due to very different trajectory patterns being seen across the 4 different modelling times on nearly half of the raindays (differences seen in 8 of 17 days at Norwich, 10 of 15 at Dublin and 6 of 14 at Birmingham). The across day variation in trajectories on 67% of the raindays for Dublin could be part of the reason why Dublin was modelled least well of the three sites, (section 4.6.2).

The results of these tests were inconclusive, often due to extremely small group sizes. For Dublin especially group sizes were either too small to be of use or no correlation was seen. The main feature that did emerge from this test was that isotope ratios from trajectories sourced in North America tended to be the most accurately portrayed for both Norwich and Birmingham (blue points in figure 4.20) though neither relationship was significant. Surprisingly the "Close" trajectories from Norwich produced more accurate isotopic ratios than the "Very Close" category. The "Close" categories had a regression equation of y = 0.2x -6.00 with an r^2 value of 0.26, which is significant at the 95% confidence level, the "Very Close" category showed no relationship at all between observed and modelled values. For Birmingham the "Very Close" trajectories were the best with a regression equation of y = 0.2x -5.99 and an r^2 value of 0.37, which is significant at the 95% confidence level. Trajectories approaching all three sites from the Atlantic direction appeared to create the modelled values that were most closely related to the observed values, though the relationship at Norwich was the only statistically significant one.

(i)

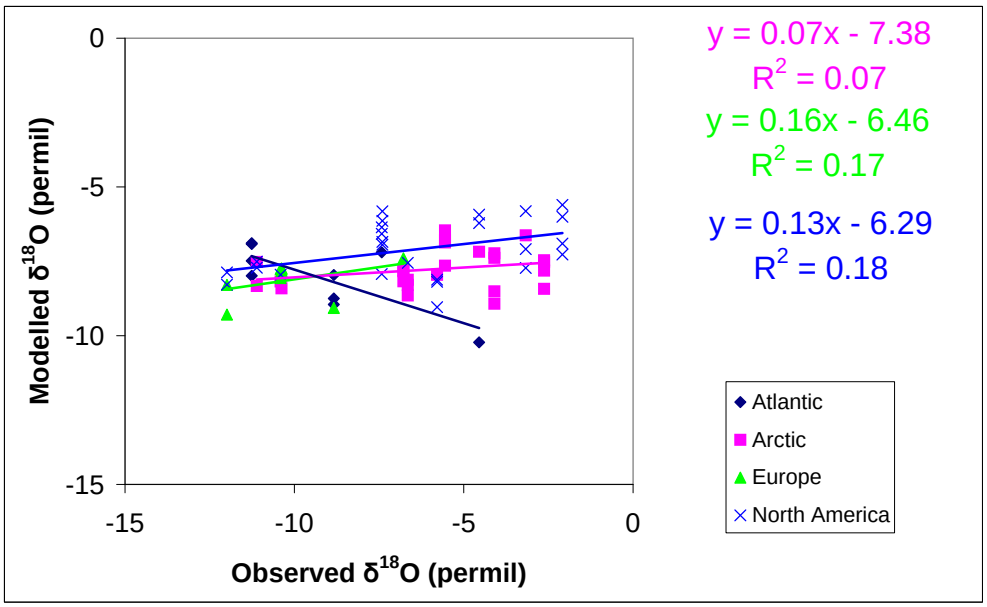

(ii)

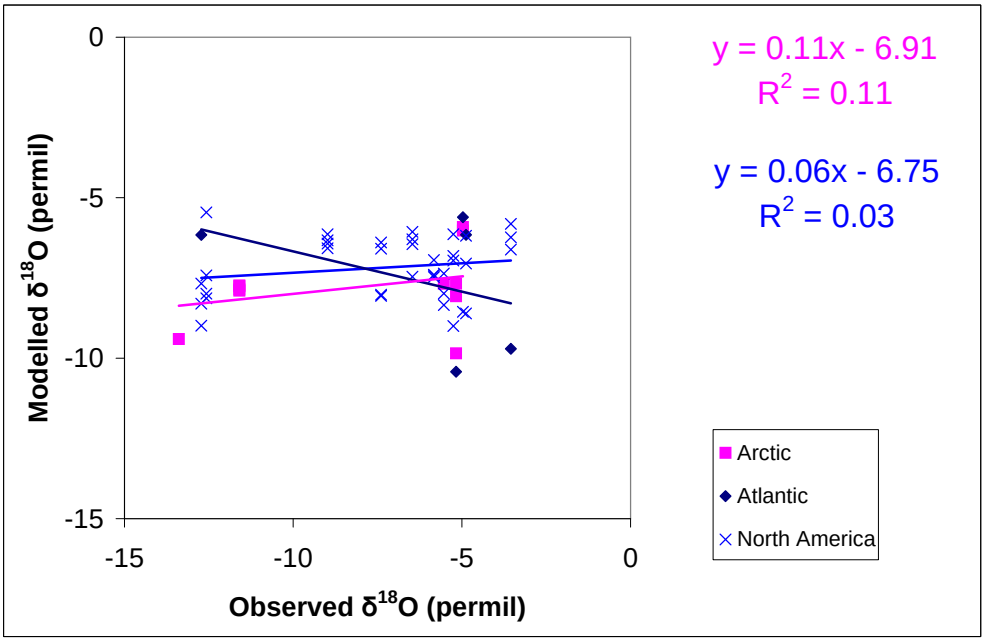

Figure 4.20: *Observed versus modelled $\delta^{18}O$ for (i) Norwich and (ii) Birmingham split into "Main source" categories. Atlantic sourced trajectories are shown in navy, Arctic sourced in pink, European sourced in green and North America sourced trajectories in blue. Regression equations and correlations coefficients are shown to the right of the figure if the relationship is positive.*

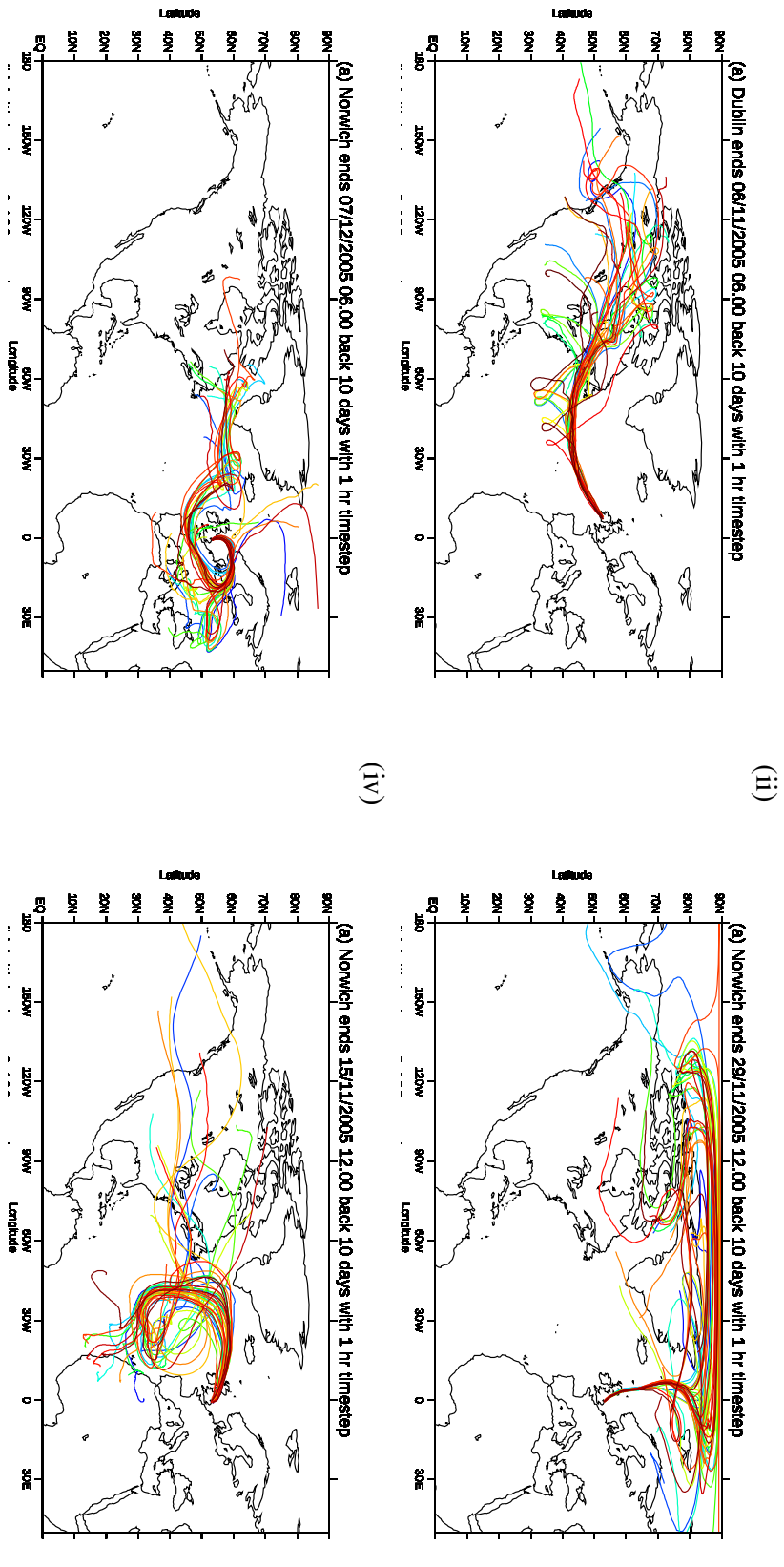

Figure 4.21: *Examples of "Main direction" FLEXPART trajectory categories (i) Atlantic, (ii) North, (iii) Cyclonic and (iv) Anticyclonic.*

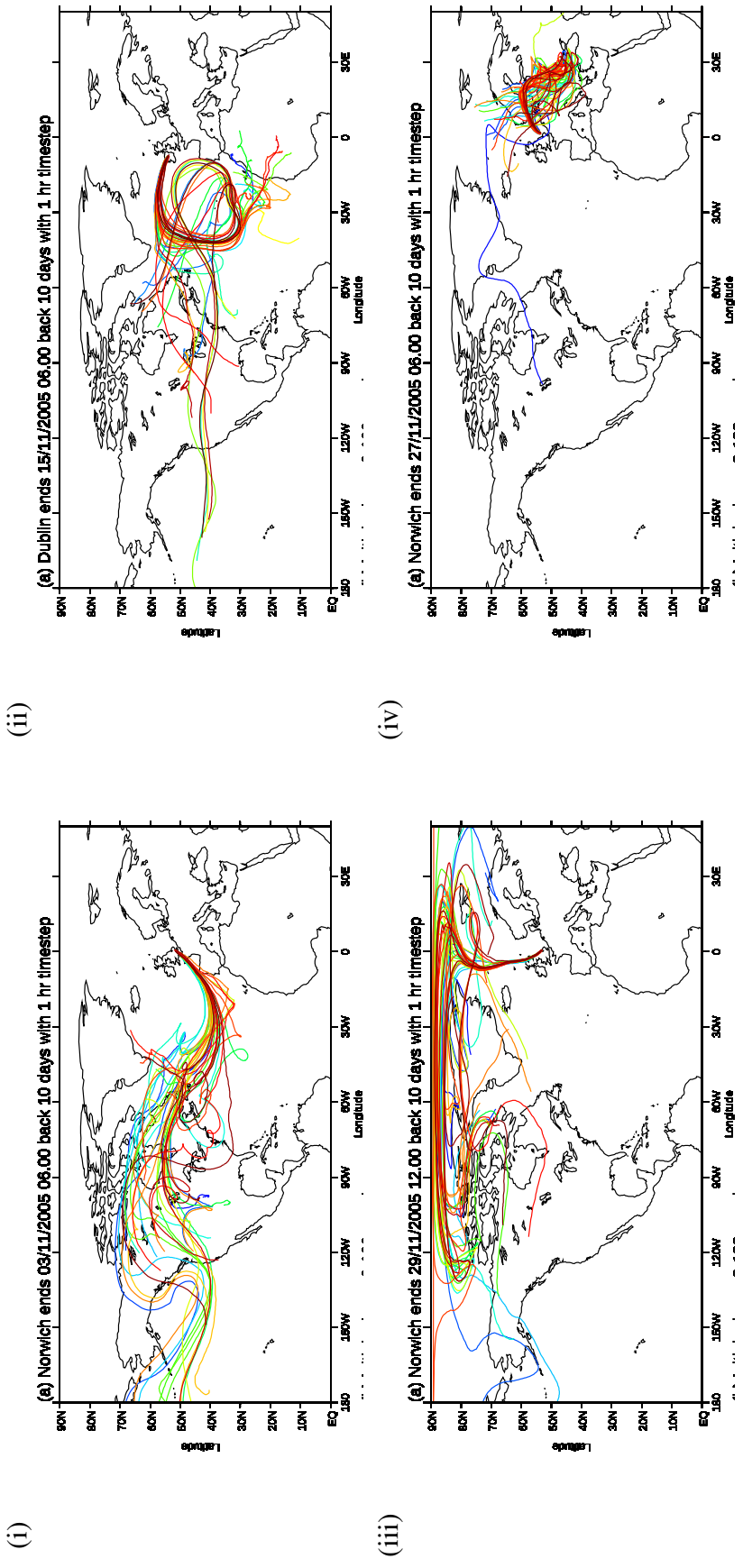

Figure 4.22: *Examples of "Main source" FLEXPART trajectory categories (i) Atlantic, (ii) North, (iii) Cyclonic and (iv) Anticyclonic.*

Feature	Category	Description
Direction	Atlantic	Majority of trajectories approach the U.K. from the Atlantic in a straight line
	North	Majority of trajectories approach the U.K. from North of North–west in a straight line
	Cyclonic	Majority of trajectories curve towards the U.K. in an anticlockwise path
	Anticyclonic	Majority of trajectories curve towards the U.K. in a clockwise path
Spread	Very Close	Trajectories are very tightly clustered moving away from the U.K. and most follow a similar path throughout the 10 day back trajectory
	Close	Trajectories are tightly clustered moving away from the U.K. and spread out further into the 10 day back trajectory
	Apart	Trajectories are disperse throughout the 10 days
Main Source	North America	Majority of trajectories are sourced in North America
	Atlantic	Majority of trajectories are sourced in the Atlantic
	Arctic	Majority of trajectories are sourced North of the U.K
	Europe	Majority of trajectories are sourced in Europe

Table 4.4: *Categories for trajectory analysis with a brief description of each situation.*

4.8 Modelling the Observed Amount of Rainfall

The MCIM outputs an estimate of the amount of precipitation that would fall from an air particle. By averaging these values in the same way as for the isotopic composition modelled values, a modelled amount of precipitation can also be obtained. These modelled values were compared with the observed values but no correlation was seen between the data sets. This is as anticipated because the particles are released in the bottom 100 m of the atmosphere, not from the cloud and therefore precipitation producing layer. The decision was made to release the particles from this lower layer because the height of clouds varies for each precipitation event and also the isotopic composition of raindrops equilibrates with that of water vapour and droplets in the air that they fall through (Rozanski et al., 1993), (see section 3.3.4 and 5.1.5). The alternative would have been that used by Helsen et al. (2006) to find the height of precipitation formation using the cloud water content information available in the ECMWF ERA-40 fields. The level of

maximum cloud water content can be assumed to be the height or pressure level of precipitation formation. However, the study of Helsen et al. (2006) was focused on snowfall over Antarctica, which would maintain the isotopic composition of cloud conditions. The sites used in this study mostly experienced rainfall, and raindrops will equilibrate with surrounding atmospheric water vapour as they fall. If cloud height was estimated and used as a initiation point for the back trajectories, then the isotope model would need to account for equilibration during falling which it does not.

4.9 Norwich Time of Precipitation Data

As the samples of precipitation were collected over a 24 hour period, the results of model runs from across this 24 hour period were averaged to give a final modelled value. However, for the Norwich site a tipping bucket raingauge was positioned next to the sampling system to obtain data on the timing of the precipitation events. This data is used in this section to investigate whether the modelled value is improved by only including model runs that were initiated close to the time of precipitation. Due to the tipping bucket raingauge malfunctioning for most of November 2005, the timing of precipitation was only obtained for 8 of the 17 raindays.

Model runs were conducted at 1500, 1800, 2100, 0000, 0300, 0600, 0900, and 1200 hours across the sample day using a 95% humidity threshold. It was not possible to conduct runs at the exact time that precipitation occurred due to events often lasting an hour or more. Instead an average was taken of the model runs closest to the time of recorded precipitation. For example, on the 28th November 2005 the tipping bucket raingauge recorded precipitation occurring between 1658 and 1719, then from 1812 to 1852, and finally from 2244 to 2318 (figure 4.23). Therefore the model runs for 1800 on the 27th November 2005 and 0000 on the 28th November 2005 were averaged to give the modelled isotopic composition for the sample collected at 1200 on the 28th November 2005. The results of this test are shown in figure 4.24, along with the results shown previously of the 4 run average, and an average of the closest times weighted by amount of precipitation that fell in each event. As can be seen from figure 4.24 there was very little difference

between the straight average and the model runs closest to the time of precipitation events. The greatest change, of 0.35 ‰ was seen for the 26th November 2005 but the average change caused was only 0.04 ‰ and is therefore negligible. More generally, the best fit lines of the data points in figure 4.24 show a slightly larger gradient (increasing from 0.08 to 0.15) and improved correlation (from 0.12 to 0.21) when the time of precipitation is taken into account, though the improved results are still not statistically significant at the 90% level. This regression equation cannot be compared with the previous results directly as it is comprised of only 8 of the total 17 Norwich raindays. Of those 8, only 3 were days when more than 3 mm of rain fell.

The results of this test suggest that the modelled values are improved when time of precipitation is taken into account. It would be interesting to see whether this improvement was even more relevant on days when more than 3 mm of rainfall occurred. Unfortunately very few data sets of isotopic composition contain accurate enough information about the within–day timing of precipitation.

4.10 Intra–site Variability in Norwich

As FLEXPART is initiated from a grid cell with a horizontal size of 0.1° x 0.1° it was hypothesised that the isotopic data collected at a single point within this grid cell might not be analagous to what was being modelled. Previous studies have shown that isotopic composition varies across synoptic systems. Lawrence et al. (1982), Gedzelman and Lawrence (1990) and Treble et al. (2005) saw that for low pressure systems the most negative values are observed at the centre of the system with less negative δ values away from the core. There is no guarantee that the entire system and range of δ values will be sampled by a stationary collector. Amount of precipitation measured at each of the 5 sites did vary, with generally more precipitation observed at the 3 sites on the UEA campus that were less sheltered. The only occasion when a larger than 1.5 mm variation was seen was on the 26th November 2005 where the Sainsbury Centre site received 10 mm more precipitation than the Bury Street sites and 7 mm more than the ZICER UEA site.

To test whether a single collection site can be legitimately compared with a modelled

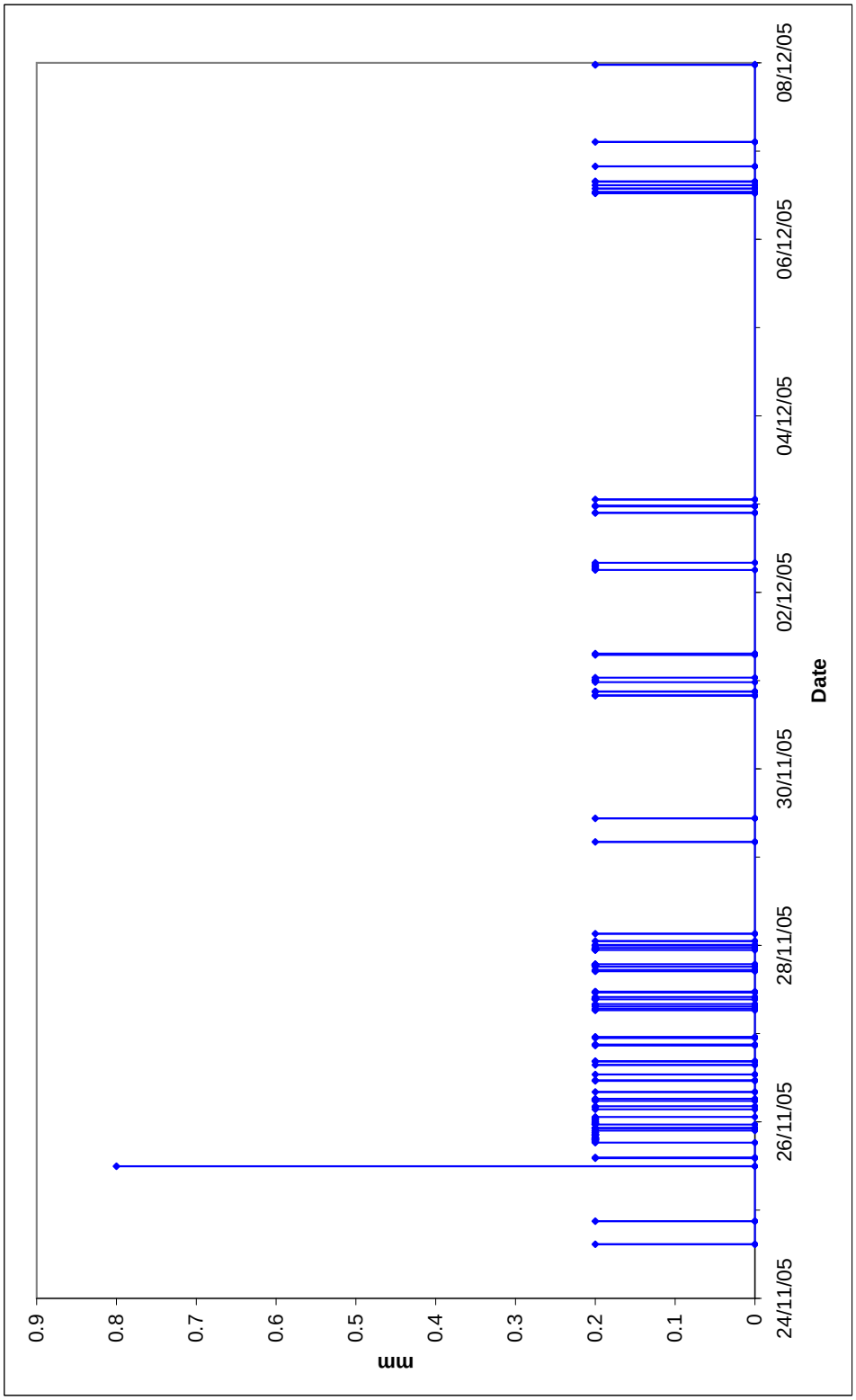

Figure 4.23: *Timing and amount of rainfall falling in Norwich from 24th November 2005 to 8th December 2005.*

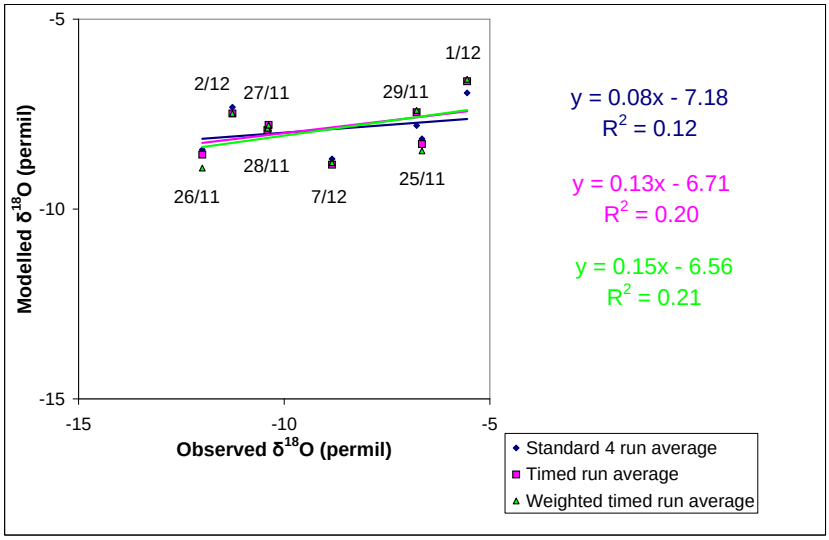

Figure 4.24: *Modelled versus observed $\delta^{18}O$ for 8 Norwich raindays where time of precipitation data was also collected. The previously shown 4 run average modelled data is in navy. Model averages calculated from only the model runs closest to the observed time of precipitation are in pink. Model averages calculated from only the model runs closest to the observed time of precipitation but weighted according to the amount of observed precipitation at each time are in green.*

value, the rainwater samples collected from 3 stations around the University of East Anglia campus and 2 stations in a residential area in Norwich were analysed for isotopic composition. The large variation in precipitation amount seen on the 26th November 2005 was not reflected in the isotopic values. Table 4.5 shows the 5 days where the maximum variation between the 5 sites was less than a 1 ‰ difference in $\delta^{18}O$ between sites, table 4.6 shows the 3 days where there was more than a 1 ‰ difference. The maximum $\delta^{18}O$ range seen across the sites was 2 ‰ on the 25th November 2005. The modelled to observed relationship is not changed when an average of the observed values is used. There is also no individual Norwich site whose isotopic value is uniformally better modelled, however the modelled results are often closest to the Sainsbury Centre UEA site values perhaps due to it being the least sheltered of the sites and therefore least likely to be affected by microscale processess. The UEA sites all lie within a 300 m radius while the distance from UEA to Bury Street is approximately 2000 m. The larger variations in isotopic composition are most likely due to synoptic situations not always passing over both UEA and Bury Street. These sub–scale variations in position would not be resolved

by the model.

In the majority of situations there is only a small variation across the 5 sites in Norwich. I would conclude that a single site is sufficient to sample any precipitation producing synoptic system, though this potential for natural variability should be considered.

4.11 Comparison of Norwich Results and GCM Output

The model approach presented in this study is a complementary approach to that of using GCMs that contain isotopic parameters. Though a detailed comparison of the results of these two approaches is beyond the scope of this study, an initial comparison is presented in this section. As isotopic fields from the ECHAM4 GCM had already been obtained, these are the GCM results used in this comparison. Following the theory that raindrops equilibrate with the atmospheric vapour surrounding them as they fall, surface layer isotopic values of water vapour over Norwich were extracted from the ECHAM4 climatological fields that had been interpolated to a daily resolution. Temperature fields were not available from the ECHAM4 data obtained so the δ values of water equilibrated to these vapour values could not be reliably calculated. Instead it was assumed that daily average temperature would not vary greatly at Norwich during November and early December and the vapour-liquid fractionation factor would remain relatively constant across the time frame involved. There would therefore be a standard enrichment factor meaning that the variations in water vapour values would be the same as that for liquid equilibrated with this water vapour. The water vapour values from ECHAM4 can therefore be used for this comparison but will be more negative by the amount of the enrichment factor (for example 10.6 $^{\circ}/_{\circ\circ}$ at 10°C from figure 3.3).

In order to assess the relative performance of the Lagrangian trajectory model approach (which utilises ECHAM4 climatologies) as opposed to extracting the final δ values straight from the ECHAM4 data, the observed data was compared with the ECHAM4 final values. The results of this comparison can be seen in figure 4.25 in red along with the previously shown observed versus modelled data in pink. Regression equations and correlation coefficients for these relationships are shown to the right of the figure. The

Date	Site	δ^{18}O ($^\circ/_{\circ\circ}$)	δD ($^\circ/_{\circ\circ}$)	Amount of Precip. (mm)
26/11/05	Residential (low roof)	-11.991	-75.71	14.34
	Residential (garden)	-11.748	-75.26	13.20
	University (ZICER building)	-12.076	-75.63	17.11
	University (Sainsbury Centre)	-11.734	-74.76	24.61
27/11/05	Residential (low roof)	-10.407	-61.46	7.17
	Residential (garden)	-10.638	-62.58	missed
	University (ZICER building)	-10.602	-61.15	9.45
	University (Sainsbury Centre)	-10.474	-61.45	10.76
28/11/05	Residential (low roof)	-10.380	-60.10	7.17
	Residential (garden)	-10.504	-60.16	6.84
	University (ZICER building)	-10.008	-57.07	9.29
	University (Sainsbury Centre)	-9.988	-54.65	8.80
01/12/05	Residential (low roof)	-5.553	-29.45	2.24
	Residential (garden)	-5.773	-29.63	2.32
	University (ZICER building)	-5.566	-29.07	2.28
	University (Sainsbury Centre)	-5.810	-30.03	2.44
	University (ENV roof)	-5.613	-29.41	2.44
07/12/05	Residential (low roof)	-8.836	-58.64	1.55
	Residential (garden)	-9.172	-57.82	1.55
	University (ZICER building)	-8.898	-57.96	1.83
	University (Sainsbury Centre)	-9.081	-58.51	1.87
	University (ENV roof)	-8.606	-54.30	1.63

Table 4.5: *Isotopic composition of precipitation collected from 5 sites in Norwich, days with less than a 1 $^\circ/_{\circ\circ}$ difference in $\delta^{18}O$ between sites.*

Date	Site	δ^{18}O ($^\circ/_{\circ\circ}$)	δD ($^\circ/_{\circ\circ}$)	Amount of Precip. (mm)
18/11/05	Residential (low roof)	-4.094	-13.34	0.45
	Residential (garden)	-3.828	-13.21	0.45
	University (Sainsbury Centre)	-4.986	-16.86	1.96
25/11/05	Residential (low roof)	-6.561	-37.27	0.37
	Residential (garden)	-6.319	-33.75	0.45
	University (ZICER building)	-5.252	-29.18	0.29
	University (Sainsbury Centre)	-4.727	-21.67	0.29
	University (ENV roof)	-4.521	-21.98	0.29
02/12/05	Residential (low roof)	-11.260	-72.70	1.22
	Residential (garden)	-11.449	-75.67	1.47
	University (ZICER building)	-10.526	-67.24	1.34
	University (Sainsbury Centre)	-10.285	-67.33	1.18
	University (ENV roof)	-10.272	-68.35	1.30

Table 4.6: *Isotopic composition of precipitation collected from 5 sites in Norwich, days where the difference in observed $\delta^{18}O$ between sites is greater than 1 $^\circ/_{\circ\circ}$.*

observed versus ECHAM4 regression equation (y = 0.01x -15.54) illustrates the lack of variation in the ECHAM4 values through the negligible gradient term of 0.01. This is as expected from a climatological data set, the temporal resolution is not high enough to pick up the daily variation, meaning there is no synoptic signal. For completeness the model results obtained in the study were compared with the ECHAM4 final values (blue line in figure 4.25). The Lagrangian trajectory model increases the range of modelled values produced by accounting for more nuances in the atmospheric conditions on a daily scale than the ECHAM4 climatology is capable of. The Lagrangian trajectory model requires input from a GCM so could potentially be used to gain higher resolution data from GCM output.

4.12 Conclusions

Daily isotopic ratios produced using the Lagrangian Trajectory Model were compared with daily observed values from sites in Norwich, Dublin and Birmingham throughout November 2005. Initial comparisons of all data points revealed small and in most cases statistically insignificant positive correlations. Filtering the data to include only **raindays where more than 3 mm** of rainfall occurred improved the correlation between observed and modelled values at both Norwich and Birmingham. The gradients of the relationship were still smaller than ideal, though the relationships were significant at the 95% level (except for the δ^{18}O comparison at Birmingham). There were too few raindays with sufficient rainfall at Dublin to allow this test to be conclusive there.

The trajectory information, both on its own and when combined with surface pressure charts, is useful in interpreting the reasons for extreme values (e.g. very negative values seen in Dublin on the 1st December 2005 due to air particles travelling over the centre of Greenland, section 4.6). This information is also useful when analysing why the isotopic ratios of precipitation on the same day varies across the country, (e.g. on the 7th November 2005 precipitation occurred at all three sites with Dublin receiving the most negative isotopic ratios and Birmingham the least negative due to varying numbers of trajectories sourced in the Davis Strait, section 4.6.4). Source region is not the sole controlling fac-

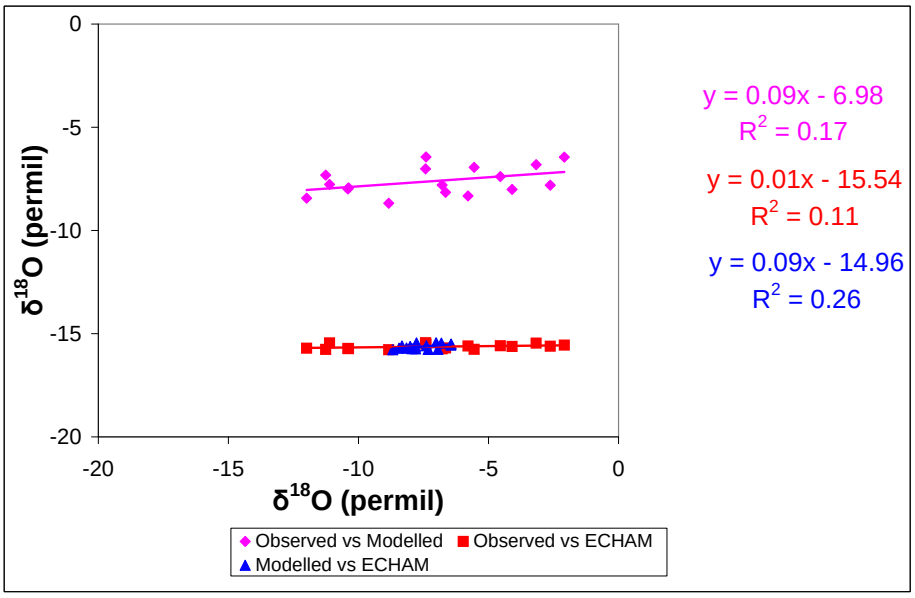

Figure 4.25: *Comparison of modelled and observed $\delta^{18}O$ with climatological values of water vapour from the ECHAM4 GCM for all Norwich raindays. The previously observed versus 4 run average modelled data is shown in pink, with the line depicting the regression equation. Observed $\delta^{18}O$ of precipitation versus ECHAM4 modelled $\delta^{18}O$ of water vapour is shown in red. The modelled $\delta^{18}O$ values of precipitation versus ECHAM4 $\delta^{18}O$ of water vapour is shown in blue. The regression equations and correlation coefficients of these comparisons are displayed to the right of the figure.*

tor on isotopic ratios as proven by the lack of correlation between source and observed isotopic ratios. The whole trajectory must be taken together to obtain a correlation.

Splitting the data according to the "Main source", "Main direction" and "Spread" suggested that trajectories approaching the British Isles from the Atlantic tend to be modelled most accurately. Other conclusions were hampered by small group sizes after splitting.

Good results were obtained when using the Norwich time of precipitation data to filter which modelled values should be averaged to create the final daily modelled value, section 4.9. Comparisons of these modelled values with observed ratios were much improved on comparisons with the standard modelled values. However, this data set was limited and similar data is extremely rare and disjointed. This would be an approach worth investigating further.

Another observed data resolution issue was highlighted by the samples collected from 5 sites around Norwich. The potential for a 2 ‰ variation in $\delta^{18}O$ across a 2000 m distance introduces significant natural variability. This observed spread is particularly

relevant due to the modelled scale being on the order of 10 km, whereas most observed data is taken from a single point. However, after comparing modelled and observed values from all 5 Norwich sites, it was concluded that a single site is sufficient in most cases.

Through comparing observed values with GCM climatological isotopic values it was concluded that the approach used in this study performs better due to it taking into account more detail of the atmospheric processes involved for each individual day. This could be a potential application of this model, used to scale down GCM output.

The comparison of modelled and observed averages in section 4.6.5 suggested that although the model does not appear to be sensitive enough for individual days, it does manage to capture the mean isotopic ratios seen over the British Isles in November and December 2005. Further tuning is required to improve the d-excess values such as changing the diffusion coefficients that control kinetic fractionation to those put forward by Cappa et al. (2003).

There was an insufficient sample size to be confident in applying these conclusions to other locations and times. A longer observed data set is required to truly test the ability of the model to reproduce isotopic ratios. Chapter 6 presents the results of a case study of observed data from Driby in Lincolnshire and Stock Hill in Somerset that spans a 5 year period.

The next chapter, Chapter 5 investigates the sensitivity of the model to initial parameters to ensure that features seen are due to processes involved and not model sensitivity.

Chapter 5

Sensitivity Studies

Both FLEXPART and the MCIM were investigated to try to assess the sensitivities to initial parameters. The results of these sensitivity tests are presented in this chapter along with conclusions about which initial parameters to use. The 2nd, 15th and 25th of November 2005 were chosen as the three test days as precipitation was observed at all three sites i.e. Norwich, Dublin and Birmingham. The test days also represent a temporal spread across the sample period and within the observed δ variations so that the effect of changing parameters on a range of δ values could be tested. These tests were mainly conducted before the conclusion had been made that the model performs better when used for rain-days where more than 3 mm of rain was observed. Of the test days used in this chapter, only at Norwich and Birmingham on 2nd November 2005 was this threshold exceeded. Also on the 25th November 2005 at Norwich, some snow would have been included in the sample as snow showers were observed for an hour from 9 p.m. on the 24th, thus contravening the requirement that only rain events should be modelled. However, the aim of these tests was to investigate the sensitivity of the model to initial parameters, and where a decision had to be made on relative ability to model the observed values, further tests were conducted for all other observation days.

5.1 FLEXPART

FLEXPART has been validated previously on many occasions (section 2.3.1) but to test its set–up on the local UEA system, FLEXPART output was qualitatively compared with surface and 850 mbar pressure charts. The output was also compared with trajectories produced by the British Atmospheric Data Centre (BADC) online trajectory service and the Hybrid Single Particle Lagrangian Integrated Trajectory model (HYSPLIT) run by the National Oceanic and Atmospheric Administration (NOAA) Air Resources Laboratory (Draxler and Rolph, 2003). FLEXPART trajectories produced on the UEA system compared well with expected flow direction caused by pressure systems and with the single trajectories output from HYSPLIT. The FLEXPART trajectories do pick up much more detail of potential paths than the HYSPLIT model is able to due to the number of trajectories produced. HYSPLIT outputs only one trajectory per initial release point whereas FLEXPART produces many, one for each particle released.

The standard FLEXPART run for this study used a Lagrangian 1 hour timestep, releasing 100 particles from a height of 0-100 metres above ground level (m agl) within a horizontal grid box of 0.1° x 0.1°. The convection scheme was turned on, and the time period covered by each trajectory was 10 days backwards in time from the release time. These parameters were then perturbed in a series of experiments to test the sensitivity of FLEXPART. The output of FLEXPART is quite complex. To more easily observe the impacts of some of the parameter perturbations, the FLEXPART output was run through the MCIM, which outputs a single, average, value. These single values could then be compared quantitatively. (Note that 3 hour not 1 hour FLEXPART timesteps were utilised in these tests when not being specifically varied themselves for all final values given in Chapter 5. This is due to the reduction in computing time required when using a 3 hour timestep.)

5.1.1 Sampling Error

FLEXPART releases particles at random locations within the initial grid box specified. Therefore there will be a sampling error, seen as a difference in δ values produced from 2

runs of FLEXPART initiated with the same conditions but with different randomly chosen release points. To test the impact of this, FLEXPART was run 10 times, backwards from 1200 on the 25th November 2005 for 10 days, with different random number seeds (and therefore different initial locations for each particle) for each test. Personal communication with Andreas Stohl confirmed that as long as sufficient particles are released from a grid box then they should be fairly evenly distributed. It can be seen in table 5.1 that when 100 particles are used the maximum variation in δ^{18}O is 0.43 $^{\circ}/_{\circ\circ}$. These tests were then repeated releasing 1000 particles. This increase in sample size reduced the variation in δ^{18}O to a maximum of 0.16 $^{\circ}/_{\circ\circ}$. To more accurately quantify the sampling error, the mean and standard deviation of the 10 modelled isotopic values for each sample size was calculated (table 5.1). This test concluded a sampling error of 0.16 $^{\circ}/_{\circ\circ}$ for δ^{18}O and 1.33 $^{\circ}/_{\circ\circ}$ for δD for a sample size of 100 particles for the 25th November 2005. For 1000 particles the standard deviation for the 25th November 2005 runs was reduced to 0.04 $^{\circ}/_{\circ\circ}$ for δ^{18}O and 0.38 $^{\circ}/_{\circ\circ}$ for δD. This decrease in sampling error would be highly desirable. However increasing the sample size from 100 to 1000 particles also increased the computational time required by a factor of 10. This increase in computing time unfortunately makes running FLEXPART with 1000 particles beyond the scope of this project.

To investigate the magnitude of error to be expected across different test days, the same 10 sets of initial locations were used for the 2nd and 15th November 2005. Again means and standard deviations were calculated with the standard deviations forming an estimate of the error involved. These results gave a mean $\pm$ standard deviation for the 2nd November 2005, as -10.163 ± 0.08 $^{\circ}/_{\circ\circ}$ for δ^{18}O and -71.69 ± 0.69 $^{\circ}/_{\circ\circ}$ for δD; and for the 15th November 2005, -13.691 ± 0.22 $^{\circ}/_{\circ\circ}$ for δ^{18}O and -99.01 ± 1.73 $^{\circ}/_{\circ\circ}$ for δD.

The average error of these three cases is 0.15 $^{\circ}/_{\circ\circ}$ for δ^{18}O and 1.25 $^{\circ}/_{\circ\circ}$ for δD. These values can be used to quantify the sampling error involved with the release of 100 particles from Norwich in November 2005 with relative confidence. As the modelled range across the 100 particles has a standard deviation in the order of 1.5 $^{\circ}/_{\circ\circ}$ for δ^{18}O and 10 $^{\circ}/_{\circ\circ}$ for δD (section 4.6), these sampling errors are negligible.

Date and Location	**Test number**	**100 particles**		**1000 particles**	
		δ^{18}**O** ($^\circ/_{\circ\circ}$)	δ**D** ($^\circ/_{\circ\circ}$)	δ^{18}**O** ($^\circ/_{\circ\circ}$)	δ**D** ($^\circ/_{\circ\circ}$)
25/11/2005	1	-10.712	-74.88	-10.948	-76.78
Norwich	2	-10.967	-77.03	-10.846	-75.96
	3	-10.898	-76.37	-10.858	-76.01
	4	-10.982	-77.10	-10.896	-76.33
	5	-10.603	-73.92	-10.793	-75.49
	6	-10.564	-73.75	-10.825	-75.75
	7	-10.870	-76.09	-10.900	-76.39
	8	-10.649	-74.48	-10.808	-75.54
	9	-10.547	-73.48	-10.83	-75.79
	10	-10.875	-76.35	-10.867	-76.11
	Mean	-10.767	-75.34	-10.857	-76.02
	Median	-10.712	-74.88	-10.858	-76.01
	St. Dev.	0.16	1.33	0.04	0.38
	Range	0.43	3.62	0.16	1.29

Table 5.1: *Modelled isotopic composition for 10 runs with different initial particle locations, for the release of 100 and 1000 particles.*

5.1.2 Timestep of FLEXPART Output

The original set–up of FLEXPART produces output every 3 hours and therefore averages over this same time period. To test the sensitivity of this timestep, FLEXPART was initiated to run backwards in time from 1200 on the test days, for 10 days, from Birmingham, Dublin and Norwich. The first set of runs were set to give output every 3 hours averaging over 15 minute sampling, (the original FLEXPART set–up). The runs were then repeated but giving output every hour with 5 minute sampling (the standard parameters in this study), and then output every 12 minutes with 1 minute sampling.

Changing the timestep appeared to have only a very small effect on the trajectories produced, especially for the first 5 days of the 10 day trajectories. This can be seen in the example of the 15th November 2005 with trajectories initiated at Norwich (figure 5.1). After 5 days backwards from the 15th November 2005 a slight variation can be seen in the spread across the North Atlantic, with fewer trajectories coming from west Africa in the 1 hour timestep run. Another significant change is in the height of the 1 hour timestep trajectories. Many trajectories reach a height of over 9000 m which is not seen in the 3 hour run. Similar results were seen for the other test days though this example shows one of the greatest variations. The observed variations are most likely caused by the

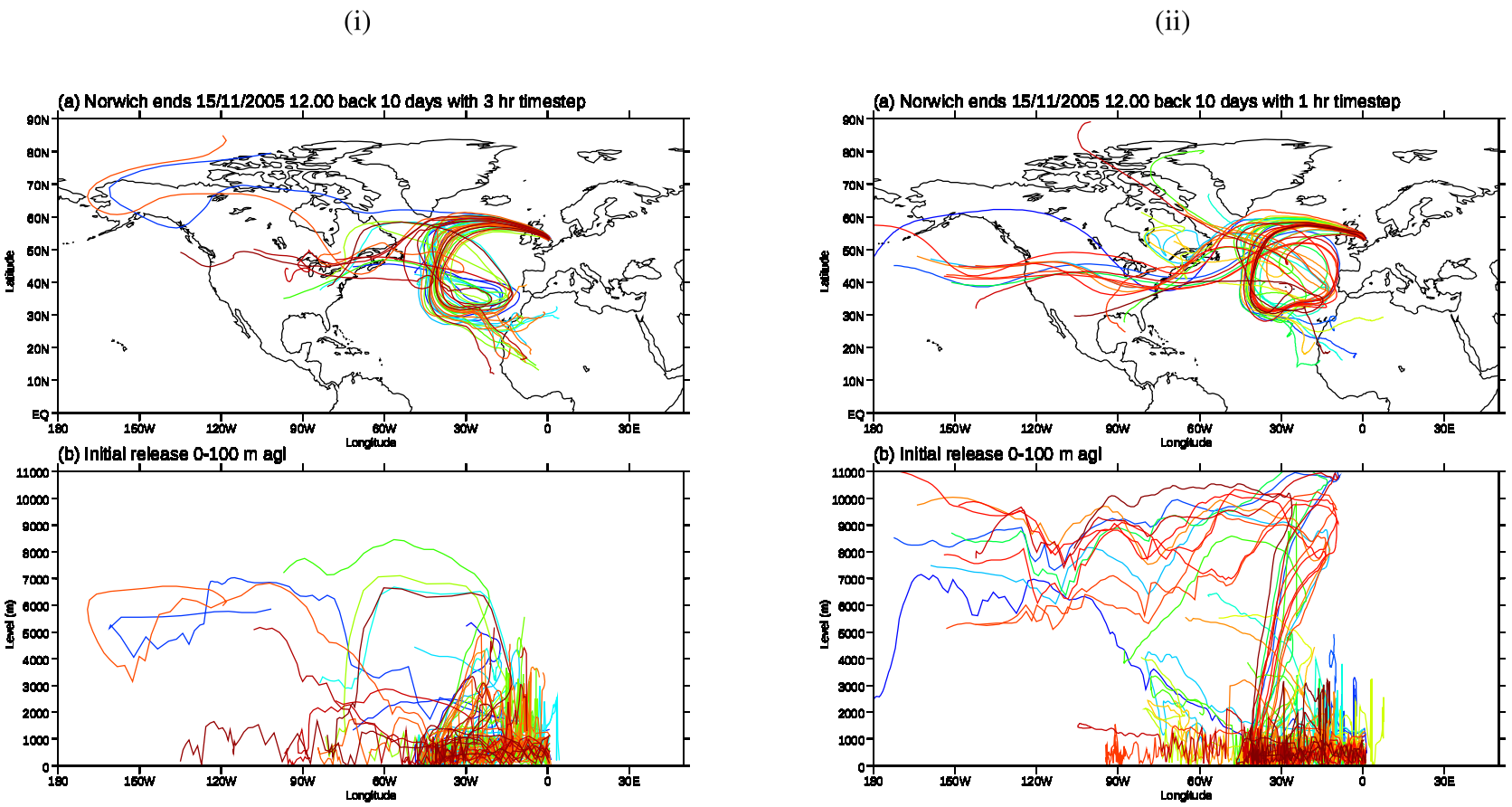

Figure 5.1: *FLEXPART particle trajectories for Norwich on the 15th November 2005 using (i) a 3 hour timestep (ii) a 1 hour timestep. Each coloured line is one particle trajectory.*

more frequent update in particle direction provided by the 1 hour timesteps. These 1 hour updates are used to correct the direction in which the parcel is moving. If rapid changes in direction of movement are occurring then a particle described by a 3 hour timestep data set might be seen to move in the "wrong" direction for 2 hours. This lack of correction in the 3 hour timestep data will be especially important in atmospheric situations where air is moving in a tightly curved streamline such as occurs close to high or low pressure centres.

Though large pattern changes can be seen by comparing the FLEXPART trajectory pictures as in figure 5.1, smaller variations between the two runs might be missed. Therefore the trajectory information was passed through the MCIM to see what effect a smaller timestep would have on the predicted isotopic values. The results of this test on the δ^{18}O values can be seen in figure 5.2.

Changing the timestep appeared to have no systematic effect on the final δ values. There is however a striking feature in these results. The isotopic values predicted for Dublin on the 2nd November 2005, and Norwich on the 15th November 2005 when using the 12 minute averages, are very much more negative than those produced using the other timesteps. Results for all of the other days show oxygen isotopic variations of the order of -1 to -2 $\permil$ between the different timestep tests. However, for the two cases mentioned previously, the change from 1 hour to 12 minute averaging produces a -10 $\permil$ change. This seems to suggest a sensitivity in the model between these two timesteps possibly due to interpolation from the 6 hourly ECMWF ERA-40 windfields,

FLEXPART was run again for the test days using the alternative method for calculating timesteps available in FLEXPART. This second method limits the timesteps with respect to the Lagrangian time scales (Stohl et al., 2005b) but outputs averages at the specified times. Lagrangian timesteps are determined by local velocity fluctuations instead of the local average velocity (Maron and Howes, 2003). Using the Lagrangian timestep also means that a shorter timestep is used for solving the equations for the vertical winds than for the horizontal winds. This method therefore allows for turbulence to be better described as well as ensuring that the density correction scheme functions properly.

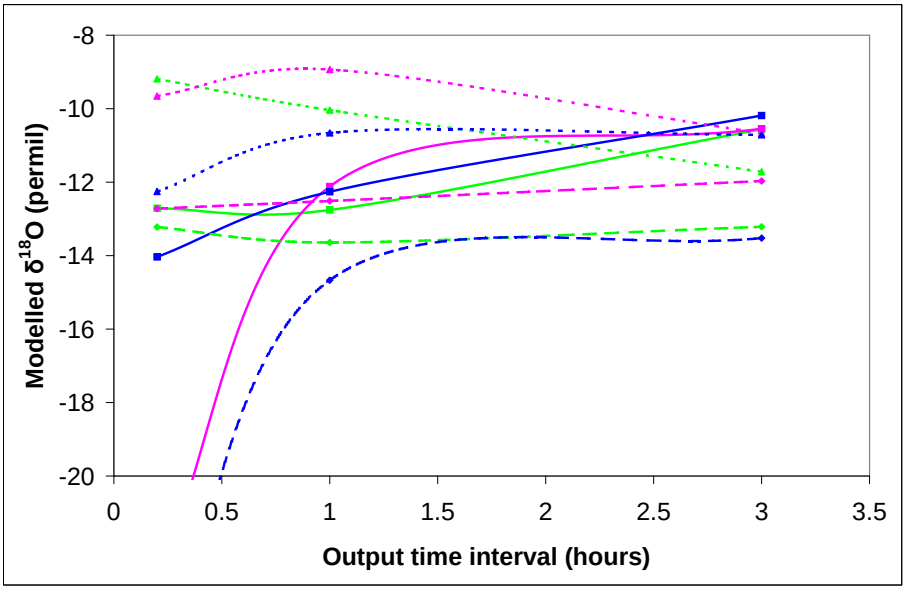

Figure 5.2: *Modelled isotopic composition from FLEXPART trajectories with different timesteps. Birmingham runs are shown in green, Dublin in purple, Norwich in blue. Solid lines with a square marker are the 2nd November 2005, dashed lines with a diamond marker are the 15th November 2005 and dotted lines with triangular markers are the 25th November 2005.*

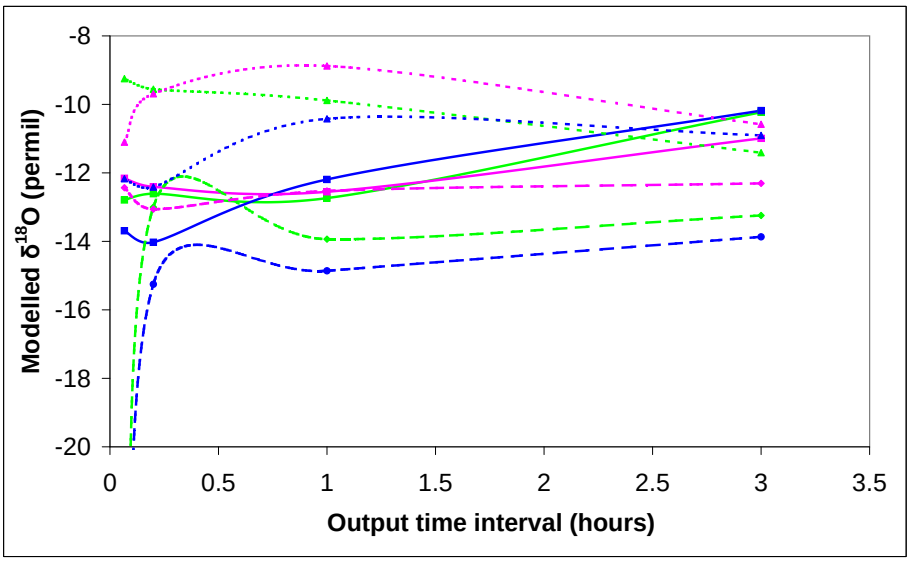

Figure 5.3: *Modelled isotopic composition from FLEXPART trajectories with Lagrangian timesteps. Birmingham runs are shown in green, Dublin in purple, Norwich in blue. Solid lines with a square marker are the 2nd November 2005, dashed lines with a diamond marker are the 15th November 2005 and dotted lines with triangular markers are the 25th November 2005.*

Using the Lagrangian timesteps seemed to move the sensitivity of the model to occur between different timesteps (see figure 5.3). The $-10\ ^{\circ}/_{\circ\circ}$ changes now do not occur in the δ^{18}O values between the 1 hour and 12 minute change, however, -1 to $-2\ ^{\circ}/_{\circ\circ}$ changes are still common. The larger changes in isotopic values reappear when a smaller 4 minute averaging period with sampling every 20 seconds output timestep is used. This is likely due to the constraining 20 second maximum timestep forcing the Lagrangian method to resemble the non–Lagrangian scheme, as it allows for less flexibility when the scheme is choosing the timesteps.

The isotopic values do not appear to converge with reducing timestep, possibly due to changes in the major source region as seen in figure 5.1 where more trajectories originated in Africa when the 3 hour timestep was used than when the 1 hour timestep was used. As a consequence the timestep magnitude and scheme to be used must be chosen with relation to how well they reproduce the observed values. To test this, FLEXPART was run for all days for which Norwich observational data was available, initiated at 1200 hours. The resulting modelled δ^{18}O values were then plotted against the observed values and an r^2 value calculated for each data set (figure 5.4). None of the r^2 values found (right hand side of figure 5.4) were significant at the 95% confidence level (i.e. the r^2 values for the 3 hour (pink) and 1 hour (navy) non–Lagrangian runs are 0.06 and 0.109 respectively). When comparing the 1 hour runs from the non–Lagrangian (navy) and Lagrangian (green) methods, the change was even smaller and still not significant, from 0.109 to 0.113 respectively. Therefore there is no conclusive indication that these changes to the timestep alter the overall results obtained significantly. The Lagrangian method was chosen to be used in the main body of data runs as it theoretically models vertical motion more accurately.

5.1.3 Duration of Back Trajectories

Another computing time versus modelled data accuracy balance that had to be found was regarding the length of time for which back trajectories should be calculated. The average residence time of water vapour in the atmosphere is around 10 days (Barry and Chorley,

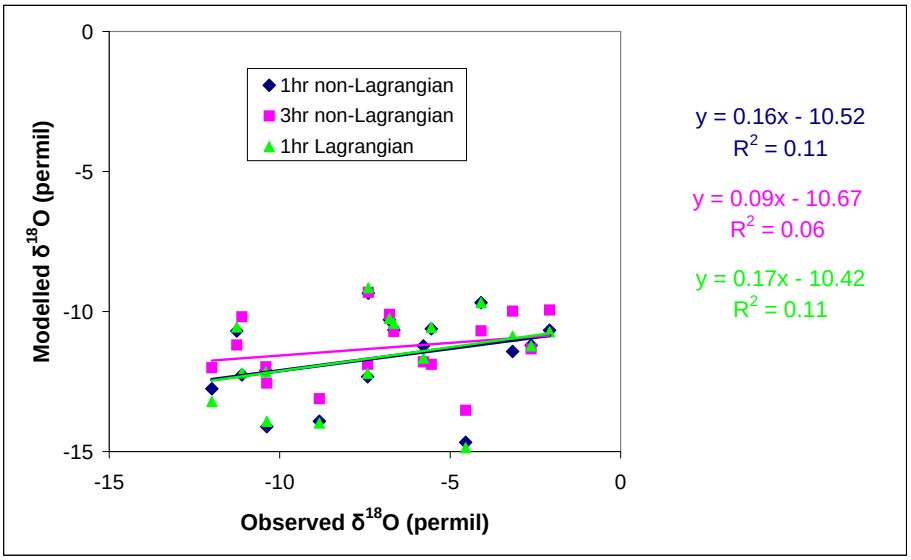

Figure 5.4: *Modelled versus observed isotopic composition for all Norwich raindays from FLEXPART trajectories using a 1 hour and 3 hour non-Lagrangian timestep (navy and pink respectively) and a 1 hour Lagrangian timestep (green) method. Regression equations of the best fit lines and the correlation coefficients of the relationships are shown on the right hand side.*

1998), so this was used as a starting point for the investigation. FLEXPART was run backwards in time for 3, 5, 8, 10, 15 and 20 days and then this output was fed into the MCIM to produce isotopic values. Figure 5.5 shows the δ^{18}O values only, as δD values varied similarly. Again the 2nd, 15th and 25th November 2005 were tested, with 100 particles, a 3 hour timestep and convection turned on.

It can be seen from these results that the final isotopic value for each day and each location asymptotes towards a single value. There is a relatively large change in value across the 3, 5, 8 and 10 day runs, (a maximum of 2.2 $^{\circ}/_{\circ\circ}$ for δ^{18}O at Norwich between 3 and 10 day trajectories from the 15th November 2005), but between 10 and 20 days the difference is much reduced (to 0.02 $^{\circ}/_{\circ\circ}$). It was therefore decided that backwards runs of 10 days would be sufficient to produce a stable estimate of isotopic composition, while keeping computational time to a minimum.

(i)

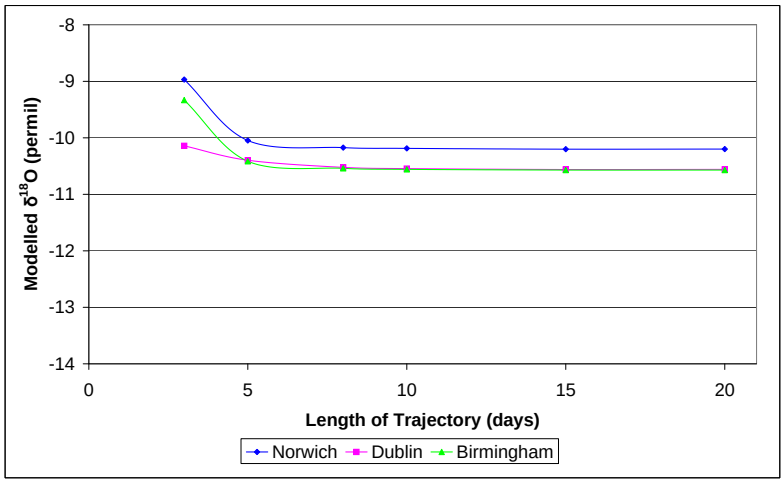

(ii)

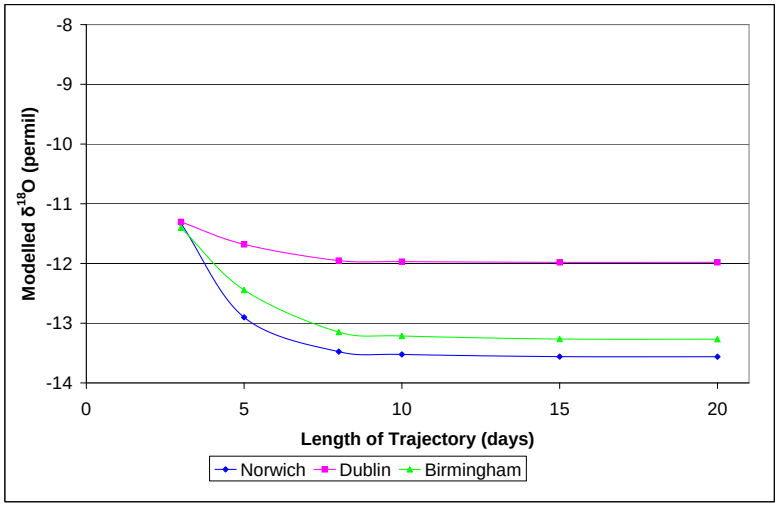

(iii)

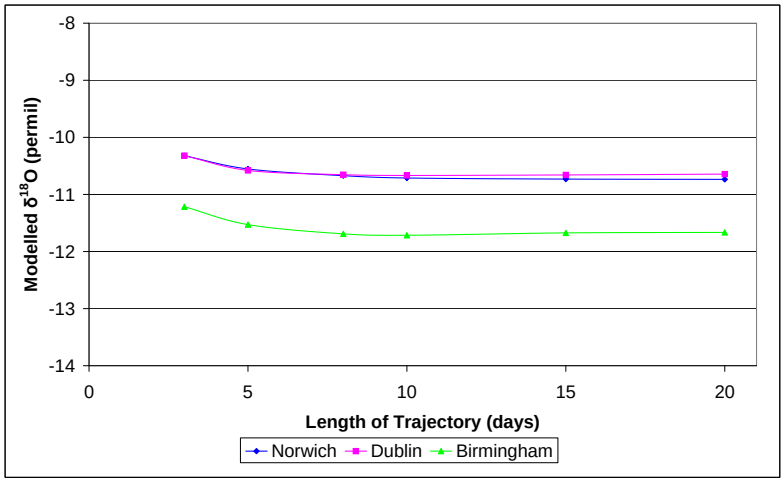

Figure 5.5: *Modelled isotopic composition with trajectories of varying length (i) 2nd November 2005, (ii) 15th November 2005, and (iii) 25th November 2005.*

5.1.4 Horizontal Size of Initial Release Grid Box

All observed isotopic data was obtained from a precipitation sample collected at a single point. FLEXPART has the ability to produce back trajectories from a single point. There are however inherent uncertainties within the ECMWF windfields used to run FLEXPART, and it is unlikely that FLEXPART itself perfectly models the entire atmospheric circulation system on these point scales. Back trajectories are therefore initiated from a grid box. The effect of varying the horizontal size of this box was tested with releases from 0.1° x 0.1° and 0.01° x 0.01° grid boxes. Using a larger, e.g. 1° scale, box was discounted due to Norwich, Dublin and Birmingham being about this distance apart from each other. Any overlap of the boxes could cause overlapping particles and would reduce the between site modelled variability.

It is necessary in all these cases to consider that the ECMWF input data is on a 1° x 1° grid so there will be some interpolation involved. Personal communication with the author of FLEXPART, Andreas Stohl, confirmed that boxes of *"0.1° or even finer does make sense, if limitations of the meteorological input data are kept in mind."*

To test the effects of a smaller release box on the MCIM results, the FLEXPART output from the 3 test days was run through the MCIM (table 5.2). Only δ^{18}O values are shown in table 5.2 as δD values varied concurrently with δ^{18}O. The changes in MCIM predicted isotopic values induced by the change in release grid box are minimal (less than 0.2 $‰$ for δ^{18}O in most cases, which is about the same as the sampling error seen before). The bigger variations were seen on the 15th November 2005 which had the largest sampling error. As the variations in δ values are minimal, the original 0.1° release box size will be used to minimise the interpolation required.

5.1.5 Release Height in the Atmosphere

The most theoretically complicated aspect of the testing of initial parameters concerned those that determine the height at which particles are released into their back trajectories. The MCIM does not model equilibration of raindrops with the surrounding atmospheric moisture as they fall, as discussed in section 3.3.4. Therefore the chosen initial height

Date	**Location**	**0.1° release box** δ^{18}**O** ($^\circ/_{\circ\circ}$)	**0.01° release box** δ^{18}**O** ($^\circ/_{\circ\circ}$)	**Observed** δ^{18}**O** ($^\circ/_{\circ\circ}$)
02/11/2005	Birmingham	-10.6	-10.6	-12.72
	Dublin	-10.5	-10.4	-12.35
	Norwich	-10.2	-10.2	-11.11
15/11/2005	Birmingham	-13.2	-13.4	-3.55
	Dublin	-12.0	-12.3	-2.78
	Norwich	-13.5	-14.0	-4.54
25/11/2005	Birmingham	-11.7	-11.6	-5.53
	Dublin	-10.7	-10.7	-8.21
	Norwich	-10.7	-10.9	-6.65

Table 5.2: *Modelled oxygen isotopic composition from FLEXPART trajectories with different release box sizes and observed Norwich* $\delta^{18}O$.

must in part deal with this process. Model runs were again conducted using the three chosen test days and a 3 hour timestep, figure 5.6. For all test days the 0-5000 m agl runs produce much (6 to 11 $^\circ/_{\circ\circ}$) more negative isotopic predictions than the 0-100 m agl. For the 2nd November 2005 runs, the 0-1000 m agl runs are consistently closer to the observed values of both δ^{18}O and δD than the runs with release heights of 0-100 and 400-500 m agl. The improvement in accuracy is in the order of 0.2 $^\circ/_{\circ\circ}$ for δ^{18}O, and 1.0 $^\circ/_{\circ\circ}$ for δD. The 0-100 m agl runs are the most accurate for the 15th November 2005 by as much as 0.4 $^\circ/_{\circ\circ}$ for δ^{18}O in Dublin but as little as 0.08 $^\circ/_{\circ\circ}$ for δ^{18}O in Norwich.

The results of the 25th November 2005 runs are not so uniform in their response to the changing release heights. For Birmingham the 400-500 m agl runs produced the most accurate predictions, whereas the 0-100 m agl prediction was best for Dublin and Norwich. Again though, the 3 lower release heights all produced very similar predictions. The improvement in accuracy across the 3 lower release heights for the 25th November 2005 was around 0.15 $^\circ/_{\circ\circ}$ for δ^{18}O, and 1 $^\circ/_{\circ\circ}$ for δD but the most accurate release height bounds varied between sites.

There does not seem to be a pattern with increased height in the lower atmosphere (less than 1000 m). These results underline the fact that release height in the atmosphere has an extremely complex role to play in reproducing the effect of equilibration of water droplets as they pass through the lower layers. However, since the variations in values predicted within the lowest 1000 metres of the model seem to be minor and of the same

order as the sampling error, the 0-100 m agl bounds will be used as this is theoretically the most sensible layer to study with this model due to equilibration of raindrops as they fall (section 3.3.4).

5.1.6 Effect of Convection

FLEXPART contains the option of computing trajectories with or without convective parameterisations. James et al. (2003) found that turning the convection scheme off has very little impact in the extra tropics but is important in the tropics. To see if this was the case for this study, FLEXPART was run with the convection scheme turned on and turned off. Table 5.3 shows the δ^{18}O results of this test on a single run (from 1200) for each of the test days. The differences made for these test days are generally larger than those seen in other sensitivity tests, with the mean change in δ^{18}O values being 0.23 $^{\circ}/_{\circ\circ}$. Again the largest changes are seen on the 15th November 2005, (up to 0.5 $^{\circ}/_{\circ\circ}$ in Norwich). The 15th November 2007 was previously shown to have the largest sampling error of the test days, so this could partially account for the larger variation seen. With respect to the observed values, modelled isotopic values at all locations for the 15th November 2005 are moved closer to observed values by adding convection, this is also the case for Dublin on the 2nd November 2005. All other runs were actually better with the convection subroutine turned off. However as it is almost a 50/50 split between the convection scheme improving the results and decreasing the accuracy, and because the differences made are only just bigger than the sampling error, it was decided to use the convection scheme as it theoretically improves the trajectories. It should also be considered that convection in November is likely to be minimal. If summer months were tested the convection scheme would potentially have more of an effect.

5.1.7 Within Day Sampling

Throughout this study modelled data is being compared with observed isotopic values from water samples collected daily. The precipitation that constitutes the water sample could therefore have fallen at anytime within the 24 hours prior to the sample being taken.

(i)

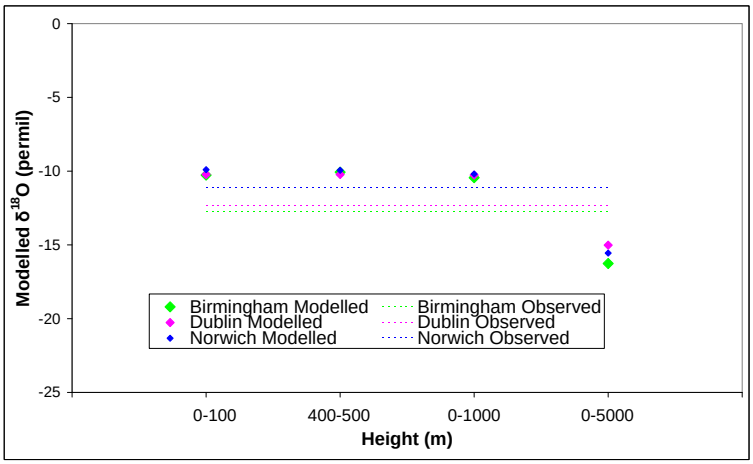

(ii)

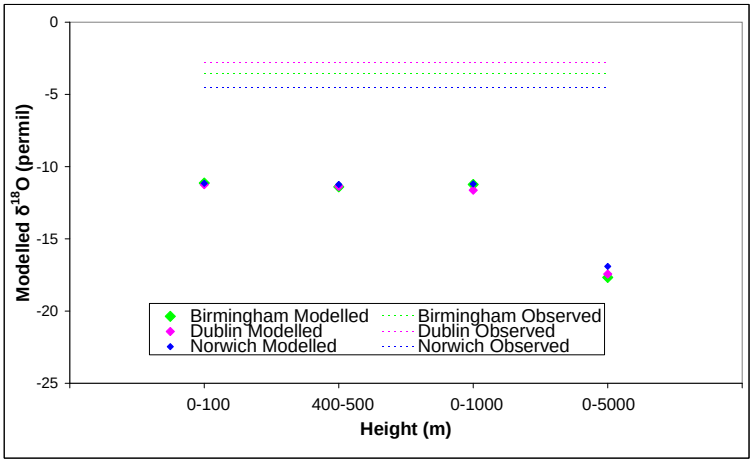

(iii)

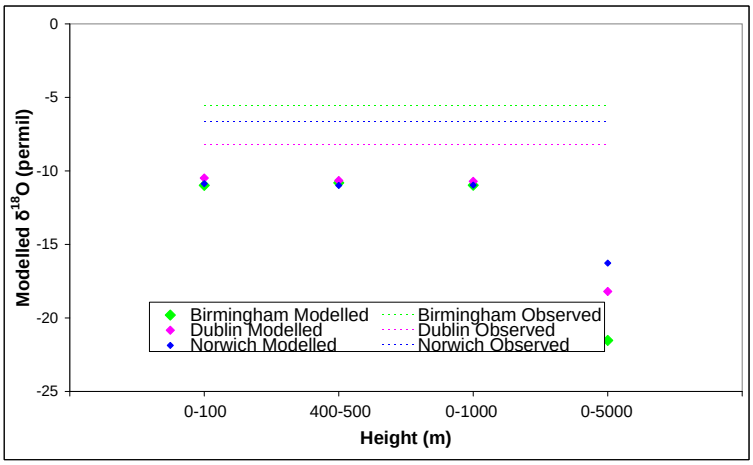

Figure 5.6: *Modelled isotopic composition of trajectories initiated at different release heights plotted as point values for (i) 2nd November 2005, (ii) 15th November 2005, and (iii) 25th November 2005. Observed values are shown as a dashed line. Norwich data is shown in blue, Birmingham in green and Dublin in pink.*

Date	Location	Convection on δ^{18}O ($^\circ/_{\circ\circ}$)	Convection off δ^{18}O ($^\circ/_{\circ\circ}$)	Observed δ^{18}O ($^\circ/_{\circ\circ}$)
02/11/2005	Birmingham	-10.6	-10.6	-12.72
	Dublin	-10.5	-10.2	-12.35
	Norwich	-10.2	-10.3	-11.11
15/11/2005	Birmingham	-13.2	-13.3	-3.55
	Dublin	-12.0	-12.4	-2.78
	Norwich	-13.5	-14.0	-4.55
25/11/2005	Birmingham	-11.7	-11.4	-5.53
	Dublin	-10.7	-10.5	-8.21
	Norwich	-10.7	-10.6	-6.65

Table 5.3: *Modelled oxygen isotopic composition from FLEXPART trajectories with convection turned on and turned off and observed $\delta^{18}O$ at Norwich.*

FLEXPART was initially set to uniformally release 100 parcels from each location during the first 3 hours of the backwards simulation. However, this three hour period will not always contain the time during which precipitation actually fell. In order not to reduce the number of particles per hour but take account of the whole 24 hour sampling period, 8 runs were initiated within each of the three test days at 3 hour intervals. The results are shown in figure 5.7. Within day variations are as large as 4.8 $^\circ/_{\circ\circ}$ for δ^{18}O (between Dublin at 2100 on the 14th and 0600 on the 15th November 2005). The maximum difference across the 8 runs ranges from 2 to 4 $^\circ/_{\circ\circ}$ for all other test days. This highlights the preference for having timed rainfall samples that are unfortunately rare at the present time. Some of the Norwich sample days have concurrent time of precipitation information investigated in section 4.9. Where timed observations are not available, it would theoretically seem that modelling the whole day using 8 runs within each day is required. This theory is tested in this section.

Running the models 8 times within each day instead of 4 doubles the computational time required so would have to greatly improve the modelled results for the computational time to be worthwhile. Therefore to test the effect of changing the number of runs within a day further, 8 runs were performed for each Norwich day and then both 8 run and 4 run averages were calculated. The resultant comparisons with the observed values are shown in figure 5.8 with 4 run averages shown in blue and 8 run averages in pink. Even though 8 runs averages cover more of the day and should therefore theoretically be more accurate,

(i)

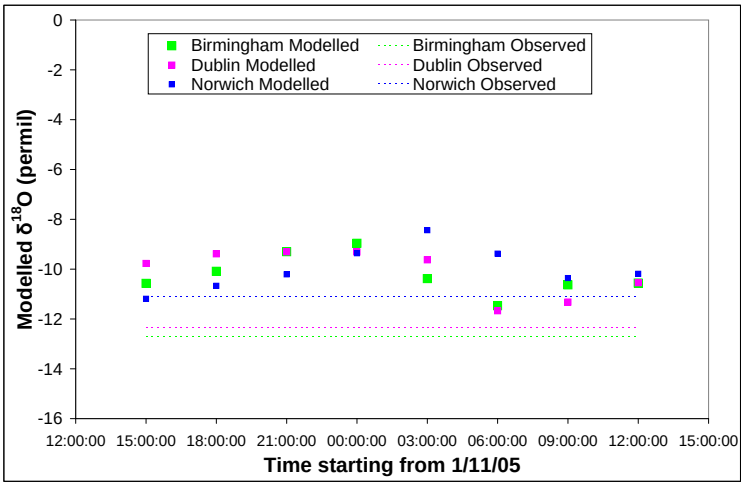

(ii)

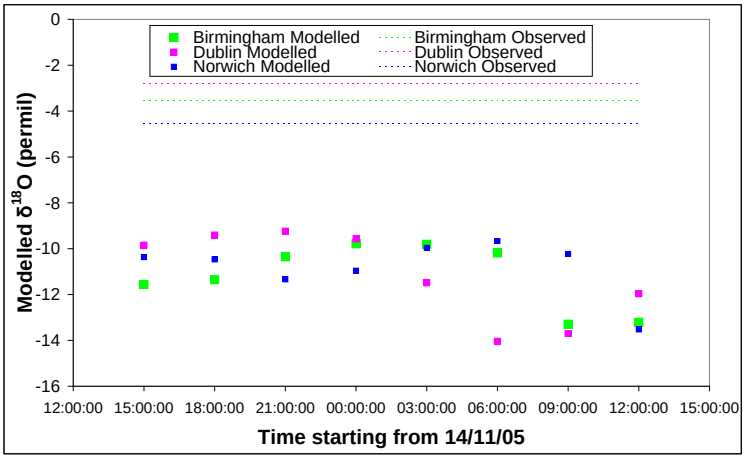

(iii)

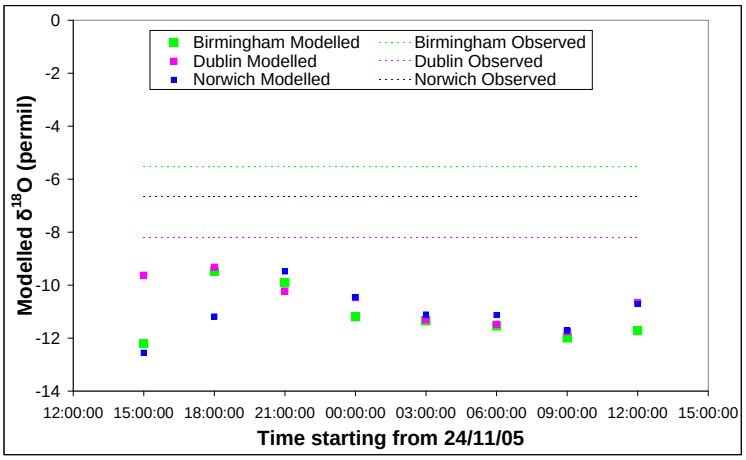

Figure 5.7: *Modelled isotopic composition of trajectories initiated at 8 times throughout the sample day plotted as point values against time for (i) 2nd November 2005, (ii) 15th November 2005, and (iii) 25th November 2005. Observed values are shown as a dashed line. Norwich data is shown in blue, Birmingham in green and Dublin in pink.*

there was no significant difference between the 4 run and 8 run averages for Norwich raindays in November 2005, as can be seen from the nearly identical regression equations of y = 0.10x -10.95 for 4 run averages and y = 0.10x -10.98 for 8 run averages both with correlation coefficients of 0.07. Therefore to save on computing time while maintaining model accuracy, 4 run averages will be used.

5.2 MCIM

The MCIM code was provided by Michiel Helsen with example input and output files included so the UEA set–up was easily verified. The standard MCIM parameters used involved all water vapour mixed into the parcels coming from the ambient air surrounding the parcel, and the use of monthly ECHAM data fields. (Note monthly not daily ECHAM fields were utilised in these tests when not being specifically varied themselves for all final values given in Chapter 5. This is due to the reduction in computing time required when using monthly fields.) The sensitivity of the model was then investigated by varying certain parameters and variables. The modelled results were again compared with isotopic data collected in November 2005 at sites in Norwich, Birmingham and Dublin.

5.2.1 Isotopic Composition of Ambient Air

As an initial test of the MCIM, global atmospheric δ^{18}O and δD were set to constant values, (0, -10, and -20 $^{\circ}/_{\circ\circ}$). Therefore all parcels were initiated with the same isotopic composition and all surrounding water vapour mixed into the air parcel would also have this composition. The results, figure 5.9, show a uniform decrease in modelled values following the decrease in the set atmospheric water vapour composition. Therefore any errors in the atmospheric data set will be passed through the MCIM but not amplified.

To more accurately set the air parcel's initial isotopic composition, and to account for changes in the surrounding water vapour's δ values, a uniform atmospheric value will not be used. Instead, monthly and daily climatologies of isotopic values on 17 atmospheric levels created using a 20 year run of the ECHAM4 climate model will be searched for

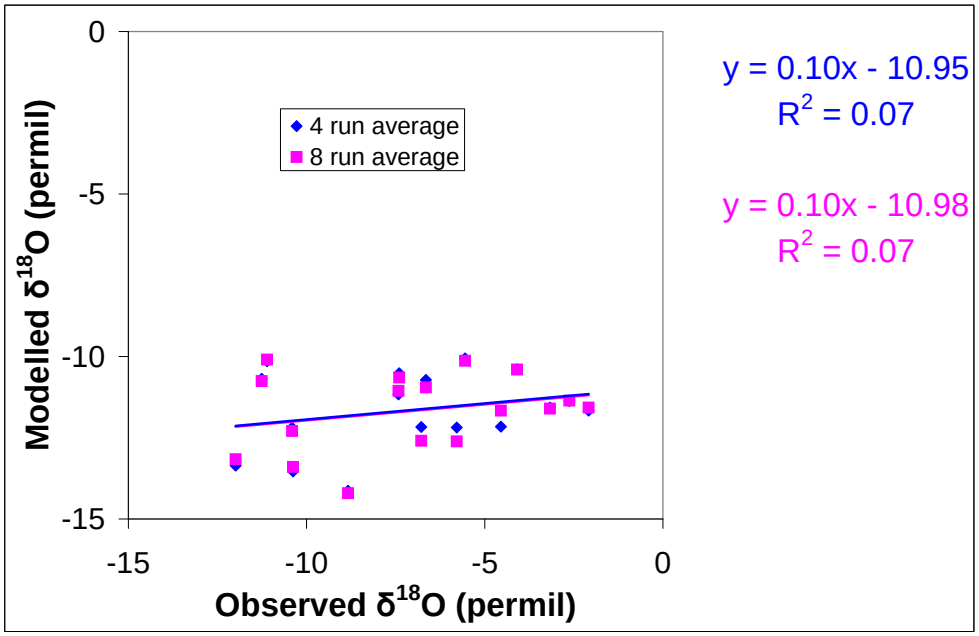

Figure 5.8: *Modelled versus observed $\delta^{18}O$ for all Norwich raindays. Modelled values are from 4 run averages (blue) and 8 run averages (pink). Best fit lines for the data are shown, as are the regression equations for these lines and the correlation coefficients of the relationships (to the right of the figure).*

time and three–dimensional location specific δ values.

5.2.2 Threshold Relative Humidity at Which Precipitation Occurs

In the original set–up of the MCIM (Helsen et al., 2006), precipitation occurs as soon as the relative humidity rises above 80%. This is a typical threshold value used in Atmospheric General Circulation Models (AGCMs). However, these large scale models are estimating precipitation from a grid box at least 1° x 1° in size that has a single relative humidity value. This single value has to describe conditions across the entire grid box area. Some areas could have 100% humidity and precipitation could be falling, but other areas in the same grid box could only have a 60% or less humidity and not be precipitating. As precipitation is occurring in the grid box, the average of 80% must also allow precipitation.

The FLEXPART trajectories are on a much smaller scale than AGCMs and therefore the relative humidity value associated with any point along a trajectory will theoretically

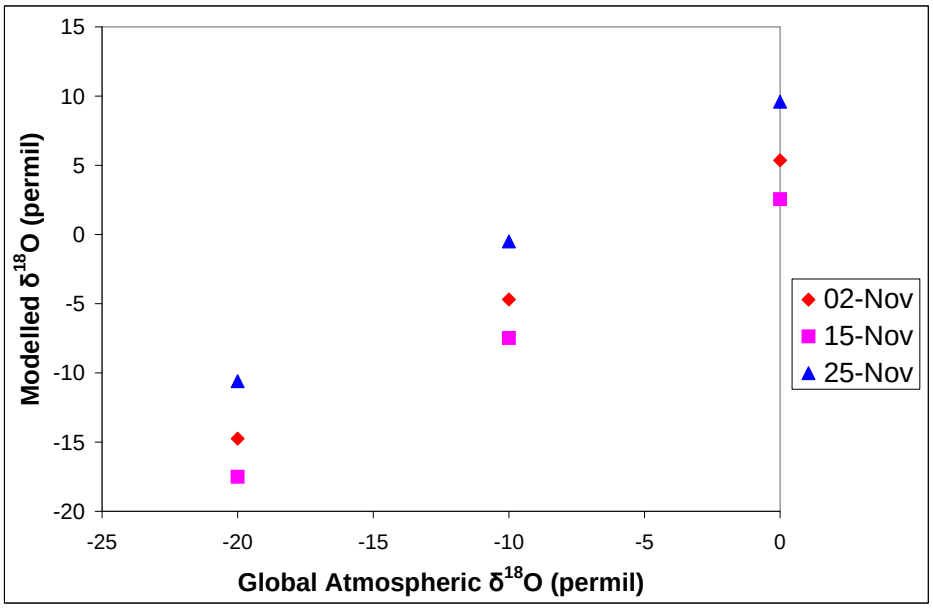

Figure 5.9: *Modelled $\delta^{18}O$ values of precipitation produced using a single initial and ambient global atmospheric $\delta^{18}O$.*

be more accurate than an average over a larger grid box. Physically, an air parcel must achieve at least 100% relative humidity before precipitation occurs. Runs were conducted with the humidity threshold at 80%, 85%, 90%, 95% and 98% to examine the sensitivity of the results to this threshold.

Figure 5.10 shows the results of this test on all Norwich raindays. All gradients and r^2 values in figure 5.10 are small and only those for 90% humidity are statistically significant at the 95% level. However, a move towards less depleted isotopic values with increased humidity threshold for all tested dates and locations can be seen. The general magnitude of the isotopic change for δ^{18}O is +5 $^{\circ}/_{\circ\circ}$ with a change in humidity from 80 to 98%. The changes are greatest between 80 and 90%. This move to less negative values is as expected as increasing the threshold value decreases the amount of precipitation occurring, so reduces the rainout that would deplete an air parcels' isotopic composition. Similar results were seen for Dublin and Birmingham raindays.

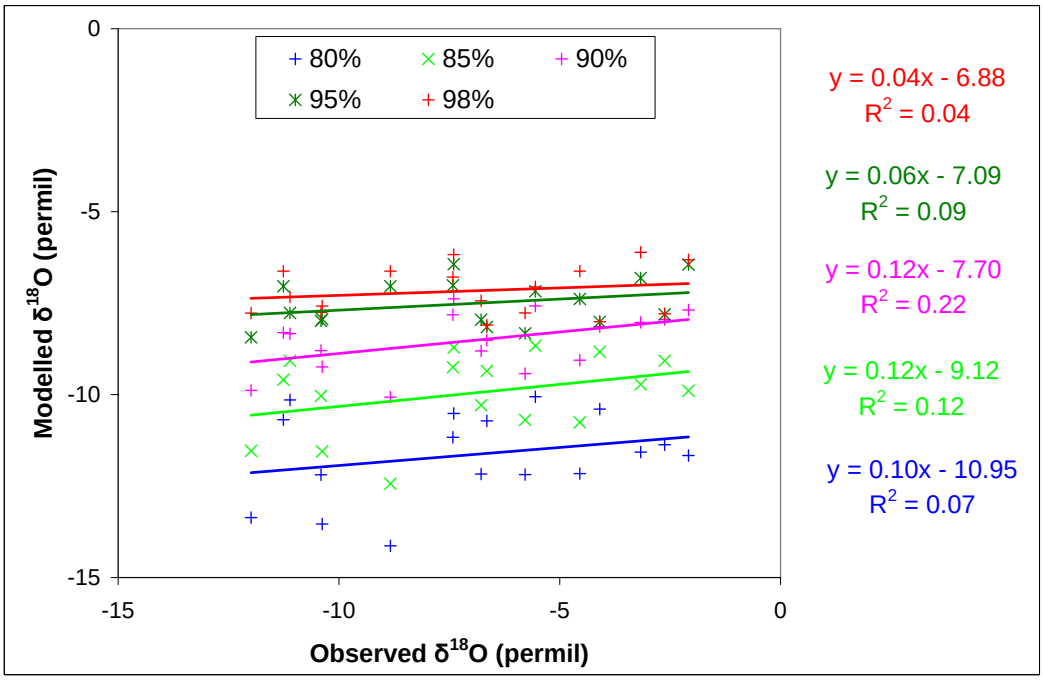

Figure 5.10: *Modelled isotopic composition from MCIM runs for Norwich raindays with varying rainout relative humidity thresholds.*

5.2.3 Relative Proportions of Ambient and Internal Air Mixing

The MCIM uses the ECMWF ERA-40 reanalysis fields for temperature, pressure and specific humidity along the FLEXPART trajectories to calculate the isotopic values. If there is an increase in specific humidity then for mass conservation to be observed water vapour must be added to the air parcel. In Michiels' version of the MCIM, all of this added water vapour is taken in from the surrounding air with an isotopic value determined by the monthly ECHAM4 climatology.

However, these ambient air values are climatological averages and it is unlikely that at any one time the air surrounding a parcel will be exactly that of these monthly averages. It is therefore suggested that the source of water vapour that is mixed into the parcel by the MCIM is slightly altered to include a proportion of water vapour of the composition currently held by the parcel. This is arguably more realistic as each parcel will most likely be surrounded by at least some parcels that have traveled with it for some distance, thereby gaining a similar isotopic composition.

This theory was tested with a 50:50 mix of ambient and internal water vapour being taken in by the MCIM whenever water vapour is required by the mass conservation elements, figure 5.11. As expected, these runs produced more negative isotopic values as the isotopic composition of the water vapour inside the parcel is more depleted in heavy isotopes than climatological water vapour due to rainout from the parcel.

The changes in modelled isotopic composition caused by this sensitivity test are different on each of the 3 test days being 1.3 ‰, 1.6 ‰ and 0.7 ‰ for the 2nd, 15th and 25th November 2005 respectively. However, the variation is similar for each location on each day. Due to the consistency of these variations a range of different ratios of internal and ambient water vapour were tested on all Norwich raindays as this parameter appeared to have the ability to affect the regression relationship between modelled and observed values. The following internal:ambient ratios were also tested 0:100, 25:75, 50:50, 72:25, and 100:0. Figure 5.11 shows the effect of these variations in internal:ambient ratios when using a 80% humidity threshold. As seen in figure 5.11, at an 80% humidity threshold there is as much as a 5 ‰ variation across the internal:ambient ratios. The gradient of the regression lines is steepest for the 100:0 internal:ambient ratio at 0.25 and the equations are only significant at the 90% level for the 100:0 and 75:25 ratios. Other humidities were also tested and at 90% humidity thresholds and above the variation in δ^{18}O caused by changing the internal:ambient ratio is reduced greatly to an average of 0.5 ‰. It was therefore decided to use a humidity threshold of 95% to minimise the effect of changing the internal:ambient ratio. Using a internal:ambient ratio of 0:100 was chosen as varying the ratio has very little effect with the higher humidity threshold and it also allows comparisons with the results of Helsen et al. (2006) while maximising the gradient and the significance of the regression equations relating observed and modelled values.

5.2.4 Temporal Resolution of Ambient Isotopic Composition Fields

When using monthly ECHAM4 fields there will be a discontinuity across month boundaries. This could theoretically affect the isotopic values produced by the model. Therefore the monthly fields were interpolated to a daily timescale to remove this possible discon-

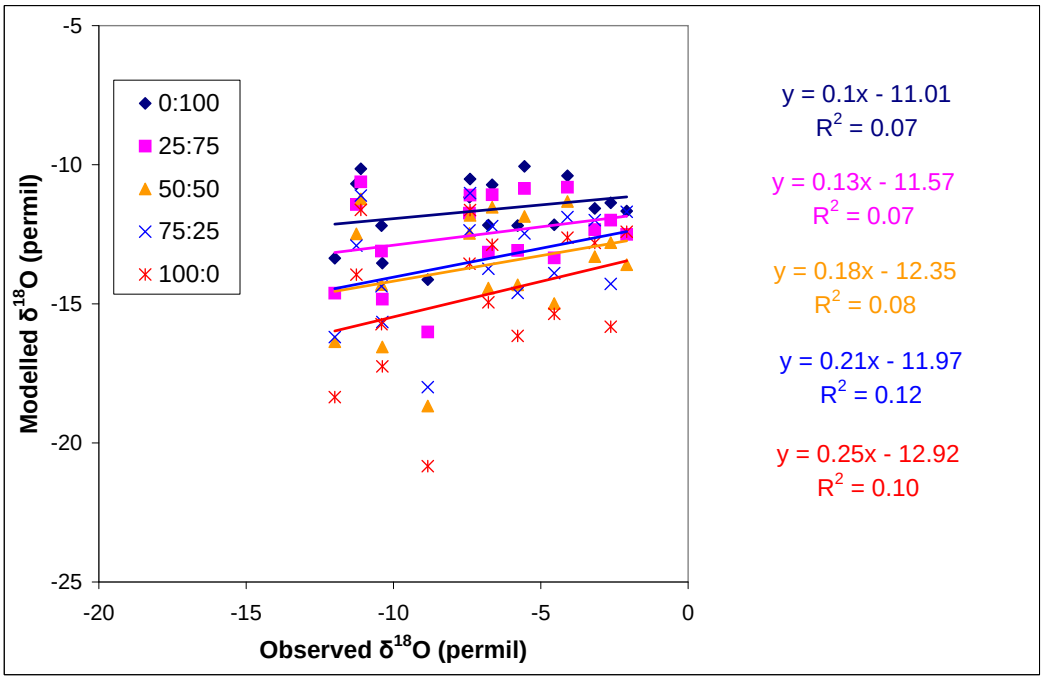

Figure 5.11: *Effect of varying the proportions of internal and external air mixed into the parcel. Internal:ambient ratios tested 0:100, 25:75, 50:50, 72:25, and 100:0. With a humidity threshold of 80%.*

tinuity. The MCIM was run for all Norwich raindays using both the daily and monthly fields and the resultant isotopic values compared. The actual changes in isotopic values seen were not significant, (for δ^{18}O most changes were less than the sampling error in the order of 0.1 $^{\circ}/_{\circ\circ}$). The daily fields will be used due to their theoretical advantage of avoiding a discontinuity across month transitions.

5.3 Post–production Processing

The method for the statistical averaging of the data was also investigated to ensure that the output data was handled in such a way as to accurately reflect the real world. All isotopic values given so far in this chapter were created by a straight average of all particles released from each location.

5.3.1 Sampling of Raining Parcels Only

As part of its output, the MCIM creates a value for the amount of liquid precipitation at each timestep along a trajectory. By selecting only the isotopic values of air parcels that the MCIM predicts to be raining at the final timestep, the average final isotopic prediction could theoretically be improved. This approach would have the drawback of assuming that the MCIM always correctly models when a parcel loses vapour as rain. However, it may also eliminate parcels that would be unlikely to contribute to the rainfall that may have experienced very different conditions along their trajectories, skewing the prediction. Data obtained from 10 day runs with a 3 hour timestep and releases at 0-100 m agl were filtered for only raining particles before being averaged and these results compared with the averages of all 100 particles, figure 5.12. There is no systematic change in accuracy seen when comparing the two sets of results. Some show an increase in accuracy and others a decrease. The magnitude of the changes are also highly variable though many of the changes are on the order of 0.5 $^{\circ}/_{\circ\circ}$, double the sampling error. This non–uniform change is also seen when 4 run daily averages are calculated. Due to the majority of results being worsened by only taking the raining particles into account, it must be concluded that the MCIM modelling of which particles are raining is not very accurate in this case. This could be due to the fact that only the last timestep has been considered. Another potential problem is that the particles released first will have already travelled away from the specified location before all particles have been released and data output from FLEXPART begins. This offset creates a slight loss of transport information that may cause the MCIM amount of rainfall calculations to be inaccurate. The most likely explanation is that rain is not being initiated within the 0-100 m agl layer. This layer is being used due to isotopic equilibration of raindrops occurring with the vapour in this layer as they fall through so that the rain obtains the isotopic composition of that layer of the atmosphere. However, the rain is falling through, not necessarily originating in, this layer.

Due to these problems, and the fact that in 7 out of 9 rainday tests the averaging of all particles created the modelled values that were closest to observations, all particles will

be averaged in all further tests.

5.4 The Model Set–up

To test the stability of the models to be used in this study, sensitivity tests were conducted as described in this chapter. These tests entailed varying initial parameters within the models and seeing the impacts that these changes had on the model output. FLEXPART output is complicated and of a very large volume making detailed comparisons between results difficult. Therefore the final MCIM isotopic results were relied upon to give an indication of the sensitivity of the model to each parameter. Table 5.4 summarises the typical variation in δ^{18}O caused by each test conducted in this chapter. Only δ^{18}O is shown as δD varied similarly relative to its magnitude. All variations shown in this table should be compared with the estimate of sampling error of 0.15 $^{\circ}/_{\circ\circ}$ found by varying the initial release locations (determined by random seed numbers) of the particles (section 5.1.1). If variations are of a similar magnitude to the sampling error then they could be due to insufficient sampling. It should also be remembered that the modelled range across 100 particles has a standard deviation of 1.5 $^{\circ}/_{\circ\circ}$ so this is likely to be the biggest error by far.

5.4.1 FLEXPART Parameters

The following standard parameter choices have been made, based on the results of the sensitivity tests. **100 particles** will be released in all further tests. 1000 particles were tested and did reduce the sampling error caused by varying the initial release locations from 0.15 to 0.04 $^{\circ}/_{\circ\circ}$. However, this increase in accuracy came at too great a computational cost to be feasible for this study (section 5.1.1). When the same random seed numbers were used for initiating 100 particles and 1000 particles the average variation in δ^{18}O seen was 0.13 $^{\circ}/_{\circ\circ}$.

A **1 hour Lagrangian timestep** was found to be marginally the best at reproducing observed values (section 5.1.2). Changing the timestep length had a large impact on the modelled isotopic value with variations in δ^{18}O of 2 $^{\circ}/_{\circ\circ}$ common. However, there

(i)

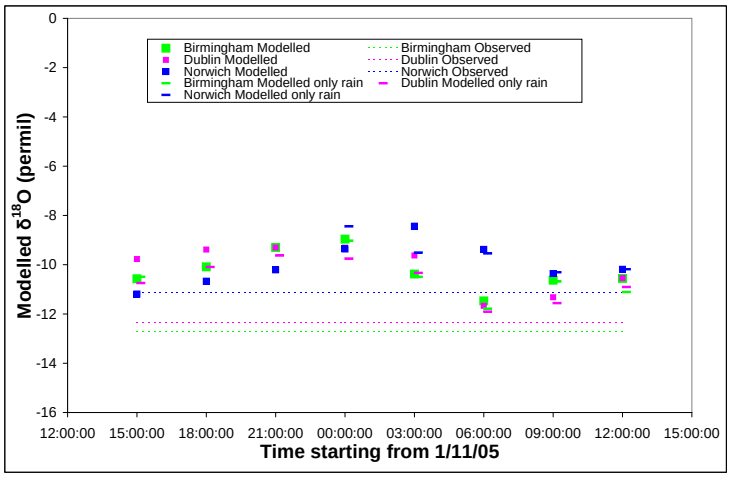

(ii)

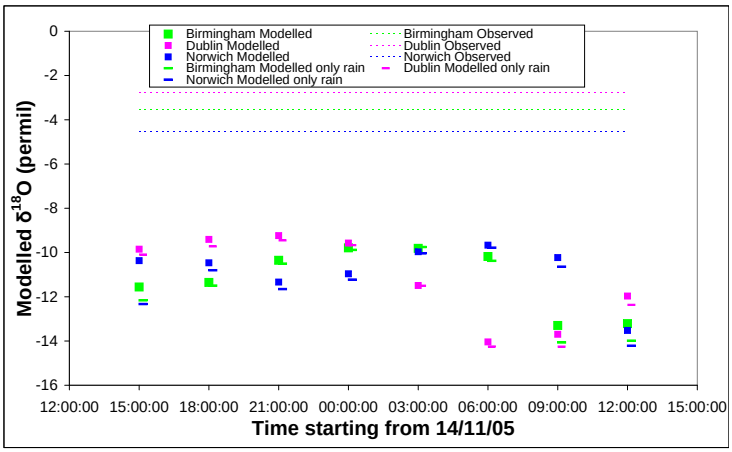

(iii)

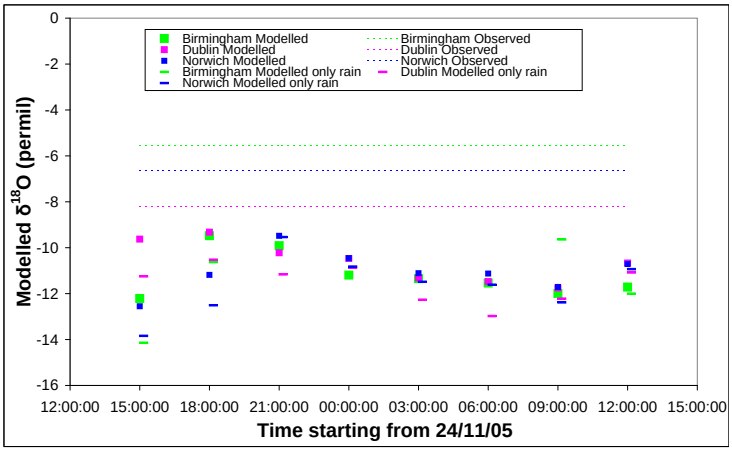

Figure 5.12: *Modelled isotopic composition of all particles and only raining particles. Trajectories initiated at 8 times throughout the sample day plotted as point values against time for (i) 2nd November 2005, (ii) 15th November 2005, and (iii) 25th November 2005. Observed values are shown as a dashed line. Squares mark averages of all particles, lines mark average of only raining particles. Norwich data is shown in blue, Birmingham in green and Dublin in pink.*

was no convergence towards a single isotopic value with varying timestep length. Using the Lagrangian or non–Lagrangian timesteps caused much smaller variations (average change in δ^{18}O of 0.2 $^{\circ}/_{\circ\circ}$). Therefore the decision on which timestep to use was made by modelling the entire Norwich rainday observed data set and the timestep that produced the best modelled to observed correlation coefficient was chosen.

Particles will be released from a horizontal grid box of **0.1 ° x 0.1 °**. Changing the release box size had very little impact on the isotopic values modelled (an average change of 0.16 $^{\circ}/_{\circ\circ}$ in δ^{18}O values). A 0.1 ° x 0.1 ° box is small enough so that the sites are in separate release boxes but is also large enough to take into account the limitations of interpolation from the ECMWF windfields grid of 1 ° x 1 ° (section 5.1.4). Turning the convection scheme on and off had a slightly larger average impact of 0.23 $^{\circ}/_{\circ\circ}$. Though this value is skewed by a few large variations and in most cases the change caused by turning the convection scheme on and off was smaller than the sampling error. These in most cases small impacts can be partly explained by the general lack of convection over Britain during winter months. FLEXPART will be run with **convection on** as this is theoretically more accurate (section 5.1.6). The duration of a trajectory back in time is set to be **10 days** (section 5.1.3). At lengths shorter than 10 days, the day to day changes in modelled δ^{18}O were an order of magnitude greater than the sampling error (maximum of 2.2 $^{\circ}/_{\circ\circ}$ change in δ^{18}O from 3 day to 10 day trajectories). Between 10 and 20 days, however, very little variation (a maximum of 0.05 $^{\circ}/_{\circ\circ}$) was seen.

Changing the number of runs required in a day to be able to compare daily modelled values with the daily observed values available had very little effect on the final δ^{18}O values (average of 0.15 $^{\circ}/_{\circ\circ}$). To reduce computational time, **4 runs** will be conducted within each 24 hour period starting at, 1800, 0000, 0600 and 1200 (section 5.1.7). Particles will be released from a height of **0-100 m agl** as results from this height range most often gave modelled isotopic values that were closest to the observed values. This height range is also theoretically most accurate for this model due to the lack of equilibration with ambient water vapour in the MCIM equations. If rainfall is assumed to almost always fully equilibrate with the water vapour in the lowest 100 m of the atmosphere as long as

rainfall is not too heavy, then the isotopic composition of this layer is the value required (section 5.1.5).

5.4.2 MCIM Parameters

The variations caused by changing MCIM parameters were less conclusive. It is important to have an accurate data set of background atmospheric δ values. This will be ensured by using climatological daily fields on 17 atmospheric levels interpolated from monthly fields created from a 20 year integration of the ECHAM4 GCM (sections 5.2.1 and 5.2.4). A **humidity threshold of 95%** will be used to minimise the effect of changing the internal:ambient ratio (section 5.2.2). Using a **internal:ambient ratio of 0:100** was chosen to maximise the gradient and the significance of the regression equations relating observed and modelled values (section 5.2.3).

5.4.3 Data Processing

Different methods of averaging the modelled particles were investigated in order to create the best results. **Averaging all particles** gave the modelled results that best matched the observed values (section 5.3.1). To be able to consider the effect of only raining particles, more confidence in the temporal and spatial scales of both the MCIM and FLEXPART would be required.

Parameter Changed	**Parameter changed to**	**Change in δ^{18}O ($^{\circ}/_{\circ\circ}$)**
Sampling error		
		0.15 (mean)
Number of particles		
100	1000	0.13 (mean)
Timestep		
3 hours	1 hour	1 to 2
Non–Lagrangian	Lagrangian	0.2 (mean)
Horizontal grid box		
0.1 x 0.1 degree	0.01 x 0.01 degree	0.16 (mean)
Convection		
On	Off	0.23 (mean)
Trajectory length		
3 days	10 days	2.2 (max)
10 days	20 days	0.05 (max)
Number of runs		
4 runs	8 runs	0.15 (mean)
Height of release		
0-100 m agl	0-5000 m agl	7 (mean)

Table 5.4: *The variation in $\delta^{18}O$ during each FLEXPART sensitivity test.*

Chapter 6

Driby, Lincolnshire and Stock Hill, Somerset Case Studies

The accuracy of the conclusions drawn in Chapter 4 are perhaps limited by the small sample size (only one month; November 2005) of the observed data. In this Chapter, two longer observed data sets of the daily isotopic composition of rainfall are modelled using the Lagrangian Isotope trajectory model. The data sets are from Driby in Lincolnshire, and Stock Hill in Somerset. The locations of these sites in relation to the Chapter 4 sites of Birmingham, Dublin and Norwich can be seen in figure 6.1. Precipitation was sampled at Driby from March 1979 until September 1979 and then again from October 1980 until June 1982, a total of 312 raindays. The Stock Hill sampling period lasted from November 1977 to February 1979, with 201 raindays.

The precipitation data from Driby, Lincolnshire were published by Heathcote and Lloyd (1986). The data were collected as part of a project funded by the Natural Environment Research Council (NERC). These data were obtained through Professor Ian Fairchild (University of Birmingham). The data from Stock Hill are as yet unpublished but were made available for this project by Professor Tim Atkinson (UCL). The data were collected by Forestry Commission personnel, co–ordinated by Peter L Smart of the University of Bristol (now Professor Peter Smart). Isotope analyses were conducted by Dr Willi Stichler of the University of Munich and International Atomic Energy Agency

Figure 6.1: *Map of the British Isles showing the location of Birmingham, Dublin and Norwich, as well as Driby and Stock Hill.*

(IAEA), Vienna. The data were collected as part of a project funded by NERC called, "Stable isotope composition of karst aquifer waters in the Mendip Hills, Somerset." (1977-80; Joint Principal Investigators T. C. Atkinson, University of East Anglia, and P. L. Smart, University of Bristol).

6.1 Observed Precipitation Amount at Driby and Stock Hill

To compare the results of this case study with those obtained from the November 2005 case study, the original observed data sets were first compared. Figure 6.2 shows the amount effect at Stock Hill and Driby by plotting observed δ^{18}O against the amount of precipitation that occurred. In Chapter 4 similar comparisons were made for the data collected at Norwich, Dublin and Birmingham and strong relationships were seen (correlation coefficients of 0.40, 0.36 and 0.26 respectively, see section 4.3). The larger data sets from Driby and Stock Hill do not show the same strength of relationship (figure 6.2). The relationships at Stock Hill and Driby have low gradients (-0.21 and -0.11 respectively) and only just significant correlation coefficients (0.05 and 0.06 respectively). This difference in situation between the two case studies may affect the relative performance of the model as amount effect is no longer an important observed feature. Care must be taken when making comparisons if this is an indication of different processes dominating across the longer Stock Hill and Driby time periods.

Another difference between the Driby and Stock Hill data sets and those of Norwich, Dublin and Birmingham is the amount of precipitation seen. The maximum amount observed during November 2005 was 17.60 mm at Birmingham on the 6th November 2005 and events of this size were rare. Across the longer Stock Hill and Driby observation periods there are many more of these larger precipitation amount days (figures 6.3 and 6.4) with the maximum amount of 41.50 mm seen at Driby on the 24th April 1981. This variation highlights the fact that a larger range of processes and atmospheric situations will be included in the Stock Hill and Driby data sets due to both the increased number

(i)

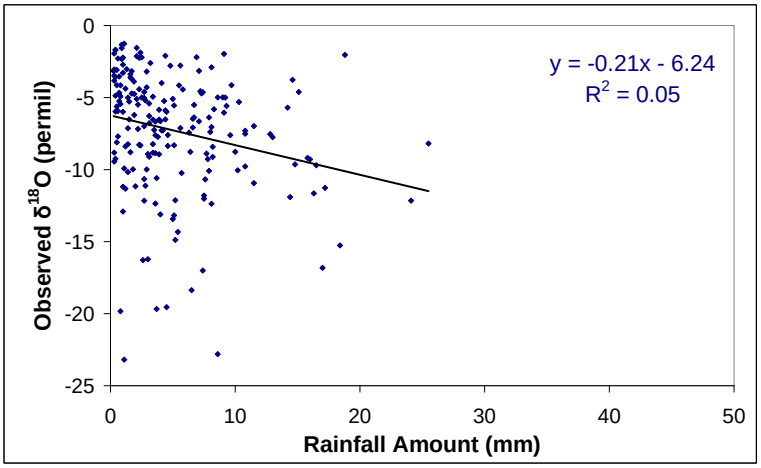

(ii)

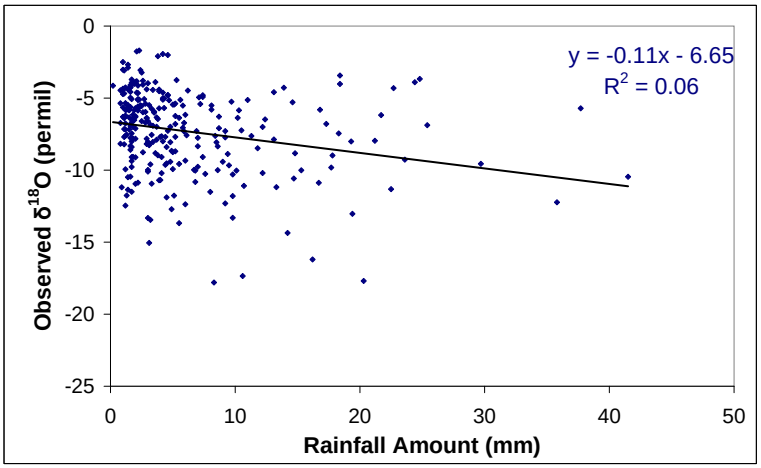

Figure 6.2: *Scatter plot of observed $\delta^{18}O$ against the daily precipitation total amount during the sampling periods at (i) Stock Hill, and (ii) Driby. The straight lines are best fits by linear regression; the regression equation and r^2 values of the lines are shown in the upper right of each panel.*

of observations and the temporal spread across all seasons rather than just the one winter month. Convective systems will be more common across the summer months, and re–evaporation will also play a more important role.

6.2 Observed Isotopic Ratio of Precipitation

The observed values at Driby ranged from a maximum of δ^{18}O = -1.70 $^{\circ}/_{\circ\circ}$ and δD = -3.20 $^{\circ}/_{\circ\circ}$ on the 22nd April 1981 to a minimum of δ^{18}O = -17.80 $^{\circ}/_{\circ\circ}$ on the 3rd October 1981 and δD = -140.30 $^{\circ}/_{\circ\circ}$ on the 22nd July 1981. The observed values at Stock Hill ranged from a maximum of δ^{18}O = -1.26 $^{\circ}/_{\circ\circ}$ on the 23rd October 1978 and δD = -4.3 $^{\circ}/_{\circ\circ}$ on the 26th September 1978 to a minimum of δ^{18}O = -23.19 $^{\circ}/_{\circ\circ}$ and δD = -175.6 $^{\circ}/_{\circ\circ}$ on the 22nd December 1978. This maximum and minimum information is summarised in table 6.1. The ranges of isotopic values seen at Driby and Stock Hill are very similar, table 6.1. The range of observed values across the whole extended sampling period is, perhaps surprisingly, not much greater than that seen at Norwich, Dublin and Birmingham during November 2005, see section 4.6. The δ^{18}O means for all sites are within 1.12 $^{\circ}/_{\circ\circ}$ of each other, which when compared to the ranges seen of close to 20 $^{\circ}/_{\circ\circ}$ is minimal. Similarly for δD, the means are all within 15.37 $^{\circ}/_{\circ\circ}$ of each other whereas the ranges seen are over 130 $^{\circ}/_{\circ\circ}$. The mean values for all sites are shown in table 6.2.

The range of deuterium excess values, however, is very much greater for Driby and Stock Hill than was seen in November 2005, see figures 4.5, 6.5 and 6.6. As discussed in section 1.2.4, d-excess values give an indication of the source region of an air parcel. The wider range of deuterium excess values seen at Driby and Stock Hill indicates a larger variety of source regions and source region conditions across the 5 year sampling period as opposed to just November 2005, as would be expected.

The regression equation linking observed δ^{18}O with observed δD at Stock Hill was y = 7.77x +6.83, (figure 6.5). At Driby the relationship was described by y = 7.51x +4.74 (figure 6.6). The gradients of these regression equations are similar to the Global Meteoric Water Line (y = 8x +10) and the November 2005 Meteoric Water Line of y = 7.87x +14.32. However, the y–intercept values are smaller than both the GMWL and the November 2005

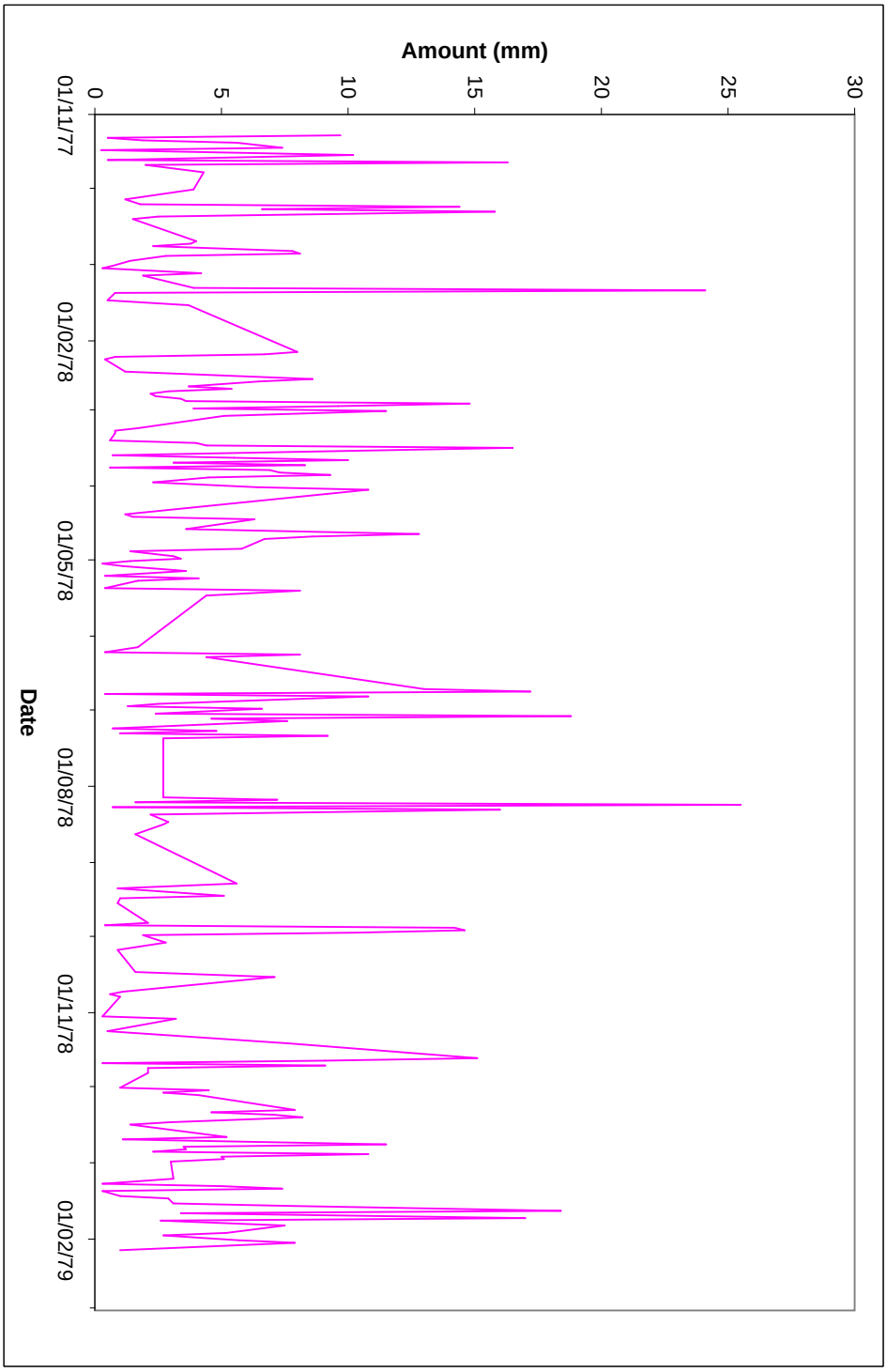

Figure 6.3: *The amount of precipitation observed at Stock Hill throughout the sampling period.*

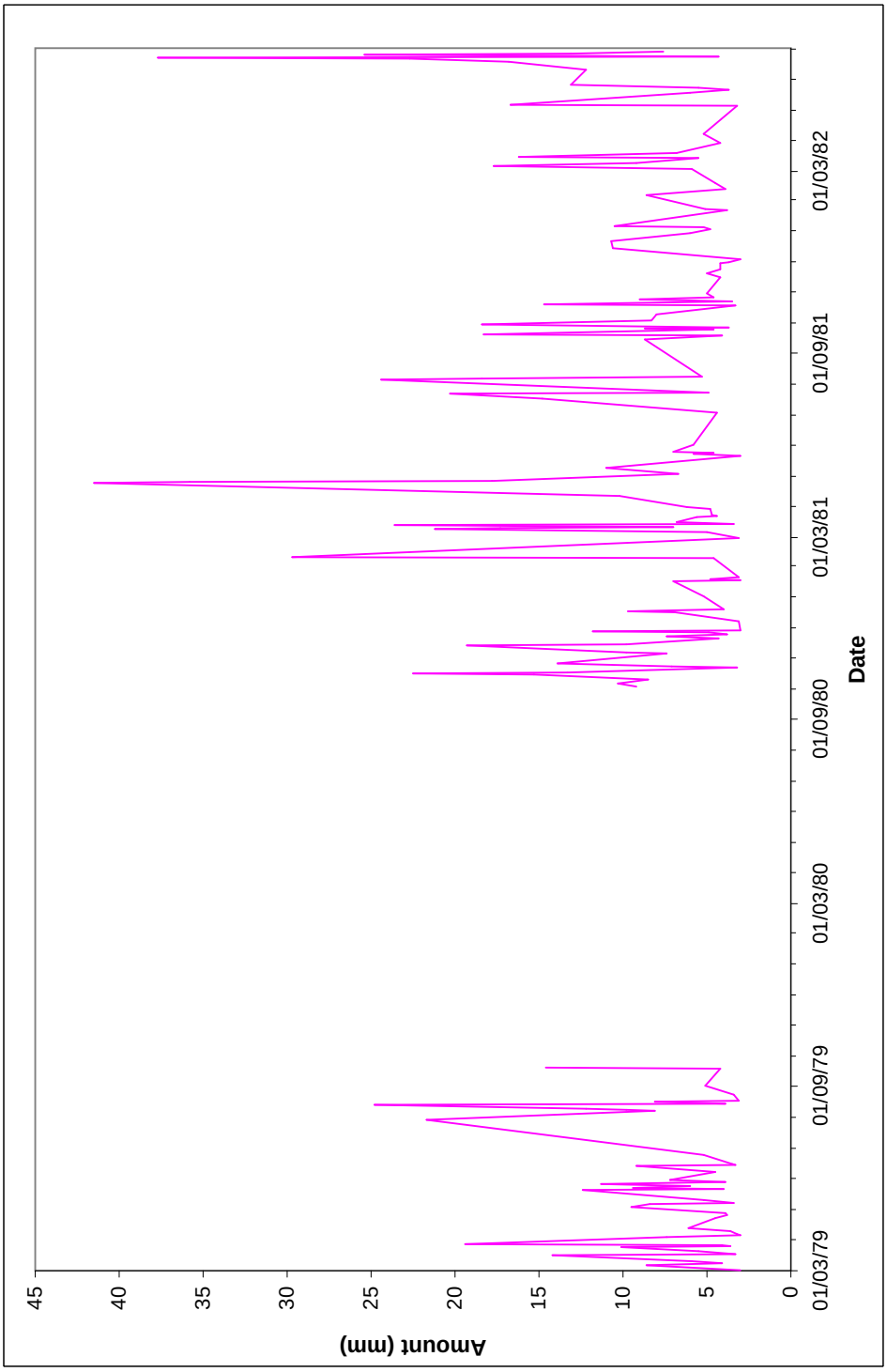

Figure 6.4: *The amount of precipitation observed at Dribyt throughout the sampling period.*

	Stock Hill			Driby		
	δ^{18}O (‰)	δD (‰)	Date	δ^{18}O (‰)	δD (‰)	Date
Maximum	−1.26		23/10/78	−1.70	−3.20	22/04/81
		−4.3	26/09/78			
Minimum	−23.19	−175.6	22/12/78	−17.80		03/10/81
					−140.30	22/07/81
Range	21.93	171.3		16.1	137.1	

Table 6.1: *Maximum and minimum observed $\delta^{18}O$ and δD at Stock Hill and Driby.*

Site	δ^{18}O (‰)	δD (‰)
Norwich	−7.06	−41.85
Dublin	−7.34	−41.53
Birmingham	−8.18	−47.91
Stock Hill	−7.71	−53.18
Driby	−7.29	−50.47

Table 6.2: *Mean observed $\delta^{18}O$ and δD at Norwich, Dublin, Birmingham, Stock Hill and Driby.*

MWL (6.83 and 4.74 as compared to the global value of 10 and November 2005 value of 14.32). Lower d-excess values tend to be found in vapour formed in areas of higher humidities (Araguás-Araguás et al., 2000). This suggests that the Stock Hill and Driby water vapour source regions were either at more oceanic locations than for Norwich, Dublin and Birmingham, or more likely that over the longer time frame higher temperatures leading to higher relative humidities were experienced more often. The lower d-excess values can also be an indication of secondary evaporative processes (Araguás-Araguás et al., 2000). If evaporation occurs below the cloud base as raindrops fall the d-excess values of the liquid phase decrease and the d-excess values of the vapour increase.

6.2.1 The Seasonal Cycle of δ^{18}O

A seasonal cycle of isotope ratios in precipitation has been observed at continental mid– to high–latitude locations (section 1.2.2). Precipitation tends to be isotopically depleted in the winter and enriched in summer due to seasonal temperature changes, or changes

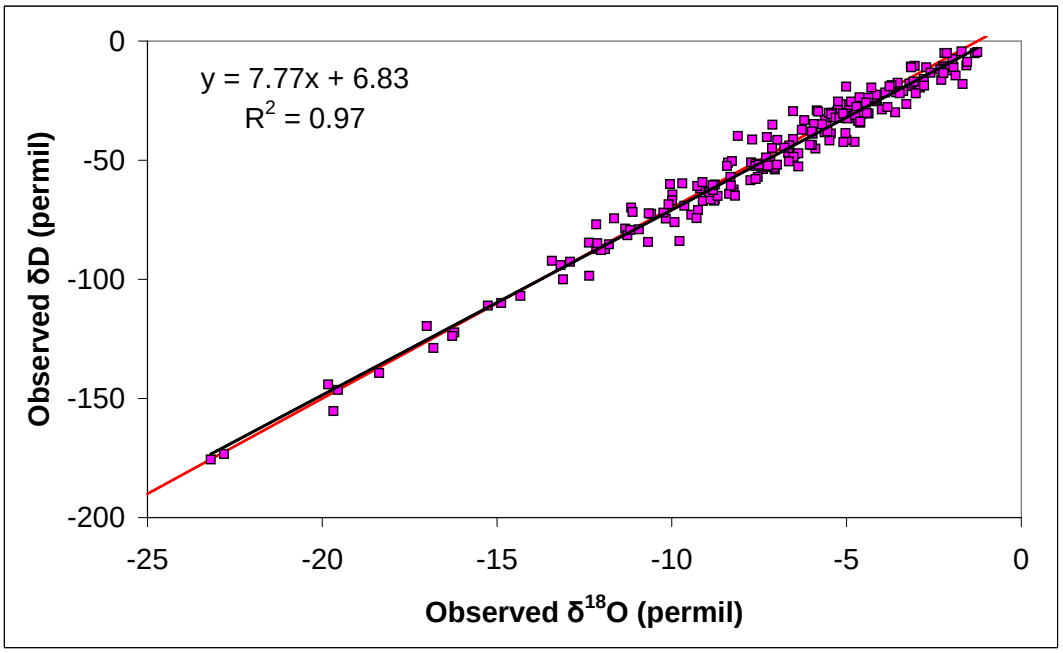

Figure 6.5: *Observed $\delta^{18}O$ versus δD for Stock Hill raindays. The black line is the best fit line through the observed values. The regression equation of this line and the correlation coefficient are displayed in the top left hand corner. The Global Meteoric Water Line (red line) is the general ($\delta D = 8*\delta^{18}O + 10$) relationship between the two variables.*

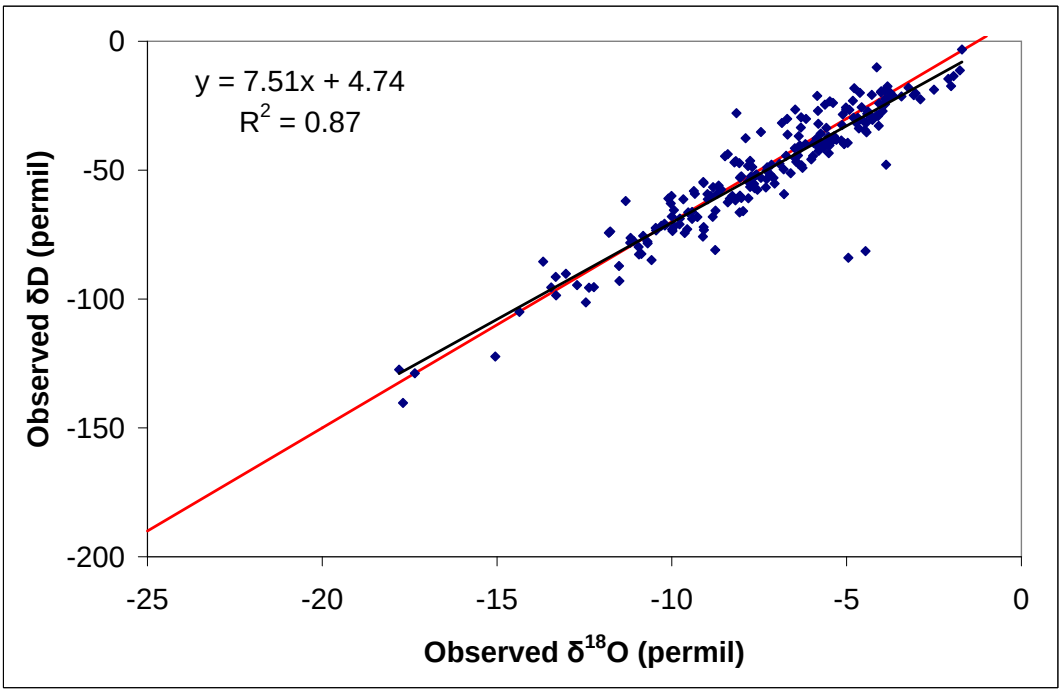

Figure 6.6: *Observed $\delta^{18}O$ versus δD for Driby raindays. The black line is the best fit line through the observed values. The regression equation of this line and the correlation coefficient are displayed in the top left hand corner. The Global Meteoric Water Line (red line) is the general ($\delta D = 8*\delta^{18}O + 10$) relationship between the two variables.*

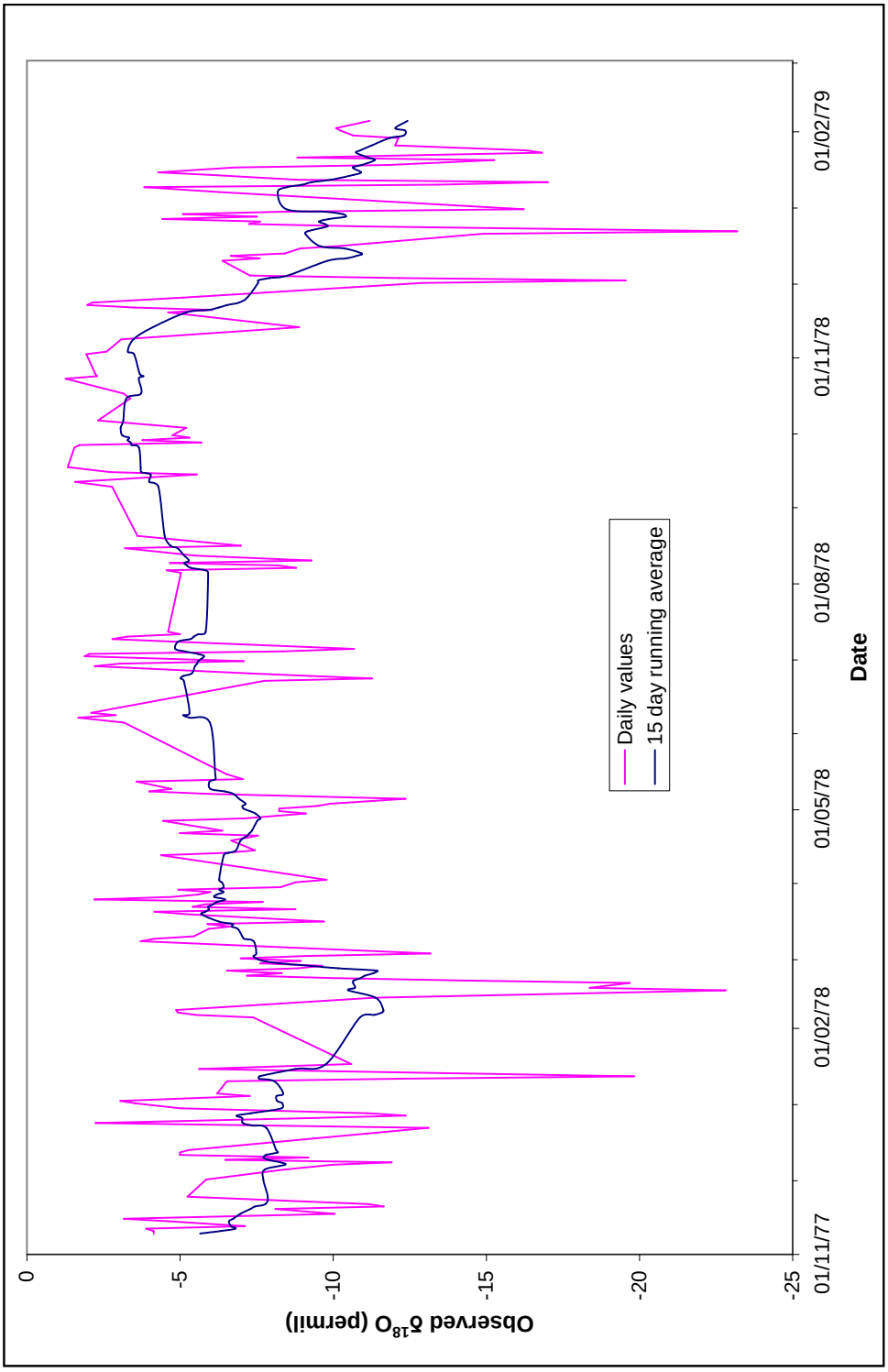

Figure 6.7: *The observed $\delta^{18}O$ of precipitation for Stock Hill from November 1977 to February 1979 (pink). The navy line shows a 15 day running average throughout the time series.*

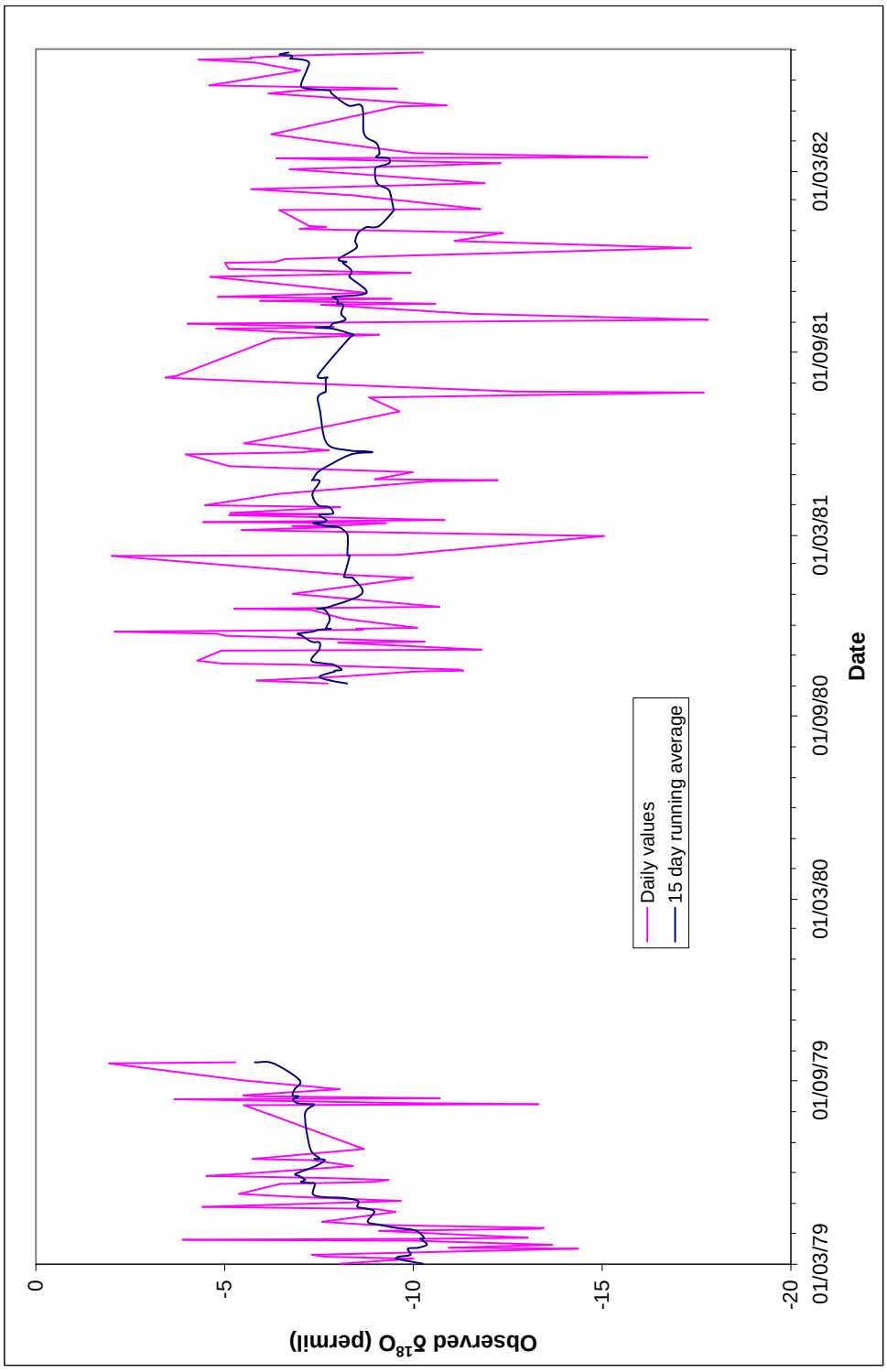

Figure 6.8: *The observed $\delta^{18}O$ of precipitation for Driby from March 1979 to September 1979, and from October 1980 to June 1982 (pink). The navy line shows a 15 day running average throughout the time series.*

in the amount of evapotranspiration occurring, or changes in water vapour source regions (Jouzel et al., 1997). Figures 6.7 and 6.8 show the observed δ^{18}O of precipitation across time at Stock Hill and Driby respectively. The Stock Hill δ^{18}O time series, figure 6.7, shows the expected seasonal cycle with more negative values in January and February of both 1978 and 1979. The situation at Driby is less defined. Starting in March 1979 the δ^{18}O values do tend to increase away from winter until September 1979. There is then a gap in the data set until September 1980 where δ^{18}O values restart with more negative values than in the previous September. From September 1980 to September 1981 the δ^{18}O values do not systematically change at Driby. There is then a slight decrease in δ^{18}O from September 1981 to January and February 1982 before a slight increase to March 1982 but none of these changes are as big as the trends seen at Stock Hill.

6.2.2 Extreme Observed δ^{18}O

In the observed time series of δ^{18}O for Stock Hill and Driby, (figures 6.7 and 6.8), there are some obvious extreme values. To try to explain why these values were unusually large or small, the trajectory information from FLEXPART and synoptic charts from the preceding days were consulted. The results of this investigation are presented here.

For Stock Hill the extremes chosen for investigation occurred on the 16th February 1978 and the 25th March 1978 with δ^{18}O values of -22.81 and -2.2 $\permil$ respectively. The amount of precipitation observed on these days was 8.6 and 6.9 mm respectively. The FLEXPART trajectories at all modelled times for these two days are shown in figures 6.9 and 6.10. The sample collected on the 16th February was known to be at least partially composed of snow, which explains the very negative δ values observed. Also it can be seen from figure 6.9 that all trajectories approached the U.K. from the North and were sourced over Scandinavia. The very cold temperatures over Scandinavia in February would also contribute to the δ^{18}O value of -22.81 $\permil$ seen.

The trajectories produced by FLEXPART for the 25th March 1978 (figure 6.10) show a very different situation from the 16th February 1978. The trajectories approached the U.K. from the west and were mainly sourced over North America. The path across the

Atlantic would have allowed freshly evaporated water vapour to enter the air parcels especially due to the majority of trajectories remaining in the lowest 2 km of the atmosphere. The synoptic situation could also play a part in making the δ values of precipitation on this day less depleted. As can be seen from figure 6.11, a warm front passed across Stock Hill between 1800 on the 24th and 0000 on the 25th March 1978. At 0000 on the 25th March 1978 rain and drizzle (shown by the meteorological current weather code of ";") are occurring close to Stock Hill in the warm sector of a low pressure synoptic system where less depleted δ values are expected (Gedzelman and Lawrence, 1990; Gedzelman and Arnold, 1994). This confluence of factors will most likely explain why the observed precipitation was very much less depleted in heavier isotopes.

As for Driby extremes, a very low δ^{18}O value of -17.69 $\permil$ was observed on the 22nd July 1981. Neither the trajectory situation nor the synoptic pattern for that day explained why such a negative value was observed. No low pressure systems were present and all trajectories approached the U.K. from the Atlantic. As the event occurred in July it is very unlikely that any of the sample was composed of snow. It appears that the only explanation for this very depleted sample is the amount of precipitation that fell. 20.3 mm was observed over the 24 hour period and if this all fell in one intense event (possibly a thunderstorm) then equilibration of the raindrops as they fell would be minimal due to the speed, size and quantity of drops present. This sort of event is therefore unlikely to be modelled well by the approach used in this study as the isotopic composition of the rain will remain keyed to that of the cloud rather than the surface layer.

The 8th February 1981 is a good example of a less depleted Driby sample with an observed δ^{18}O value of -2.01 $\permil$. 4.60 mm of precipitation was recorded during the 24 hour collection period. From a trajectory perspective all trajectories at 1800, 0000 and 0600, and around half at 1200 were sourced over the tropical Atlantic (figure 6.12). On the 9th February 1981 a δ^{18}O value of -9.56 $\permil$ was observed at Driby. This sudden change could have been caused by more trajectories being sourced over the Davis Strait between North America and Greenland in a similar pattern to half of the trajectories on the 8th February 1981 at 1200 (figure 6.12). The more depleted δ^{18}O value may also be

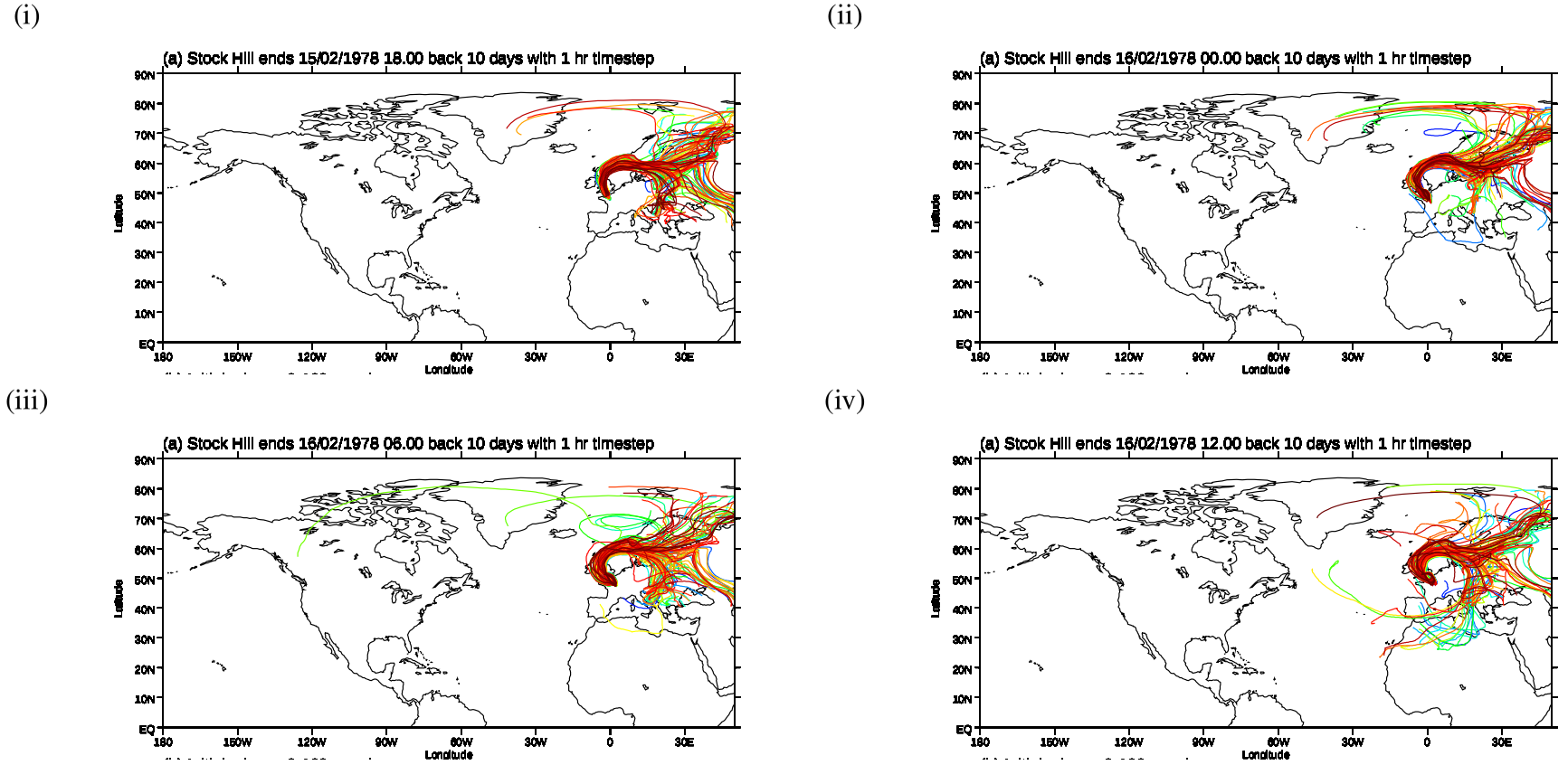

Figure 6.9: *FLEXPART trajectories for Stock Hill on the (i) 15th February 1978 at 1800 and the 16th February 1978 at (ii) 0000, (iii) 0600 and (iv) 1200 when an extremely negative $\delta^{18}O$ value of -22.81 ‰ was observed.*

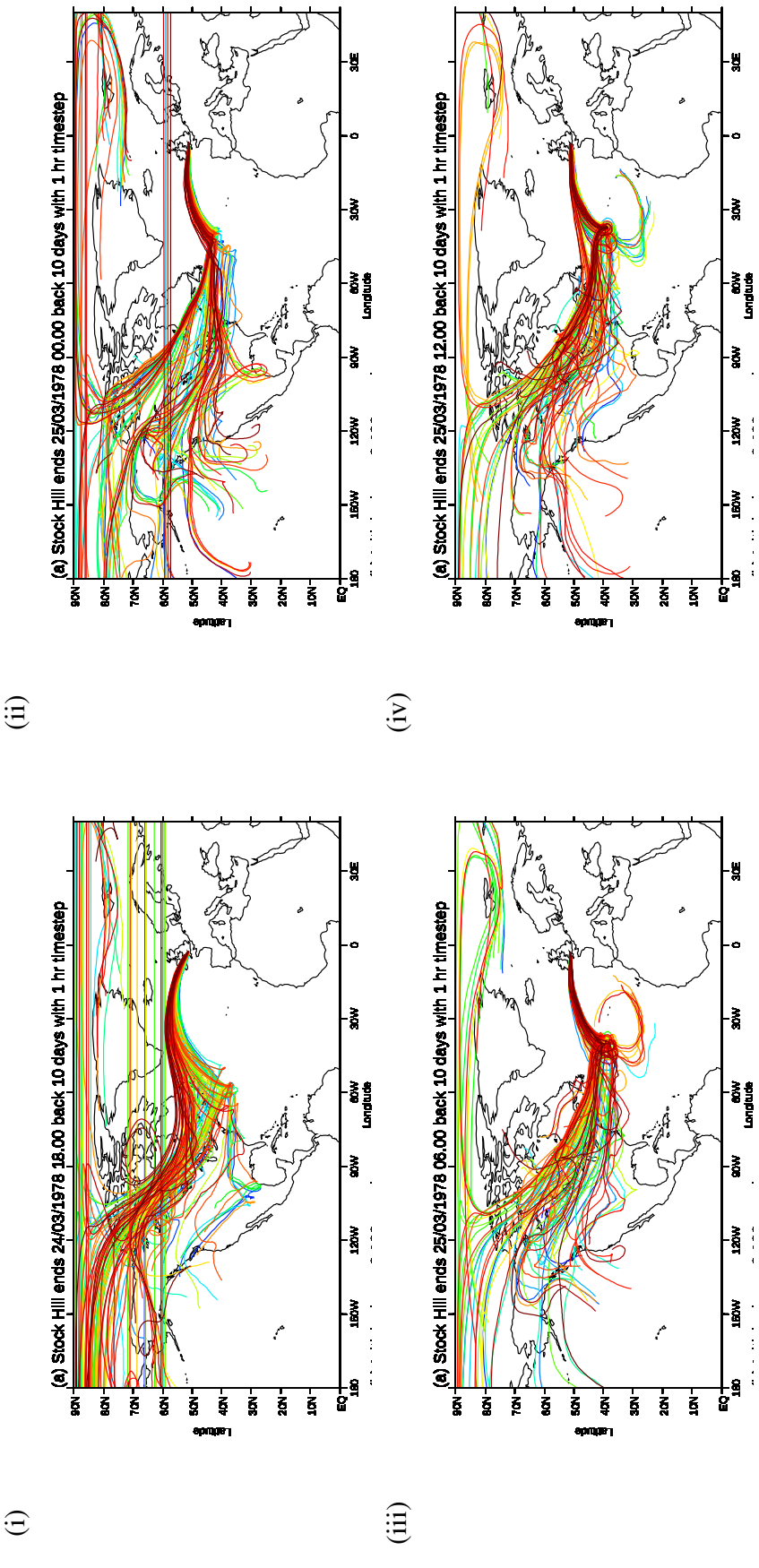

Figure 6.10: *FLEXPART trajectories for Stock Hill on the (i) 24th March 1978 at 1800 and the 25th March 1978 at (ii) 0000, (iii) 0600 and (iv) 1200 when an extremely undepleted $\delta^{18}O$ value of -2.2 ‰ was observed.*

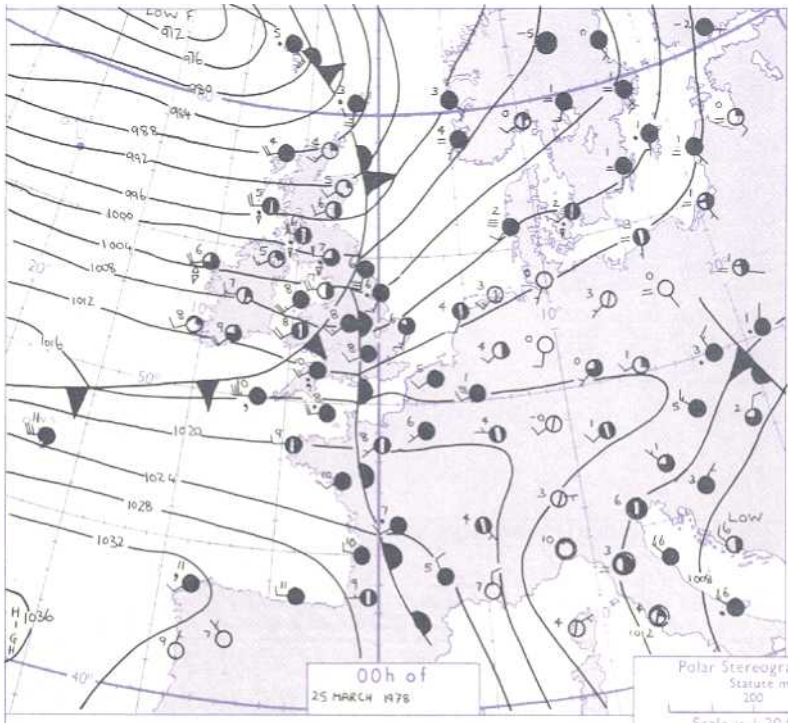

Figure 6.11: *Surface pressure chart for 0000 on the 25th March 1978 taken from the Daily Weather Report of the British Meteorological Office.*

due to the location of a low pressure system across the U.K. as seen in figure 6.13. Driby is located very close to the centre of a low pressure system at 1200 on the 9th February 1981, and more negative δ values are expected in this region of a low pressure system (Gedzelman and Lawrence, 1990).

6.3 Modelling the Observed Isotopic Composition

6.3.1 Modelling the Daily Values

Due to a combination of "no data" recordings for amount of precipitation and isotopic compositions, and the threshold of 3 mm of precipitation set due to the results in section 4.6, the data sets were reduced in size. Six of the Stock Hill days were known to have been composed entirely of snowfall and so were also removed from the data set to be modelled as snow does not equilibrate with the surrounding atmosphere. The use of a 0-100 m agl release height to model the equilibration would therefore not model snow accurately. δ^{18}O values were therefore available for 105 days at Stock Hill and 169 days

(i)

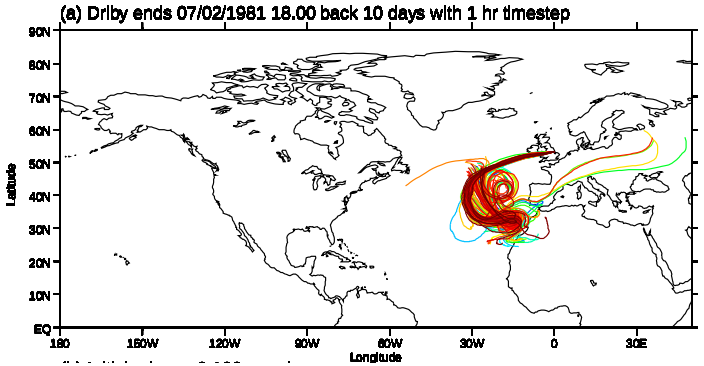

(ii)

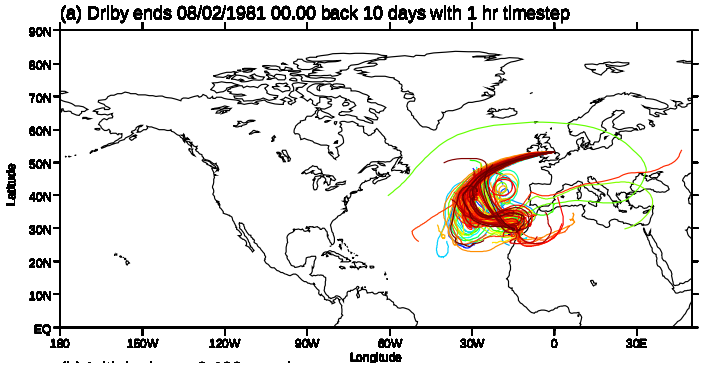

(iii)

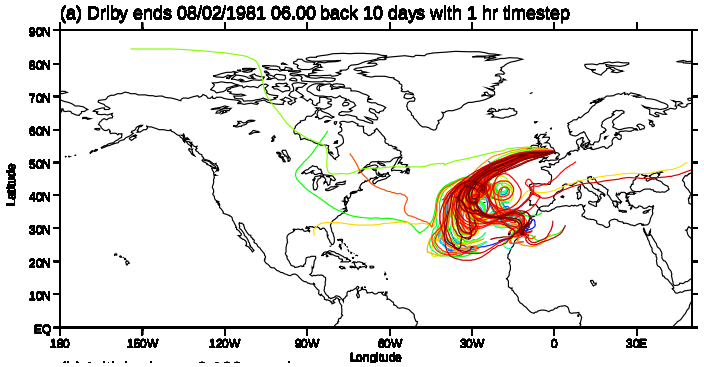

(iv)

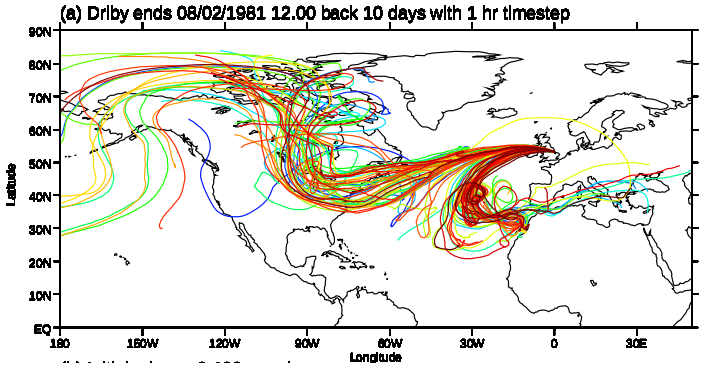

Figure 6.12: *FLEXPART trajectories for Driby on the (i) 7th February 1981 at 1800 and the 8th February 1981 at (ii) 0000, (iii) 0600 and (iv) 1200 when an extremely undepleted $\delta^{18}O$ value of -2.01 ‰ was observed.*

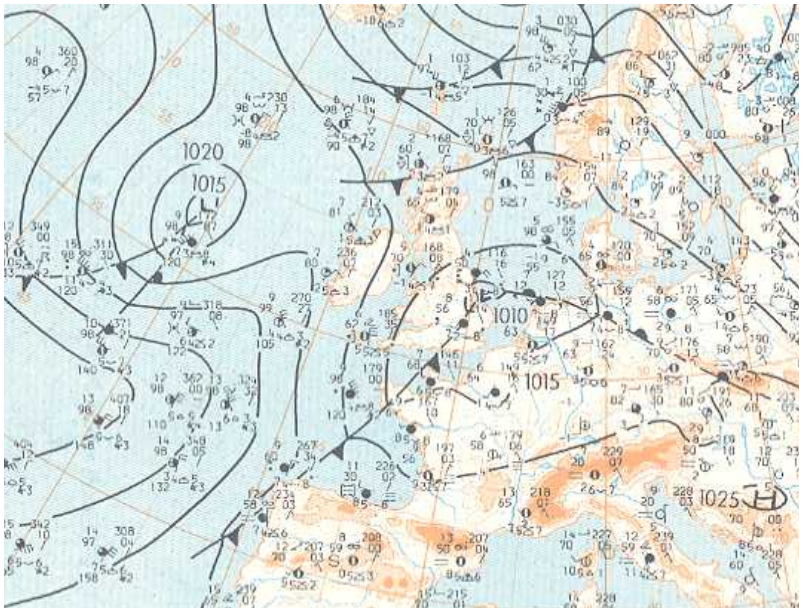

Figure 6.13: *Surface pressure chart for 0000 on the 25th March 1978 taken from the Daily European Meteorological Bulletin.*

at Driby. Appendices D and E give the observed and modelled δ^{18}O and δD values for Stock Hill and Driby respectively for days when more than 3 mm of precipitation was observed.

As in Chapter 4, a modelled isotopic value for each of the Driby and Stock Hill rain-days where over 3 mm of rain fell was produced and then compared with the observed value for that day. Figures 6.14 and 6.15 show all the daily observed isotopic values against the modelled values for (i) δ^{18}O (ii) δD and (iii) d-excess for Stock Hill and Driby respectively. A best fit line was fitted to each set of points and a regression equation and correlation efficient calculated, figures 6.14 and 6.15. All comparisons except for δD at Stock Hill show a positive relationship that is significant at the 90% confidence level. The regression equations for δ^{18}O are y = 0.04x -6.67 for Stock Hill, and y = 0.03x -6.71 for Driby and for δD are y = 0.02x -43.51 for Stock Hill, and y = 0.03x -44.26 for Driby. For a perfect match between the model and observations, the regression equation would be y = x. These equations are very similar to each other though very different from the Norwich, Birmingham and Dublin data regression equations (section 4.6), having much smaller gradients and correlation coefficients. As for d-excess, the regression equations are y = 0.23x +9.40 for Stock Hill, and y = 0.08x +10.17 for Driby. The Stock Hill mod-

elled to observed d-excess relationship has a correlation coefficient of 0.34, much higher than any of the other coefficients for Stock Hill and Driby data, and is the only one to get even close to the gradients seen in the November 2005 case study. This improvement at Stock Hill suggests that the source of water vapour processes are better handled at Stock Hill than at Driby. Further investigation would be required to see if this conclusion is robust and to look into the possible differences in processes involved. An investigation into this is outside the scope of this project.

A further test was conducted on this initial comparison, not only filtering the data for raindays where more than 3 mm was observed, but also capping the amount of rain at 15 mm (optimised through a suite of tests). This was done due to the fact that raindrops in heavy rainfall events do not equilibrate as much as those in light events meaning that heavy event isotopic compositions tend to reflect cloud conditions rather than that of the lower atmosphere (Peng et al., 2005). Figure 6.16 shows the results of this new comparison of observed to modelled δ^{18}O. Gradients of the new regression equations are 0.01 and 0.02 greater for Stock Hill and Driby respectively. The correlation coefficient for the Stock Hill data did not change, but for Driby an increase from 0.01 to 0.02 was seen. These improvements are minimal but this factor is worth considering in future work. This test was not possible for the Norwich, Dublin and Birmingham data sets due to only 2 days at Birmingham exceeding 15 mm of observed rainfall. Removing these days would leave too small a data set to be useful.

To better compare these longer data sets with the November 2005 case study results, the Stock Hill and Driby data was split into monthly time periods and observed and modelled values were compared again i.e. for November 1977, December 1977, etc. The results of these comparisons are summarised in tables 6.3 and 6.4 and displayed in full in Appendix F and G. The results for Stock Hill showed mostly positive correlations. Within these positive relationships there is a mixture of significant and non–significant r^2 values, table 6.3. Only positive relationships with more than 3 data points can be tested for significance due to the one–tailed distribution involved as explained in section 4.2. The number of significant relationships seen across the months is close to the number that

(i)

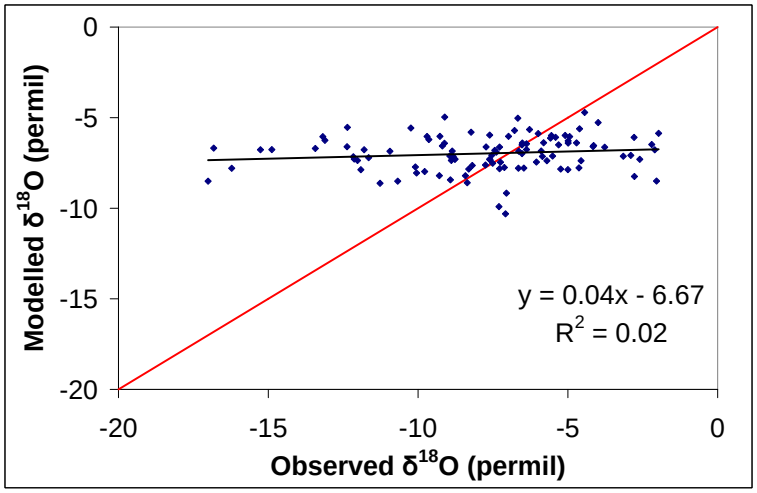

(ii)

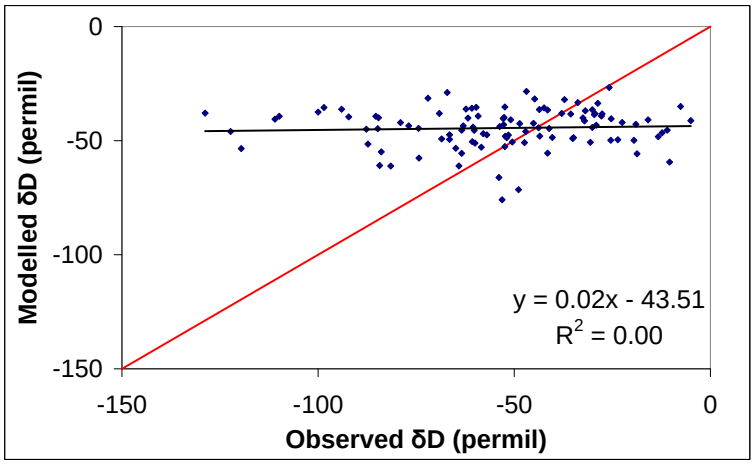

(iii)

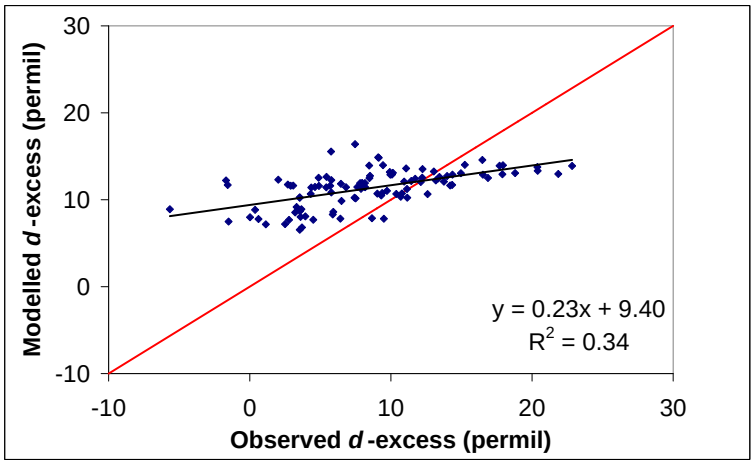

Figure 6.14: *Observed versus modelled $\delta^{18}O$, δD and d-excess for all raindays with over 3 mm of rain at Stock Hill, shown in blue, with the regression equation and correlation coefficient shown in the bottom right hand corner. The red line in each graph is the optimum 1:1 line.*

(i)

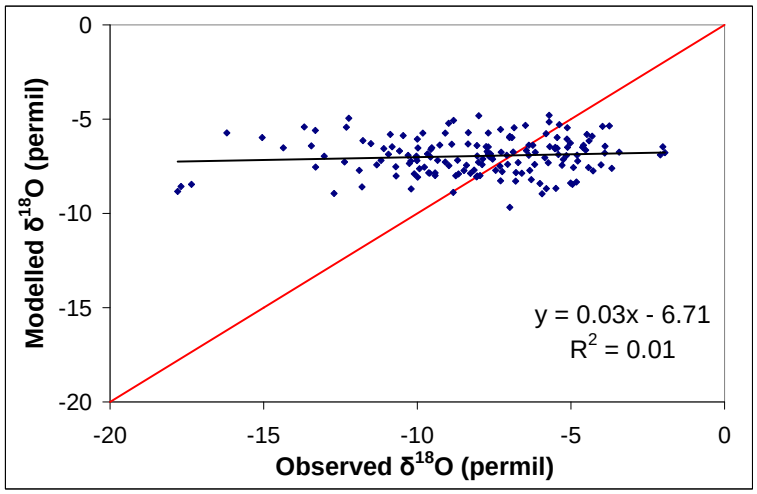

(ii)

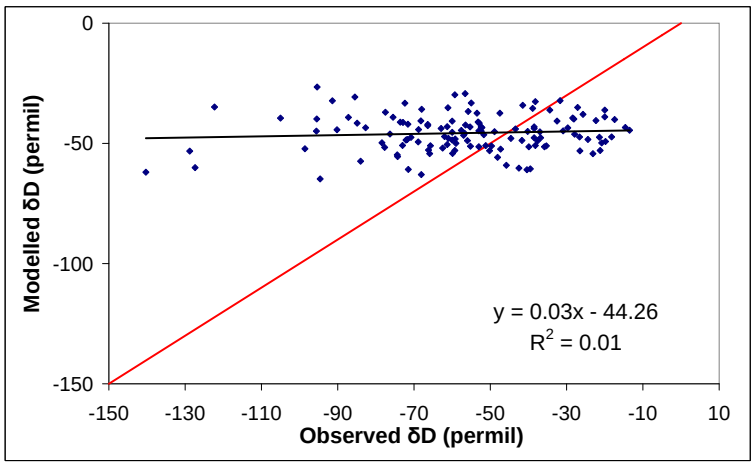

(iii)

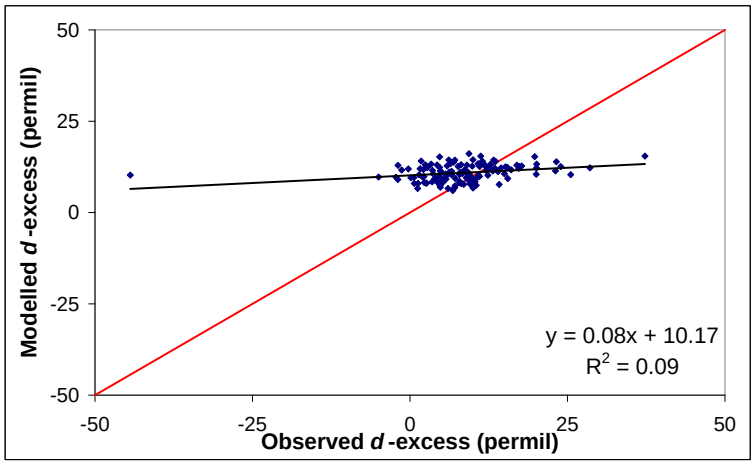

Figure 6.15: *Observed versus modelled $\delta^{18}O$, δD and d-excess for all raindays with over 3 mm of rain at Driby, shown in blue, with the regression equation and correlation coefficient shown in the bottom right hand corner. The red line in each graph is the optimum 1:1 line.*

(i)

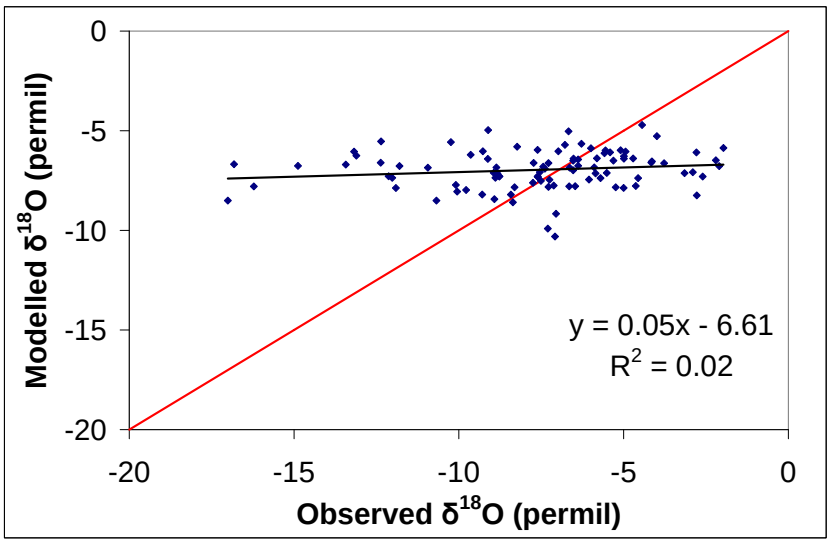

(ii)

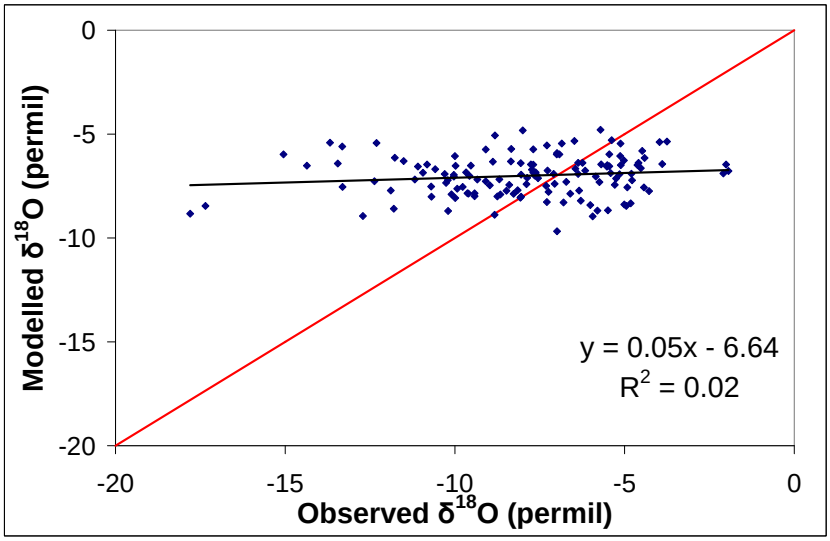

Figure 6.16: *Observed versus modelled $\delta^{18}O$ for all raindays with between 3 and 15 mm of rain (i) Stock Hill, (ii) Driby, shown in blue, with the regression equation and correlation coefficient shown in the bottom right hand corner. The red line in each graph is the optimum 1:1 line.*

would be expected to occur by chance (i.e. when using a significance level of 95%, 5% of occurrences could be significant by chance). Similarly the Driby monthly data split into equal numbers of positive and negative correlations and again a mixture of significant and non–significant r^2 values, table 6.4. This situation is improved when the data is compacted further by month i.e. combining March 1979 and 1981 to form one March group. 9 of these monthly groups had a positive correlation with r^2 values in the order of 0.1, the other 3 showed a negative correlation. The sampling period for Stock Hill only covered 4 months repeatedly, 3 of these 4 when compared by month had a positive correlation.

The high number of positive rather than negative correlations seen suggests that the model is capturing some of the processes involved on a monthly basis. However the low gradients and r^2 values seen when comparing the modelled values with the observed values (figures 6.14 and 6.15) highlights the smaller range of modelled values produced than the observed range. As for the November 2005 observations (Chapter 4), the amplitude of the modelled variations for Driby and Stock Hill does not capture that of the observed data. Therefore some process affecting the isotopic composition is either not included in the model or is included but is not given enough importance. Another explanation for this lack of modelled range is that by modelling many back trajectories in an attempt to capture all possibilities and then averaging these 400 modelled isotopic values, the variation of the system has been smoothed too much. Section 4.6 discussed the range of values seen across the 100 modelled trajectories for each time and within these 100 isotopic values the observed δ value was usually found. The problem could then become how to know which of the 400 modelled values available for each rainday to choose, unless this too is due to chance and a large enough sample size.

6.3.2 Stock Hill Sensitivity Tests

Though a full suite of sensitivity tests to attempt to tune the model to Stock Hill processes was beyond the scope of this study, an initial investigation was conducted to find out if such tuning for each site would be useful. Figure 6.17 shows the previously shown results as well as those of these tests. In the first test a humidity threshold for precipitation occur-

Month	Number of raindays	Sign of Correlation	r^2 value	Significance
November 1977	6	+	0.05	Not Significant
December 1977	9	-	0.01	
January 1978	3	+	0.01	
February 1978	7	-	0.99	
March 1978	15	-	0.00	
April 1978	10	+	0.21	Significant at 90%
May 1978	4	-	0.00	
June 1978	6	+	0.32	Significant at 90%
July 1978	5	+	0.26	Not Significant
August 1978	3	+	0.76	
September 1978	5	-	0.40	
October 1978	1			
November 1978	5	+	0.24	Not Significant
December 1978	14	+	0.05	Not Significant
January 1979	10	+	0.45	Significant at 95%
February 1979	2			

Table 6.3: *Summary of the monthly split of modelled vs observed $\delta^{18}O$ at Stock Hill comprised of: the number of raindays with over 3 mm of rainfall within each month; the sign of the relationship between modelled and observed $\delta^{18}O$; the correlation coefficient of the relationship; and for positive relationships, whether or not the r^2 value is significant.*

Month	Number of raindays	Sign of Correlation	r^2 value	Significance
March 1979	11	-	0.11	
April 1979	8	-	0.02	
May 1979	11	+	0.13	Not Significant
June 1979	5	-	0.07	
July 1979	1			
August 1979	8	-	0.00	
September 1979	3	+	0.05	Not Significant
October 1980	9	-	0.02	
November 1980	10	+	0.44	Significant at 95%
December 1980	4	+	0.38	Not Significant
January 1981	5	-	0.41	
February 1981	3	-	0.46	
March 1981	12	+	0.00	
April 1981	4	-	0.70	
May 1981	6	+	0.37	Not Significant
June 1981	1			
July 1981	4	+	0.30	
August 1981	3			
September 1981	7	-	0.00	
October 1981	8	-	0.00	
November 1981	5	+	0.09	
December 1981	4	+	0.13	
January 1982	5	-	0.26	
February 1982	3	+	0.99	
March 1982	7	-	0.12	
April 1982	1			
May 1982	6	+	0.03	
June 1982	8	+	0.57	Significant at 95%

Table 6.4: *Summary of the monthly split of modelled vs observed $\delta^{18}O$ at Driby comprised of: the number of raindays with over 3 mm of rainfall within each month; the sign of the relationship between modelled and observed $\delta^{18}O$; the correlation coefficient of the relationship; and for positive relationships, whether or not the r^2 value is significant.*

ring of 80% rather than the previously chosen 95% was used in the MCIM. In the second test the supersaturation over ice parameterisation at temperatures lower than 248 K was changed from 1.02-0.0038T to 0.9-0.0038T. Neither of these tests had any impact on the correlation coeffients seen when comparing observed and modelled δ^{18}O values at Stock Hill. Changing the supersaturation value had no effect on the regression equation either though individual modelled values were altered slightly. As expected from the results of previous tests on varying the relative humidity threshold (section 5.2.2), reducing the threshold caused a larger offset from the ideal 1:1 line, changing from -6.67 to -11.57, due to more rainout occurring when a lower threshold is used. The changes induced by these two tests are minimal though further tuning may still improve the results if the right combination of parameters is used.

6.3.3 Modelling Monthly Averages

Although the comparisons of observed and modelled daily isotopic values do not show the ideal 1:1 relationship, monthly averages of these daily values were produced and compared with the monthly observed average. This was done as most observed data sets are on a monthly resolution e.g. the GNIP database. These monthly values with modelled versus observed δ^{18}O are shown in figure 6.18. As with previous graphs of this type the regression equation and correlation coefficient are in the bottom right hand corner of the graphs and the ideal 1:1 line is shown in red. The Stock Hill data shows a small negative relationship though this is greatly influenced by a few extreme observed values. The larger Driby data set shows a positive though non–significant relationship between the modelled and observed monthly averages. The regression equation for Driby is y = 0.09x-6.25, which is close to the equations found for Driby and Stock Hill daily data though with a slightly higher gradient, (0.09 as opposed to 0.04 and 0.03). These results lead to the conclusion that the problems with the model would extend into lower temporal resolution studies.

(i)

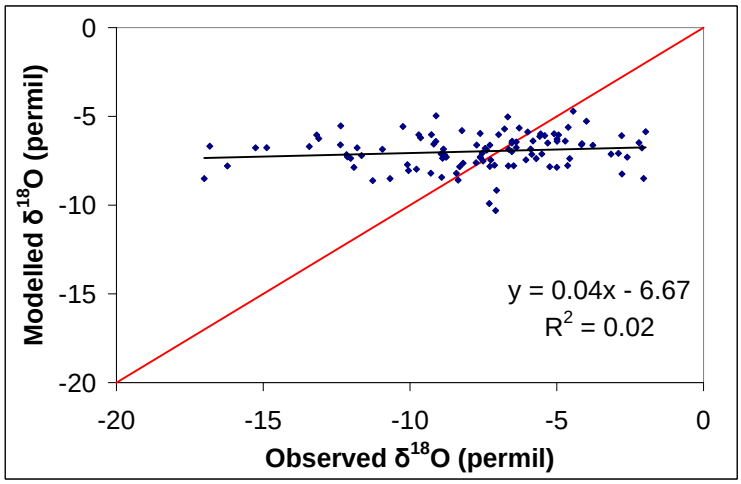

(ii)

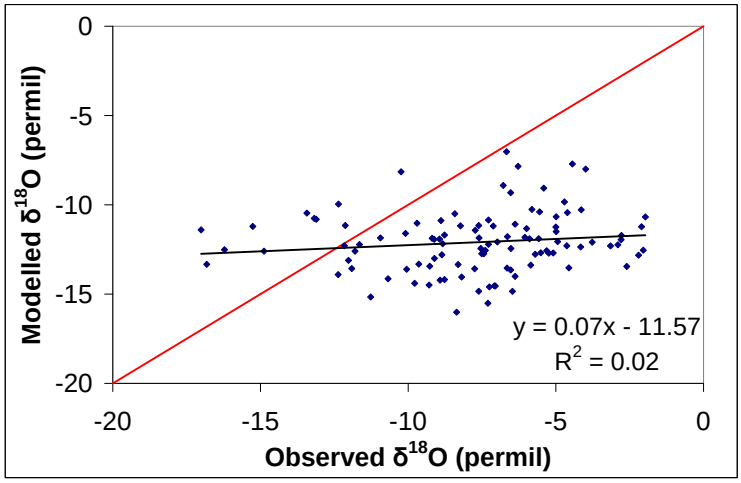

(iii)

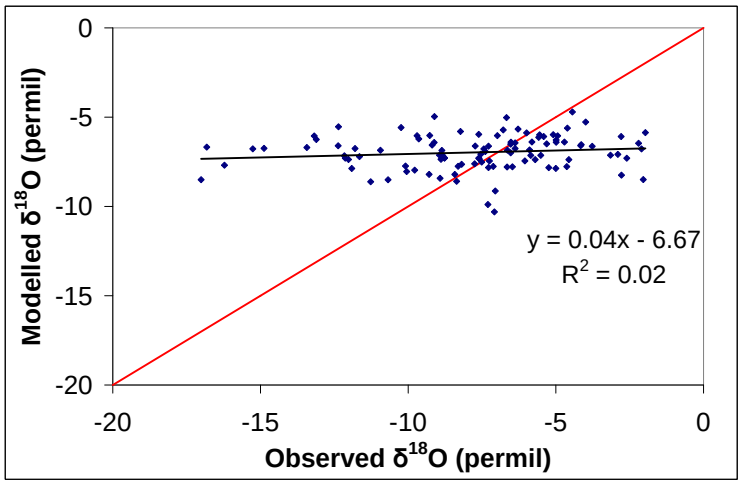

Figure 6.17: *Observed versus modelled for all Stock Hill raindays with over 3 mm of rain (i) previously used parameters, (ii) with a 80% humidity threshold instead of 95% and (iii) a different supersaturation parameter of 0.09-0.0038T. The red line in each graph is the optimum 1:1 line.*

(i)

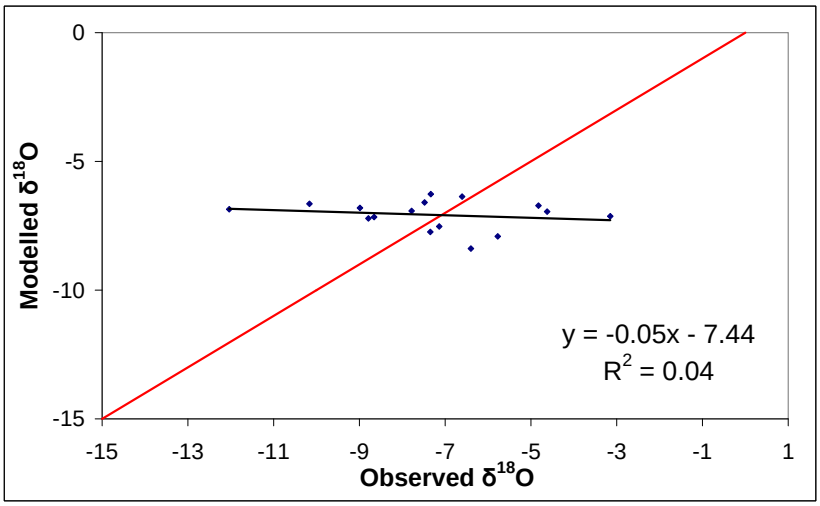

(ii)

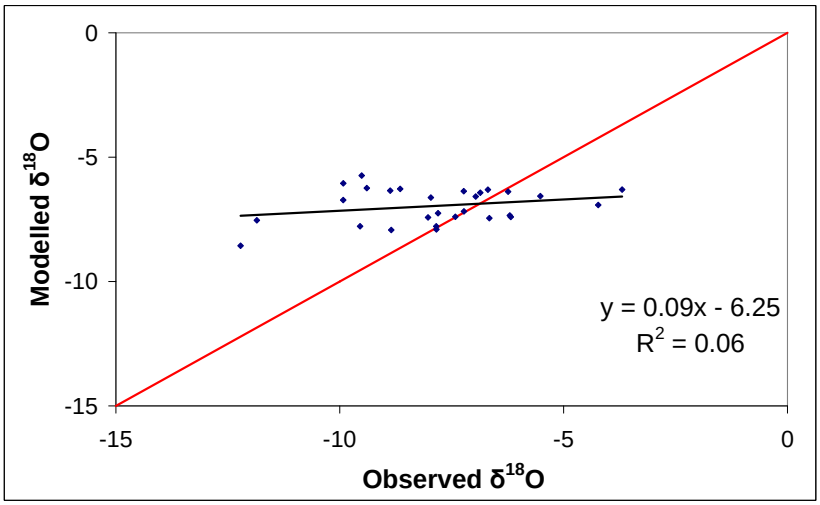

Figure 6.18: *Monthly averages of observed versus monthly averages of modelled $\delta^{18}O$ values (i) Stock Hill, (ii) Driby, shown in blue, with the regression equation and correlation coefficient shown in the bottom right hand corner. The red line in each graph is the optimum 1:1 line.*

Site	Observed			Modelled		
	δ^{18}O (‰)	δD (‰)	d-excess	δ^{18}O (‰)	δD (‰)	d-excess
Norwich	−7.06	−41.85	14.66	−7.60	−48.49	12.34
Dublin	−7.34	−41.53	16.00	−7.41	−46.95	12.36
Birmingham	−8.18	−47.91	15.35	−7.40	−46.97	12.22
Stock Hill	−7.71	−53.18	8.50	−6.97	−44.46	11.30
Driby	−7.29	−50.47	7.85	−6.95	−44.92	10.68
Wallingford	−7.25					

Table 6.5: *Mean observed and modelled $\delta^{18}O$, δD and d-excess at Norwich, Dublin, Birmingham, Stock Hill and Driby, and observed $\delta^{18}O$ from Wallingford (Darling and Talbot, 2003)*

6.3.4 Observed and Modelled Averages

As in section 4.6.5, averages of modelled and observed δ^{18}O, δD and d-excess at Stock Hill and Driby were calculated for the entire data set (table 6.5). There is very good agreement between all modelled and observed averages. The modelled averages also compare well with the average observed δ^{18}O for Wallingford from 1982-2001 from the study by Darling and Talbot (2003) of -7.25 ‰. This supports the conclusion of section 4.6.5 that although the model sensitivity is not large enough to pick up the full range of daily variations, it is capable of producing an accurate average value for the British Isles. It would be interesting to see if this is maintained further afield and to further investigate why this is so. However, an investigation into this is beyond the scope of the present study.

6.3.5 Modelling the Seasonal Cycle

As a seasonal cycle was seen in the observed data for Stock Hill, time series of the modelled data for Stock Hill and Driby were created so as to test the ability of the model to capture this phenomenon, see figures 6.19 and 6.20. The observed Stock Hill data displayed clearly more negative δ^{18}O values in the winter months than in the summer months, figure 6.7. The modelled data however does not truly capture this cycle. There is a small increase in modelled δ^{18}O in April and May 1978 compared to winter 1977 but no change is apparent from May 1978 until the end of the Stock Hill sampling period in February 1979, figure 6.19. Part of this deficiency could be due to the observed data set

incorporating all raindays whereas only raindays with greater than 3 mm of rainfall were modelled and included here. However, it would appear that the model does not manage to satisfactorily capture the seasonal cycle seen at Stock Hill.

The observed data from Driby exhibited no clear seasonal cycle, figure 6.8. The modelled data, (figure 6.20), shows small variations across the Driby sampling period, and has picked up the very negative values seen around the 23rd July 1981, though not to sufficient amplitude. The increase in δ^{18}O values from March 1979 to September 1979 is not captured by the model, nor is the slight decrease seen in winter 1982.

6.3.6 Lamb Classifications

Heathcote and Lloyd (1986), when analysing the Driby observed data, proposed a localised "weather effect" present in precipitation isotope ratios over the U.K. This theory grouped precipitation into types based on the subjective weather classification system developed by Lamb (1972) and developed into an objective system by Jenkinson and Collison, (1977) (Jones et al., 1993). The direction the air parcel came from and whether precipitation was deposited by a cyclonic or anticyclonic system was seen to be important. Air parcels originating over the Northern Atlantic had the least negative isotopic precipitation composition, whereas air parcels from further south or over continents had the most negative isotopic composition (Heathcote and Lloyd, 1986). To see if splitting the data from this study into these subsets would help to reveal where in the model any problems lie, Lamb classifications were obtained for all raindays from Hulme and Barrow (1997). The observed and modelled values for all days with the same classification were then compared for both Stock Hill and Driby sites. There are 28 Lamb categories, though not all of these were represented within the samples. The codes for the Lamb categories are directions of main atmospheric flow (e.g. N is North), and system type involved (e.g. C is cyclonic, A is anticyclonic).

As for the splitting of Norwich, Dublin and Birmingham sites into categories (section 4.7), there were no clear conclusions to be drawn from this analysis as no one type was especially well modelled, in fact no individual type was modelled well at all. The

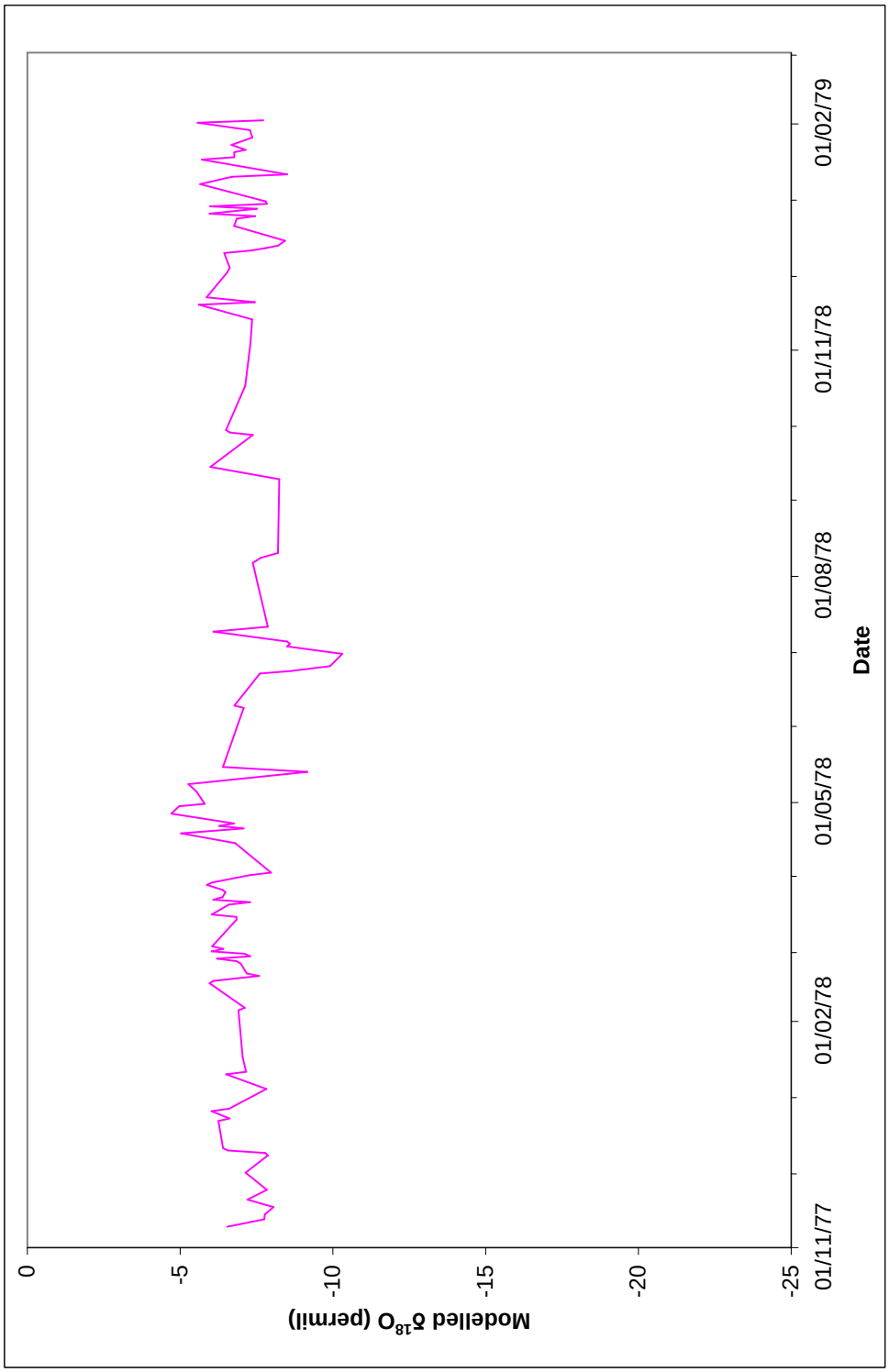

Figure 6.19: *The modelled $\delta^{18}O$ of rainfall for Stock Hill from November 1977 to February 1979.*

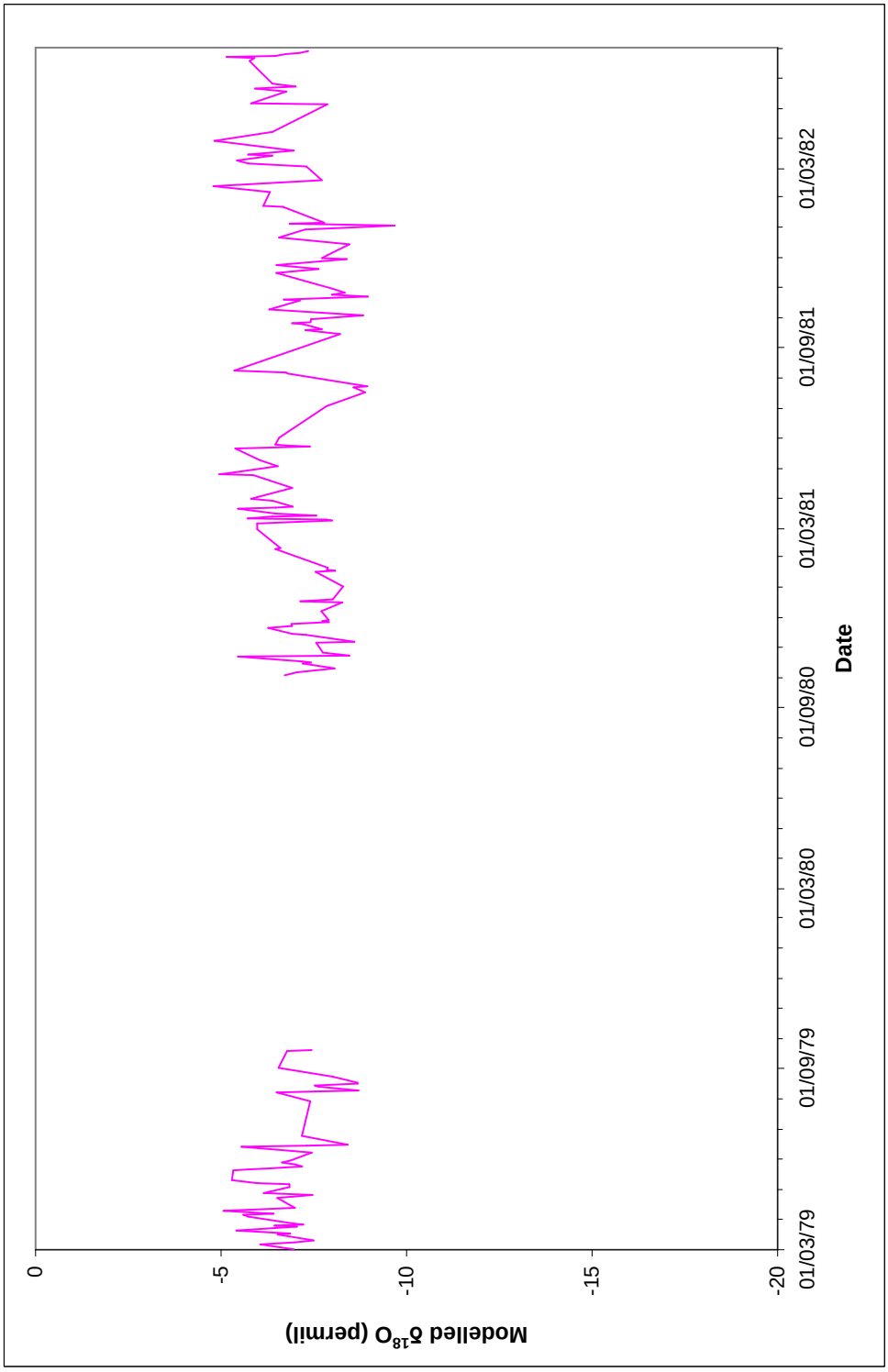

Figure 6.20: *The modelled $\delta^{18}O$ of rainfall for Driby from March 1979 to September 1979, and from October 1980 to June 1982.*

results of these tests can be seen in figures 6.21 and 6.22. Many categories had only a few examples. None of the relationships seen were significant when the r^2 values of the regression equations were compared with the critical values. To increase the sample size the groups created by Heathcote and Lloyd (1986) were used. Weather types C, NW, CN and CNE were combined, as were S, N, A, SW and CS, and finally W and CW formed the third group. Again no significant relationships were seen in this comparison as can be seen in figures 6.23 and 6.24.

6.4 Conclusions

The aim of this chapter was to test the Lagrangian trajectory model on a longer time scale data set. The two observed data sets available spanned the period from November 1977 to June 1982 but were split between two U.K. sites at Stock Hill in Somerset and Driby in Lincolnshire. The hypothesis was that a longer data set would provide more information on the accuracy of the model. Significant positive relationships were seen between observed and modelled data at both Driby and Stock Hill. However the range of modelled values was still insufficient to cover that of the observed values, (section 6.2). The source of this problem was not determinable through splitting the data sets into different conditions to see if some conditions were better modelled than others, (section 6.3.6).

The model is not able to capture the observed seasonal cycle of isotopic ratios though some individual extremes are captured, (section 6.3.5).

A comparison of monthly observed values with monthly modelled values exhibited the same relationship as seen when comparing daily values, (section 6.3.3). This suggests that though at the moment the model does not capture the range of values required, if this problem could be rectified then the model could be useful at lower resolutions of observed data. A comparison of an average of all modelled values with that of all observed values for Driby and Stock Hill suggested that although the range of δ values is not captured, the mean δ value is.

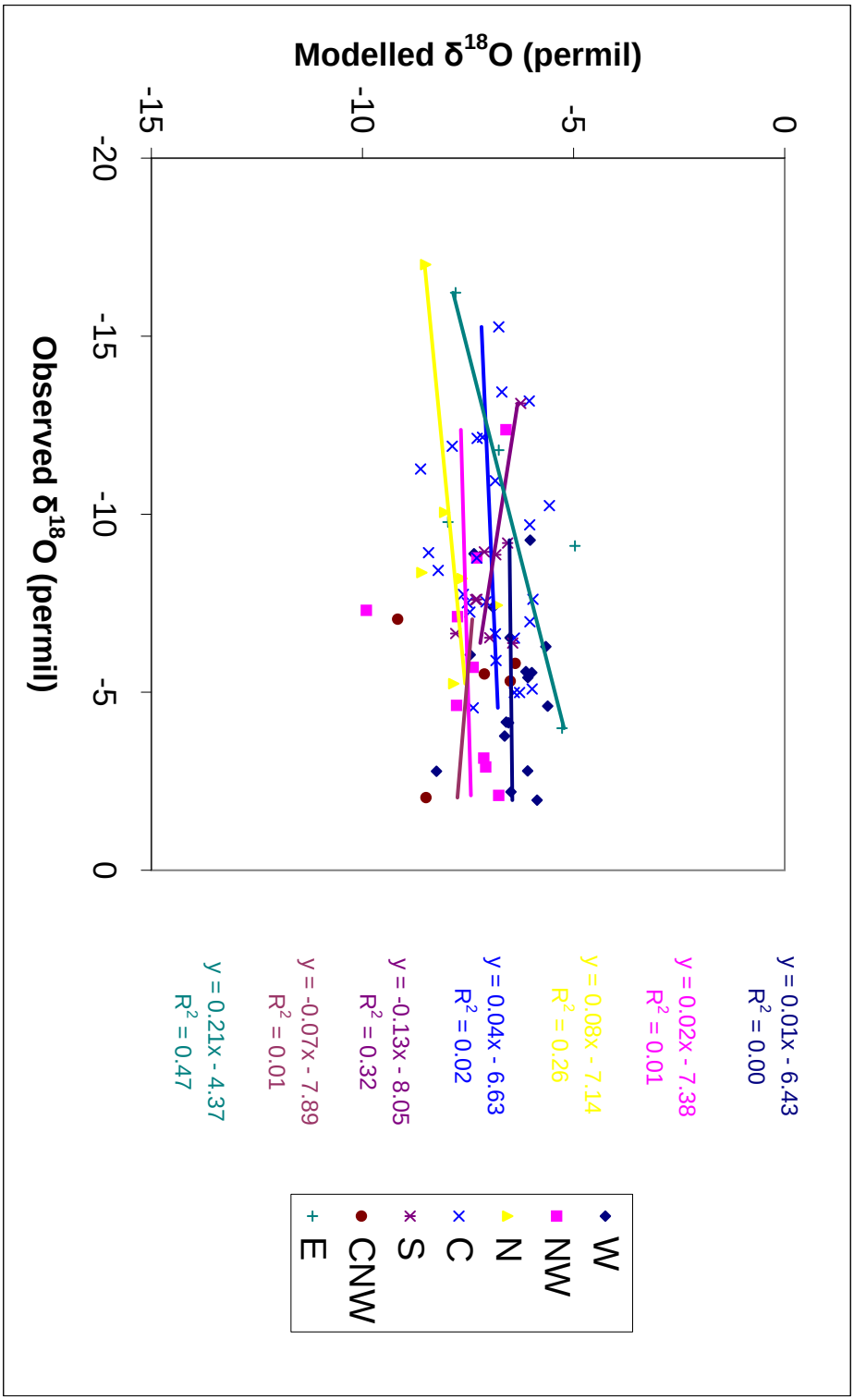

Figure 6.21: *Modelled versus observed $\delta^{18}O$ for all Stock Hill raindays, split by Lamb categories.*

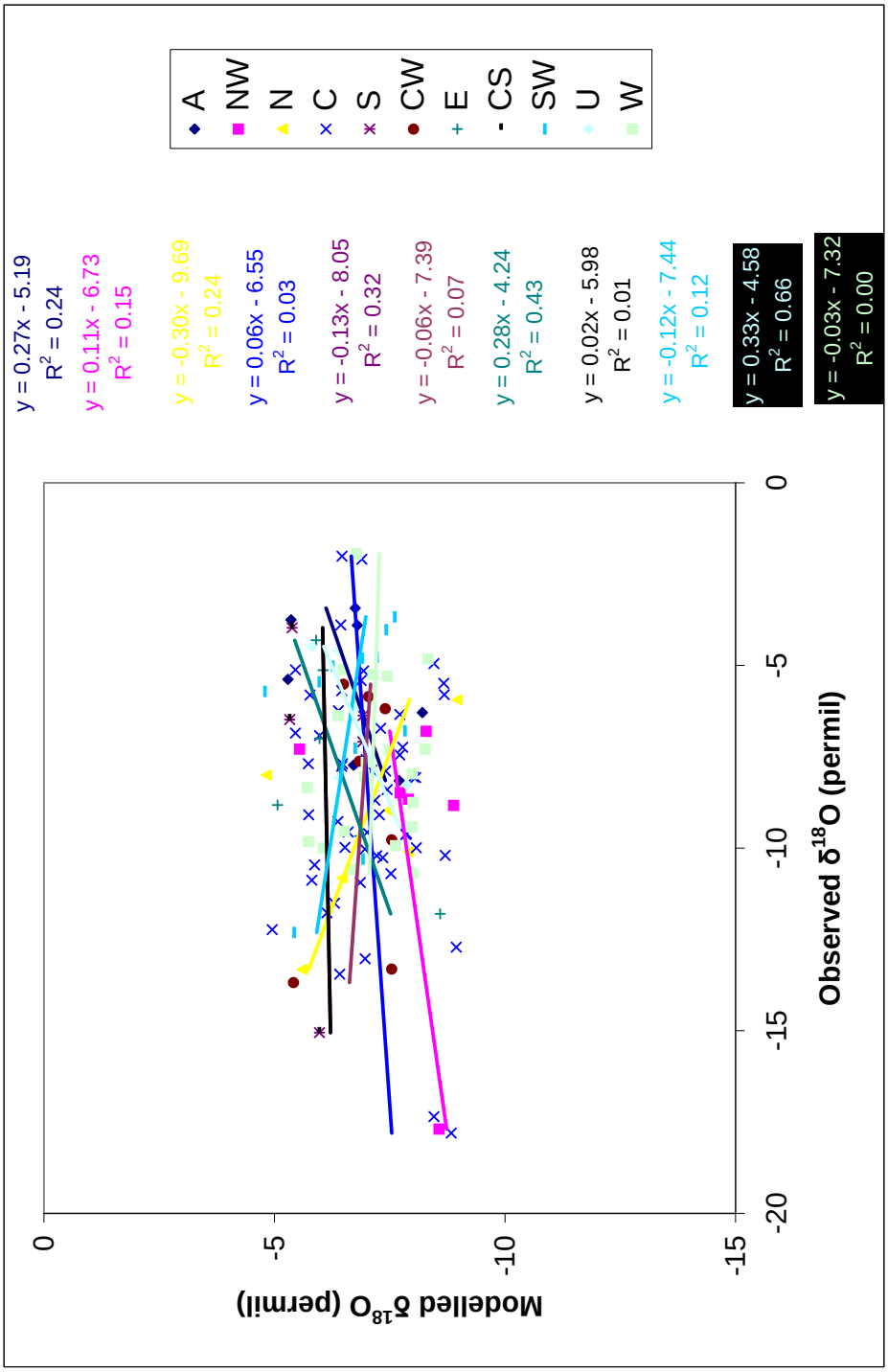

Figure 6.22: *Modelled versus observed $\delta^{18}O$ for all Driby raindays, split by Lamb categories.*

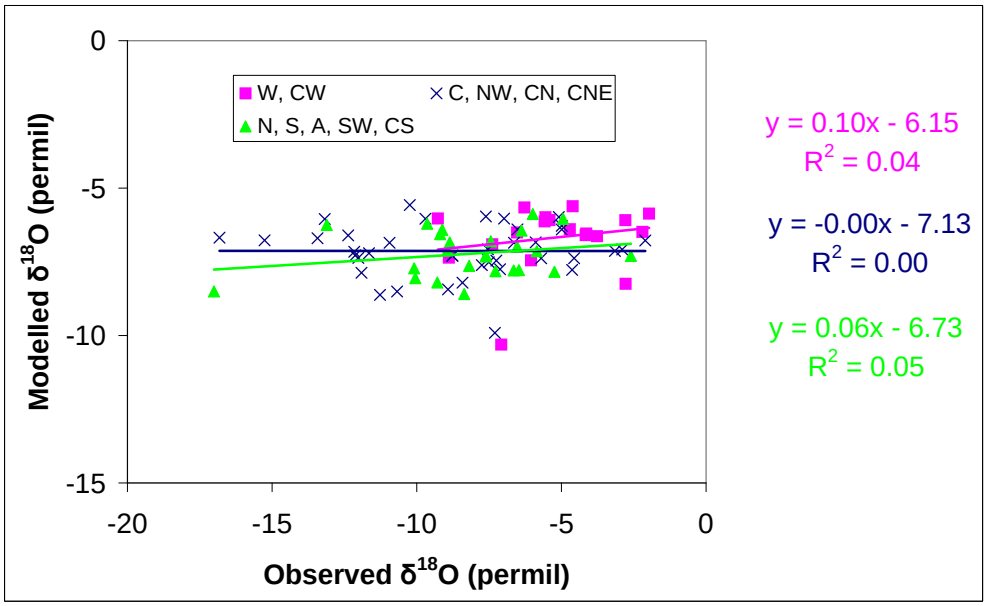

Figure 6.23: *Modelled versus observed $\delta^{18}O$ for all Stock Hill raindays, split into 3 groups of Lamb categories.*

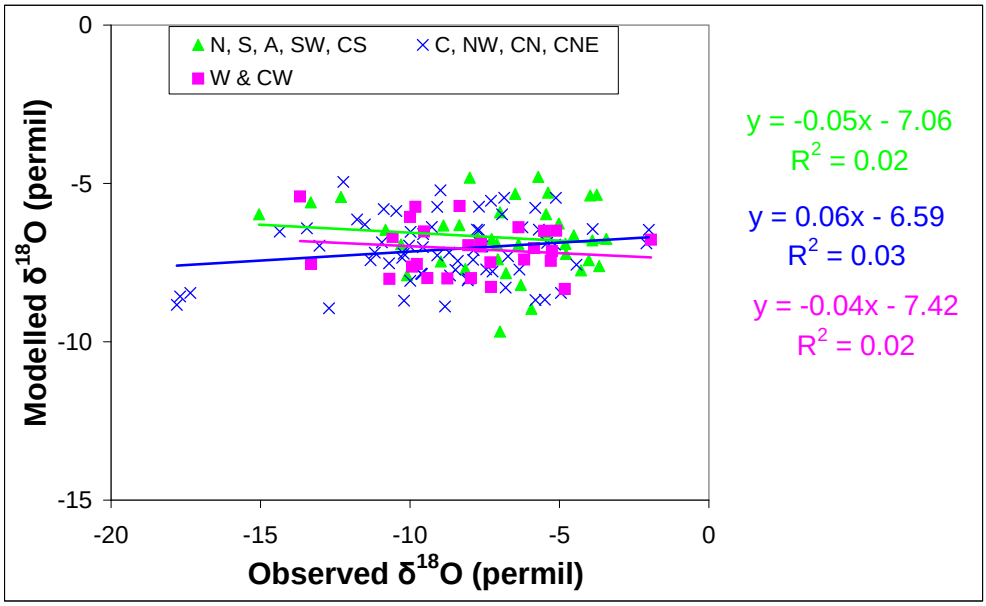

Figure 6.24: *Modelled versus observed $\delta^{18}O$ for all Driby raindays, split into 3 groups of Lamb categories.*

Chapter 7

Conclusions

Isotopes are extremely useful tools for studying our environment, both past and present. The stable isotopes of oxygen and hydrogen have been used to trace the movement of water through the hydrological cycle (e.g. Darling et al. (2003); Clark and Fritz (1997); Gat and Gonfiantini (1981)), as well as being used as indicators of temperature. The ratio of heavy to light oxygen (δ^{18}O) and hydrogen (δD) in ice layers has been used extensively to interpret climatic fluctuations (specifically temperature changes). δ^{18}O of precipitation is also preserved in modified form in cave carbonate precipitates (speleothems), through rainwater infiltrating into the ground above caves (Lauritzen and Lundberg, 1999). Analysis of these cave formations can provide valuable continental records once a thorough interpretation has been conducted (Fricke and O'Neil, 1999). However any use of isotopes to uncover information about the past relies on an understanding of the isotopic systems in the present gained through observing and modelling the system.

This study has investigated a new approach to modelling the isotopic composition of rainfall over the British Isles. The approach involves combining a Lagrangian Particle Dispersion model (FLEXPART) with a Mixed Cloud Isotope model (MCIM). FLEXPART tracks air particles backwards in time from a precipitation event using ECMWF ERA-40 reanalysis fields, more specifically the 3–dimensional wind fields. FLEXPART also extracts temperature, pressure and humidity data along each back trajectory from the ECMWF fields. These atmospheric parameters are then used by the MCIM to calculate changes in the isotopic composition of the water vapour in the air particle and the isotopic

ratio of any precipitation that occurs from the particle. The initial isotopic value is taken from a climatology of isotopic ratios in atmospheric water vapour provided by a 20 year run of the ECHAM4 climate model with isotopic parameters included.

Throughout this study modelled isotopic compositions were compared with observed ratios to test the ability of the model. The results of these comparisons are summarised in this chapter but are shown and discussed in more detail in Chapters 4 and 6. Table 7.1 summarises the time periods for which observed data sets used in this study were available from Birmingham, Dublin, Norwich, Stock Hill and Driby.

Internal parameters of the model were investigated in Chapter 5 to optimise model performance and identify any sensitivity. For FLEXPART, output averaged over every hour was chosen, as was the use of the Lagrangian method of selecting the timestep of interpolation between wind fields, (i.e. using longer timescales when the atmospheric situation is stable and shorter timesteps when the situation is changeable). 100 particles were released over a 3 hour period at 4 times throughout each day to be modelled. The release box was 0.1° x 0.1° and the particles were traced back in time for 10 days. FLEXPART's convection scheme was used in all model runs.

Most precipitation observed over the British Isles occurs as rain. Isotope theory suggests that the isotopic composition of rainfall alters as it falls through the atmosphere and equilibrates with the surrounding atmospheric vapour. This would suggest that modelling the isotopic composition of liquid water condensed from atmospheric vapour in the bottom layers of the atmosphere would be more accurate than trying to model the precip-

Site	**Latitude**	**Longitude**	**Altitude**	**Months Available**
Birmingham (U.K.)	52°28'58"N	1°53'37"W	458 ft	11/05
Dublin (Ireland)	53°19'48"N	6°15'0"W	46 ft	11/05
Norwich (U.K.)	52°37'21"N	1°16'45"E	86 ft	11/05 to 12/05
Stock Hill (U.K.)	51°14'46"N	2°31'12"W	172 m	11/77 to 02/79
Driby (U.K.)	53°14'52"N	0°05'00"E		03/79 to 09/79 10/80 to 06/82

Table 7.1: *Locations of daily data sites and the dates $\delta^{18}O$ data is available for each.*

itation directly. Especially as to model the precipitation the particles would need to be released from the height of condensation, which varies for each precipitation event. Equilibration and re–evaporation as the droplets fall would also need to be modelled greatly increasing the complexity of the model required. Modelling the isotopic composition of water vapour in the lower layers of the atmosphere and assuming equilibration would appear to be a simpler but still accurate method to use. This theory was tested by releasing particles in FLEXPART at different heights in the atmosphere. In most cases the isotopic ratios obtained from modelling particles released in the lowest 1000 m of the atmosphere compared best with observations. The model was finally run releasing the particles between 0 and 100 m above ground level so as to standardise the results. This decision means that the model created for this study is only capable of modelling the isotopic composition of rain. Rain will equilibrate with the modelled isotopic composition of the lower atmosphere; snow and hail will not. The model is also not able to accurately predict which of the air parcels will contribute to the rainfall as rain will be initiated higher in the atmosphere than the 0 to 100 m layer (section 5.1.5).

When internal parameters of the MCIM were investigated, the most accurate modelled values were produced when the humidity threshold was set to 95% (section 5.2.2) and the internal:ambient ratio of mixing of 0:100 (section 5.2.3). The concept of a humidity threshold is used in many models involving precipitation and is a threshold humidity above which precipitation occurs in the model. 80% is the generally used threshold in GCMs due to the humidity being an average across a large area in the GCM resolution. This humidity has to take into account the fact that there will be regions of each grid box where precipitation is occurring and regions where it is not. Due to the much smaller resolution involved in the Lagrangian approach used in this study, this threshold can be raised towards the more theoretically accurate value of over 100%. 100% is not used due to potential errors in the ECMWF reanalysis fields, however 95% was found to produce generally more accurate modelled values than 80%. The internal:ambient ratio of mixing parameters control the source of water vapour mixed into the air parcels when specific humidity increases and mass conservation requires water vapour to be added to the parcel

(section 3.4.1). Using a internal:ambient ratio of mixing of 0:100 allows evaporation from the surface to interact with each air particle at least on a limited basis. The ECHAM4 isotope fields used as the ambient isotopic compositions will be affected by each grid box's position in comparision to water vapour sources and average circulation patterns. Therefore by allowing mixing of isotopic ratios into the parcels from this ambient source, evaporation into the parcel can be accounted for to a certain extent. It was found that when using a humidity threshold of 95% varying the ratio of ambient to internal mixing made very little difference to the modelled values.

Through comparing observed and modelled values from Norwich, Dublin and Birmingham it was concluded that the model is most accurate for days where more than 3 mm of rainfall is experienced. A potential source of error was noted as being caused by point observations for the observed data but greater than point resolution being modelled. This mis–match of scales was found to be non–significant by comparing observations from sites 2000 m apart across Norwich. Insufficient data was available to allow this variability to be quantified satisfactorily on a general basis but for the 8 days where multiple samples were collected in Norwich and analysed the standard deviation of the observed δ^{18}O values were between 0.11 and 0.92 $^{\circ}/_{\circ\circ}$, (section 4.10). The modelled sampling error caused by releasing only 100 particles was estimated to be 0.15 $^{\circ}/_{\circ\circ}$ for δ^{18}O, (section 5.1.1). It should also be considered that there will be a modelled error involving the use of trajectories based on reanalysis fields. Using many trajectories reduces the impact of individual trajectory errors but there will still be positional errors and therefore atmospheric parameter errors passed through FLEXPART into the MCIM and then into the final modelled δ values.

Generally the observed deuterium excess values were modelled more accurately than the individual isotopic ratios, though this was less pronounced for the Driby case study. Table 7.2 summarises the relationships seen in Chapters 4 and 6 between observed and modelled δ^{18}O and d-excess for raindays where more than 3 mm occurred at all 5 U.K. locations and their significance.

A second filtering was applied to the larger data sets from Driby and Stock Hill to

compare modelled and observed values for raindays where more than 3 mm but less than 15 mm of precipitation was seen. This second filter was employed as during heavy rainfall events equilibration with lower atmosphere water vapour is limited, meaning that the raindrops retain more of an in–cloud isotopic signature, which the model approach used in this study is not able to account for. The results of applying this second filter increased the gradient of the regression equations comparing observed and modelled δ^{18}O values by 0.01 and 0.02 for Stock Hill and Driby respectively. The correlation coefficient for the Stock Hill data did not change, but for Driby an increase from 0.01 to 0.02 was seen. These improvements are minimal but this factor is worth considering in future work. This test was not possible for the Norwich, Dublin and Birmingham data sets due to only 2 days at Birmingham exceeding 15 mm of observed rainfall. Removing these days would have left too small a data set to be useful, (section 6.3.1).

The relationships seen for Norwich are the strongest, which is perhaps due to most of the model tuning having used the Norwich observed data. It is possible that retuning the model to each individual site could produce better results. An initial investigation into this was conducted for Stock Hill. A humidity threshold of 80% was used, as was a different linear function for the calculation of supersaturation over ice, (S_i), in clouds composed purely of ice crystals. The results of these two tests were discussed in section 6.3.2. No change in the overall observed to modelled relationship was seen when changing the S_i function. A small change in gradient (from 0.04 to 0.07) of the observed to modelled relationship was seen when a threshold humidity of 80% was used, as was a change in the offset from the ideal 1:1 line (from -6.67 to -11.57). These results were not conclusive as the changes seen were so minimal and only 2 parameters were varied once. A more detailed investigation of this theory was outside the scope of this study due to time constraints but it is possible that an optimum combination of initial parameters could be found with further study into individual site conditions and the results of the model could be improved.

Norwich, Dublin and Birmingham were all quite limited data sets. The observed data from Driby and Stock Hill was used to investigate the model's applicability to longer

time scale case studies. The range of modelled values was still insufficient on the longer time scales and this impacted on the model's ability to capture the seasonal cycle seen at Stock Hill, (section 6.3.5). The insufficient range was also seen when comparing monthly observed and modelled isotopic compositions (section 6.3.3). In an effort to identify the problems with the model the Driby and Stock Hill data sets were split according to Lamb classifications, (section 6.3.6). No one type of circulation pattern or approach direction to the U.K. was better handled by the model so the error cannot be pinned down to a mishandling of one specific atmospheric situation. It is likely that a process such as evaporation into the air parcel along the trajectory is not expressed correctly .

Overall the model does seem to produce isotopic ratios that have a positive relationship to the observed ratios seen (i.e. a more negative modelled value corresponds to a more negative observed value). The model is seen to perform better when time of rainfall data is available to filter the model runs that contribute to the daily modelled isotopic composition, though only limited observations were available for this test, (section 4.9). However, the range of modelled values produced across the study is not sufficient to cover that seen in the observations. This could partly be due to some as yet unidentified error in how the model deals with some of the processes involved in the isotopic water cycle, or perhaps a process is not included. Alternatively the fact that so many particles are averaged together could remove some of the signal with the noise. The fact that averages of all modelled values compare well with averages of all observed values is also interesting and has a potential application in proxy studies if average values in other locations can be modelled. The method does seem to have promise as a complimentary approach to that of including isotope parameterisations into GCMs. The Lagrangian trajectory model combined with the MCIM allows complex cloud microphysics to be modelled and fractionation to be accounted for at every change of phase of water in the atmosphere, as well as a suite of possible atmospheric paths to be examined. Smaller resolutions of processes can be modelled and comparisons with point observations are easier to make. Computer processing power and time required is also much reduced for this type of study as compared to a GCM approach. However, though the results of this study are positive, more

Site	Observed vs modelled regression equation		r^2 value		Critical r^2 value
	δ^{18}**O**	d**-excess**	δ^{18}**O**	d**-excess**	**at 90%**
Birmingham (U.K.)	y = 0.10x -6.19	y = 0.24x +8.74	0.33	0.86	0.52
Dublin (Ireland)	y = -0.48x -12.47	y = 0.14x +9.73	0.81	0.65	0.73
Norwich (U.K.)	y = 0.35x -4.18	y = 0.17x +9.26	0.84	0.89	0.52
Stock Hill (U.K.)	y = 0.04x -6.67	y = 0.23x +9.40	0.02	0.34	0.02
Driby (U.K.)	y = 0.03x -6.71	y = 0.08x +10.17	0.01	0.09	0.01

Table 7.2: *Regression equations and r^2 values for observed versus modelled $\delta^{18}O$ and d-excess for all days where more than 3 mm of rainfall occurred at all sites.*

investigation is required into why the modelled range is so much smaller than the observed range.

7.1 Further Work

It is clear from the results of this study that further investigation is required into the method of using a back trajectory model combined with a Mixed Cloud Isotope Model before it would be widely applicable. The model should be adapted to use the kinetic fractionation scheme of Cappa et al. (2003) to see if this would improve the modelled results. Further study would require more daily observed data on the isotopic composition of rainfall to be available. Information on the timing of rainfall would also be needed. Then further tuning tests could be conducted to optimise results as well as an investigation into which other processes are missing or mis–represented in the models. The strength of these Lagrangian small scale models is that processes can be removed or added fairly easily when compared with altering GCMs, thus allowing a thorough test of the relative impacts of each process to be carried out.

Once the model has been improved it would be interesting to test it on some more of the IAEA GNIP sites where monthly resolution isotopic ratios are available in some cases across a 30 year time period (e.g. Valentia, Ireland). The initial test of the ability of this

modelling approach to be translated to lower temporal resolution studies was conducted in section 6.3.3. Rainday data for Valentia is available through the European Climate Assessment and Dataset website from 1941 to the present. This dataset could be used initially to test the model as previously only raindays where over 3 mm of rainfall were modelled and averaged into modelled monthly averages for comparison with the observed monthly averages. Further tests would then be required to work out how many randomly chosen days from each month must be modelled to model the monthly average accurately where rainday data is not available. With these longer GNIP datasets it may even be possible to extend the use of the model further into modelling annual averages.

If the model is shown to be able to handle these lower temporal resolutions then it would be possible to extend the use of the model into interpreting speleothem records. Palaeoclimate GCM runs would be required to force the trajectory calculations of FLEXPART. Many GCMs, such as HadCM3 and ECHAM5, have already been run in palaeoclimate mode. The second phase of the Palaeoclimate Modelling Intercomparison Project (PMIP2) involved comparing the results of 13 such models (Braconnot et al., 2007) giving plenty of scope for FLEXPART input to be found. In effect the ultimate best use of the type of modelling approach used in this study may be as an extension to GCM model runs to allow modelling on much smaller scales. Another use of this modelling approach is, as stated before, to allow the dominant processes involved in the Isotopic Cycle to be better understood therefore improving models and the interpretation of observations.

References

L. Araguás-Araguás, K. Froelich, and K. Rozanski. Deuterium and Oxygen-18 Isotope Composition of Precipitation and Atmospheric Moisture. *Hydrological Processes*, 14:1341–1355, 2000.

L. Barlow, J. White, R. Barry, J. Rogers, and P. Grootes. The North Atlantic Oscillation Signature in Deuterium and Deuterium Excess Signals in the Greenland Ice Sheet Project 2 Ice Core, 1840-1970. *Geophysical Research Letters*, 20(24):2901–2904, 1993.

V. Barras and I. Simmonds. Synoptic Controls Upon δ^{18}O in Southern Tasmanian Precipitation. *Geophysical Research Letters*, 35, L02707, doi:10.1029/2007GL031835, 2008.

R. Barry and R. Chorley. *Atmosphere, Weather and Climate. 7th Edition*, chapter 3. Atmospheric Moisture Budget, pages 51–61. Routledge. London, 1998.

K. Baumann and A. Stohl. Validation of a Long-Range Trajectory Model Using Gas Balloon Tracks from the Gordon Bennett Cup 1995. *Journal of Applied Meteorology*, 36:711–720, 1997.

S. Beirle, N. Spichtinger, A. Stohl, K. Cummins, T. Turner, D. Boccippio, O. Cooper, M. Wenig, M. Grzegorski, U. Platt, and T. Wagner. Estimating the NOx Produced by Lightning from GOME and NLDN Data: A Case Study. *Atmospheric Chemistry and Physics*, 6:1075–1089, 2006.

A. Berto, A. Buzzi, and D. Zardi. Back-tracking Water Vapour Contributing to a Precipitation Event Over Trentino: A Case Study. *Meteorologische Zeitschrift*, 13(3):189–200, 2004.

P. Braconnot, B. Otto-Bliesner, S. Harrison, S. Jousaumme, J.-Y. Peterchmitt, A. Abe-Ouchi, M. Crucifix, E. Driesschaert, T. Fichefet, C. Hewitt, M. Kageyama, A. Kitoh, A. Laîné, M.-

F. Loutre, O. Marti, U. Merkel, G. Ramstein, P. Valdes, S. Weber, Y. Yu, and Y. Zhao. Results of PMIP2 Coupled Simulations of the Mid-Holocene and Last Glacial Maximum - Part 1: Experiments and Large-Scale Features. *Climate of the Past*, 3:261–277, 2007.

W. Brutsaert. A Theory for Local Evaporation (or Heat Transfer) from Rough and Smooth Surfaces at Ground Level. *Water Resources Research*, 11(4):543–550, 1975.

C. Cappa, M. Hendricks, D. DePaolo, and R. Cohen. Isotopic Fractionation of Water During Evaporation. *Journal of Geophysical Research*, 108(D16), 4525, doi:10.1029/2003JD003597, 2003.

P. Ciais and J. Jouzel. Deuterium and Oxygen-18 in Precipitation - Isotopic Model, Including Mixed Cloud Processes. *Journal of Geophysical Research*, 99(D8):16793–16803, 1994.

I. Clark and P. Fritz. *Environmental Isotopes in Hydrogeology.* Lewis Publishers, New York, 1997.

J. Cole, D. Rind, R. Webb, J. Jouzel, and R. Healy. Climatic Controls on Interannual Variability of Precipitation δ^{18}O: Simulated Influence of Temperature, Precipitation Amount, and Vapour Source Region. *Journal of Geophysical Research*, 104(D12):14223–14235, 1999.

O. Cooper, A. Stohl, G. Hubler, E. Hsie, D. Parrish, A. Tuck, G. Kiladis, S. Oltmans, B. Johnson, M. Shapiro, J. Moody, and A. Lefohn. Direct Transport of Midlatitude Stratospheric Ozone into the Lower Troposphere and Marine Boundary Layer of the Tropical Pacific Ocean. *Journal of Geophysical Research*, 110(D23):Art. No. 310, 2005.

C. Covey and P. Haagenson. A Model of Oxygen Isotope Composition of Precipitation: Implications for Paleoclimate Data. *Journal of Geophysical Research*, 89(D3):4647–4655, 1984.

H. Craig. Isotopic Variations in Meteoric Waters. *Science*, 133(3465):1702–1703, 1961.

H. Craig and L. Gordon. Isotopic Oceanography: Deuterium and Oxygen 18 Variations in the Ocean and the Marine Atmosphere. *Scripps Institution of Oceanography Contributions*, 39(1): 837–858, 1965.

P. Cristofanelli, P. Bonasoni, W. Collins, J. Feichter, C. Forster, P. James, A. Kentarchos, P. Kubik, C. Land, J. Meloen, G. Roelofs, P. Siegmund, M. Sprenger, C. Schnabel, A. Stohl, L. Tobler, L. Tositti, T. Trickl, and P. Zanis. Stratosphere-to-Troposphere Transport: A Model and Method

Evaluation. *Journal of Geophysical Research*, 108(D12), 8525, doi:10.1029/2002JD002600, 2003.

R. Damoah, N. Spichtinger, C. Forster, P. James, I. Mattis, U. Wandinger, S. Beirle, T. Wagner, and A. Stohl. Around the World in 17 Days - Hemispheric-Scale Transport of Forest Fire Smoke from Russia in May 2003. *Atmospheric Chemistry and Physics*, 4:1311–1321, 2004.

E. Danielsen. Trajectories: Isobaric, Isentropic and Actual. *Journal of Meteorology*, 18:479–486, 1961.

W. Dansgaard. Stable Isotopes in Precipitation. *Tellus*, 4:436–468, 1964.

W. Darling, A. Bath, and J. Talbot. The O & H Stable Isotopic Composition of Fresh Waters in the British Isles. 2. Surface Waters and Groundwater. *Hydrology and Earth System Sciences*, 7 (2):183–195, 2003.

W. Darling and J. Talbot. The O & H Stable Isotopic Composition of Fresh Waters in the British Isles. 1. Rainfall. *Hydrology and Earth System Sciences*, 7(2):163–181, 2003.

P. Dennis, P. Rowe, and T. Atkinson. The Recovery and Isotopic Measurement of Water from Fluid Inclusions in Speleothems. *Geochimica et Cosmochimica Acta*, 65(6):871–884, 2001.

S. Dorling, T. Davies, and C. Pierce. Cluster Analysis: A Technique for Estimating the Synoptic Meteorological Controls on Air and Precipitation Chemistry - Method and Applications. *Atmospheric Environment*, 26A(14):2575–2581, 1992.

R. Draxler and G. Rolph. HYSPLIT (HYbrid Single-Particle Lagrangian Integrated Trajectory) Model access via NOAA ARL READY Website (http://www.arl.noaa.gov/ready/hysplit4.html). NOAA Air Resources Laboratory, Silver Spring, MD., 2003.

P. Eden. Weather Log. November 2005. *Weather*, 61(1):i–iv, 2006.

K. Emanuel. A Scheme for Representing Cumulus Convection in Large-Scale Models. *Journal of the Atmospheric Sciences*, 48(21):2313–2335, 1991.

K. Emanuel and M. Živković-Rothman. Development and Evaluation of a Convection Scheme for use in Climate Models. *Journal of the Atmospheric Sciences*, 56:1766–1782, 1999.

G. Faure. *Principles of Isotope Geology.*, chapter 18. Oxygen and Hydrogen in the Hydrosphere and the Atmosphere., pages 323–349. Wiley, 1977.

G. Faure and T. Mensing. *Isotopes: Principles and Applications.*, chapter 26. Hydrogen and Oxygen., pages 693–701. John Wiley & Sons, New Jersey, 2005.

D. Fisher. Remarks on the Deuterium Excess in Precipitation in Cold Regions. *Tellus*, 43B: 401–407, 1991.

D. Flothmann, K. Muennich, and H. Vogt. Evaporation Study by Isotopic Fractionation of Water in a Circular Wind Tunnel. *Transactions of the American Geophysical Union*, 58(9):898, 1977.

C. Forster, O. Cooper, A. Stohl, S. Eckhardt, P. James, E. Dunlea, D. Nicks, Jr, J. Holloway, G. Hubler, D. Parrish, T. Ryerson, and M. Trainer. Lagrangian Transport Model Forecasts and a Transport Climatology for the Intercontinental Transport and Chemical Transformation 2002 (ITCT 2k2) Measurement Campaign. *Journal of Geophysical Research*, 109(D7), doi: 10.1029/2003JD003589, 2004.

C. Forster, U. Wandinger, G. Wotawa, P. James, I. Mattis, D. Althausen, P. Simmonds, S. O'Doherty, S. Jennings, C. Kleefeld, J. Schneider, T. Trickl, S. Kreipl, H. Jäger, and A. Stohl. Transport of Boreal Forest Fire Emissions from Canada to Europe. *Journal of Geophysical Research*, 106(D19):22887–22906, 2001.

H. Fricke and J. O'Neil. The Correlation Between $^{18}O/^{16}O$ Ratios of Meteoric Water and Surface Temperature: Its Use in Investigating Terrestrial Climate Change Over Geologic Time. *Earth and Planetary Science Letters*, 170:181–196, 1999.

J. Gat. *Handbook of Environmental Isotope Geochemistry. Vol. 1. The Terrestrial Environment, A.*, chapter 1. The Isotopes of Hydrogen and Oxygen in Precipitation. Elsevier, Amsterdam, 1980.

J. Gat. Oxygen and Hydrogen Isotopes in the Hydrologic Cycle. *Annual Review of Earth Planetary Sciences*, 24:225–262, 1996.

J. Gat. Atmospheric Water Balance - The Isotopic Perspective. *Hydrological Processes*, 14:1357–1369, 2000.

J. Gat and R. Gonfiantini, editors. *Stable Isotope Hydrology. Deuterium and Oxygen-18 in the Water Cycle.* IAEA, Austria, 1981.

S. Gedzelman and R. Arnold. Modeling the Isotopic Composition of Precipitation. *Journal of Geophysical Research*, 99(D5):10455–10471, 1994.

S. Gedzelman and J. Lawrence. The Isotopic Composition of Precipitation from Two Extratropical Cyclones. *Monthly Weather Review*, 118:495–509, 1990.

R. Gonfiantini. *Handbook of Environmental Isotope Geochemistry. Vol. 2. The Terrestrial Environment, B.*, chapter 3. Environmental Isotopes in Lake Studies. Elsevier, Amsterdam, 1986.

S. Gupta, R. McNider, M. Trainer, R. Zamora, K. Knupp, and M. Singh. Nocturnal Wind Structure and Plume Growth Rates Due to Inertial Oscillations. *Journal of Applied Meteorology*, 36: 1050–1063, 1997.

P. Haagenson, K. Gao, and Y.-H. Kuo. Evaluation of Meteorological Analyses, Simulations, and Long-Range Transport Calculations Using ANATEX Surface Tracer Data. *Journal of Applied Meteorology*, 29:1268–1283, 1990.

P. Haagenson, Y.-H. Kuo, M. Skumanich, and N. Seaman. Tracer Verification of Trajectory Models. *Journal of Climate and Applied Meteorology*, 26(3):410–426, 1987.

J. Heathcote and J. Lloyd. Factors Affecting the Isotopic Composition of Daily Rainfall at Driby, Lincolnshire. *Journal of Climatology*, 6:97–106, 1986.

M. Helsen. *On the Interpretation of Stable Isotopes in Antarctic Precipitation.* PhD thesis, Institute for Marine and Atmospheric Research, Utrecht., 2006.

M. Helsen, R. van de Wal, and M. van den Broeke. The Isotopic Composition of Present-Day Antarctic Snow in a Lagrangian Atmospheric Simulation. *Journal of Climate*, 20:739–756, 2007.

M. Helsen, R. van de Wal, M. van den Broeke, E. Kerstel, V. Masson-Delmotte, H. Meijer, C. Reijmer, and M. Scheele. Modelling the Isotopic Composition of Snow Using Backward Trajectories: A Particular Precipitation Event in Dronning Maud Land, Antarctica. *Annals of Glaciology*, 39:293–299, 2004.

M. Helsen, R. van de Wal, M. van den Broeke, V. Masson-Delmotte, H. Meijer, M. Scheele, and M. Werner. Modeling the Isotopic Composition of Antarctic Snow Using Backward Trajectories: Simulation of Snow Pit Records. *Journal of Geophysical Research*, 111, D15109, doi: 10.1029/2005JD006524, 2006.

M. Hendricks, D. DePaolo, and R. Cohen. Space and Time Variation of δ^{18}O and δD in Precipitation: Can Palaeotemperature be Estimated from Ice Cores? *Global Biogeochemical Cycles*, 14 (3):851–861, 2000.

H. Hoffmann, J. Jouzel, and V. Masson. Stable Water Isotopes in Atmospheric General Circulation Models. *Hydrological Processes*, 14:1385–1406, 2000.

H. Hoffmann, M. Werner, and M. Heimann. Water Isotope Module of the ECHAM Atmospheric General Circulation Model: A Study on Timescales from Days to Several Years. *Journal of Geophysical Research*, 103(D14):16871–16896, 1998.

J. Horita and D. Wesolowski. Liquid-vapor Fractionation of Oxygen and Hydrogen Isotopes of Water from the Freezing to the Critical Temperature. *Geochimica et Cosmochimica Acta*, 58 (16):3425–3437, 1994.

M. Hulme and E. Barrow, editors. *Climates of the British Isles.* Routledge, London, 1997.

H. Jacob and C. Sonntag. An 8–year Record of the Seasonal Variation of ^{2}H and ^{18}O in Atmospheric Water Vapour and Precipitation at Heidelberg, Germany. *Tellus*, 43B:291–300, 1991.

P. James, A. Stohl, C. Forster, and S. Eckhardt. A 15-year Climatology of Stratosphere-Troposphere Exchange with a Lagrangian Particle Model: 1. Methodology and Validation. *Journal of Geophysical Research*, 108(D12), 8519, doi:10.1029/2002JD002637, 2003.

P. Jones, M. Hulme, and K. Briffa. A Comparison of Lamb Circulation Types With An Objective Classification Scheme. *International Journal of Climatology*, 13:655–663, 1993.

S. Joussaume, R. Sadourny, and J. Jouzel. A General Circulation Model of Water Isotope Cycles in the Atmosphere. *Nature*, 311:24–29, 1984.

J. Jouzel. Perspectives: Geoscience - Calibrating the Isotopic Palaeothermometer. *Science*, 286 (5441):910–911, 1999.

J. Jouzel, K. Froehlich, and U. Schotterer. Deuterium and Oxygen-18 in Present-Day Precipitation: Data and Modelling. *Hydrological Sciences Journal*, 42(5):747–763, 1997.

J. Jouzel, G. Hoffmann, R. Koster, and V. Masson. Water Isotopes in Precipitation: Data/Model Comparison for Present-Day and Past Climates. *Quarternary Science Reviews*, 19:363–379, 2000.

J. Jouzel and R. Koster. A Reconsideration of the Initial Conditions Used for Stable Water Isotope Models. *Journal of Geophysical Research*, 101(D17):22933–22938, 1996.

J. Jouzel, R. Koster, and V. Masson. Climate Reconstruction from Water Isotopes: What do We Learn from Isotopic Models? *Climatic Variations and Forcing Mechanisms of the Last 2000 Years.*, NATO ASI Series, Vol. 141:213–241, 1996.

J. Jouzel, R. Koster, R. Suozzo, G. Russell, J. White, and W. Broecker. Simulations of the HDO and $H_2{}^{18}O$ Atmospheric Cycles Using the NASA GISS General Circulation Model: Sensitivity Experiments for Present-Day Conditions. *Journal of Geophysical Research*, 96(D4):7495–7507, 1991.

J. Jouzel and L. Merlivat. Deuterium and Oxygen 18 in Precipitation: Modeling of the Isotopic Effects During Snow Formation. *Journal of Geophysical Research*, 89(D7):11749–11757, 1984.

J. Jouzel, G. Russell, R. Suozzo, R. Koster, J. White, and W. Broecker. Simulations of the HDO and $H_2{}^{18}O$ Atmospheric Cycles Using the NASA GISS General Circulation Model: The Seasonal Cycle for Present-Day Conditions. *Journal of Geophysical Research*, 92(D12):14739–14760, 1987.

J. Jouzel, F. Vimeux, N. Caillon, G. Delaygue, G. Hoffmann, V. Masson-Delmotte, and F. Parrenin. Magnitude of Isotope/Temperature Scaling for Interpretation of Central Antarctic Ice Cores. *Journal of Geophysical Research*, 108(D12), 4361, doi:10.1029/2002JD002677, 2003.

J. Kaye. Analysis of the Origins and Implications of the ^{18}O content of Stratospheric Water Vapor. *Journal of Atmospheric Chemistry*, 10:39–57, 1990.

S. Lauritzen and J. Lundberg. Speleothems and Climate: A Special Issue of The Holocene. *The Holocene*, 9(6):643–647, 1999.

J. Lawrence, S. Gedzelman, J. White, D. Smiley, and P. Lazov. Storm Trajectories in Eastern US D/H Isotopic Composition of Precipitation. *Nature*, 296:638–640, 1982.

M. Lawrence, P. Rasch, R. von Kuhlmann, J. Williams, H. Fischer, M. de Reus, J. Lelieveld, P. Crutzen, M. Schultz, P. Stier, H. Huntrieser, J. Heland, A. Stohl, C. Forster, H. Elbern, H. Jakobs, and R. Dickerson. Global Chemical Weather Forecasts for Field Campaign Planning: Predictions and Observations of Large-Scale Features During MINOS, CONTRACE and INDOEX. *Atmospheric Chemistry and Physics*, 3:267–289, 2003.

J.-E. Lee, I. Fung, D. DePaolo, and C. Henning. Analysis of the Global Distribution of Water Isotopes Using the NCAR Atmospheric General Circulation Model. *Journal of Geophysical Research*, 112, D16306, doi:10.1029/2006JD007657, 2007.

M. Majoube. Fractionnement en Oxygẹne 18 Entre la Glace et la Vapeur d'eau. *Journal de Chimie Physique*, 68(4):625, 1971a.

M. Majoube. Fractionnement en Oxygẹne 18 et en Deutêrium Entre L'eau et sa Vapeur. *Journal de Chimie Physique*, 68(10):1423, 1971b.

J. Maron and G. Howes. Gradient Particle Magnetohydrodynamics: A Lagrangian Particle Code for Astrophysical Magnetohydrodynamics. *Astrophysical Journal*, 595:564–572, 2003.

R. Mathieu, D. Pollard, J. Cole, J. White, R. Webb, and S. Thompson. Simulation of Stable Water Isotope Variations by the GENESIS GCM for Modern Conditions. *Journal of Geophysical Research*, 107(D4):Art. No. 4037, 2002.

J. Meloen, P. Siegmund, P. van Velthoven, H. Kelder, M. Sprenger, H. Wernli, A. Kentarchos, G. Roelofs, J. Feichter, C. Land, C. Forster, P. James, A. Stohl, W. Collins, and P. Cristofanelli. Stratosphere-Troposphere Exchange: A Model and Method Intercomparison. *Journal of Geophysical Research*, 108(D12), 8526, doi:10.1029/2002JD002274, 2003.

L. Merlivat. Molecular Diffusivities of $H_2{}^{16}O$, $HD^{16}O$, and $H_2{}^{18}O$ in Gases. *Journal of Chemical Physics*, 69(6):2864–2871, 1978.

L. Merlivat and J. Jouzel. Global Climatic Interpretation of the Deuterium-Oxygen 18 Relationship for Precipitation. *Journal of Geophysical Research*, 84(C8):5029–5033, 1979.

L. Merlivat and G. Nief. Fractionnement Isotopique lors des Changements d'état Solide-Vapeur et Liquide-Vapeur de l'eau à des Températures Inférieures à 0°C. *Tellus*, 19(1):122–127, 1967.

D. Noone and I. Simmonds. Associations Between δ^{18}O of Water and Climate Parameters in a Simulation of Atmospheric Circulation for 1979-95. *Journal of Climate*, 15:3150–3169, 2002.

S. Oltmans and D. Hofmann. Increase in Lower-Stratospheric Water Vapour at a Mid-Latitude Northern Hemisphere Site from 1981 to 1994. *Nature*, 374:146–149, 1995.

H. Peng, B. Mayer, A.-L. Norman, and H. R. Krouse. Modelling of Hydrogen and Oxygen Isotope Compositions for Local Precipitation. *Tellus*, 57B:273–282, 2005.

J. Petit, J. White, N. Young, J. Jouzel, and Y. Korotkevich. Deuterium Excess in Recent Antarctic Snow. *Journal of Geophysical Research*, 96(D3):5113–5122, 1991.

S. Petterssen. *Weather Analysis and Forecasting. 2nd Edition.*, pages 22–32. McGraw-Hill, New York, 1956.

M. Rindsberger, S. Jaffe, S. Rahamim, and J. Gat. Patterns of the Isotopic Composition of Precipitation in Time and Space: Data from the Israeli Storm Water Collection Program. *Tellus*, 42B: 263–271, 1990.

K. Rozanski, J. Araguás-Araguás, and R. Gonfiantini. Isotopic Patterns in Modern Global Precipitation. Climate Change in Continental Isotopic Records. *Geophysical Monograph*, 78:1–36, 1993.

K. Rozanski, L. Araguás-Araguás, and R. Gonfiantini. Relation Between Long-Term Trends of Oxygen-18 Composition of Precipitation and Climate. *Science*, 258(5024):981–985, 1992.

K. Rozanski, C. Sonntag, and K. Munnich. Factors Controlling Stable Isotope Composition of European Precipitation. *Tellus*, 34:142–150, 1982.

G. Schmidt, G. Hoffmann, D. Shindell, and Y. Hu. Modeling Atmospheric Stable Water Isotopes and the Potential for Constraining Cloud Processes and Stratosphere-Troposphere Water Exchange. *Journal of Geophysical Research*, 110, D21314, doi:10.1029/2005JD005790, 2005.

G. Schmidt, R. Ruedy, J. Hansen, I. Aleinov, N. Bell, M. Bauer, S. Bauer, B. Cairns, V. Canuto, Y. Cheng, A. del Genio, G. Faluvegi, A. D. Friend, T. Hall, Y. Hu, M. Kelley, N. Kiang, D. Koch,

A. Lacis, J. Lerner, K. Lo, R. Miller, L. Nazarenko, V. Oinas, J. Perlwitz, D. Rind, A. Romanou, G. Russell, M. Sato, D. Shindell, P. Stone, S. Sun, N. Tausnev, D. Thresher, and M. Yao. Present-Day Atmospheric Simulations Using GISS ModelE: Comparison to In Situ, Satellite, and Reanalysis Data. *Journal of Climate*, 119:153–191, 2006.

C. Schmutz, J. Luterbacher, D. Gyalistras, E. Xoplaki, and H. Wanner. Can We Trust Proxy-Based NAO Index Reconstructions? *Geophysical Research Letters*, 27(8):1135–1138, 2000.

U. Schotterer, F. Oldfield, and K. Frohlich. Global Network for Isotopes in Precipitation. *Climatic Variations and Forcing Mechanisms of the Last 2000 Years.*, pub. Druckerei Laderach, Switzerland:47, 1996.

P. Seibert and A. Frank. Source-Receptor Matrix Calculation with a Lagrangian Particle Dispersion Model in Backward Mode. *Atmospheric Chemistry and Physics*, 4:51–63, 2004.

P. Seibert, B. Krüger, and A. Frank. Parametrisation of Convective Mixing in a Lagrangian Particle Dispersion Model. *In: Proceedings of the 5th GLOREAM Workshop, Wengen, Switzerland.*, 2002.

H. Sodemann. *Tropospheric Transport of Water Vapour: Lagrangian and Eulerian Perspectives.* PhD thesis, Swiss Federal Institute of Technology, Zurich., 2006.

C. Sonntag, K. Munnich, H. Jacob, and K. Rozanski. Variations of Deuterium and Oxygen-18 in Continental Precipitation and Groundwater, and Their Causes. In: Variations in the Global Water Budget. Street Perrott et al., (eds.). Reidel Publ,. pages 107–124, 1983.

N. Spichtinger, M. Wenig, P. James, T. Wagner, U. Platt, and A. Stohl. Satellite Detection of a Continental-Scale Plume of Nitrogen Oxides from Boreal Forest Fires. *Geophysical Research Letters*, 28(24):4579–4582, 2001.

M. Stewart. Stable Isotope Fractionation Due to Evaporation and Isotopic Exchange of Falling Waterdrops: Applications to Atmospheric Processes and Evaporation of Lakes. *Journal of Geophysical Research*, 80(9):1133–1146, 1975.

A. Stohl. Computation, Accuracy and Applications of Trajectories - A Review and Bibliography. *Atmospheric Environment*, 32(6):947–966, 1998.

A. Stohl. *The FLEXTRA Trajectory Model. Version 3.0 User Guide.* . http://zardoz.nilu.no/∼andreas/flextra/flextra3.pdf, 1999.

A. Stohl. Characteristics of Atmospheric Transport into the Arctic Troposphere. *Journal of Geophysical Research*, 111, D11306, doi:10.1029/2005JD006888, 2006.

A. Stohl, O. Cooper, R. Damoah, F. Fehsenfeld, C. Forster, E. Hsie, G. Hubler, D. Parrish, and M. Trainer. Forecasting for a Lagrangian Aircraft Campaign. *Atmospheric Chemistry and Physics*, 4:1113–1124, 2004a.

A. Stohl, O. Cooper, and P. James. A Cautionary Note on the Use of Meteorological Analysis Data for Quantifying Atmospheric Mixing. *Journal of the Atmospheric Sciences*, 61:1446–1453, 2004b.

A. Stohl, S. Eckhardt, C. Forster, P. James, N. Spichtinger, and P. Seibert. A Replacement for Simple Back Trajectory Calculations in the Interpretation of Atmospheric Trace Substance Measurements. *Atmospheric Environment*, 36:4635–4648, 2002.

A. Stohl, C. Forster, S. Eckhardt, N. Spichtinger, H. Huntrieser, J. Heland, H. Schlager, S. Wilhelm, F. Arnold, and O. Cooper. A Backward Modeling Study of Intercontinental Pollution Transport Using Aircraft Measurements. *Journal of Geophysical Research*, 108(D12), 4370, doi:10.1029/2002JD002862, 2003.

A. Stohl, C. Forster, A. Frank, P. Seibert, and G. Wotawa. Technical Note: The Lagrangian Particle Dispersion Model FLEXPART Version 6.2. *Atmospheric Chemistry and Physics*, 5:2461–2474, 2005a.

A. Stohl, L. Haimberger, M. Scheele, and H. Wernli. An Intercomparison of Results From Three Trajectory Models. *Meteorological Applications*, 8:127–135, 2001.

A. Stohl, M. Hittenberger, and G. Wotawa. Validation of the Lagrangian Particle Dispersion Model Flexpart Against Large-Scale Tracer Experiment Data. *Atmospheric Environment*, 32 (24):4245–4264, 1998.

A. Stohl and P. James. A Lagrangian Analysis of the Atmospheric Branch of the Global Water Cycle: Part 1. Method Description, Validation, and Demonstration for the August 2002 Flooding in Central Europe. *Journal of Hydrometeorology*, 5:656–678, 2004.

A. Stohl and N. Koffi. Evaluation of Trajectories Calculated From ECMWF Data Against Constant Volume Balloon Flights During ETEX. *Atmospheric Environment*, 32:4151–4156, 1998.

A. Stohl and P. Seibert. Accuracy of Trajectories as Determined from the Conservation of Meteorological Tracers. *Quarterly Journal of the Royal Meteorological Society*, 124:1465–1484, 1998.

A. Stohl, P. Seibert, and C. Forster. *The FLEXPART Particle Dispersion Model. Version 6.0 User Guide.* http://zardoz.nilu.no/∼andreas/flexpart/flexpart60.pdf, 2005b.

A. Stohl and D. Thompson. A Density Correction for Lagrangian Particle Dispersion Models. *Boundary-Layer Meteorology*, 90:155–167, 1999.

A. Stohl and T. Trickl. A Textbook Example of Long-Range Transport: Simultaneous Observation of Ozone Maxima of Stratospheric and North American Origin in the Free Troposphere Over Europe. *JGR*, 104(D23):30445–30462, 1999.

A. Stohl and G. Wotawa. A Method for Computing Single Trajectories Representing Boundary Layer Transport. *Atmospheric Environment*, 29:3235–3239, 1995.

A. Stohl, G. Wotawa, P. Seibert, and H. Kromp-Kolb. Interpolation Errors in Wind Fields as a Function of Spatial and Temporal Resolution and Their Impact on Different Types of Kinematic Trajectories. *Journal of Applied Meteorology*, 34:2149–2165, 1995.

K. Sturm, G. Hoffmann, B. Langmann, and W. Stichler. Simulation of δ^{18}O in Precipitation by the Regional Circulation Model REMO$_{iso}$. *Hydrological Processes*, 19:3425–3444, 2005.

P. Treble, W. Budd, P. Hope, and P. Rustomji. Synoptic-scale Climate Patterns Associated with Rainfall δ^{18}O in Southern Australia. *Journal of Hydrology*, 302:270–282, 2005.

T. Trickl, O. Cooper, H. Eisele, P. James, R. Mucke, and A. Stohl. Intercontinental Transport and its Influence on the Ozone Concentrations Over Central Europe: Three Case Studies. *Journal of Geophysical Research*, 108(D12), 8530, doi:10.1029/2002JD002735, 2003.

F. Vimeux, V. Masson, J. Jouzel, J. Petit, E. Steig, M. Stievenard, R. Vaikmae, and J. White. Holocene Hydrological Cycle Changes in the Southern Hemisphere Documented in East Antarctic Deterium Excess Records. *Climate Dynamics*, 17(7):503–513, 2001.

F. Vimeux, V. Masson, J. Jouzel, M. Stievenard, and J. Petit. Glacial-Interglacial Changes in Ocean Surface Conditions in the Southern Hemisphere. *Letters to Nature*, 398(6726):410–413, 1999.

D. Vogelezang and A. Holtslag. Evaluation and Model Impacts of Alternative Boundary–Layer Height Formulations. *Boundary-Layer Meteorology*, 81:245–269, 1996.

M. Wenig, N. Spichtinger, A. Stohl, G. Held, S. Beirle, T. Wagner, B. Jahne, and U. Platt. Intercontinental Transport of a Power Plant Plume of Nitrogen Oxides. *Atmospheric Chemistry and Physics*, 3:387–393, 2003.

D. Wilks. *Statistical Methods in Atmospheric Sciences.* Academic Press Inc., London., 1995.

H. Willard, L. Merritt, Jr, J. Dean, and F. Settle, Jr. *Instrumental Methods of Analysis. 7th Edition.* Wadsworth Publishing Company, California., 1988.

J. Wilson and B. Sawford. Review of Lagrangian Stochastic Models for Trajectories in the Turbulent Atmosphere. *Boundary-Layer Meteorology*, 78:191–210, 1996.

A. Zahn, P. Franz, C. Bechtel, J.-U. Grooß, and T. Röckmann. Modelling the Budget of Middle Atmospheric Water Vapour Isotopes. *Atmospheric Chemistry and Physics*, 6:2073–2090, 2006.

P. Zanis, T. Trickl, A. Stohl, H. Wernli, O. Cooper, C. Zerefos, H. Gaggeler, C. Schnabel, L. Tobler, P. Kubik, A. Priller, H. Scheel, H. Kanter, P. Cristofanelli, C. Forster, P. James, E. Gerasopoulos, A. Delcloo, A. Papayannis, and H. Claude. Forecast, Observation and Modeling of a Deep Stratospheric Intrusion Event Over Europe. *Atmospheric Chemistry and Physics*, 3:763–777, 2003.

Appendices

Appendix A

Photographs of Norwich Precipitation Collection Sites

Figure A.1: *The roof precipitation collection site at 87 Bury Street, Norwich*

Figure A.2: *The garden precipitation collection site at 87 Bury Street, Norwich*

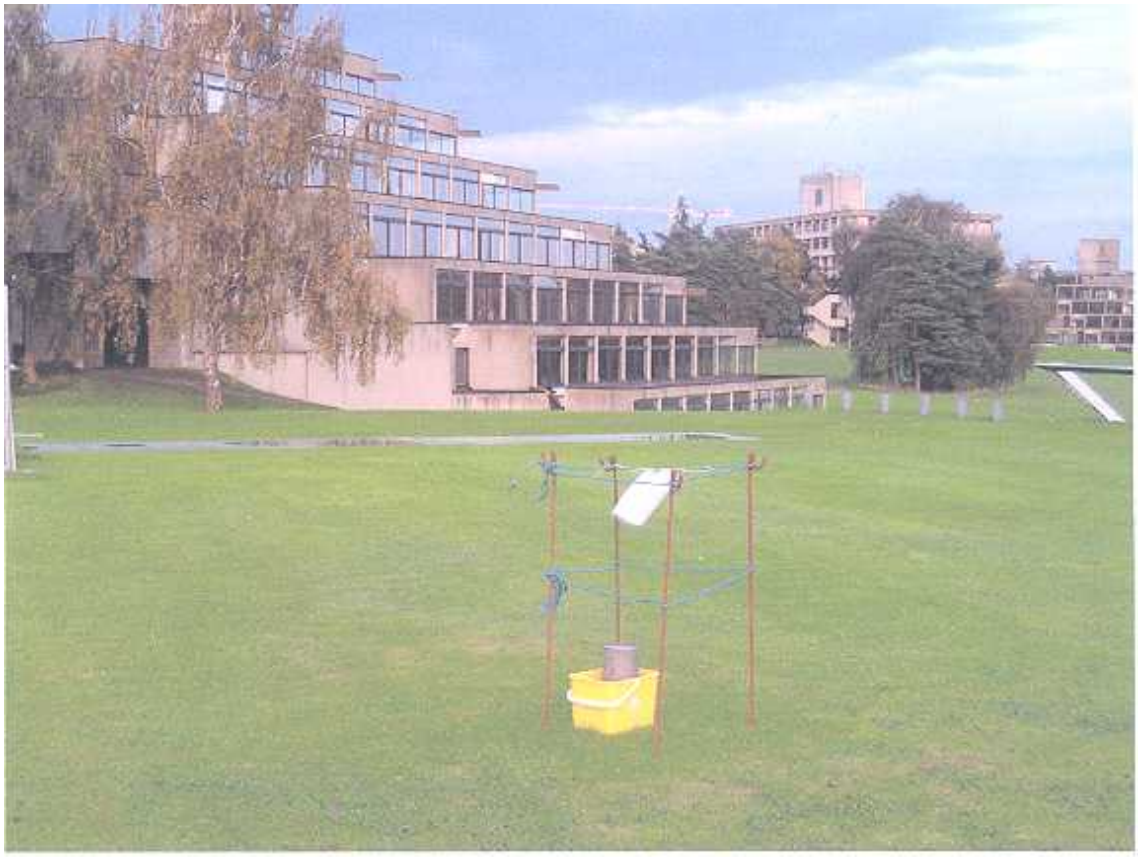

Figure A.3: *The Sainsbury Centre precipitation collection site at the University of East Anglia, Norwich*

Figure A.4: *The Zicer precipitation collection site at the University of East Anglia, Norwich*

Appendix B

Observed and Modelled δ^{18}O and δD values, and amount of precipitation for Norwich, Dublin and Birmingham

Date	δ^{18}O (‰)		δD (‰)		Amount
	Observed	Modelled	Observed	Modelled	(mm)
01/11/05	-7.42	-7.01	-47.82	-45.03	7.82
02/11/05	-11.11	-7.77	-78.35	-51.57	3.26
03/11/05	-3.17	-6.81	-20.82	-43.83	0.81
07/11/05	-7.40	-6.44	-47.98	-39.80	4.40
12/11/05	-2.08	-6.45	-8.16	-39.04	0.65
15/11/05	-4.55	-7.39	-27.88	-47.57	2.28
16/11/05	-5.79	-8.33	-29.42	-54.15	0.86
17/11/05	-2.63	-7.81	-9.53	-48.89	0.33
18/11/05	-4.09	-8.01	-13.34	-50.97	0.45
25/11/05	-6.56	-8.15	-37.27	-50.50	0.37
26/11/05	-11.99	-8.44	-75.71	-54.15	14.34
27/11/05	-10.41	-7.99	-61.46	-51.01	7.17
28/11/05	-10.38	-7.94	-60.10	-50.41	7.17
29/11/05	-6.78	-7.80	-32.98	-49.18	0.20
01/12/05	-5.55	-6.94	-29.45	-43.01	2.24
02/12/05	-11.26	-7.32	-72.70	-45.82	1.22
07/12/05	-8.84	-8.68	-58.64	-58.59	1.55

Table B.1: *Observed and modelled $\delta^{18}O$ and δD values, and amount of precipitation for all Norwich raindays collected at the roof site at 87 Bury Street.*

Date	δ^{18}O (‰)		δD (‰)		Amount
	Observed	Modelled	Observed	Modelled	(mm)
02/11/05	-12.35	-7.07	-88.90	-44.94	10.00
03/11/05	-5.66	-7.52	-29.56	-49.48	2.60
04/11/05	-7.06	-9.11	-42.39	-62.27	9.50
05/11/05	-5.69	-7.61	-27.04	-48.80	1.00
06/11/05	-9.41	-6.36	-65.31	-38.69	1.70
07/11/05	-12.66	-7.11	-90.81	-43.92	3.25
10/11/05	-3.21	-6.71	-8.50	-42.01	negligible
11/11/05	-3.20	-6.19	-13.20	-37.42	1.00
12/11/05	-5.81	-7.50	-20.60	-46.82	1.50
15/11/05	-2.78	-7.52	-10.60	-48.48	negligible
24/11/05	-5.15	-6.93	-14.50	-42.76	negligible
25/11/05	-8.21	-7.63	-40.40	-45.73	1.00
29/11/05	-8.17	-8.25	-48.30	-51.36	negligible
30/11/05	-10.14	-8.90	-66.40	-59.42	2.00
01/12/05	-14.07	-6.80	-102.00	-42.12	11.50

Table B.2: *Observed and modelled $\delta^{18}O$ and δD values, and amount of precipitation for all Dublin raindays.*

Date	δ^{18}**O** ($^{\circ}/_{\circ\circ}$)		δ**D** ($^{\circ}/_{\circ\circ}$)		**Amount**
	Observed	**Modelled**	**Observed**	**Modelled**	**(mm)**
01/11/05	-5.25	-7.23	-27.27	-46.36	1.80
02/11/05	-12.72	-7.78	-89.46	-51.07	8.60
03/11/05	-4.88	-7.00	-32.20	-45.02	6.40
04/11/05	-5.17	-9.00	-29.54	-61.70	0.60
05/11/05	-5.83	-7.31	-32.41	-46.33	0.40
06/11/05	-8.98	-6.37	-57.44	-39.40	17.60
07/11/05	-6.47	-6.57	-35.07	-40.31	0.40
09/11/05	-12.57	-7.25	-86.66	-45.91	17.20
10/11/05	-7.40	-7.27	-43.28	-46.45	1.00
15/11/05	-3.55	-7.09	-12.10	-45.01	0.40
24/11/05	-4.97	-6.53	-21.24	-39.09	0.40
25/11/05	-5.53	-7.84	-24.80	-47.61	0.60
27/11/05	-13.39	-8.54	-90.30	-55.41	1.00
29/11/05	-11.59	-7.81	-69.80	-47.88	4.00

Table B.3: *Observed and modelled $\delta^{18}O$ and δD values, and amount of precipitation for all Birmingham raindays.*

Appendix C

Observed δ^{18}O and δD values, and amount of precipitation for all 5 Norwich precipitation collection sites

Date	87 Bury Street Sites					
	Roof Site			Garden Site		
	Observed		Amount	Observed		Amount
	δ^{18}O	δD	mm	δ^{18}O	δD	mm
01/11/05	-7.42	-47.82	7.82			8.15
02/11/05	-11.11	-78.35	3.26			3.75
03/11/05	-3.17	-20.82	0.81			0.81
07/11/05	-7.40	-47.98	3.91			3.91
12/11/05	-2.08	-8.16	0.65			0.65
15/11/05	-4.55	-27.88	2.28			2.28
16/11/05	-5.79	-29.42	0.86			0.98
17/11/05	-2.63	-9.53	0.33			0.49
18/11/05	-4.09	-13.34	0.45	-3.83	-13.21	0.45
19/11/05			0.04			0.24
25/11/05	-6.65	-37.27	0.37	-6.32	-33.75	0.45
26/11/05	-11.99	-75.71	14.34	-11.75	-75.26	13.2
27/11/05	-10.41	-61.46	7.17	-10.64	-62.58	
28/11/05	-10.38	-60.10	7.17	-10.50	-60.16	6.84
29/11/05	-6.78	-32.98	0.20			0.33
01/12/05	-5.55	-29.45	2.24	-5.77	-29.63	2.32
02/12/05	-11.26	-72.70	1.22	-11.45	-75.67	1.47
07/12/05	-8.84	-58.64	1.55	-9.17	-57.82	1.55

Table C.1: *Observed $\delta^{18}O$ and δD values, and amount of precipitation for all Norwich raindays collected at both 87 Bury Street precipitation collection sites. All δ values are given in permil ($^{\circ}/_{\circ\circ}$).*

Date	University of East Anglia Sites								
	Sainsbury Centre Site			ZICER Site			ENV roof Site		
	Observed		Amount	Observed		Amount	Observed		Amount
	δ^{18}O	δD	mm	δ^{18}O	δD	mm	δ^{18}O	δD	mm
01/11/05			8.96			8.96			
02/11/05			4.24			4.07			
03/11/05			0.90			0.81			
07/11/05			5.22			4.89			
12/11/05			0.73			0.90			
15/11/05			2.44			2.85			
16/11/05			1.81			1.10			
17/11/05			0.49			0.49			
18/11/05	-4.99	-16.86	1.96	9.45					
19/11/05			0.37			0.37			
25/11/05	-4.73	-21.67	0.29	-5.25	-29.18	0.29	-4.52	-21.98	0.29
26/11/05	-11.73	-74.76	24.61	-12.08	-75.63	17.11			
27/11/05	-10.47	-61.45	10.76	-10.60	-61.15	9.45			
28/11/05	-9.99	-54.65	8.80	-10.00	-57.07	9.29			
29/11/05			0.61			0.45			0.45
01/12/05	-5.81	-30.03	2.44	-5.57	-29.07	2.28	-5.61	-29.41	2.44
02/12/05	-10.29	-67.33	1.18	-10.53	-67.24	1.34	-10.27	-68.35	1.30
07/12/05	-9.08	-58.51	1.87	-8.90	-57.96	1.83	-8.61	-54.30	1.63

Table C.2: *Observed $\delta^{18}O$ and δD values, and amount of precipitation for all Norwich raindays collected at all University of East Anglia precipitation collection sites. All δ values are given in permil ($^{\circ}/_{\circ\circ}$).*

Appendix D

Observed and Modelled δ^{18}O and δD values, and amount of precipitation for Stock Hill

Please contact Professor Tim Atkinson, Department of Earth Sciences, University College London, t.atkinson@ucl.ac.uk for permission to use this data.

Date	Observed		Modelled		Amount
	δ^{18}**O** ($^\circ/_{\circ\circ}$)	δ**D** ($^\circ/_{\circ\circ}$)	δ^{18}**O** ($^\circ/_{\circ\circ}$)	δ**D** ($^\circ/_{\circ\circ}$)	**(mm)**
09/11/1977	-4.14	-25.3	-6.54	-40.41	9.7
12/11/1977	-7.12	-35.1	-7.75	-49.05	5.6
14/11/1977	-4.63	-23.6	-7.77	-49.57	7.4
17/11/1977	-10.05	-60	-8.05	-51.09	10.2
20/11/1977	-11.65	-74.4	-7.21	-44.59	16.3
24/11/1977	-5.24	-25.4	-7.84	-49.83	4.3
01/12/1977	-5.85	-29.1	-7.14	-43.23	3.9
08/12/1977	-11.91	-87.3	-7.87	-51.51	14.4
09/12/1977	-6.47	-47.4	-7.78	-50.85	6.6
10/12/1977	-9.19	-61.8	-6.56	-40.09	15.8
11/12/1977	-4.99	-27.8	-6.40	-39.19	9
22/12/1977	-13.11	-100	-6.25	-37.48	4
23/12/1977	-7.73	-50.9	-6.62	-40.84	3.8
26/12/1977	-9.27	-60.8	-6.03	-35.78	7.8
27/12/1977	-12.37	-84.6	-6.60	-39.94	8.1
04/01/1978	-7.28	-40.3	-7.82	-48.60	4.2
10/01/1978	-6.53	-29.4	-6.51	-38.16	3.9
11/01/1978	-12.16	-76.9	-7.16	-43.50	24.1
05/02/1978	-7.39	-53.7	-6.91	-43.83	8
06/02/1978	-5.51	-30.1	-7.12	-44.21	6.7
24/02/1978	-6.53	-41.1	-6.99	-44.66	3.4
25/02/1978	-8.86	-63	-6.84	-43.50	3.6
26/02/1978	-9.64	-69.1	-6.21	-38.05	14.8
27/02/1978	-7.61	-51.5	-7.29	-47.56	9.6
28/02/1978	-8.94	-63.4	-7.11	-45.42	3.9
01/03/1978	-6.98	-41.5	-6.03	-36.56	11.5
02/03/1978	-9.12	-59.2	-6.41	-39.23	8.2
03/03/1978	-13.18	-94	-6.05	-36.23	5.1
14/03/1978	-6.64	-43.8	-6.85	-44.33	4
15/03/1978	-5.89	-45.1	-6.84	-42.40	4.4
16/03/1978	-9.7	-59.7	-6.04	-35.38	16.5
20/03/1978	-4.16	-22.5	-6.59	-42.03	5.5
21/03/1978	-8.77	-60.2	-7.29	-45.47	10
22/03/1978	-5.41	-30.1	-6.08	-36.44	3.1
23/03/1978	-5.81	-29.6	-6.38	-38.57	8.3
25/03/1978	-2.2	-5	-6.48	-41.23	6.9
26/03/1978	-4.71	-27.6	-6.39	-38.26	7.3
27/03/1978	-5.58	-35.6	-6.13	-38.33	9.3

Table D.1: *Observed and modelled $\delta^{18}O$ and δD values, and amount of precipitation for all Stock Hill raindays. Unpublished, please contact Professor Tim Atkinson, Department of Earth Sciences, University College London, t.atkinson@ucl.ac.uk for permission to use this data.*

Date	Observed		Modelled		Amount
	δ^{18}**O** ($^{\circ}/_{\circ\circ}$)	δ**D** ($^{\circ}/_{\circ\circ}$)	δ^{18}**O** ($^{\circ}/_{\circ\circ}$)	δ**D** ($^{\circ}/_{\circ\circ}$)	**(mm)**
28/03/1978	-5.99	-43.6	-5.88	-36.36	4.5
29/03/1978	-4.94	-31.9	-6.04	-36.89	3.4
01/04/1978	-8.77	-66.5	-7.29	-49.43	6.4
02/04/1978	-9.78	-83.9	-7.97	-54.89	10.8
14/04/1978	-7.44	-52.7	-6.80	-42.99	6.3
18/04/1978	-6.67	-46.9	-5.03	-28.41	3.6
20/04/1978	-7.54	-57	-7.07	-47.44	12.8
21/04/1978	-4.99	-32.5	-6.28	-39.99	8.6
22/04/1978	-6.38	-47.1	-6.76	-45.99	6.7
26/04/1978	-4.44	-25.8	-4.71	-26.68	5.8
29/04/1978	-9.11	-67.1	-4.97	-28.90	3.1
30/04/1978	-8.23	-62.3	-5.80	-36.14	3.4
05/05/1978	-12.36	-98.5	-5.54	-35.46	3.6
08/05/1978	-3.99	-28.7	-5.27	-33.64	4.1
13/05/1978	-7.05	-53.9	-9.17	-66.14	8.1
15/05/1978	-6.52	-48.6	-6.40	-42.51	4.4
08/06/1978	-2.9	-19.5	-7.08	-49.85	8.1
09/06/1978	-2.1	-12.3	-6.78	-46.51	4.4
22/06/1978	-7.75	-58.4	-7.61	-52.87	13
23/06/1978	-11.27	-81.5	-8.62	-61.11	17.2
25/06/1978	-7.3	-48.9	-9.91	-71.46	10.8
30/06/1978	-7.08	-53.1	-10.31	-75.91	6.6
03/07/1978	-2.04	-10.4	-8.50	-59.39	18.8
04/07/1978	-8.36	-64.1	-8.59	-61.08	4.6
05/07/1978	-10.68	-84.3	-8.51	-60.88	7.6
09/07/1978	-2.79	-15.9	-6.09	-40.88	4.8
11/07/1978	-5	-41.5	-7.87	-55.47	9.2
06/08/1978	-4.56	-30.6	-7.38	-50.71	7.2
08/08/1978	-8.19	-64.9	-7.64	-53.33	25.5
10/08/1978	-9.29	-74.3	-8.20	-57.63	16
09/09/1978	-2.78	-18.7	-8.25	-55.74	5.6
14/09/1978	-5.55	-37.9	-5.99	-38.05	5.1
27/09/1978	-5.7	-34.9	-7.38	-48.69	14.2
28/09/1978	-3.77	-19	-6.63	-42.82	14.6
29/09/1978	-5.31	-32.1	-6.50	-41.34	10.3
17/10/1978	-3.15	-11	-7.13	-45.40	7.1
03/11/1978	-2.6	-13.3	-7.30	-48.25	3.2

Table D.1: *continued. Please contact Professor Tim Atkinson, Department of Earth Sciences, University College London, t.atkinson@ucl.ac.uk for permission to use this data.*

Date	Observed		Modelled		Amount
	δ^{18}**O** ($^\circ/_{\circ\circ}$)	δ**D** ($^\circ/_{\circ\circ}$)	δ^{18}**O** ($^\circ/_{\circ\circ}$)	δ**D** ($^\circ/_{\circ\circ}$)	**(mm)**
13/11/1978	-8.89	-66.5	-7.36	-47.41	7.7
19/11/1978	-4.61	-33.8	-5.61	-33.29	15.1
20/11/1978	-6.05	-43.5	-7.45	-48.00	9.1
22/11/1978	-1.97	-7.6	-5.86	-34.99	9.1
04/12/1978	-7.28	-52.8	-6.62	-40.34	4.1
10/12/1978	-6.38	-52.6	-6.44	-39.84	7.9
11/12/1978	-7.6	-57.9	-7.32	-46.94	4.6
12/12/1978	-6.65	-50.5	-7.79	-50.59	7.1
13/12/1978	-8.42	-52.4	-8.21	-52.60	8.2
15/12/1978	-8.92	-63.4	-8.43	-55.54	3
21/12/1978	-14.88	-109.9	-6.77	-39.30	5.2
24/12/1978	-10.94	-79	-6.85	-42.08	11.5
25/12/1978	-7.25	-52.3	-7.46	-48.05	3.5
26/12/1978	-7.61	-52.4	-5.96	-35.21	3.6
28/12/1978	-7.51	-51.9	-7.52	-48.68	10.8
29/12/1978	-5.09	-42.4	-5.98	-35.63	5
30/12/1978	-8.31	-60.7	-7.84	-50.45	5.1
31/12/1978	-16.22	-122.3	-7.80	-45.98	3
07/01/1979	-6.28	-37.2	-5.66	-32.00	3.1
10/01/1979	-13.43	-92.2	-6.70	-39.57	5
11/01/1979	-17.01	-119.6	-8.50	-53.46	7.4
17/01/1979	-6.78	-44.8	-5.71	-31.71	3.1
18/01/1979	-11.8	-85.3	-6.77	-39.30	7.5
20/01/1979	-15.26	-111	-6.77	-40.57	18.4
21/01/1979	-8.83	-60.5	-7.14	-44.06	3.4
23/01/1979	-16.82	-128.8	-6.68	-37.91	17
26/01/1979	-12.02	-87.7	-7.37	-44.99	7.5
29/01/1979	-12.13	-84.8	-7.28	-44.74	5.2
01/02/1979	-10.24	-72	-5.57	-31.41	5.7
02/02/1979	-10.09	-68.5	-7.72	-49.23	7.9

Table D.1: *continued. Please contact Professor Tim Atkinson, Department of Earth Sciences, University College London, t.atkinson@ucl.ac.uk for permission to use this data.*

Appendix E

Observed and Modelled δ^{18}O and δD values, and amount of precipitation for Driby

The null value for lack of observed δ values is 100.00

Date	Observed		Modelled		Amount
	δ^{18}**O** ($^\circ/_{\circ\circ}$)	δ**D** ($^\circ/_{\circ\circ}$)	δ^{18}**O** ($^\circ/_{\circ\circ}$)	δ**D** ($^\circ/_{\circ\circ}$)	**(mm)**
01/03/1979	-8.05	-52.90	-6.95	-41.59	3.00
06/03/1979	-10.00	-68.00	-6.06	-35.82	8.60
08/03/1979	-7.65	-55.30	-6.99	-43.14	4.10
10/03/1979	-7.31	-56.70	-7.49	-45.85	5.90
16/03/1979	-14.36	-105.00	-6.52	-39.49	14.20
17/03/1979	-10.94	-82.70	-6.86	-43.49	3.30
20/03/1979	-13.68	-85.50	-5.41	-30.72	5.50
24/03/1979	-10.03	-62.90	-7.05	-43.78	10.10
25/03/1979	-3.89	-22.30	-6.44	-40.50	3.60
26/03/1979	-10.21	-70.80	-7.22	-47.50	4.10
27/03/1979	-13.03	-90.20	-6.96	-44.32	19.40
03/04/1979	-9.09	-55.00	-5.74	-33.18	7.40
05/04/1979	-13.32	-91.40	-5.60	-32.27	3.00
06/04/1979	-13.45	-95.50	-6.42	-39.84	3.20
09/04/1979	-8.82	-56.60	-5.07	-29.31	3.60
12/04/1979	-7.58	-51.70	-6.99	-46.38	6.10
22/04/1979	-9.53	-66.40	-6.52	-42.61	4.50
25/04/1979	-8.97	-61.30	-7.47	-50.48	3.80
27/04/1979	-4.41	-28.10	-6.15	-39.86	3.90
03/05/1979	-9.67	-61.30	-6.84	-43.04	9.50
06/05/1979	-7.62	-52.20	-6.84	-43.43	8.40
07/05/1979	-6.92	-47.50	-5.98	-37.42	3.40
10/05/1979	-5.38	-38.20	-5.29	-32.63	5.20
20/05/1979	-6.48	-41.50	-5.33	-34.14	12.40
21/05/1979	-7.69	-55.80	-5.73	-36.71	4.00
22/05/1979	-8.88	-60.00	-6.33	-40.75	9.40
24/05/1979	-9.34	-59.20	-7.18	-48.17	6.00
26/05/1979	-7.63	-57.00	-6.99	-46.64	11.30
28/05/1979	-4.52	-30.90	-6.64	-44.80	3.90
30/05/1979	-5.41	-38.50	-6.88	-47.66	7.20
07/06/1979	-8.40	-62.50	-7.45	-51.94	4.50
13/06/1979	-7.29	-53.50	-5.55	-37.44	9.20
14/06/1979	-5.74	-35.80	-7.31	-51.40	3.30
15/06/1979	-6.01	-45.80	-8.41	-59.10	3.50

Table E.1: *Observed and modelled $\delta^{18}O$ and δD values, and amount of precipitation for all Driby raindays from Heathcote and Lloyd (1986). Null value for δ values is 100.00.*

Date	Observed		Modelled		Amount
	δ^{18}**O** ($^\circ/_{\circ\circ}$)	δ**D** ($^\circ/_{\circ\circ}$)	δ^{18}**O** ($^\circ/_{\circ\circ}$)	δ**D** ($^\circ/_{\circ\circ}$)	**(mm)**
24/06/1979	-8.69	-59.00	-7.18	-49.98	5.20
29/07/1979	-6.18	-39.90	-7.40	-51.42	21.70
07/08/1979	-5.51	-43.40	-6.50	-44.00	8.10
08/08/1979	-13.31	-98.60	-7.54	-52.22	9.80
09/08/1979	-10.20	-71.50	-8.70	-60.84	12.20
13/08/1979	-3.67	-21.20	-7.61	-52.95	24.80
14/08/1979	-10.70	-77.70	-7.52	-51.68	3.90
16/08/1979	-5.80	-42.50	-8.68	-60.30	8.10
17/08/1979	-5.49	-40.40	-8.67	-60.96	3.10
23/08/1979	-8.05	-59.90	-8.01	-54.18	3.40
01/09/1979	-5.45	-38.50	-6.55	-43.79	5.10
18/09/1979	-1.94	-13.50	-6.78	-44.53	4.20
19/09/1979	-5.29	-38.20	-7.44	-50.88	14.60
03/10/1980	-7.73	-52.40	-6.71	-43.18	9.20
06/10/1980	-5.85	-40.20	-7.04	-45.03	10.30
10/10/1980	-8.07	-47.30	-8.06	-52.38	8.50
15/10/1980	-10.01	-60.00	-7.20	-45.39	15.30
16/10/1980	-11.32	-62.00	-7.42	-47.14	22.50
17/10/1980	-11.18	-76.30	-7.17	-46.11	13.30
22/10/1980	-6.85	-31.70	-5.45	-32.23	3.20
23/10/1980	-4.95	-84.00	-8.46	-57.42	7.10
26/10/1980	-4.28	-20.80	-7.74	-49.78	13.90
05/11/1980	-4.92	-26.60	-7.56	-47.34	7.40
06/11/1980	-11.80	-74.30	-8.59	-55.50	9.80
13/11/1980	-8.01	-52.40	-7.28	-44.88	19.30
14/11/1980	-10.30	-71.60	-6.92	-42.02	9.80
20/11/1980	-5.02	-25.70	-6.27	-37.92	4.30
22/11/1980	-4.80	-29.70	-6.91	-43.54	7.40
24/11/1980	-2.09	-14.60	-6.89	-43.39	3.80
26/11/1980	-8.66	-56.00	-7.91	-48.87	4.90
27/11/1980	-8.48	-44.60	-7.73	-47.92	11.80
28/11/1980	-10.10	-61.00	-7.90	-47.89	3.00
07/12/1980	-8.15	-27.90	-7.70	-46.17	3.10
16/12/1980	-7.29	-50.20	-8.27	-53.05	6.90
17/12/1980	-5.25	100.00	-7.14	-44.10	9.70

Table E.1: *continued*

Date	Observed		Modelled		Amount
	δ^{18}**O** ($^\circ/_{\circ\circ}$)	δ**D** ($^\circ/_{\circ\circ}$)	δ^{18}**O** ($^\circ/_{\circ\circ}$)	δ**D** ($^\circ/_{\circ\circ}$)	**(mm)**
19/12/1980	-10.69	-78.40	-8.01	-49.74	4.00
01/01/1981	-6.80	-49.70	-8.29	-51.09	5.20
16/01/1981	-9.77	-68.80	-7.54	-44.24	7.00
17/01/1981	-9.99	-73.00	-8.08	-50.84	3.00
18/01/1981	-9.42	-68.90	-7.85	-49.39	4.80
20/01/1981	-8.27	-60.00	-7.88	-48.61	3.10
08/02/1981	-2.01	-17.40	-6.46	-40.08	4.60
09/02/1981	-9.56	-72.90	-6.60	-41.28	29.70
28/02/1981	-15.05	-122.30	-5.97	-34.88	3.10
06/03/1981	-5.45	-38.90	-5.97	-35.43	5.00
09/03/1981	-7.96	-65.90	-7.99	-54.27	21.20
10/03/1981	-6.79	-59.30	-7.83	-52.94	17.30
11/03/1981	-8.34	-61.10	-5.71	-35.18	7.00
13/03/1981	-9.27	-68.20	-6.38	-40.63	23.60
14/03/1981	-4.43	-35.30	-7.57	-51.02	3.40
16/03/1981	-10.82	-75.50	-6.46	-39.11	6.80
21/03/1981	-5.12	100.00	-5.46	-32.50	5.60
22/03/1981	-7.69	-53.20	-6.47	-41.10	4.40
23/03/1981	-5.15	-38.50	-6.93	-43.12	4.70
29/03/1981	-8.06	-66.40	-6.40	-42.13	4.80
31/03/1981	-4.48	-34.40	-5.81	-36.15	6.20
11/04/1981	-6.37	-36.80	-6.92	-47.65	10.20
24/04/1981	-10.46	-72.40	-5.87	-33.28	41.50
25/04/1981	-12.23	-95.40	-4.95	-26.54	35.80
26/04/1981	-8.98	-59.30	-5.22	-29.78	17.80
03/05/1981	-9.98	-73.60	-6.53	-41.17	6.70
09/05/1981	-5.13	-32.50	-6.05	-40.72	11.00
21/05/1981	-3.97	-27.10	-5.38	-35.03	3.00
23/05/1981	-7.06	-55.20	-7.39	-51.19	5.80
24/05/1981	-7.27	-48.90	-6.75	-45.12	4.60
25/05/1981	-7.76	-56.50	-6.46	-42.36	7.00
01/06/1981	-5.52	-37.00	-6.57	-45.21	5.80
03/07/1981	-9.63	-74.40	-7.85	-54.76	4.40

Table E.1: *continued*

Date	Observed		Modelled		Amount
	δ^{18}**O** ($^\circ/_{\circ\circ}$)	δ**D** ($^\circ/_{\circ\circ}$)	δ^{18}**O** ($^\circ/_{\circ\circ}$)	δ**D** ($^\circ/_{\circ\circ}$)	**(mm)**
17/07/1981	-8.83	-68.10	-8.89	-62.99	14.80
22/07/1981	-17.69	-140.30	-8.57	-61.97	20.30
23/07/1981	-12.71	-94.60	-8.94	-64.78	4.90
05/08/1981	-3.90	-24.40	-6.80	-48.36	24.40
06/08/1981	-3.43	-21.40	-6.75	-47.42	18.40
08/08/1981	-3.75	-20.00	-5.36	-36.14	5.30
14/09/1981	-6.29	-48.10	-8.21	-55.80	8.70
18/09/1981	-9.09	-72.10	-7.27	-48.61	4.10
19/09/1981	-7.45	-53.00	-7.72	-51.40	18.30
24/09/1981	-4.78	-18.20	-7.22	-47.32	4.60
25/09/1981	-7.09	-53.00	-6.91	-44.77	8.70
26/09/1981	-7.89	-37.60	-7.41	-48.93	3.70
29/09/1981	-4.02	-19.80	-7.42	-49.20	18.40
03/10/1981	-17.80	-127.40	-8.83	-60.07	8.30
09/10/1981	-11.51	-87.20	-6.30	-39.17	8.00
18/10/1981	-7.55	-57.60	-7.12	-44.60	3.30
19/10/1981	-10.58	-84.90	-6.69	-41.58	14.70
22/10/1981	-5.94	-39.50	-8.96	-60.59	3.50
24/10/1981	-9.42	-66.20	-7.99	-52.78	9.00
26/10/1981	-4.82	-23.10	-8.33	-54.28	4.60
30/10/1981	-8.75	-65.70	-8.00	-50.98	5.00
15/11/1981	-4.62	-20.00	-6.49	-38.97	4.20
19/11/1981	-9.93	-71.80	-7.63	-48.39	5.00
23/11/1981	-5.11	-28.40	-6.49	-39.44	4.20
29/11/1981	-5.01	-26.50	-8.39	-53.11	4.20
30/11/1981	-6.34	-41.70	-7.72	-48.77	3.70
03/12/1981	-6.60	-51.20	-7.87	-50.93	3.00
14/12/1981	-17.35	-128.80	-8.46	-53.21	10.60
21/12/1981	-11.09	-77.50	-6.56	-37.05	10.70
29/12/1981	-12.37	-95.60	-7.27	-44.90	6.00
02/01/1982	-6.99	100.00	-9.68	-65.27	4.80
04/01/1982	-7.69	100.00	-6.85	-42.70	5.20
05/01/1982	-7.24	100.00	-7.78	-50.53	10.50
21/01/1982	-6.45	100.00	-6.67	-41.02	3.80
22/01/1982	-11.77	100.00	-6.14	-35.74	5.10
05/02/1982	-8.35	100.00	-6.32	-38.60	8.60

Table E.1: *continued*

Date	Observed		Modelled		Amount
	δ^{18}**O** ($^\circ/_{\circ\circ}$)	δ**D** ($^\circ/_{\circ\circ}$)	δ^{18}**O** ($^\circ/_{\circ\circ}$)	δ**D** ($^\circ/_{\circ\circ}$)	**(mm)**
11/02/1982	-5.71	100.00	-4.79	-26.46	3.90
17/02/1982	-11.89	100.00	-7.72	-50.18	4.50
03/03/1982	-6.72	100.00	-7.30	-46.32	5.90
06/03/1982	-9.82	100.00	-5.74	-34.00	17.70
09/03/1982	-12.31	100.00	-5.43	-30.46	9.20
14/03/1982	-6.37	100.00	-6.38	-38.96	5.50
15/03/1982	-16.20	100.00	-5.73	-34.41	16.20
19/03/1982	-10.03	100.00	-6.96	-44.17	6.80
29/03/1982	-8.00	100.00	-4.82	-27.29	4.20
07/04/1982	-6.24	100.00	-6.39	-42.21	5.20
05/05/1982	-9.60	100.00	-7.86	-51.89	3.20
06/05/1982	-10.88	100.00	-5.81	-35.92	16.70
18/05/1982	-6.16	100.00	-6.76	-46.33	6.00
21/05/1982	-6.99	100.00	-5.91	-40.29	3.70
23/05/1982	-9.57	100.00	-7.01	-47.94	5.50
26/05/1982	-4.59	100.00	-6.38	-42.54	13.10
10/06/1982	-7.00	100.00	-5.98	-41.74	12.20
18/06/1982	-5.81	100.00	-5.77	-38.49	16.80
21/06/1982	-4.31	100.00	-5.90	-40.41	22.70
22/06/1982	-5.71	100.00	-5.15	-33.77	37.70
23/06/1982	-5.69	100.00	-6.46	-44.33	4.30
25/06/1982	-6.88	100.00	-6.74	-47.11	25.40
26/06/1982	-7.87	100.00	-7.11	-49.31	13.10
28/06/1982	-10.26	100.00	-7.35	-51.37	7.60

Table E.1: *continued*

Appendix F

Observed versus modelled δ^{18}O for all raindays with over 3 mm of rain at Stock Hill split by month

(i)

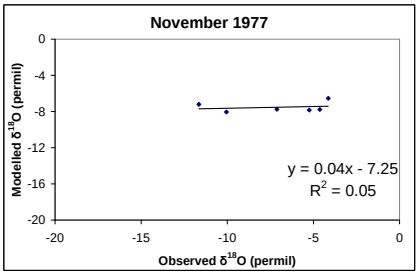

(ii)

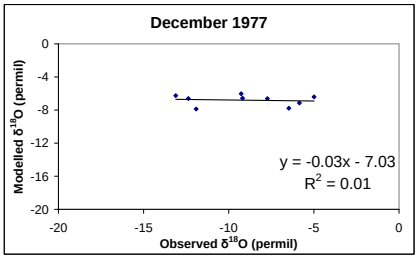

(iii)

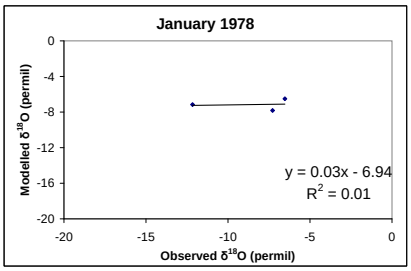

(iv)

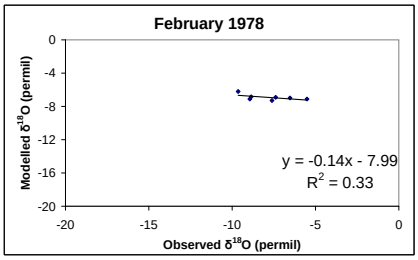

(v)

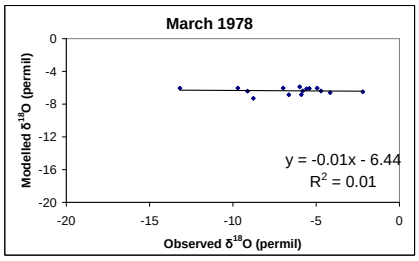

(vi)

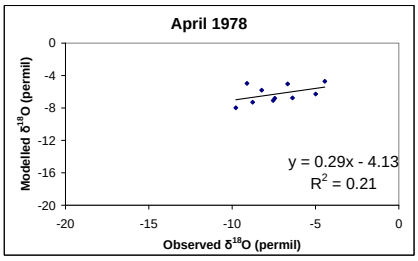

(vii)

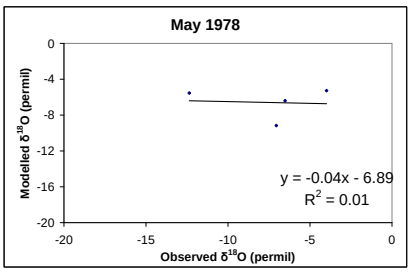

(viii)

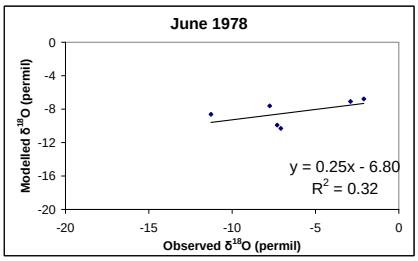

(ix)

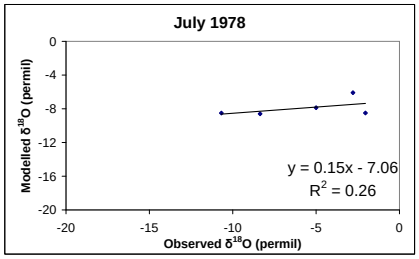

(x)

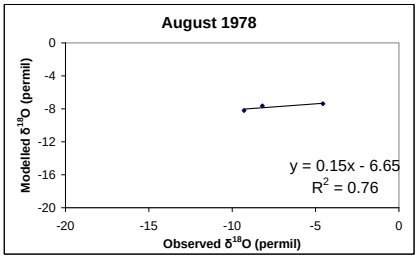

(xi)

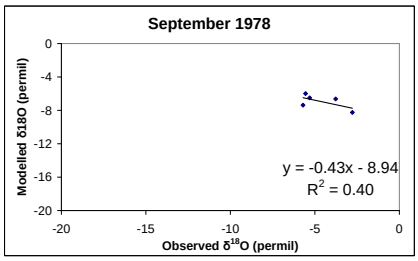

(xii)

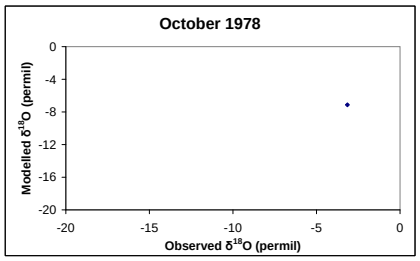

(xiii)

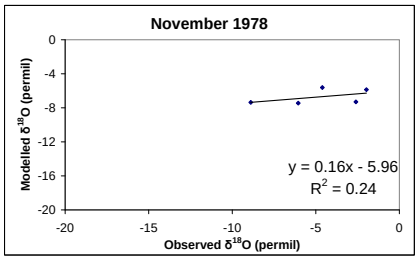

(xiv)

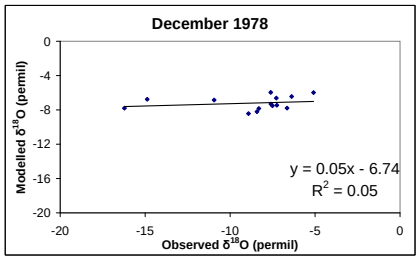

(xv)

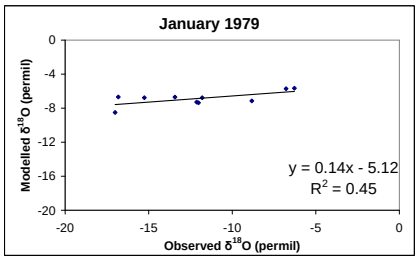

(xvi)

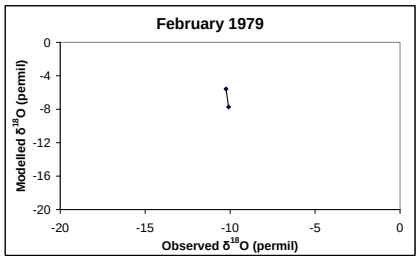

Appendix G

Observed versus modelled δ^{18}O for all raindays with over 3 mm of rain at Driby split by month

(i)

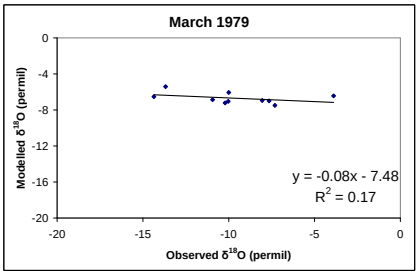

(ii)

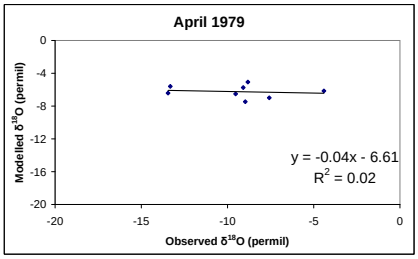

(iii)

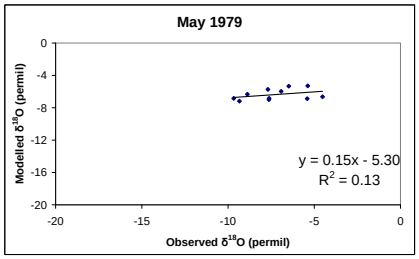

(iv)

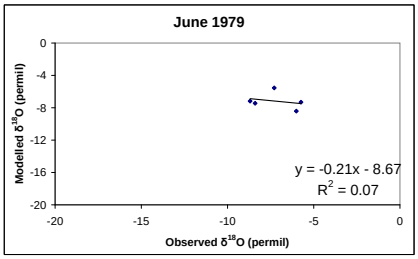

(v)

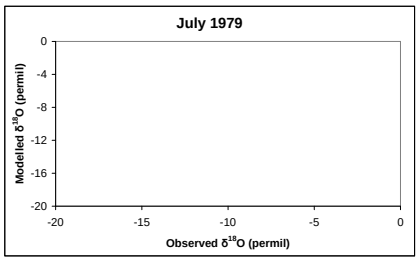

(vi)

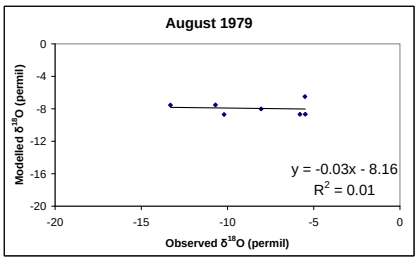

(vii)

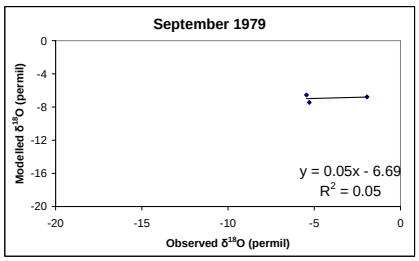

(viii)

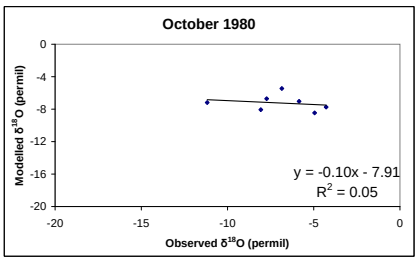

(ix)

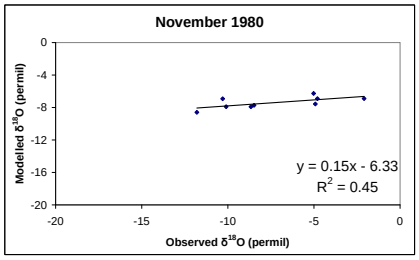

(x)

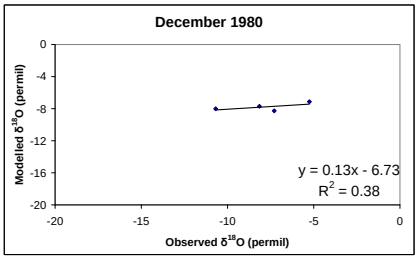

(xi)

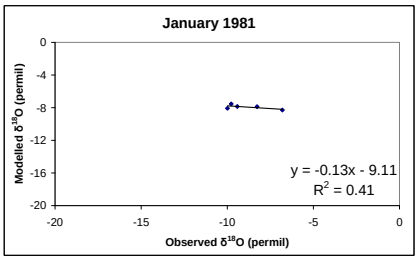

(xii)

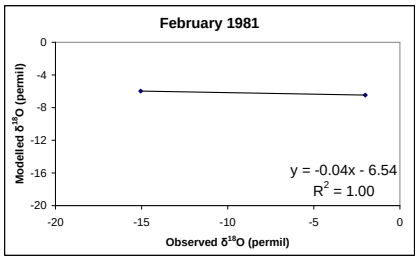

(xiii)

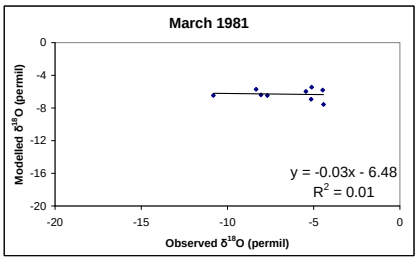

(xiv)

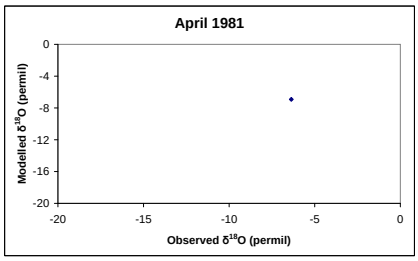

(xv)

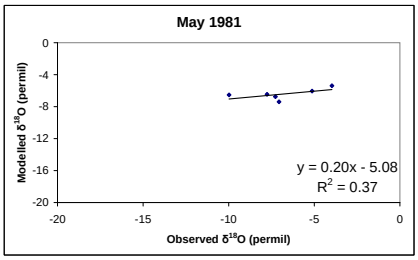

(xvi)

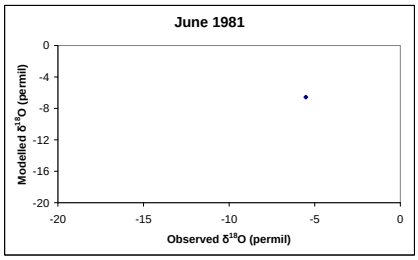

(xvii)

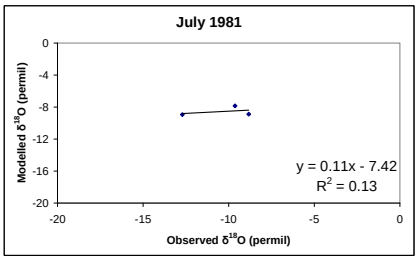

(xviii)

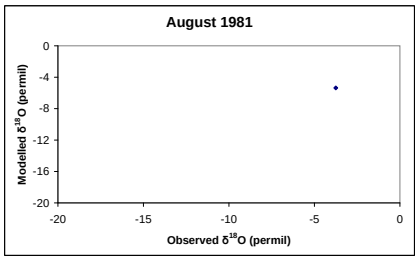

(xix)

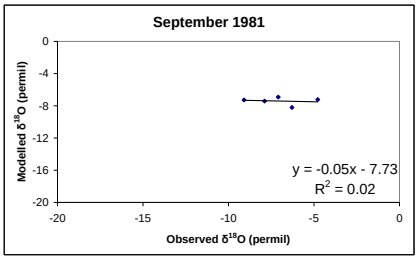

(xx)

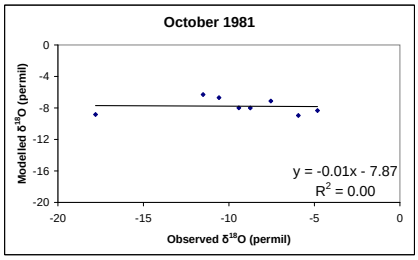

(xxi)

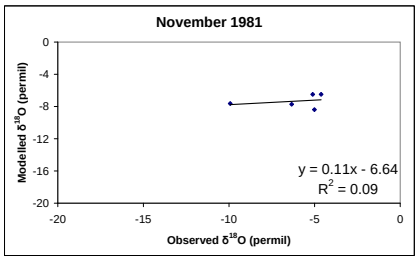

(xxii)

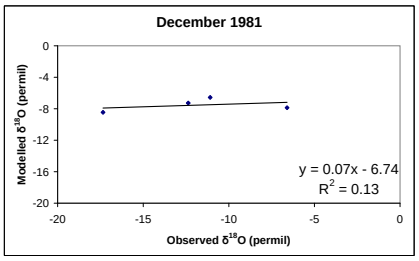

(xxiii)

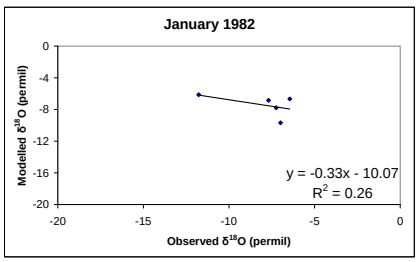

(xxiv)

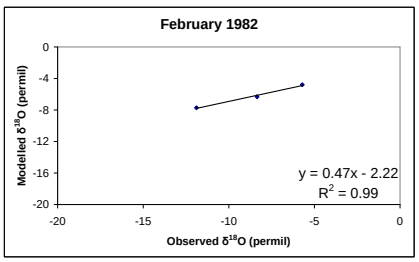

(xxiii)

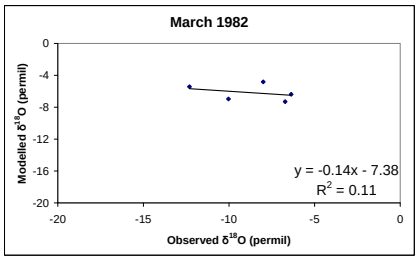

(xxiv)

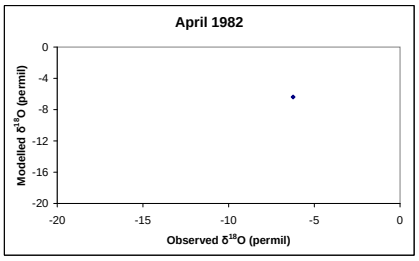

(xxiii)

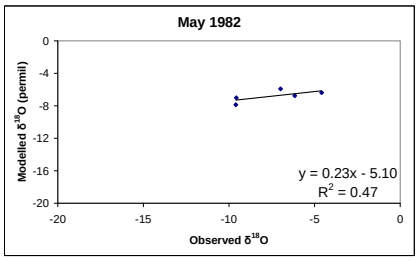

(xxiv)